1993

Tectonic Implications of Fission-Track Thermochronology and Amphibole Thermobarometry Studies of the Northern Peninsular Ranges Batholith, Southern California.

Peter Gillham George
Louisiana State University and Agricultural & Mechanical College

Order Number 9401525

Tectonic implications of fission-track thermochronology and amphibole thermobarometry studies of the northern Peninsular Ranges batholith, Southern California

George, Peter Gillham, Ph.D.

The Louisiana State University and Agricultural and Mechanical Col., 1993

U·M·I
300 N. Zeeb Rd.
Ann Arbor, MI 48106

TECTONIC IMPLICATIONS OF FISSION-TRACK THERMOCHRONOLOGY AND AMPHIBOLE THERMOBAROMETRY STUDIES OF THE NORTHERN PENINSULAR RANGES BATHOLITH, SOUTHERN CALIFORNIA

A Dissertation

Submitted to the Graduate Faculty of the
Louisiana State University and
Agricultural and Mechanical College
in partial fulfillment of the
requirements for the degree of
Doctor of Philosophy

in

The Department of Geology and Geophysics

by
Peter Gillham George
B.S., Duke University, 1980
M.S., Texas A&M University, 1985
May 1993

ACKNOWLEDGEMENTS

I would like to thank Dr. Dag Nummedal, Dr. Andrew Schedl, and Dr. Chad McCabe for reviewing this dissertation, as well as their encouragement and friendship. I would especially like to acknowledge Dr. Darrell Henry and my advisor, Dr. Roy Dokka, for their guidance and interest in this work. Darrell's knowledge of metamorphic petrology and Roy's understanding of the geology of southern California helped to greatly improve this dissertation. While at LSU I made a number of friends, including both faculty and graduate students, and I would also like to acknowledge their support and friendship. My family also provided a great deal of encouragement, as they have always done. Work in the field was much easier with the help of my four-legged field assistant, Olaf. Not only was he good company, but he also taste-tested the batholith for me. Given time he may have been able to differentiate tonalite from low-K granodiorite. Finally, I would like to acknowledge the support and patience of my wife Brenda.

TABLE OF CONTENTS

LIST OF TABLES

LIST OF FIGURES

ABSTRACT

Fission-track data from the San Jacinto Mountains and the Palomar Mountain-Escondido study area indicate that the Late Cretaceous history of the Peninsular Ranges batholith is marked by a series of major cooling events. Coupled with geobarometry measurements and field observations, these data allow for a greater understanding of the nature and timing of both local and regional tectonic events. In the eastern Peninsular Ranges, west-vergent thrusting along the Santa Rosa mylonite belt at ~99-94 Ma was followed by major extensional faulting between ~94 and 92 Ma. Amphibole geobarometry of mylonites indicate that ~10-18 km of crustal thickening occurred as a consequence of thrusting. Fission-track thermochronology and amphibole-plagioclase thermobarometry from footwall rocks (i.e. tonalitic plutons in the San Jacinto Mountains) indicate that subsequent extension resulted in ~10-14.5 km of exhumation. This was accompanied by synextensional intrusion and concomitant cooling of footwall tonalites from crystallization temperatures (730-760°C) to below the closure temperature of zircon (~235°C) in less than ~1 to 2 m.y. Fission-track data from the Palomar Mountain to Escondido study area indicate that the western Peninsular Ranges underwent several intervals of surface uplift and associated erosion between ~100 and 82 Ma. At ~77-76 Ma both eastern and western parts of the batholith experienced additional surface uplift that was likely brought on by changes in plate motions associated with the beginning of the Laramide orogeny. Surface uplift at ~77-76 Ma may explain the development of regional erosional unconformities that are common throughout Baja and southern California. The repeated intervals of Cretaceous and early Tertiary surface uplift also incrementally tilted the batholith and its fission-track age surfaces to the southwest by an amount that is compatible with estimates based on previous geochronologic and thermobarometric data. Tilting to the southwest brings discordant paleomagnetic directions of plutonic

rocks from the batholith into alignment with the expected Cretaceous direction, and thus eliminates the need for long-distance northward transport (~11°) of peninsular California as advocated by some workers.

CHAPTER 1

INTRODUCTION

FISSION-TRACK THERMOCHRONOLOGY

In minerals such as apatite, zircon, and sphene the spontaneous fission of ^{238}U (i.e. the breakup of its nucleus into two less massive nuclei) produces a trail of defects consisting of displaced atoms and vacancies, which is a fission-track (Fleischer et al., 1975; Naeser, 1976; Crowley et al., 1989). Fission tracks are stable in these minerals at temperatures less than their respective "closure" temperatures (i.e. less than ~300°C for sphene, ~250°C for zircon, and ~100°C for apatite). At higher temperatures, atomic movement in a mineral increases and displaced ions along the damage zone will diffuse back into the track and cause the damage zone to either partially or completely fade or "anneal" (Naeser, 1976; Crowley et al., 1989). The density of tracks in a mineral grain is a function of uranium concentration and the time elapsed since cooling below its closure temperature (Dodson, 1973; Naeser, 1976). Once the uranium concentration and track density are obtained a "cooling age" can be calculated using the fission-track age equation (see appendix A). In addition, apatite track lengths can be measured to evaluate the degree of "partial annealing." Fission-track thermochronology (i.e. an analysis of both fission-track ages and apatite track-length distributions), therefore, provides important information on the low-temperature cooling history (< 300°C) of a sample or group of samples, which in turn can be interpreted in terms of tectonic history. This is especially useful in areas that have experienced major cooling, due either to uplift and erosion and/or tectonic denudation. The following study is based mainly on fission-track analysis of tonalites and granodiorites from the northern Peninsular Ranges batholith of southern California, and includes age data for sphene, zircon, and apatite, as well as apatite track-length distributions. The data are then applied, in the context of previous geologic studies, to the Late Cretaceous tectonic

history of the batholith. The study also includes thermobarometry data from batholithic rocks in and adjacent to a regional ductile shear zone in the eastern Peninsular Ranges (i.e. the Santa Rosa mylonite belt). Pressure and temperature conditions estimated using an Al-in-hornblende geobarometer and an amphibole-plagioclase geothermometer, along with the fission-track thermochronologic data, help constrain the age and origin of the shear zone.

GEOLOGIC SETTING OF THE PENINSULAR RANGES

The study areas are shown in Figure 1 and include parts of the eastern Peninsular Ranges between the San Jacinto Mountains and Borrego Springs, and the western Peninsular Ranges from Palomar Mountain to Escondido, California. Both the western and the eastern Peninsular Ranges are composed primarily of plutonic and metamorphic rocks of the Peninsular Ranges batholith. However, there are major differences in the geology of the two regions, so much so that Silver et al. (1979) separated them into *western* and *eastern* batholiths. The boundary between the two trends northwest to southeast along the center of the batholith. There is a greater diversity of plutonic rocks in the west than the east. Western lithologies range from silica-undersaturated gabbros to leucogranites, with gabbro constituting up to 20% of the plutonic rocks (Larsen, 1948; Walawender and Smith, 1980; Gastil, 1983; Baird and Miesch, 1984; Silver and Chappell, 1988). Rocks in the east are primarily tonalites and granodiorites (Gastil, 1983; Silver and Chappell, 1988). U-Pb dating of zircon indicate that plutonic rocks in the western half of the batholith are older than those to the east, ~140 to 105 Ma as opposed to ~105 to 80 Ma (Silver et al., 1979; Silver and Chappell, 1988). Depth of exposure also increases from west to east across the batholith. Plutonic bodies in the westernmost part of the batholith show irregular outlines, and have brittle contact relations with surrounding country rock (Gastil, 1975). Volcanic rocks (i.e. the Santiago Peak Volcanics) are confined to the western edge of the batholith, where there

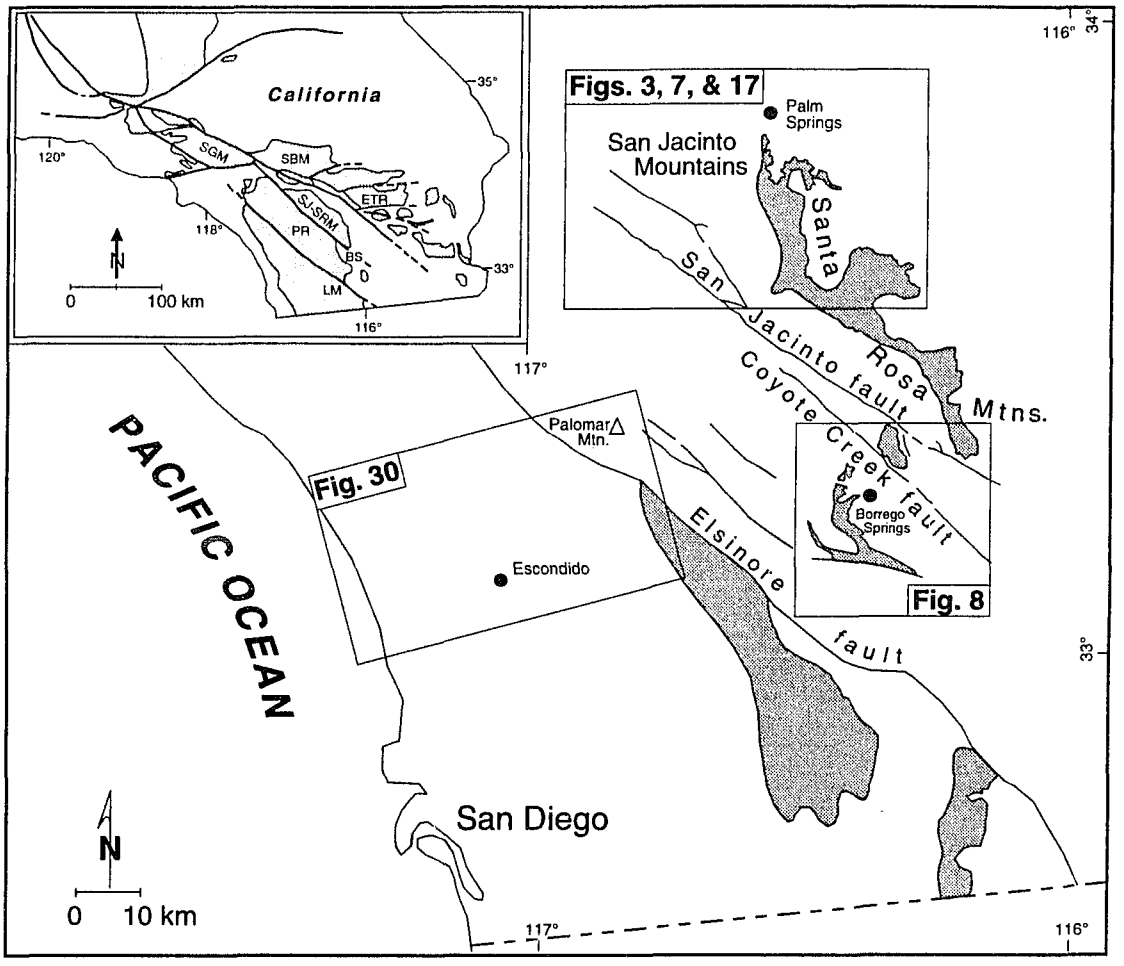

Figure 1. Location of study areas; 1. San Jacinto Mountains area (covered in chapters 2 and 3), 2. the Borrego Springs area (covered in chapters 2 and 3), 3. Palomar Mountain to Escondido, California (covered in chapter 4). Dark stipple represents major ductile shear zones in the eastern Peninsular Ranges. Inset shows the distribution of crystalline terranes and Cenozoic faults of southern California. Abbreviations are as follows: SGM, San Gabriel Mountains; SBM, San Bernardino Mountains; ETR, eastern Transverse Ranges; PR, northern Peninsular Ranges; SJ-SRM, San Jacinto and Santa Rosa Mountains; and LM, Laguna Mountains. Modified from Sharp (1967), Simpson (1984), Todd et al. (1988), and May (1989).

is some evidence that they may be part of a coeval volcanic cover to the batholith (Walawender et al., 1991). Plutons increase in size towards the east and their contacts become more ductile in appearance. Those near the center of the batholith are subcircular in outline with exposed diameters of 5 to 10 km. Plutons in the east measure as much as 40 km in width, and have even greater lengths parallel to the longitudinal axis of the batholith (Gastil, 1975) Metamorphic grade increases from lower greenschist facies in the west to upper amphibolite facies in the east, although this is a generalization (Todd et al., 1988).

The physiographic differences between the *western* and *eastern* batholiths are not as pronounced as the lithologic and structural differences. Both are the product of relatively recent (post ~5.5 Ma) right-lateral movements along the San Andreas fault system. Transpression and transtension between faults, such as the Elsinore and San Jacinto faults, has at various times in the past both uplifted and down-dropped large basement blocks of southern California (Larsen, 1948; Crowell, 1974; Christie-Blick and Biddle, 1985). The landscapes are generally composed of steep-sloped mountains and hills separated by northwest-oriented valleys (Weber, 1963). Some slopes are especially steep, such as the western side of Palomar Mountain and the eastern slopes of the San Jacinto Mountains. Rivers and streams flow to the west-southwest across the Peninsular Ranges where they enter the Pacific Ocean along a narrow continental shelf. Topographic relief increases towards the east from low hills and mountains to a chain of high mountains in the east. This chain of mountains extends NNW-SSE from southern California into northern Baja California along the eastern side of the Peninsular Ranges, and includes the voluminous tonalitic plutons of the San Jacinto Mountains and the La Posta pluton in the Laguna Mountains.

ORGANIZATION

The following study is subdivided into three parts (chapters 2, 3, and 4). Each was written in the Journal style as a separate paper. However, they all concern the Late Cretaceous tectonic history of the northern Peninsular Ranges and are intended to complement one another. Because each was written as an individual journal article, there is some overlap with regard to content. This mainly occurs in those parts of the dissertation concerning the Santa Rosa mylonite belt.

The first part of this study, Chapter 2, is based on fission-track ages and apatite track-length distributions from the San Jacinto Mountains in the eastern Peninsular Ranges. The data indicate major cooling events at ~92 and ~76 Ma, which are related to the tectonic history of the region. The prefered interpretation involves major west-vergent thrusting along the Santa Rosa mylonite belt at ~99-94 Ma, which produced an overthickened crustal welt in the eastern part of the batholith. This crustal welt subsequently collapsed by extension between ~94 and 92 Ma, and the mylonite belt along with its footwall rocks (i.e. the San Jacinto Mountains) were exhumed and rapidly cooled as a result of tectonic denudation. The fission-track data, specifically the sphene and zircon fission-track ages, therefore help constrain both the age and origin of the Santa Rosa mylonite belt when interpreted in the context of previous studies. The apatite fission-track ages and track-length distributions indicate regional cooling in the eastern Peninsular Ranges at ~76 Ma. This major cooling event is interpreted as resulting from regional surface uplift and erosion, which is supported by previous studies in the area. This uplift event coincided with major changes in plate motions along the Farallon (or Kula)-North American plate boundary located just west of the study area in Late Cretaceous time. These changes in plate motions are attributed to the initiation of low-angle subduction that, in turn, was responsible for the Laramide deformation of the Cordilleran foreland. Therefore, a part of Chapter 2 concerns the

Laramide orogeny, and specifically the linkage between low-angle subduction and cooling of the crust. Chapter 2 also deals with the stratigraphic and sedimentologic consequences of surface uplift. These consequences include the formation of Late Cretaceous age regional unconformities throughout Baja and southern California, as well as a major reorganization of marine facies in Late Cretaceous strata along the western edge of the batholith.

Chapter 3 examines the tectonic history of the Santa Rosa mylonite belt in light of new amphibole-plagioclase thermobarometry measurements. Geobarometry data, based on original electron microprobe data of Anderson (1983) from the Borrego Springs area, indicate major increases in pressure (~3-5 kb) during mylonitization. Combining these data with new thermobarometry measurements from the Palm Springs area, I have evaluated the tectonic history proposed in Chapter 2. These data support the notion of major Late Cretaceous thrusting along the mylonite belt followed by extension and exhumation of the shear zone. Also, evidence is presented that suggests the Santa Rosa mylonite belt is part of a larger Late Cretaceous belt of ductile deformation that extended from the Transverse Ranges into the eastern Peninsular Ranges, and included the Cuyamaca-Laguna Mountains shear zone of Todd et al. (1988).

Discordant paleomagnetic directions from the Peninsular Ranges batholith (Teissere and Beck, 1973; Hagstrum et al., 1985) have been interpreted as indicating ~25° of clockwise tectonic rotation and ~11° (~1200 km) northward translation of peninsular California with respect to cratonic North America during late Mesozoic and early Cenozoic time. Lithologic correlations between peninsular California and Sonora, however, support only 300 ± 10 km of north-northwest translation along the San Andreas transform system (Gastil et al., 1991). To resolve this enigma, Butler et al. (1991) proposed that southwest tilting of the batholith is responsible for the present paleomagnetic directions, and thus eliminates the need for long-distance transport. In

Chapter 4, fission-track data from a NE-SW sample transect between Palomar Mountain and Escondido, California are used to test the notion of structural tilting. The distribution of fission-track ages in the study area is compatible with southwest tilting of the batholith. The data, along with additional geologic evidence, also suggests that tilting was accomplished incrementally over an extended period from Early Cretaceous into Tertiary time.

Appendix A describes the methods of fission-track analysis in greater detail than is presented in Chapters 2 and 4. Appendix B includes all amphibole and plagioclase electron microprobe analyses of the samples from the San Jacinto Mountains (i.e. those of chapter 3).

CHAPTER 2

MAJOR LATE CRETACEOUS COOLING EVENTS IN THE EASTERN PENINSULAR RANGES, CALIFORNIA AND THEIR IMPLICATIONS FOR CORDILLERAN TECTONICS

INTRODUCTION

Causal links between plate tectonics and Cordilleran orogenesis have been well-supported by numerous regional studies over the years (e.g., Hamilton, 1969; Atwater, 1970; Coney, 1972; Burchfiel and Davis, 1972, 1975; Page and Engebretson, 1984; Engebretson et al., 1985). The plate tectonics paradigm has been particularly effective in understanding the underlying controls behind continental arc magmatism (e.g., Lipman et al., 1971; Coney and Reynolds, 1977; Dickinson and Snyder, 1978; Keith, 1978), the San Andreas fault system (e.g., Atwater, 1970), and accretion of "suspect" terranes (e.g., Coney et al., 1980). This chapter describes a fission-track thermochronologic study that was designed to test causal links through comparison of the timing of plate tectonic changes with the geologic history of a region that lay near the western edge of the North American plate in Cretaceous time. The study had two major goals. The first was to test explicit and implied features of recent geodynamical models by Bird (1984, 1988) and Hamilton (1988, 1989) that require significant tectonic erosion of the leading edge and base of the North American plate in association with low-angle subduction of the Farallon (or Kula) plate. Implicit in these models is that tectonically induced changes in the density distribution of the North American plate should have resulted in *surface uplift.* As defined by England and Molnar (1990) "surface uplift" is the displacement of the earth's surface on a regional scale ($>10^3$ km^2) with respect to the geoid. Thus a testable feature of these models centers on whether areas along the western edge of North America were the sites of Late Cretaceous surface uplift. The San Jacinto Mountains would have been among the regions to record such an event. Furthermore, surface uplift should have begun at ~74 Ma , the time of change

from steep to low-angle subduction (Engebretson et al., 1985). Shallowing of the subduction angle is thought to have been responsible for the development of the classic Laramide orogeny of the western interior (Coney, 1972). The second goal of the study was to constrain the tectonic history of a major Cretaceous brittle-ductile shear zone of the region, the Santa Rosa mylonite belt, by fission-track analysis of footwall rocks in the San Jacinto Mountains.

GEOLOGIC SETTING

The San Jacinto Mountains are located in the northern Peninsular Ranges of southern California (Fig. 2), and are a part of the *eastern* batholith defined by Silver et al. (1979). They consist mainly of Cretaceous plutonic rocks and older metamorphic rocks (Fig. 3; Dibblee, 1971, 1981; Brown, 1981; Hill, 1984). Three large bodies of tonalite dominate the plutonic rocks, although there are many smaller igneous bodies that range in composition from olivine gabbro to granite (Hill et al., 1986; Hill, 1988). Metamorphic rocks consist of pre-middle Cretaceous schist and gneiss. U-Pb isotopic studies on zircon by Hill and Silver (1979) and Silver (1986) establish a crystallization age for the tonalites between 94 and 93 Ma. The smaller intrusions of gabbro to granite crystallized between 99 and 94 Ma, based also on U-Pb isotopic studies on zircon and on cross-cutting relationships (Hill, 1984; Hill et al., 1986; Silver, 1986). Depth of emplacement of the tonalites has been estimated at 12-16 km (3.2-4.3 kb) based on metamorphic mineral assemblages (Hill et al., 1986), and 15-17 km (4.0-4.4 kb) based on amphibole geobarometry (Ague and Brimhall, 1988).

Rocks of the San Jacinto Mountains lie structurally beneath the Santa Rosa mylonite belt (SRMB), which is the northern segment of the eastern Peninsular Ranges mylonite zone (Sharp, 1979); rocks of the northern Santa Rosa Mountains form the hanging wall. The SRMB is a Cretaceous shear zone that strikes north-northwest and dips 30°-40° to the east (Sharp, 1966, 1967, 1979; Theodore, 1967; Dokka, 1984; Engel and

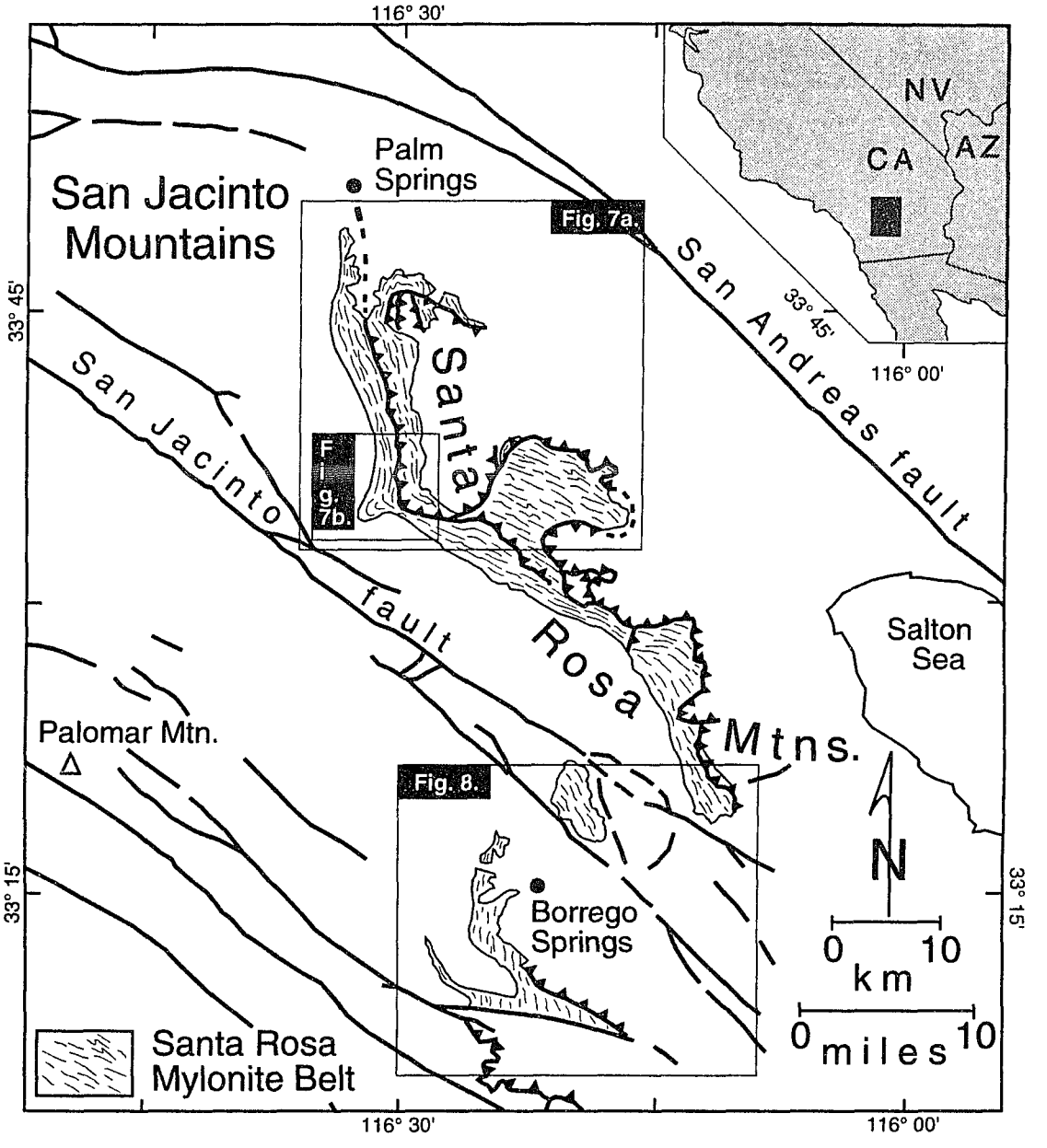

Figure 2. Map of southern California showing locations of the San Jacinto Mountains, Santa Rosa Mountains, and the Santa Rosa mylonite belt (modified from Sharp, 1967 and Simpson, 1984). Also shown are areas covered by figures 7 and 8.

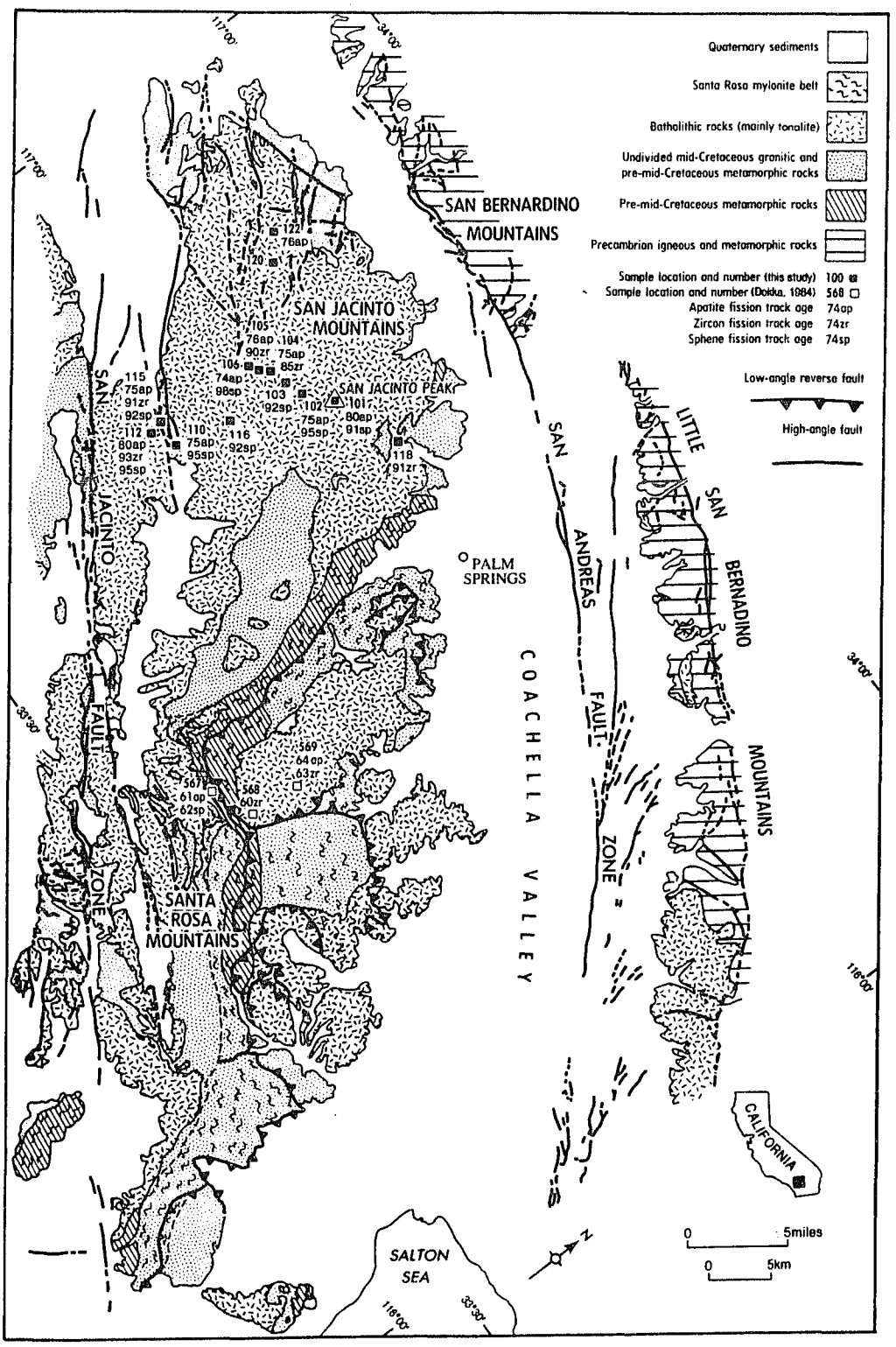

Figure 3. Geologic map of the study area showing sample locations from this study and those of Dokka (1984). Modified from the Geologic Map of California, Santa Ana Sheet (Rodgers, 1965).

Schultejann, 1984; Simpson, 1984; Erskine and Wenk, 1985; O'Brien et al., 1987). Two schools of thought exist regarding its origin. The shear zone was first interpreted by Sharp (1979), and later by Simpson (1984), Engel and Schultejann (1984), and Hamilton (1988) to be a major, Late Cretaceous west-vergent thrust fault. In contrast, Erskine and Wenk (1985) postulated that the SRMB is a Late Cretaceous extensional fault zone. This latter interpretation is based solely on observations of the mylonite zone from between the San Jacinto and northern Santa Rosa Mountains, while the studies of Engel and Schultejann (1984) and Simpson (1984) were concentrated to the south in the vicinity of Borrego Springs.

METHODS

Fission-Track Thermochronology

Fission-track thermochronology (FTT) has proven to be a powerful tool for tectonic studies by providing information on the timing of orogenic events and on the thermal environment in which deformation occurred (e.g., Wagner et al., 1977; Parrish, 1983; Dokka et al., 1986; Holm and Dokka, 1991). FTT can establish cooling points with which to reconstruct the thermal history of a rock. This requires that the age of several mineral species be determined and that the temperature sensitivity range of each of the thermochronometers is known. Sphene and zircon are typically interpreted in terms of the closure temperature concept (Dodson, 1973). Estimates of closure temperatures for sphene are between 250°C and 350°C (Naeser and Faul, 1969), and for zircon they range from 175°C (Harrison et al., 1979) to 240° ± 50°C (Hurford, 1986). Closure temperatures of ~285°C for sphene and ~235°C for zircon are adopted here (values based on cooling rates of ~10 to 100°C/Ma; Zeitler et al., 1982). Because the annealing characteristics of apatite are well known from laboratory studies, the time-temperature history of a sample can be modeled after determining its age and track-length distribution (Laslett et al., 1987; Jones and Dokka, 1990). This technique yields information for a

temperature range of 70°-130°C. The low temperature stability of fission-tracks allows tectonic changes in cooling history to be related to near-surface processes such as faulting, uplift, erosion, and sedimentation. FTT can also provide information concerning the rate of *exhumation* for a body of rock if a depth can be assigned to a given closure temperature. The term "exhumation" is used here as the displacement of rocks with respect to the surface where the rate of exhumation is the rate of erosion and/or tectonic denudation (England and Molnar, 1990).

Analytical Procedures

Samples were collected from low-K granodiorites and tonalites at locations shown in Figure 3. Their mineral assemblages typically include plagioclase, quartz, K-feldspar, biotite, hornblende, sphene, and accessory zircon, apatite, allanite, and ilmenite. Separates of apatite, zircon, and sphene, in the size range of 62-250 μm were recovered from crushed and pulverized rock using a concentration table, non-toxic heavy liquids, and a magnetic separator (see appendix A for a more detailed description of methods used in this study). All minerals were dated using the external detector method (Naeser, 1976) following procedures described in Dokka et al. (1986). Apatite samples were also prepared for track-length measurements according to methods outlined by Green (1981) and Laslett et al. (1982). Track lengths were measured using an optical microscope (1500x) linked by way of a camera lucida to a digitizing pad and microcomputer. Ages were calculated using the "zeta" method of Hurford and Green (1983) using National Bureau of Standards Fission-Track Glasses 962 and 963a and coupled muscovite detectors; these standards have been calibrated using apatite and zircon from the Fish Canyon tuff. Statistical uncertainty for all age determinations was calculated by the method of Johnson et al. (1979). A chi-square test at the 5% level was applied to all age data as proposed by Galbraith (1981).

RESULTS

Fission-track age data are given in Table 1. Sphene and zircon ages in rocks sampled from San Jacinto Peak to near the base of the mountains (2.5 km of vertical relief) have ages that are concordant at ~92 Ma (midpoint of the overlap of 2 σ error bars), thus implying a major cooling event when temperatures dropped from above ~285°C to below ~235°C (Fig. 4a). Amphibole-plagioclase thermobarometry of the main tonalitic plutons indicate crystallization at 730°-760°C and 4-5 kb (15-19 km) (data presented in chapter 3). Because the tonalites of the San Jacinto Mountains have U-Pb zircon ages of 94-93 Ma (Hill and Silver, 1979; Silver, 1986), and crystallized at 730°-760°C, temperatures must have dropped between 500°-530°C in less than ~1 to 2 m.y. The thermobarometry and thermochronology data, together, imply ~10-14.5 km of exhumation between 94-93 Ma and ~92 Ma.

Apatites range in age from 74.1 Ma to 79.9 Ma (Table 1). There is no significant variation within the ages of the apatites, regardless of elevation (Fig. 4b). Concordance of apatite ages from an ~2.3 km vertical exposure of rock indicates a second cooling event at ~76 Ma (midpoint of the overlap of 2 σ error bars) when temperatures fell through the 70°-130°C range.

The distribution of lengths of confined fission-tracks in apatite provides additional information on the cooling history of a rock. Gleadow et al. (1986) has shown that slowly cooled granitic terranes tend to have negatively skewed track-length distributions with mean track lengths of 12-13 μm and standard deviations of 1.2-2.0 μm. Skewness increases with the amount of time spent in the temperature range ~70°-130°C, within which substantial annealing occurs. Rapidly cooled granitic terranes have normal to positively skewed distributions with mean lengths >14.0 μm and standard deviations between 0.8 μm and 1.2 μm (Dokka et al., 1986; Gleadow et al., 1986). Track-length distributions of apatites from the study area have mean track lengths between 13.9 μm

Table 1: Fission-Track Data for the San Jacinto Mountains

Field # [Lab #]	Elevation meters	Mineral Dated	Spontaneous Track Density, tracks/cm^2 [tracks counted]	Induced Track Density, tracks/cm^2 [tracks counted]	Standard Track Density, tracks/cm^2 [tracks counted]	Grains Counted	Chi-Square Statistic [X^2]$	Correlation Coefficient*	Age [Ma]#	±1sigma [Ma]
101 [880018]	3293	Apatite	8.140E+05 [407]	2.278E+06 [1139]	4.196E+04 [2026]	20	3.349	0.951	79.7	4.9
102 [910036]	2365	Apatite	8.646E+05 [198]	2.603E+06 [596]	4.226E+04 [2009]	6	1.044	0.991	74.6	6.3
104 [880014]	1984	Apatite	5.507E+05 [413]	1.652E+06 [1239]	4.213E+04 [2026]	29	9.429	0.494	74.6	4.6
105 [880011]	1856	Apatite	8.553E+05 [272]	2.503E+06 [796]	4.187E+04 [2026]	7	1.036	0.972	76.1	5.6
106 [880015]	1756	Apatite	8.376E+05 [356]	2.527E+06 [1074]	4.205E+04 [2026]	16	15.733	0.494	74.1	4.8
122 [880019]	1359	Apatite	9.067E+05 [476]	2.676E+06 [1405]	4.221E+04 [2026]	21	27.114	0.654	76.0	4.3
110 [880013]	1353	Apatite	1.084E+06 [271]	3.264E+06 [816]	4.259E+04 [2026]	9	5.618	0.804	75.2	5.5
112 [880057]	1231	Apatite	1.213E+06 [455]	3.411E+06 [1279]	4.229E+04 [2026]	15	23.539	0.640	79.9	4.7
115 [880012]	1003	Apatite	8.855E+05 [294]	2.599E+06 [863]	4.162E+04 [2015]	8	2.04	0.953	75.4	5.4
104 [880021]	1984	Zircon	7.824E+06 [1154]	3.003E+06 [443]	1.960E+05 [4150]	6	4.678	0.965	84.9	4.9
105 [890042]	1856	Zircon	1.163E+07 [872]	4.133E+06 [310]	1.916E+05 [4150]	5	1.458	0.999	89.6	6.1
112 [890001]	1231	Zircon	1.139E+07 [1463]	3.938E+06 [506]	1.928E+05 [4150]	6	7.023	0.926	92.6	5.0
115 [880022]	1003	Zircon	6.215E+06 [839]	2.170E+06 [293]	1.922E+05 [4150]	7	0.377	0.996	91.4	6.4
118 [880053]	811	Zircon	1.656E+07 [911]	5.836E+06 [321]	1.935E+05 [4150]	6	0.375	0.995	91.2	6.1
101 [880004]	3293	Sphene	5.895E+06 [1179]	2.180E+06 [436]	2.023E+05 [4150]	8	13.703	0.498	90.9	5.3
102 [880006]	2731	Sphene	5.531E+06 [968]	2.017E+06 [353]	2.079E+05 [4150]	7	3.185	0.979	94.7	6.1
103 [890002]	2365	Sphene	6.585E+06 [1238]	2.484E+06 [467]	2.092E+05 [4150]	5	2.089	0.701	92.2	5.2
106 [880007]	1756	Sphene	7.663E+06 [1341]	2.577E+06 [451]	1.992E+05 [4150]	7	2.075	0.940	98.4	5.6
110 [880009]	1353	Sphene	4.531E+06 [1246]	1.585E+06 [436]	2.010E+05 [4150]	11	7.255	0.804	95.4	5.5
112 [880058]	1231	Sphene	4.973E+06 [1119]	1.720E+06 [387]	1.972E+05 [4150]	9	2.087	0.789	94.7	5.8
115 [880001]	1003	Sphene	5.116E+06 [1105]	1.792E+06 [387]	1.928E+05 [4150]	6	0.396	0.998	91.5	5.6
116 [890045]	3293	Sphene	1.023E+07 [818]	3.788E+06 [303]	2.041E+05 [4150]	5	0.481	0.925	91.6	6.3

$ X^2 value according to Galbraith [1981] for n degrees of freedom [n is number of grains minus 1]; all samples pass at 5% level.

* comparison between individual crystal track counts

calculated according to Hurford and Green [1983] using zeta values of 10692 and 335 for apatite and zircon-sphene, respectively

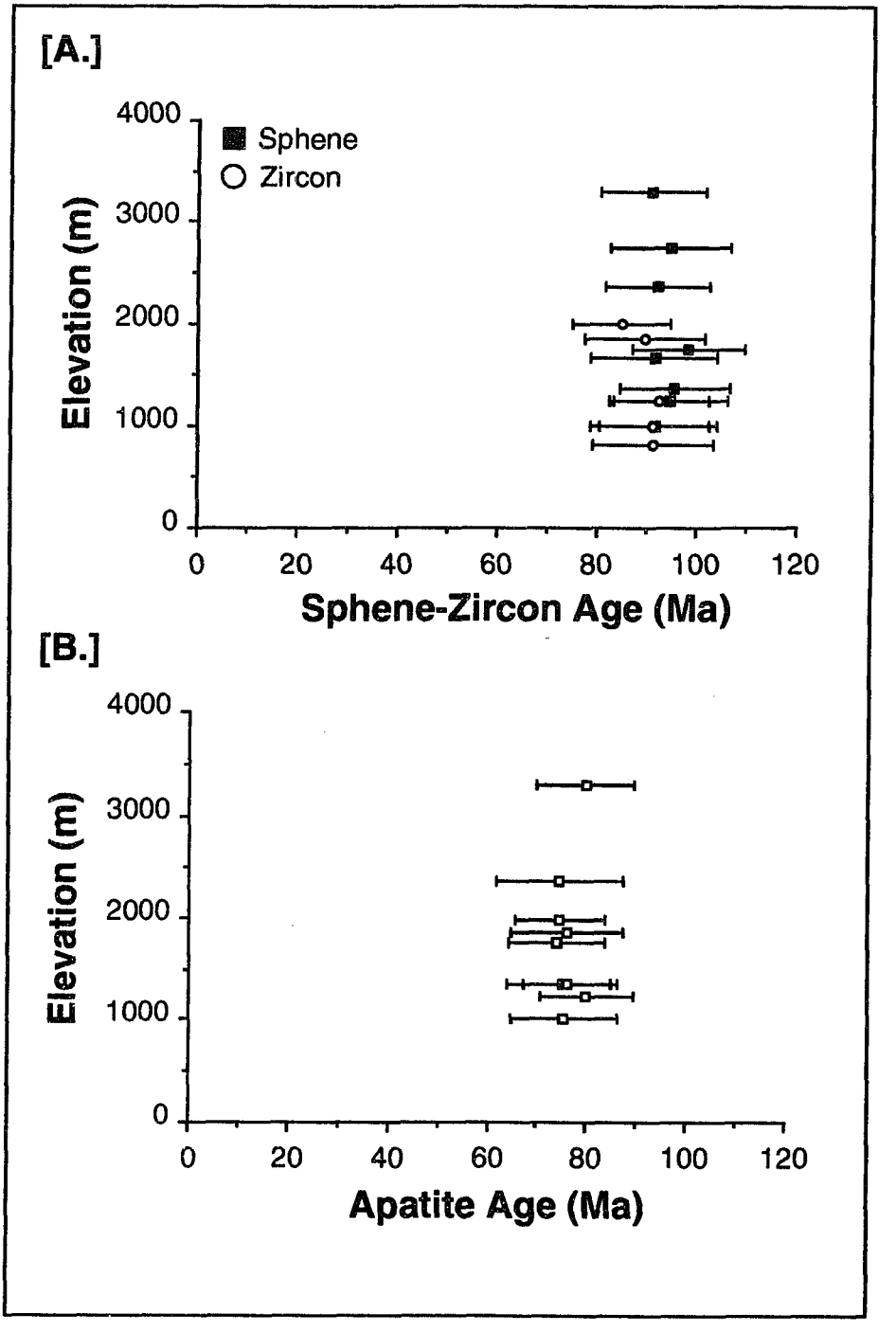

Figure 4. a) Sphene and zircon fission-track ages plotted against elevation. Samples range in age between 85.0 Ma and 98.4 Ma. b) Apatite fission-track ages plotted against elevation. Samples range in age between 74.1 Ma and 79.9 Ma. Precision estimates expressed as 2 sigma.

and 14.4 μm with standard deviations of 0.7 μm to 1.2 μm and are, therefore, similar to the those of a rapidly cooling basement terrane (Fig. 5a). Mean track lengths do not correlate with elevation (Fig. 5b). Because all samples from the San Jacinto Mountains have indistinguishable cooling ages and apatite track-length distributions, 2.3 km of exposed vertical section must have cooled over a short period in Late Cretaceous time (~76 Ma). It is not known how much rock with the same cooling history has been removed from above the present erosion surface or exists below the lower sample. Figure 6 shows a hypothetical thermal history for rocks of the San Jacinto Mountains that is consistent with available thermochronologic data.

DISCUSSION

Fission-track data reported here have important implications for local, regional, and Cordillera-wide tectonics. Sphene and zircon fission-track ages, coupled with observations from earlier studies (Anderson, 1983; Dokka, 1984; Engel and Schultejann, 1984; Simpson, 1984; Erskine and Wenk, 1985; Erskine, 1986; O'Brien et al., 1987), help constrain the deformational history of the SRMB, while providing insights into its tectonic origin. The apatite fission-track data allow testing of models that relate the Laramide orogeny to Late Cretaceous plate interactions along the west edge of the North American plate. In addition, the fission-track ages constrain the timing of formation of major erosional surfaces in Baja California and southern California, and help explain the general Late Cretaceous-early Tertiary stratigraphic development of the region.

Age and Origin of the Santa Rosa Mylonite Belt

Two general hypotheses have been proposed to explain deformation along the Santa Rosa mylonite belt. Proponents of one model, initially suggested by Sharp (1979), consider the SRMB to have originated as a west-vergent thrust fault. A second model,

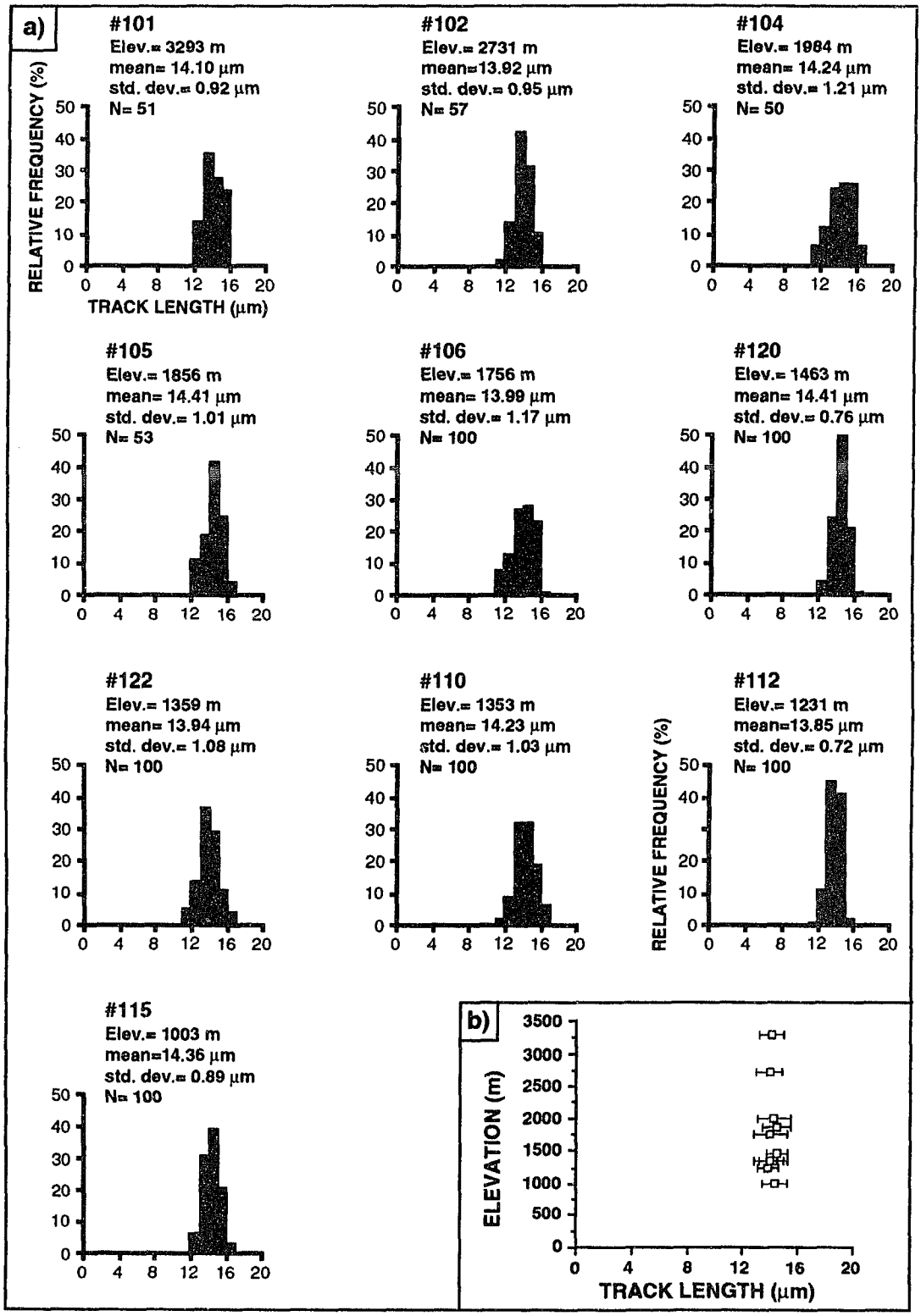

Figure 5. a) Frequency distributions of confined fission-tracks in apatite of samples from the San Jacinto Mountains. Means (13.9-14.4 µm) and standard deviations (0.8-1.2 µm) are similar to apatites from rapidly cooling basement terranes. b) Mean track lengths of apatite plotted against elevation show no correlation.

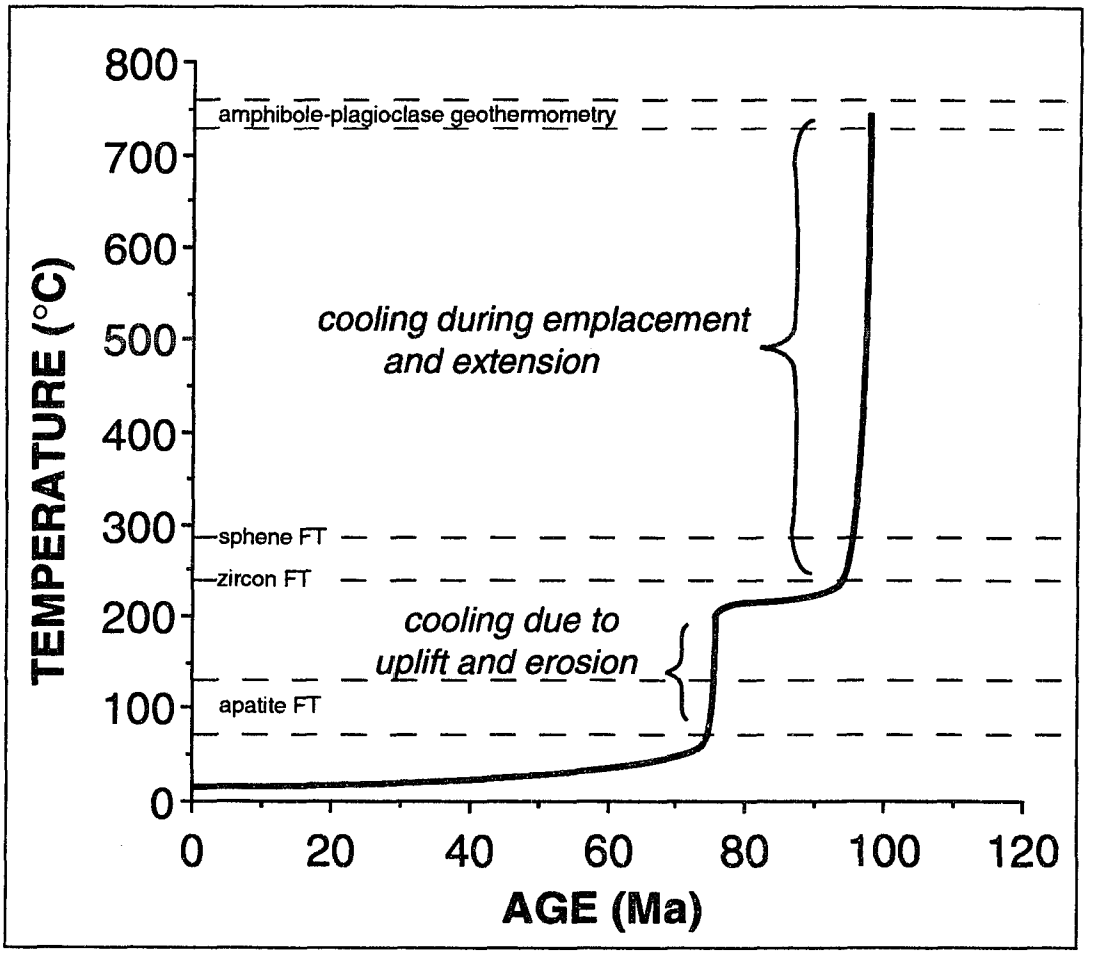

Figure 6. Hypothetical thermal history of rocks of the San Jacinto Mountains consistent with U-Pb zircon ages reported in Silver (1986), fission-track ages from this study, and thermobarometry results presented in Chapter 3.

proposed by Erskine and Wenk (1985), attributes mylonitization to extensional detachment faulting. Fission-track data presented here, along with other complementary data, provide additional constraints on these models. The data also indicate that mylonitization in the Palm Springs area occurred during Late Cretaceous (Cenomanian) time. Previously, deformation along the SRMB was more broadly constrained as Late Cretaceous to early Paleocene in age (Dokka, 1984).

Abundant large- and small-scale structures support the notion of west-directed thrusting along the SRMB. In the portion of the mylonite belt located between the San Jacinto Mountains and northern Santa Rosa Mountains, microstructures indicate a top towards the southwest sense of shear. These include S-C structures (Erskine and Wenk, 1985) and asymmetric porphyroclasts (Simpson and Schmid, 1983) in lower-plate, mylonitic plutonic rocks (unit Kmgr; Fig. 7). Within these mylonites are lenses or pods of highly deformed mylonitic gneiss, ultramylonite, and phyllonite (O'Brien et al., 1987). They are nearly identical in terms of mineralogy and bulk composition to the surrounding mylonitic plutonic rock, indicating that both share a common protolith. Microstructures in these intensely deformed rocks also indicate an east-over-west sense of shear. The rocks display ubiquitous S-C surfaces and local shear bands, coherent rotated clasts of feldspar and quartz with sigmoidal shadows, asymmetric pole figures from biotite, and some asymmetry in quartz fabrics (O'Brien et al., 1987).

Upper-plate rocks of the Palm Canyon Complex (Fig. 7) also contain evidence supporting the notion of west-vergent thrusting along the SRMB. These rocks are characterized by substantial volumes of mylonitic, garnetiferous leucogranite anatexites associated, in a lit-par-lit manner, with metasedimentary rocks and orthogneiss (Todd et al., 1988). The anatexites are strongly foliated and display a well developed downdip lineation that are parallel to east-northeast lineations in lower-plate, mylonitic plutonic rocks. The development of foliation and lineation is considered coeval with anatexis of

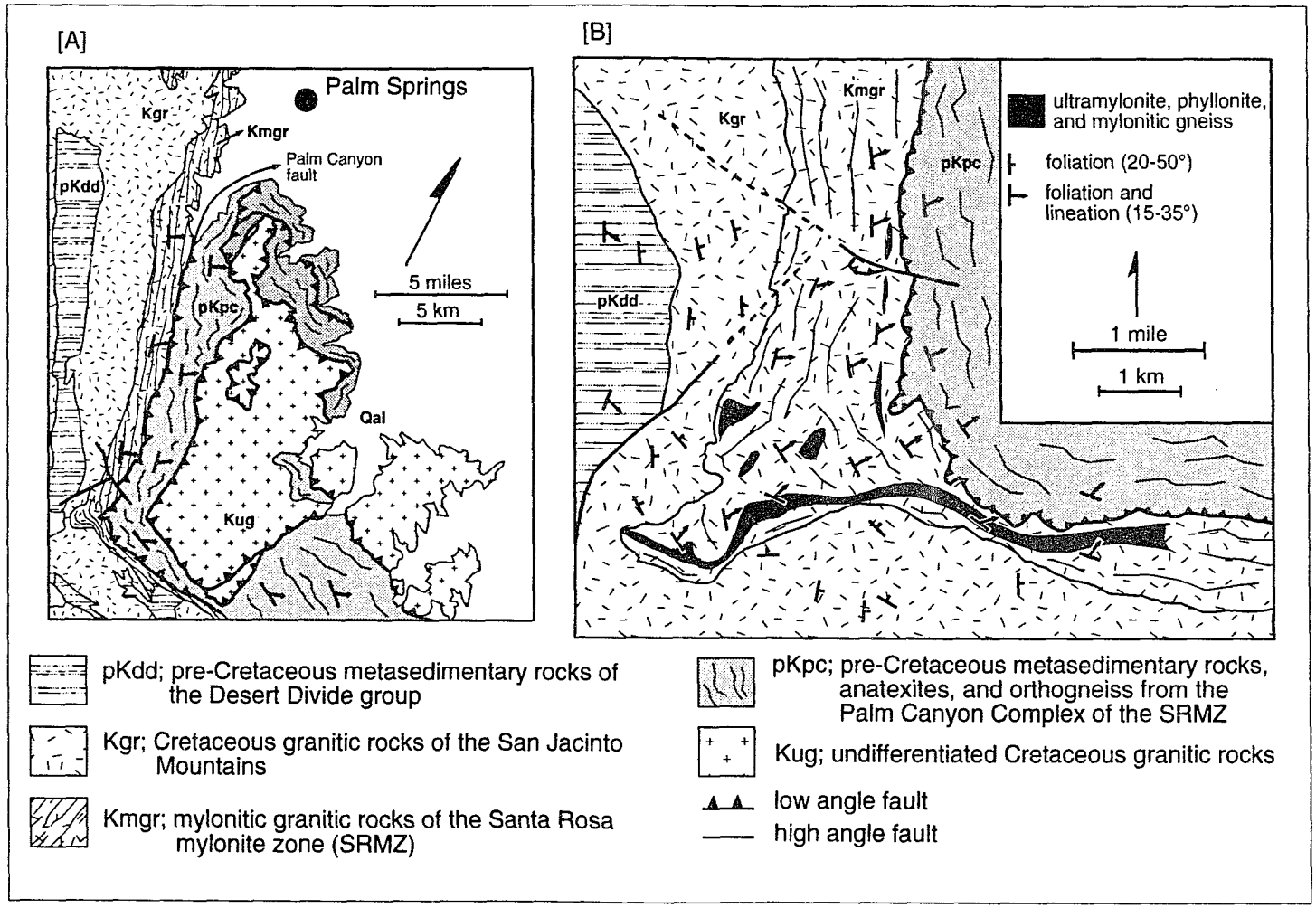

Figure 7. a) Geologic map of the Santa Rosa mylonite belt between the San Jacinto and Santa Rosa Mountains. Modified from maps of Erskine and Wenk (1985) and Todd et al. (1988). b) Geologic map of a highly deformed part of the mylonite belt. Modified from O'Brien et al. (1987)

pelitic schists during high grade metamorphism (Todd et al., 1988). Todd et al. (1988) interpreted the lack of similar anatexis and high grade metamorphism of metasedimentary rocks in the footwall of the SRMB (i.e. the Desert Divide Group of Brown, 1981) as indicating that the Palm Canyon Complex was uplifted from deep structural levels during west-vergent thrusting and mylonitization.

Microstructural and mesoscopic-scale evidence from the SRMB in the Borrego Springs area also indicate west-vergence. Southwest of Borrego Springs, Simpson (1984) described S and C planes and shear bands in deformed granodiorites that consistently indicate an east-over-west sense of shear (Fig. 8). She also noted various other microstructures, all indicating west-vergence. They include, "(1) small relict biotite grains that have tails of fine-grained recrystallized biotite asymmetrically distributed relative to the S planes, (2) antithetic offset along microfaults in feldspar grains, and (3) elongate subgrains and recrystallized new grains of quartz that have long axes perpendicular to the direction of the last increment of maximum compression." Mapping by Engel and Schultejann (1984) and Schultejann (1984) in the mylonites west and southwest of Borrego Springs, at Coyote Mountain, and in the southern Santa Rosa Mountains indicate west and NNW-vergent thrusting (Figs. 2 and 8). All three localities contain overthrusts and associated drag folds and nappes that form imbricate stacks of metasediments, plutonic rocks, and mylonites. Thrusting to the west and NNW is indicated by the geometry and vergence of large and small folds, from stratigraphic reconstructions, and the displacement of crosscutting pegmatites. They also noted an east to ENE-plunging mineral lineations that is similar to those in both upper- and lower-plate rocks of the SRMB from the Palm Springs area.

In addition to the evidence that imply west-directed thrusting along the mylonite belt in both the Palm Springs and Borrego Springs areas, there are also extensional structures. Marbles of the Palm Canyon Complex between the San Jacinto Mountains

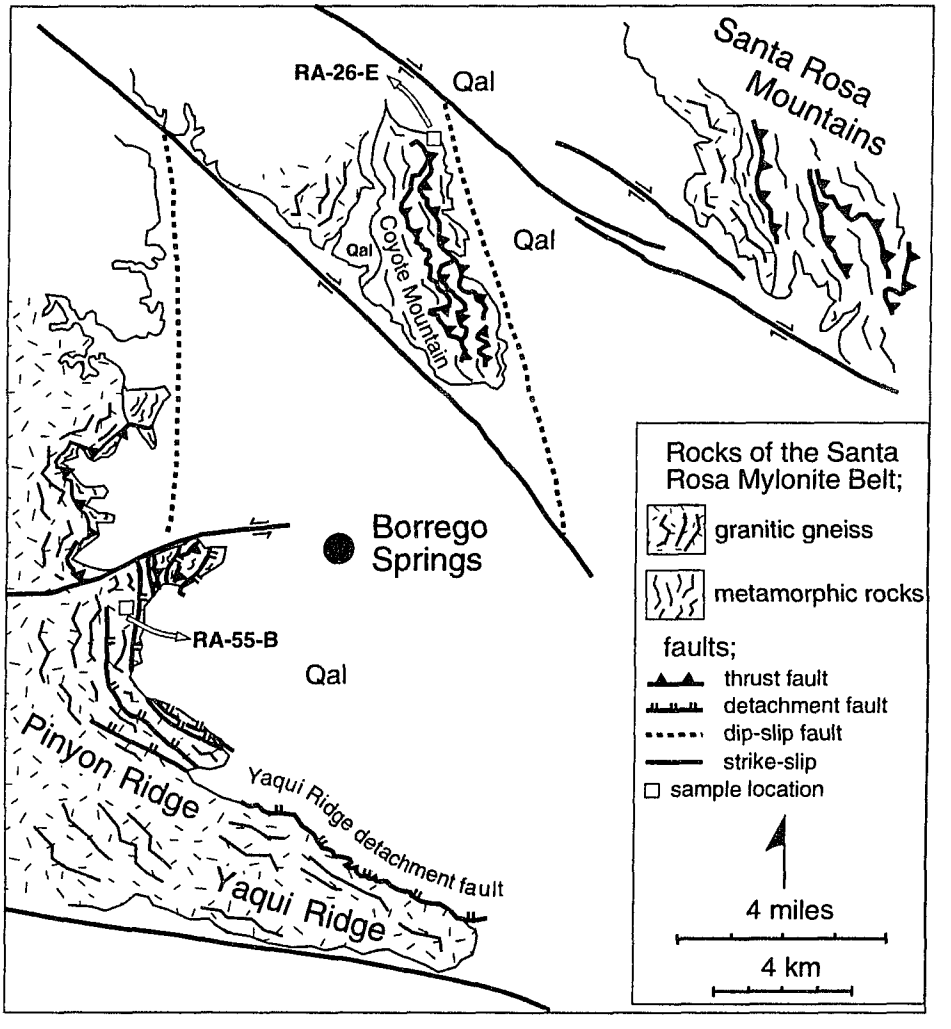

Figure 8. Simplified geologic map of the Santa Rosa mylonite belt in the Borrego Springs area. Modified from maps of Engel and Shultejann (1984) and Shultejann (1984). Samples RA-26-E and RA-55-B of Anderson (1983) have amphiboles with Al-rich rims that formed during mylonitization, as ~10-18 km of crust was thrust over the eastern margin of the Peninsular Ranges.

and northern Santa Rosa Mountains yield calcite pole figures indicating orthorhombic symmetry (Fig. 7; Erskine and Wenk, 1985). Pole figures from quartz bands in the lower-plate, mylonitic plutonic rocks display similar geometry. Orthorhombic symmetry of quartz and calcite fabrics suggests coaxial deformation under conditions of plane strain, pure shear (Wagner et al., 1982). Erskine and Wenk (1985) interpreted these data as representing flattening normal to the mylonitic foliation of the SRMB, which strikes north-northwest and dips 35-55° to the east. Deformation was thought to also involve extension parallel to the stretching lineation that trends ~N55°E. In the same area lying above the Palm Canyon fault are several low-angle, east-dipping normal faults that parallel or locally cut the mylonitic foliation at a low angle; these faults do not, however, cut across the Palm Canyon fault. Fault surfaces commonly have a well developed chloritic breccia zone, and some display northeast-vergent drag folds. These surfaces also have linear slip-related structures that are subparallel to lineations in the SRMB. Erskine and Wenk (1985) cited these relations, along with the relative attitudes of the low-angle faults and the mylonite belt, as evidence for kinematic linkage between down-to-the-east low-angle faulting and mylonitization. Todd et al. (1988) proposed that the Palm Canyon fault was the basal décollement to the structurally higher low-angle faults.

Low-angle faults, similar to those in the Palm Springs area, have also been described along the mylonite belt to the south. Southwest of Borrego Springs on Pinyon Ridge and Yaqui Ridge, Engel and Schultejann (1984) and Schultejann (1984) identified a family of northeast-dipping detachment faults (Fig. 8). The faults are terraced surfaces with pervasively lineated blastomylonites to ultramylonites and refoliated gneisses along their contacts with underlying orthogneiss or mylonitic granodiorite of the SRMB. On the north flank of Yaqui Ridge, the Yaqui Ridge detachment fault dips 10°-40° to the northeast and separates a lower core of mylonitic

granodiorite of the SRMB from an unconsolidated, unmetamorphosed megabreccia of Miocene(?) age (Schultejann, 1984). The fault surface is smooth and planar with striations that indicate movement subparallel to the northeast dip direction of the fault. Directly below the fault surface is a band of intensely sheared cataclasite, which is in turn underlain by a zone of intense brecciation and chloritization. Schultejann (1984) attributed these features to a "mid-Cenozoic low temperature episode of ENE-WSW extension and detachment faulting accompanied by lower greenschist facies metamorphism and brittle deformation." Simpson (1985a), in comment of the studies by Engel and Schultejann (1984) and Schultejann (1984), noted that some of the structures they described along the low-angle faults in the Borrego Springs area are indicative of ductile deformation and, therefore, are not entirely brittle.

Along with the observations of structures along low-angle faults at Pinyon Ridge and Yaqui Ridge, Engel and Schultejann (1984) noted that many of the Late Cretaceous, west-vergent folds in the Borrego Springs area, at Coyote Mountain, and in the southern Santa Rosa Mountains, have been detached from their substrates and transported eastward. This eastward "backsliding" produced secondary drag folds and related shear zones. They considered these down-to-the east structures as forming contemporaneously with the Miocene(?) detachment faults at Pinyon Ridge and Yaqui Ridge.

Todd et al. (1988) proposed that mylonitization and low-angle faulting along the SRMB in the Palm Springs area were part of a single protracted episode of deformation. They argued that this period of deformation occurred between 97 and 62 Ma. They further proposed that some low-angle faults were reactivated during Miocene(?) time, based on the study of the Yaqui Ridge detachment fault by Schultejann (1984).

The notion of kinematic linkage between mylonitization and low-angle faulting, as well as later reactivation of the low-angle faults is likely, but based on the current

fission-track andU-Pb thermochronometry from the study area mylonitization occurred between ~99 and 92 Ma and involved initial west-vergent thrusting followed soon thereafter by major extension. This contention is based on the following observations. Concordant sphene and zircon fission-track ages from this study indicate that the plutonic rocks of the San Jacinto Mountains had cooled to less than ~235°C by ~92 Ma. Because these rocks lie in the footwall of the SRMB, the overlying mylonite belt must have been below ~235°C by this time. Temperatures of >300°C are needed for the crystal-plastic deformation of quartz (Sibson, 1977). Therefore, mylonitization had to have occurred before ~92 Ma. The mylonite belt must be younger than the oldest rock deformed along the SRMB; the oldest known rock in the San Jacinto Mountains is 99 Ma (U-Pb zircon age, Hill et al., 1986).

Based on the microstructural evidence and larger structures, mylonitization (at ~99 and 92 Ma) involved both west-vergent thrusting and extension. It is our thesis that the former preceded, and was responsible for, the latter. In a manner described by Dewey (1988), and which has been documented in the Himalayas (England and Houseman, 1988), west-vergent thrusting thickened the lithosphere, which in turn experienced extensional orogenic collapse. Geobarometry data from the SRMB at Coyote Mountain and to the west of Borrego Springs indicate that the crust was thickened by ~10 to 18 km (revised from George et al., 1991). This is based on amphibole core to rim increases from 1.6 to 3.2 f.u. in Al_{total} from deformed plutonic rocks in the mylonite belt (Fig. 8; samples RA-26-E and RA-55-B of Anderson, 1983). When employing the Al-in-hornblende geobarometer of Schmidt (1992), these data indicate an ~3-5 kb increase in pressure during mylonitization (see chapter 3 for an evaluation of these data). West-vergent thrusting was probably over by ~94 Ma, based on minor comparable compositional zoning of Al_{total} in amphiboles from the 94-93 Ma footwall tonalites in the San Jacinto Mountains (George et al., 1991).

Compositional data from plagioclase, as well as from amphibole, in the sample from Coyote Mountain (RA-26-E) were used as inputs for the amphibole-plagioclase geothermometer of Blundy and Holland (1990). The results indicate that rim temperatures, which represent conditions during mylonitization, are only slightly higher than those based on core compositions, and generally the difference is less than the ± 75°C uncertainty of the geothermometer (see chapter 3 for a more complete description of the geothermometry results). Estimated rim temperatures range from ~740°-820°C, and temperatures during crystallization of the core are from 720°-800°C. These data are consonant with the notion of west-vergent thrusting that was soon followed, and may have been accompanied in part, by extensional collapse of the overthickened crustal welt. Extension resulted in tectonic denudation and exhumation of the mylonite belt, which explains why rim temperatures are not higher.

Tectonic denudation and exhumation of batholithic rocks in the eastern Peninsular Ranges through extension along the SRMB provides an explanation for major cooling of the tonalitic plutons of the San Jacinto Mountains. As discussed in *Results*, these rocks cooled some 500° to 530°C in less than ~1 to 2 m.y. (i.e. between 94-93 Ma and ~92 Ma) during ~10-14.5 km of post-emplacement exhumation.

There is abundant structural evidence in the San Jacinto Mountains that the rapid cooling of the tonalitic plutons took place as they intruded into an active, synextensional shear zone. The overall dimensions of the three major tonalitic plutons indicate they are tabular in form (Hill, 1984). The oldest pluton is an elongate body with dimensions of 40 by 8 km, and the next oldest is an irregular mass 25 km long and 3 km wide. The dimensions of these igneous bodies, characterized by large length to width ratios, would be expected in an area where semi-lithified magmas intruded into an active shear zone and were subsequently extended along a fault. Also, internal and external foliations in the plutons are parallel or subparallel with contacts with metasedimentary and/or igneous

wall rocks (Hill, 1988). Hill (1988) interpreted the internal structures, which include banding, schlieren, and mafic inclusion trains, as the product of magmatic flow within the plutons. He described the external foliations as forming during emplacement of the plutons. Both sets of structures are consistent with the emplacement of tonalitic magmas into an actively extending shear zone. Similar observations in other parts of the mylonite belt support the notion that shearing along the SRMB was accompanied by the emplacement of Late Cretaceous plutonic rocks (Anderson, 1983; Matti et al., 1983).

Figure 9 illustrates a proposed sequence of geologic events that led to the development of the mylonite belt. These events include: (1) regional west-vergent thrusting and mylonitization between ~99 and 94 Ma. This resulted in thickening of the continental crust beneath the eastern Peninsular Ranges by ~10-18 km; (2) major crustal extension at ~94-92 Ma. The SRMB served as an extensional detachment fault that facilitated extension; (3) voluminous synextensional intrusion of tonalite beneath the active mylonite belt at depths of ~15-19 km followed by ~10-14.5 km of exhumation, and accompanied by rapid cooling from crystallization temperatures (730°-760°C) to below ~235°C in 1 to 2 m.y.; (4) a second interval of major cooling and unroofing at ~76 Ma (to be discussed in the following section); (5) a third interval of major cooling and unroofing at ~62 Ma (based on concordant fission-track ages from the northern Santa Rosa Mountains, see Dokka, 1984); and (6) brittle normal faulting during mid-Tertiary time. It is also possible that events (1) and (2) overlapped in time, i.e. extension within an actively thickening contractional belt. For example, such relations have been proposed for the Himalayan Mountains (Burchfiel and Royden, 1985).

Other portions of the Peninsular Ranges batholith experienced tectonic events similar to those that affected the SRMB. These include the Cuyamaca-Laguna Mountains shear zone (CLMSZ) and the La Posta pluton, both located ~130 km south to southeast of the SRMB. Evidence for east-over-west sense of movement along the CLMSZ has been

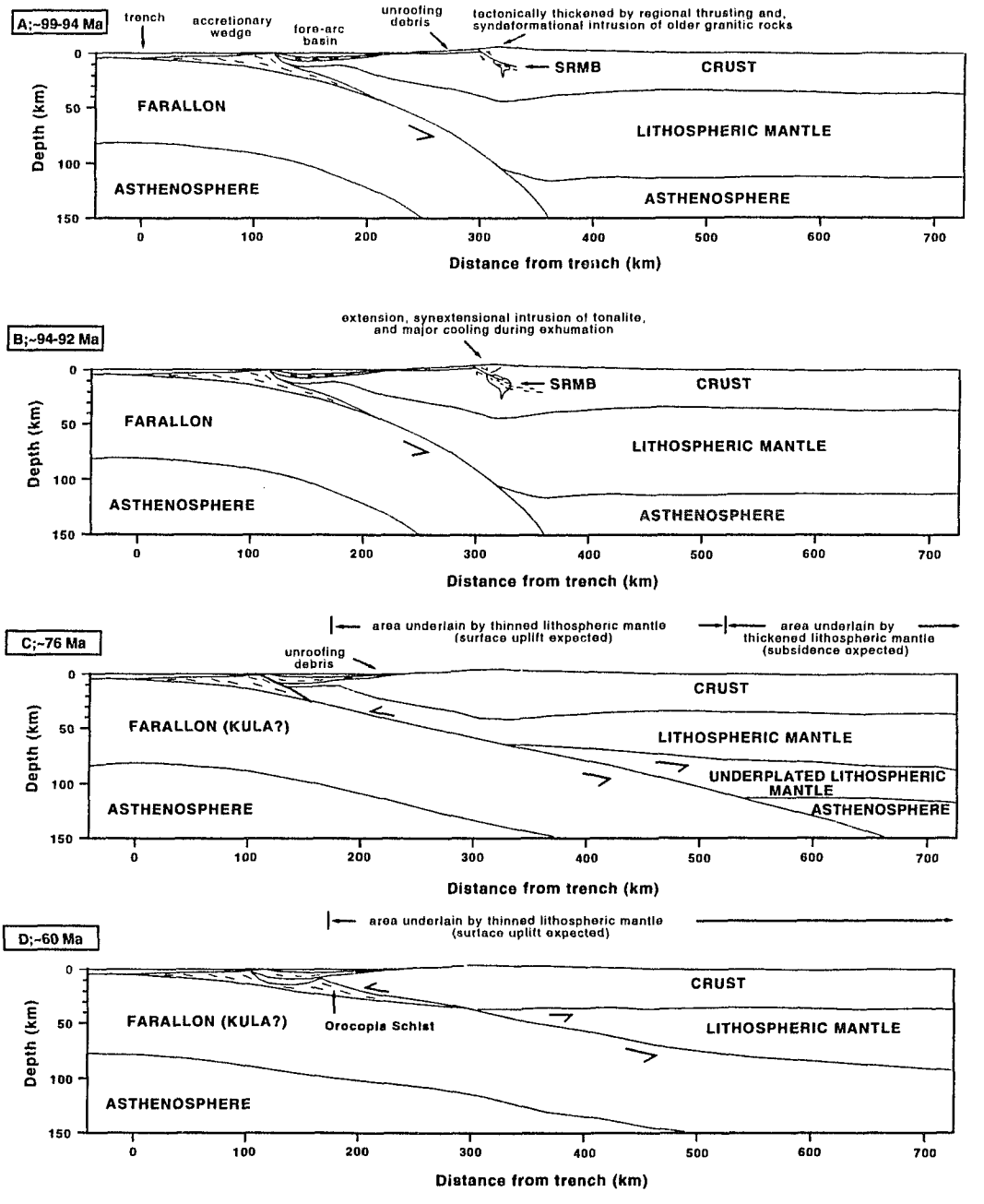

Figure 9. Plate tectonic history of the northern Peninsular Ranges with emphasis on the development of the Santa Rosa mylonite belt (SRMB); a) Regional west-vergent thrusting and mylonitization between ~99 and 94 Ma. b) Major extension and synextensional intrusion of voluminous tonalite between ~94-92 Ma (the tonalites are exhumed from depths of 15-26 km and rapidly cool from crystallization temperatures to below ~235°C). c) Tectonic erosion of the North American lithospheric mantle during low-angle subduction led to surface uplift, erosion, and cooling in the eastern Peninsular Ranges beginning at ~76 Ma. d) Continued low-angle subduction and erosion of the lithospheric mantle results in further surface uplift and cooling, as occurred in the Santa Rosa Mountains at ~62 Ma (Dokka, 1984).

reported by Todd et al. (1988), Grove (1986), and Clinkenbeard (1987). Leeson (1989) and Leeson et al. (1989) also presented mesoscopic and microscopic structural data from an S-C mylonite within the shear zone that indicate a down-to-the-east sense of movement. The occurrence of both east-over-west and down-to-the-east sense of shear along the CLMSZ is similar to that found in the SRMB, and can be interpreted as indicating west-vergent thrusting followed by extension. East of the CLMSZ, in an upper-plate position, are tonalites and granodiorites of the La Posta pluton. The La Posta pluton is similar in lithology, geochemistry, and age to the tonalitic plutons of the San Jacinto Mountains (Hill, 1984; Hill et al., 1986; Walawender et al., 1990). U-Pb ages on multiple zircon fractions from three different samples from the pluton are 94 ± 2 Ma (Walawender et al., 1990). Walawender et al. (1991) speculate that this voluminous pluton (~1400 km^2) was emplaced into a synbatholithic extensional zone (i.e. the CLMSZ). Timing of deformation along the shear zone is presently constrained to between 118 Ma and 94 ± 2 Ma (Todd and Shaw, 1979; Leeson, 1989; Walawender et al., 1991). The CLMSZ may be a southern extension to the SRMB. After removing 30 km of dextral slip (Sage, 1973) along the Elsinore fault and 24 km of dextral slip along the San Jacinto fault (Sharp, 1967), the SRMB and the CLMSZ line up north to south (see chapter 3). Based on this and the similar geology of the two shear zones, it seems probable that both are part of one shear zone active at approximately the same time.

The eastern Peninsular Ranges mylonite zone begins in the San Jacinto Mountains and may extend as far south as Baja California Sur (Sharp, 1979). It includes the SRMB, and possibly the CLMSZ of Todd et al. (1988). It may also extend northward into the Transverse Ranges, as part of a much larger mylonite belt. May (1989) presented a palinspastic restoration of the San Andreas and older fault systems, and reconstructed the distribution of basement terranes in southern California. After reconstruction, Late Cretaceous age mylonite zones, including the SRMB, form a

discontinuous belt extending ~northwest-southeast from the Transverse Ranges into the eastern Peninsular Ranges. Deformation in all of these mylonites, including the Santa Rosa mylonite belt, occurred under similar conditions and produced similar structures (May, 1989). Ductile deformation generally occurred under upper greenschist to amphibolite facies conditions, although commonly there is evidence for late-stage brittle deformation. Mylonitization was coeval with emplacement of upper Cretaceous granitic rocks, and locally post-dates intrusion. After the removal of net rotations of fault-bounded blocks in the Transverse Ranges, based on studies of Luyendyk et al. (1980) and Hornafius et al. (1986), foliations and lineations from the various mylonites indicate west-vergent thrusting in directions from 270° to 235° (May, 1989, the latter value is from the Santa Rosa mylonite belt). In the Cucamonga region and in the Limerock Complex both located in the San Gabriel Mountains to the north of the study area, mylonitization occurred within major sinestral transcurrent shear zones along directions from 260° to 250° (May and Walker, 1989). These transcurrent fault systems have been interpreted as left-lateral tear faults that offset the major ductile thrusts in the Transverse Ranges from those in the eastern Peninsular Ranges (May, 1989; May and Walker, 1989). Therefore, west-vergent thrusting and subsequent extension, as seen in the SRMB, may represent a larger Cordillera-wide tectonic event, which is consistent with the hypothesis proposed by Coney and Harms (1984) that in Late Cretaceous time western North America was the site of an unstable crustal welt that subsequently collapsed through major extension.

Mechanisms for Rapid Cooling of the San Jacinto Mountains at ~76 Ma

The range of geological mechanisms that could have resulted in the abrupt cooling of the San Jacinto Mountains at ~76 Ma includes: (1) tectonic denudation by extensional faulting; (2) cooling of the North American plate due to the subduction of a cold Farallon (or Kula) plate; and (3) erosion in response to surface uplift. Rapid cooling at ~76 Ma,

unlike at ~92 Ma, did not likely occur as a consequence of tectonic denudation associated with extensional faulting. Sphene and zircon fission-track ages indicate that temperatures dropped below those required for mylonitization by that time. Cooling due to refrigeration caused by a subducted, cold oceanic plate is also discounted because it should have resulted in similar cooling of rocks lying structurally below the rocks of the San Jacinto Mountains; similar or somewhat older fission-track ages would also be expected for underlying rocks and from rocks of the SRMB due to their proximity to the cold plate. Geological evidence is consistent, however, with the notion that cooling occurred as the result of erosion associated with regional surface uplift. The occurrence of regional unconformities throughout northern Baja California and southern California (Gastil, 1961; Minch, 1979) supports our contention that the Peninsular Ranges was the site of major surface uplift and erosion during Late Cretaceous time. These unconformities are erosional surfaces cut into the granitic and metamorphic rocks of the Cretaceous Peninsular Ranges batholith. The age of the surfaces is not precisely known, although they are thought to have been initiated in late Mesozoic time and were probably well-established by 70 Ma (Minch, 1979). It is likely that the surface uplift that led to the development of the regional erosion surfaces is also responsible for the major cooling of rocks of the San Jacinto Mountains at ~76 Ma.

Regional uplift and erosion, and resultant cooling, at ~76 Ma is also supported by recent geochronologic studies elsewhere in the northern Peninsular Ranges. Concordant zircon and apatite fission-track ages, and apatite track-length distributions in the vicinity of Palomar Mountain indicate major cooling in the western Peninsular Ranges at ~77 Ma (George and Dokka, 1992; chapter 4). To the south of the study area, near the Cuyamaca-Laguna Mountains, plutonic rocks from the batholith have $^{40}Ar/^{39}Ar$ ages for K-feldspar of between 72 and 78 Ma (Grove and Harrison, 1992). The blocking

temperature of K-feldspar for $^{40}Ar/^{39}Ar$ dating is comparable to the fission-track closure temperatures of zircon and apatite (McDougall and Harrison, 1988).

Northern Peninsular Ranges Paleogeography and Stratigraphy

Major west-vergent thrusting between ~99 and 94 Ma in the eastern Peninsular Ranges should have created considerable topographic relief and resulted in high rates of erosion of the batholith and its volcanic cover. There is stratigraphic evidence for major erosion of the Peninsular Ranges at about this time. Peterson and Nordstrom (1970) and Minch (1979) described the transport of coarse unroofing debris from the ancestral Peninsular Ranges to the west along narrow channels cut into a surface of rugged topography. The debris was deposited by fluvial and debris flow processes as alluvial fans in a semi-arid climate forming along the edge of the Late Cretaceous forearc basin (Peterson and Nordstrom, 1970). The alluvial fan deposits, designated the Lusardi Formation by Nordstrom (1970), contain a mixture of plutonic, metamorphic, and volcanic clast types typical of the Peninsular Ranges to the east (Fig. 10; Nilsen and Abbott, 1981). The age of the Lusardi Formation is tentatively constrained between 105 Ma and a Turonian age (91-88.5 Ma; Nordstrom, 1970). It unconformably overlies Late Jurassic to Early Cretaceous metavolcanic rocks of the Santiago Peak Volcanics and Early Cretaceous batholithic rocks (~140-105 Ma; Silver and Chappell, 1988). The contact has over 460 m of relief (Nordstrom, 1970). The lower part of the Point Loma Formation of Campanian age overlies the Lusardi Formation along a possible unconformity (Nilsen and Abbott, 1981). Nordstrom (1970) stated that the Lusardi Formation may be stratigraphically equivalent to a thick terrestrial boulder conglomerate that lies conformably below Turonian age marine strata of the Trabuco Formation (Popenoe, 1941) from the Santa Ana Mountains.

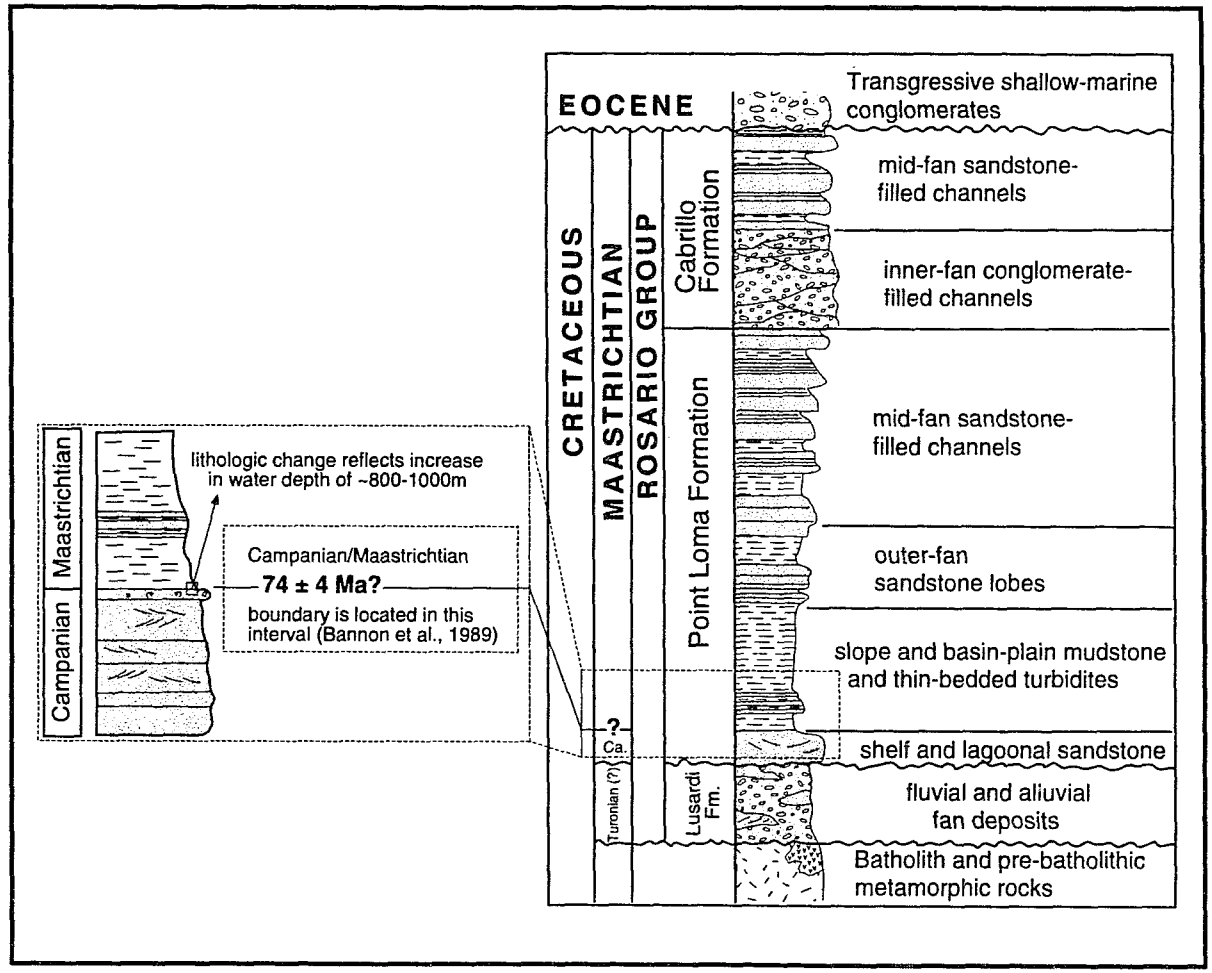

Figure 10. Stratigraphic column of the Point Loma and overlying and underlying formations from the San Diego area (from Nilsen and Abbott, 1981 and Bannon et al., 1989). At the Campanian-Maastrichtian boundary there is lithologic and paleontologic evidence for a large increase in water depth and a major reorganization of marine facies. A transition from shelf to slope or basin plain deposition coincided with surface uplift in the central and eastern Peninsular Ranges.

Surface uplift at ~76 Ma and subsequent cutting of regional unconformities also produced a large amount of unroofing debris that was then shed west to the adjacent forearc basin. This debris was transported ~50-100 km to the southwest and deposited in the San Diego area as the shelf and deep marine fan deposits of the Point Loma Formation (Nilsen and Abbott, 1981; Girty, 1987). At the Campanian-Maastrichtian boundary a major change in lithology from shallow-marine sandstone to deep-water shale occurs in the basin (Fig. 10; Nilsen and Abbott, 1981; Bannon et al., 1989). The faunal record, including macro-fossils (Sundberg, 1979) and foraminifers (Sliter, 1979), implies a change in water depth from "shallow" to depths of 900-1000 m. Deep-water shale, interpreted as slope or basin-plain deposits, are overlain by a progradational sequence of outer, middle, and inner-fan sandstone and conglomerate (Nilsen and Abbott, 1981). It is probable that the large increase in water depth and the transition from shelf to slope or basin plain deposition were primarily the result of tectonic causes and not to eustasy. The eustatic sea level curve for the Maastrichtian, according to Haq et al. (1987), includes only short-term rises and falls of <50 m, and a long-term fall of ~40 m. Thus, major reorganization of marine facies ~100 km to the west at the Campanian-Maastrichtian boundary (74.4 ± 4.0 Ma) was coincident with abrupt cooling in the eastern Peninsular Ranges. Subsequent to this reorganization, erosion of the ancestral San Jacinto Mountains during the Maastrichtian resulted in progradation of the Late Cretaceous fan system as seen higher in the section in the Point Loma Formation. Sediments shed from the Peninsular Ranges during the younger ~62 Ma period of cooling and unroofing (Dokka, 1984) have not been found in the region. Paleocene strata are generally missing throughout southern and Baja California (Nilsen and McKee, 1979), as would be expected in a region undergoing major uplift (Dokka, 1984). The sediments may have been deposited farther west into the forearc basin and later transported to the north along faults of the San Andreas transform system. Bartling

and Abbott (1984) described such northward translation of Upper Cretaceous and Eocene strata from the San Diego area to their present exposure on San Miguel Island.

Following a Paleocene hiatus, deposition of alluvial fan conglomerates (Poway Conglomerates) and coarse marine turbidites occurred during the Eocene in the forearc basin to the west. The source area for the distinctive Poway Conglomerates is in Sonora which was located just to the east of the ancestral eastern Peninsular Ranges during the Eocene (Merriam, 1979; Minch, 1979; Abbott and Smith, 1978, 1989). This implies that the eastern ancestral Peninsular Ranges had been breached by west flowing streams by this time and that uplift in the study area had ceased. The present offset of the Sonoran source area from the southern California conglomerates is the result of right-slip along the San Andreas fault and the opening of the Gulf of California (e.g., Merriam, 1979).

Plate Tectonics and the Laramide Orogeny

The Laramide orogeny resulted in major mountain-building along a belt extending from Montana to Arizona and New Mexico during latest Cretaceous, Paleocene, and Eocene time (80-40 Ma; Armstrong, 1968; Coney, 1972, 1976; Tweto, 1975; Hamilton, 1988, 1989). Deformation during Laramide time was characterized by fault-bounded, basement-cored uplifts separated by intervening basins in which synorogenic sediment accumulated (Coney, 1972; 1976; Dickinson and Snyder, 1978; Dickinson et al., 1988).

Most current models relate Laramide tectonism to the low-angle subduction of the Farallon (or Kula) plate beneath North America (Coney, 1976; Cross and Pilger, 1978; Dickinson and Snyder, 1978; Bird, 1984, 1988; Engebretson et al., 1985; Hamilton, 1988, 1989). Plate reconstructions using global hot spots indicate that low-angle subduction was initiated along the west coast at ~74 Ma (Engebretson et al., 1985); it should be pointed out that the timing quoted by Engebretson et al. (1985) of initiation of low-angle subduction does not reflect the uncertainties involved in their plate

reconstructions. Although beyond the scope of this study, these uncertainties are likely to be several million years (Stock and Molnar, 1988). Models by Bird (1984, 1988) and Hamilton (1988, 1989) predict significant tectonic erosion of the leading edge and base of the North American plate in association with low-angle subduction. Implicit in these models is that tectonically induced changes in the density distribution of the North American plate should have resulted in isostatic rise of the crust and surface uplift. Thus, a testable feature of these models centers on whether areas along the western edge of North America were the site of Late Cretaceous regional uplift. The San Jacinto Mountains were located along the continental margin adjacent to Sonora during Cretaceous time (Gastil, 1985) and is, therefore, an appropriate area with which to test the models.

The factors that give rise to low-angle subduction of the lithosphere have been evaluated by Cross and Pilger (1982). They concluded that such a geometry can be the result of an increase in the convergence rate between interacting plates, an increase in the absolute velocity of the overriding plate towards the trench, or the subduction of low-density lithosphere. Although satisfactorily argued for areas well north of the study area (Livaccari et al., 1981; Henderson et al., 1984), subduction of low-density lithosphere can be discounted here because of lack of evidence. In contrast, the plate tectonic record indicates that combinations of the other factors were operative. Engebretson et al. (1985) showed in their analysis of the displacement history of the North American plate relative to hotspots that the motion normal to and towards the trench along its western edge was more rapid during the Laramide orogeny. Their reconstruction also indicates that a steep rise in the convergence rate between the two plates occurred at ~74 Ma (Fig. 11). Data presented by Debiche et al. (1987) also show a major change in the direction of Farallon plate motion at approximately the same time (i.e. at 75 Ma; Fig. 12). Thus,

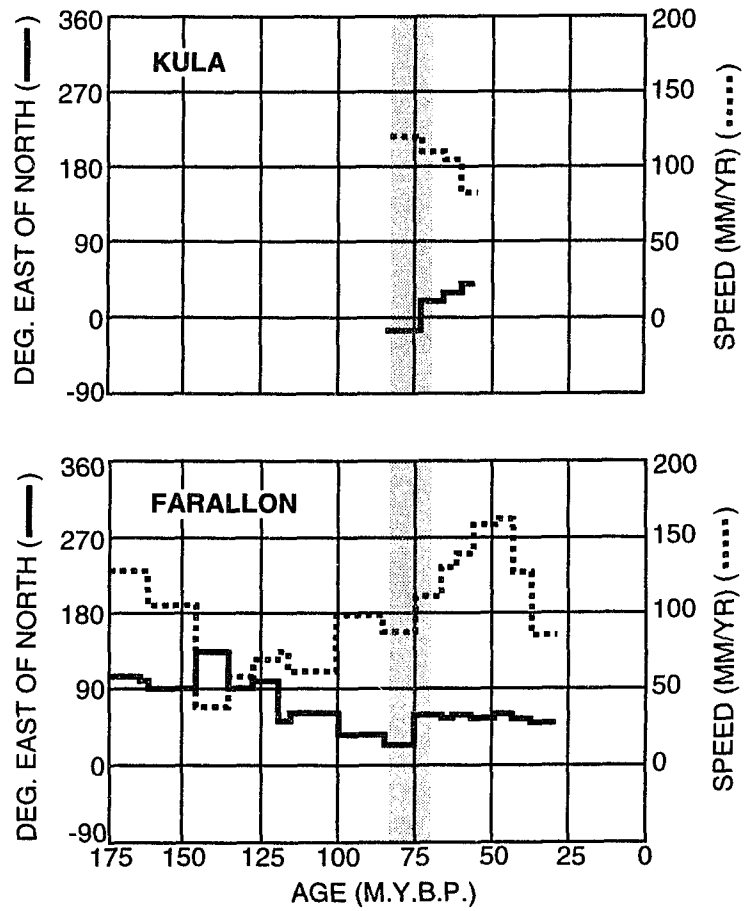

Figure 11. Azimuth and speed of linear velocities of the Farallon and Kula plates relative to North America at Baja, California (site coordinates of Lat. 26°, Long. 248°; from Engebretson et al., 1985). Shaded area represents the overlap of concordant apatite fission-track ages (at 2 sigma) reported here from the San Jacinto Mountains.

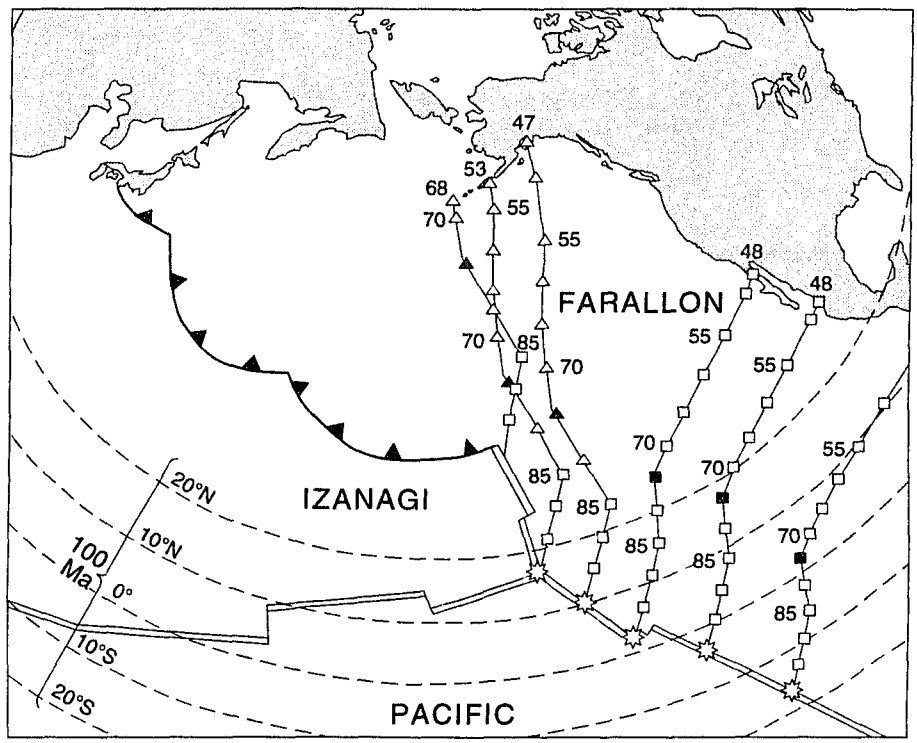

Figure 12. Forward-modeled trajectories for 100 m.y. old Farallon crust forming at the Farallon-Pacific ridge (heavy line). Numbers at the ends of the trajectories are arrival times. Note the change in direction of plate motion at ~75 Ma (75 Ma symbols have been darkened; from Debiche et al., 1987).

low-angle subduction followed by surface uplift along the North American plate margin likely began at this time.

The quantitative mechanical model of Bird (1988) and geological model of Hamilton (1988) provide a useful conceptual framework with which to assess the geodynamic effects of low-angle subduction on the North American plate in Late Cretaceous-Early Tertiary time. An important feature predicted by both models is the decoupling and removal (i.e. *tectonic erosion*) of the lithospheric mantle in response to low-angle subduction-induced shear. Such tectonic erosion was probably a major cause of the surface uplift and cooling observed in the San Jacinto Mountains at ~76 Ma (Fig. 9).

Bird (1988) created a finite-element model for Laramide deformation of the North American plate involving northeast directed shear produced by the shallow subduction of the Farallon (or Kula) plate. The model successfully accounts for the location, orientation, and magnitude of regional Laramide and later surface strains. The model also predicts that the North American lithospheric mantle was detached from the overlying continental crust and then transported northeast in response to the low-angle subduction-induced shear. Tectonic erosion of the lithospheric mantle is thought to have taken place along a weak zone in the lower crust without disrupting the overlying crust. The model predicts that all the lithospheric mantle beneath much of the region west of the Rocky Mountains was removed during the Laramide. Decoupled lower crustal rocks were then transported east and underplated to the North American plate (Bird, 1988; Hamilton, 1988). This resulted in a change in density distribution and contributed to the buoyancy of the North American plate. Eventually the oceanic Farallon (or Kula) plate came in direct contact with the bottom of North American crust.

Implicit in the removal of the lithospheric mantle beneath western North America is the reconfiguration of the density distribution of the plate. Bird (1979) modeled the regional geologic and geophysical effects of vertical separation or "*delamination* " of the

lithospheric mantle from the continental crust and predicted the amplitude of such effects. Bird calculated maximum surface uplifts of 1.30 km and 1.05 km for a 120 km thick plate given crustal thicknesses of 30 km and 40 km, respectively. These results are considered grossly applicable to Late Cretaceous southern California because of the similarities of crustal and mantle dimensions (Hamilton, 1988, 1989). A conservative value of 1 km of surface uplift caused by the removal of the lithospheric mantle seems an appropriate estimate for the case considered here. Furthermore, geodynamic modeling by Nunn (1990) indicates that the inevitable erosion of a topographic uplift also results in substantial additional *uplift of rocks* as a consequence of isostatic rebound. "Uplift of rocks," as defined by England and Molnar (1990), is the displacement of rocks with respect to the geoid (i.e. the absolute upward movement of a point within the earth). Studies by Nunn (1990) of the Sabine uplift of Louisiana indicate that such isostatic rebound amplifies by ~2 to 3 times an original increment of surface uplift. By applying this concept to Late Cretaceous southern California, ~1 km of surface uplift should result in ~2-3 km of uplift of rocks within the lithosphere. The amount of uplift of rocks predicted by geodynamic models does not, however, account for all of the exhumation indicated by the apatite fission-track data from the study area (i.e., uplift of rocks = surface uplift + exhumation). The amount of exhumation of a 2.3 km rock column located below the 130°C isotherm prior to 76 Ma is 3.8 km and 5.3 km, using geothermal gradients of 40°C and 20°C, respectively. These boundingvalues for the geothermal gradients seem appropriate given that the area was the site of fairly recent continental arc magmatism (~17 m.y. prior to cooling). To account for this additional uplift of rocks another feature of the models of Bird (1988) and Hamilton (1988) is called upon. Both models involve underplating of low density rocks, such as continental margin sediments and lower crustal rocks, beneath North America (Fig. 9). This underplating could have contributed to the buoyancy of the plate, and in

conjunction with tectonic erosion of the mantle lithosphere, explain the 3.8 km to 5.3 km of exhumation indicated by the apatite fission-track data.

The Bird (1988) model, when considered in the context of this study in the San Jacinto Mountains, predicts that as the Farallon (or Kula) plate moves eastward, additional surface uplift and cooling occurs. The geologic history, as well as the results of a fission-track study in Colorado by Bryant and Naeser (1980), provide simple tests of this hypothesis. The plate tectonic record indicates that the leading edge of the low-angle subducted slab would have migrated relatively northeast at a rate equal to the convergence rate (Fig. 13). Using the convergence rate of 110 mm/yr determined by Engebretson et al. (1985), the leading edge of the shallow subducted slab would have reached the classic Laramide terrane of central Colorado, a distance of ~1000 km after removing the effects of mid-Tertiary extension of the Basin and Range, at ~67 Ma. This model time corresponds to the age of deposition of the Laramie Formation, the primary evidence for the Laramide orogeny (~66.5 Ma) in its type area as documented by Tweto (1975). This corresponds closely to the time of marked cooling of basement rocks of the Front and Sawatch Ranges of central Colorado (Bryant and Naeser, 1980).

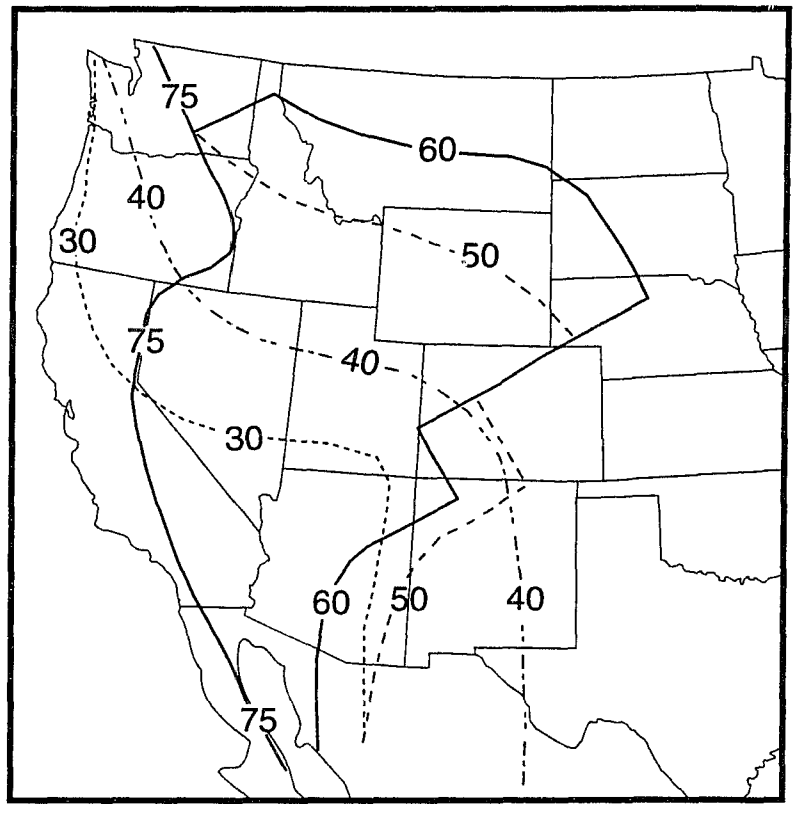

Figure 13: Geographic extent of areas underlain by a shallowly subducting Farallon-Kula plate at various times in the past (from Bird, 1988). Curves are labeled in millions of years before present. The map was constructed using the palinspastic base map of Hamilton (1978) and cooling ages of Cenozoic volcanic rocks from studies by Snyder et al. (1976) and Lipman (1980).

CONCLUSIONS

The following are conclusions reached during this thermochronologic study of the tonalitic basement rocks of the San Jacinto Mountains, California:

1. New fission-track data identify two intervals of Late Cretaceous rapid cooling, the first at ~92 Ma and the second at ~76 Ma. These data are important because they help clarify the nature of the Cretaceous Santa Rosa mylonite belt, the unroofing history of the Peninsular Ranges, and plate tectonic controls on the Laramide orogeny.

2. Concordant sphene and zircon fission-track dates and previously published U-Pb zircon ages from tonalites at all elevations indicate that the 2.5 km of exposed vertical section, and perhaps more, cooled from crystallization temperatures at 94-93 Ma to below 235°C at ~92 Ma. Such rapid cooling is attributed to exhumation during regional extension. Rocks of the San Jacinto Mountains sit in the footwall of the Santa Rosa mylonite belt, the major tectonic element of the ~92 Ma extension. Following their intrusion into the active extensional shear zone at a depth of ~15-19 km, the tonalite plutons underwent an additional ~10-14.5 km of exhumation along the Santa Rosa mylonite belt

3. Amphibole thermobarometry of mylonites and footwall rocks of the SRMB, previous U-Pb dating of footwall rocks in the San Jacinto Mountains, and deformational structures from the SRMB indicate that extensional faulting was preceded by west-vergent thrusting at ~99-94 Ma. This sequence of tectonic thickening followed by extension supports the concept of the construction of a crustal-scale unstable welt during the Sevier orogeny that subsequently collapsed by regional extension. Other areas with a similar Cretaceous history occur along a

regional shear zone that extends from the Transverse Ranges to the Cuyamaca-Laguna Mountains, located ~130 km to the south of the study area.

4. Fission-track ages and indistinguishable track-length distributions from apatite at all elevations indicate rapid cooling of the tonalites through the apatite partial annealing zone (~130°-70°C) at ~76 Ma. The occurrence of Late Cretaceous-age regional unconformities throughout Baja and southern California suggests that the cooling was the result of surface uplift and erosion. This surface uplift coincided with several important changes in the North American and Farallon (or Kula) plate motions. The surface uplift, erosion, and associated cooling of rocks of the eastern Peninsular Ranges was probably the consequence of tectonic erosion of the North American lithospheric mantle triggered by low-angle subduction. It is likely, therefore, that these phenomena represent the initial manifestations of the Laramide orogeny in North America.

CHAPTER 3

EVIDENCE OF REGIONAL LATE CRETACEOUS THRUSTING FOLLOWED BY EXTENSION IN THE EASTERN PENINSULAR RANGES OF SOUTHERN CALIFORNIA BASED ON AMPHIBOLE THERMOBAROMETRY

INTRODUCTION

There is abundant evidence of west-directed thrusting along north-south trending shear zones in the eastern Peninsular Ranges (Fig. 14; Sharp, 1979; Todd and Shaw, 1979; Engel and Schultejann, 1984; Simpson, 1984; Grove, 1986; Clinkenbeard, 1987; O'Brien et al., 1987; Todd et al., 1988). Deformational structures in the shear zones, however, also indicate a down-to-the-east sense of movement (Erskine and Wenk, 1985; Leeson, 1989; Leeson et al., 1989). Several contrasting tectonic models involving either thrusting or extensional faulting have been proposed based on these studies (Sharp, 1979; Engel and Schultejann, 1984; Simpson, 1984; Erskine and Wenk, 1985; Todd et al., 1988; Walawender et al., 1991). Using thermochronologic and preliminary thermobarometric data, George and Dokka (in review) and George et al. (1991) proposed a revised tectonic history that reconciles these divergent explanations for the development of the shear zones. These workers argued that fission-track ages from footwall rocks of the Santa Rosa mylonite belt and thermobarometry of amphiboles from plutonic rocks in and adjacent to the shear zone indicate a deformational history involving Late Cretaceous west-vergent thrusting followed closely by regional extension. This chapter presents the thermobarometry measurements reported in George and Dokka (in review) in greater detail. Integration of these data with existing information creates a test for the model of George and Dokka (in review), as well as providing insight into the relationship between large Cretaceous shear zones of southern California.

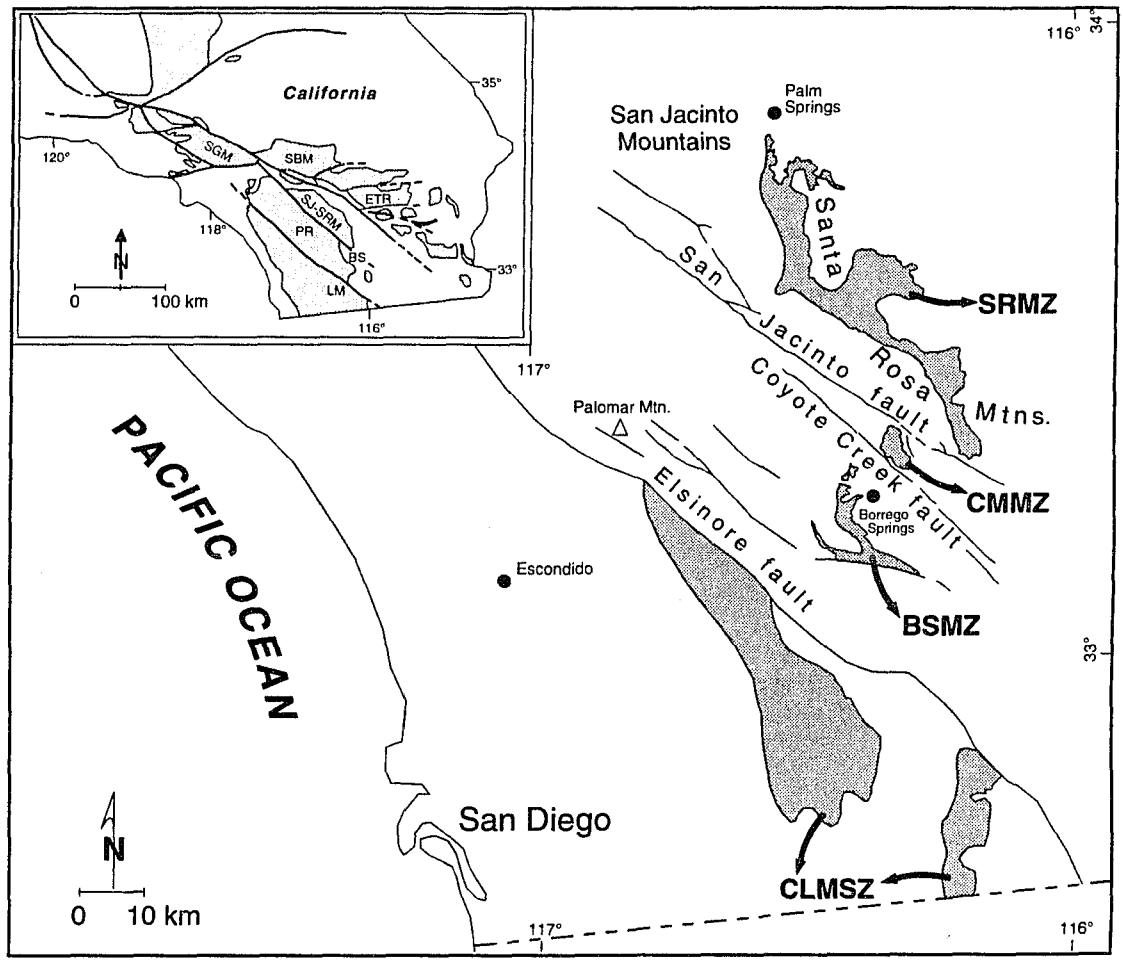

Figure 14. Map showing the distribution of major ductile shear zones of the eastern Peninsular Ranges (dark stipple). They include the Santa Rosa mylonite zone (SRMZ), the Coyote Mountain mylonite zone (CMMZ), the Borrego Springs mylonite zone (BSMZ), and the Cuyamaca-Laguna Mountains shear zone (CLMSZ). All but the latter are part of the Santa Rosa mylonite belt. Inset map shows the location of the figure with respect to crystalline terranes and Cenozoic faults of southern California. Abbreviations are as follows: SGM, San Gabriel Mountains; SBM, San Bernardino Mountains; ETR, eastern Transverse Ranges; PR, northern Peninsular Ranges; SJ-SRM, San Jacinto and Santa Rosa Mountains; and LM, Laguna Mountains. Modified from Sharp (1967), Simpson (1984), Todd et al. (1988), and May (1989).

GEOLOGY OF THE EASTERN PENINSULAR RANGES

The Santa Rosa mylonite belt lies within the leucotonalite belt of Gastil (1983), which encompasses the eastern half of the Peninsular Ranges batholith (Figs. 14 and 15). The belt is composed mainly of leucocratic tonalites and granodiorites containing <2.7 % K_2O, with <10% of the plutonic rocks being gabbro (Gastil, 1983; Silver and Chappell, 1988). Individual plutons are larger (up to 40 km in diameter) than those of the western half of the batholith, which are <10 km in exposed diameter (Gastil, 1983). They are generally undeformed, having been emplaced late (Todd and Shaw, 1979; Walawender et al., 1990). Walawender et al. (1990) consider these plutons petrographically and structurally distinct from those in the western part of the Peninsular Ranges, and have termed them "La Posta-type" for the voluminous La Posta pluton in the Laguna Mountains. La Posta type plutons comprise the majority of rock exposed in the highest mountain ranges of the batholith. Extending NNW-SSE from southern California into northern Baja California along the eastern side of the Peninsular Ranges, these include the large tonalitic plutons of the San Jacinto Mountains, the La Posta pluton in the Laguna Mountains, the Laguna Juárez pluton of the Sierra de Juárez, and the Sierra San Pedro Martir pluton in the mountains of the same name.

Initial U-Pb dating of zircons constrained the timing of emplacement of plutons in the eastern Peninsular Ranges to between ~105 and 80 Ma (Silver et al., 1979). Silver et al. (1979) proposed that during this period the Cretaceous magmatic arc migrated to the east. Additional age and isotopic data, as well as a reevaluation of previous U-Pb ages, has further constrained the timing of emplacement to between ~99 and 89 Ma (Silver, 1986; Walawender et al., 1990, 1991). Walawender et al. (1990,1991) also proposed that emplacement occurred along a static arc, as in the western half of the batholith between ~120 to 105 Ma. They further suggested that a shift in the axis of magmatism

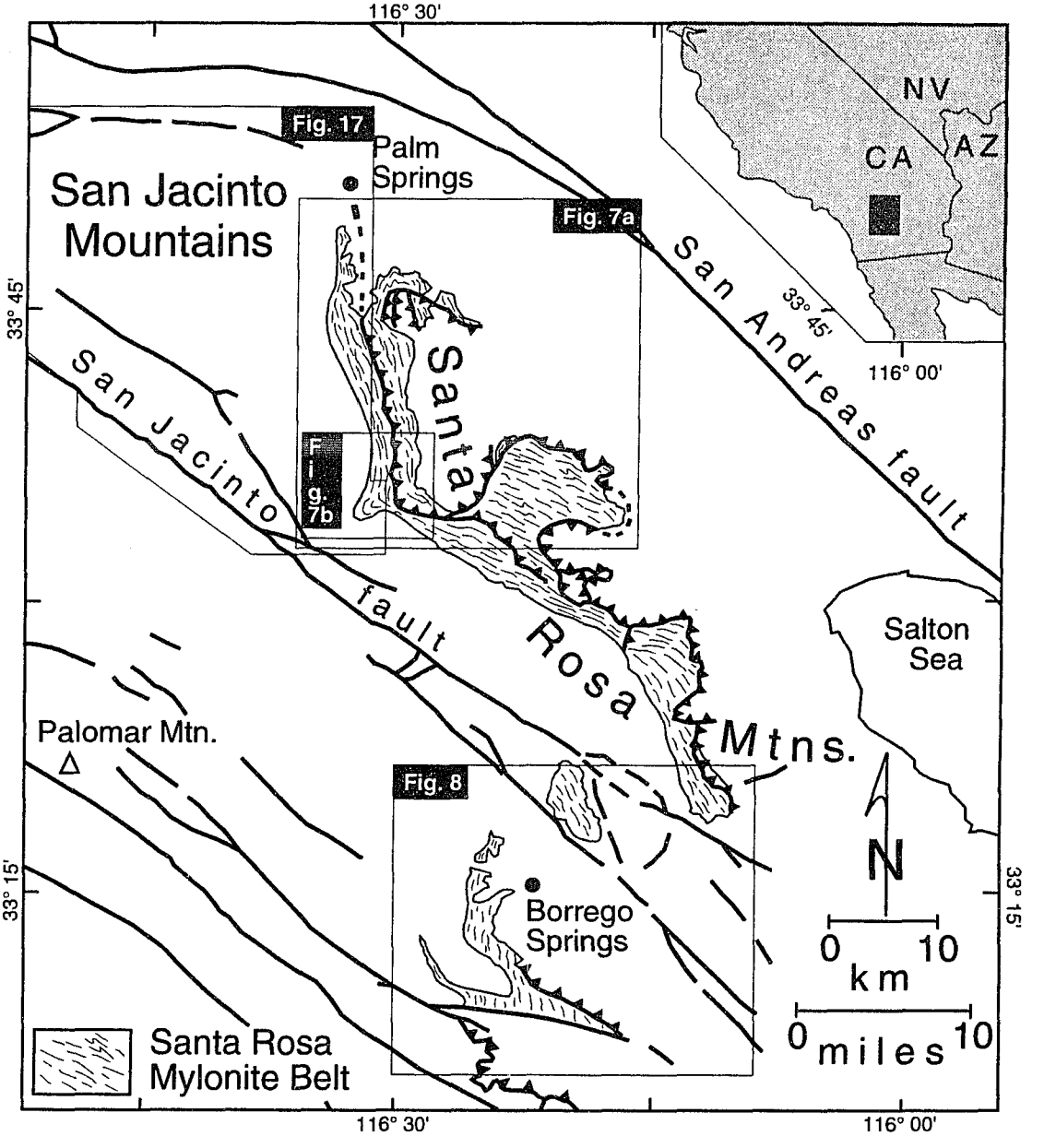

Figure 15. Map showing the location of the Santa Rosa mylonite belt, and areas covered in Figures 7, 8, and 17 (modified from Sharp, 1967 and Simpson, 1984).Inset map shows location of figure.

at or near 105 Ma took place as a result of a shallowing in the angle of subduction of the Farallon plate beneath North America.

The voluminous tonalitic and granodioritic plutons of the eastern Peninsular Ranges intruded into a miogeoclinal wedge of carbonate rocks and siliciclastic strata derived from the North American craton to the east (Gastil et al., 1975; Gastil and Miller, 1984; Gastil et al., 1986; Todd et al., 1988). These host rocks are generally Paleozoic in age, but may include some Mesozoic age sedimentary rocks (Todd et al., 1988). They were metamorphosed during intrusion to coarse schist, gneiss, and marble, and are presently exposed in screens and roof pendants surrounded by younger plutonic rocks. The majority of these rocks are included within a sillimanite-bearing amphibolite facies, which covers most of the eastern Peninsular Ranges (Todd et al., 1988).

The areas of interest to this study are the north-south trending shear zones near Palm Springs and Borrego Springs (Figs. 7, 8 and 15). Simpson (1984) grouped the shear zones between the two areas into the Santa Rosa mylonite belt, and divided the mylonite belt into the Santa Rosa mylonite zone (SRMZ), the Coyote Mountain mylonite zone (CMMZ), and the Borrego Springs mylonite zone (BSMZ). The Cuyamaca-Laguna Mountains shear zone to the south (Fig. 14) is not considered part of the eastern Peninsular Ranges mylonite zone (Todd et al., 1988), although it may be the southern continuation of the Santa Rosa mylonite belt.

The Santa Rosa mylonite belt extends a minimum of ~80 km to the south from the Palm Springs area, and has an estimated maximum thickness of ~8 km (Sharp, 1979). Tonalites and granodiorites of the Peninsular Ranges batholith, along with some prebatholithic metasedimentary rocks, are ductilely deformed along the mylonite belt (Theodore, 1970; Sharp, 1979; Dibblee, 1981; Anderson, 1983; Engel and Schultejann, 1984; Simpson, 1984; Erskine and Wenk, 1985; Erskine, 1986; O'Brien et al., 1987). Ductile deformation has produced a range of rock types including, mylonitic gneiss,

mylonite, phyllonite, and ultramylonite. These rocks display a well-defined foliation and stretching lineation (Sharp, 1979; Engel and Schultejann, 1984; Simpson, 1984; Erskine, 1986; O'Brien et al., 1987). The attitude of the foliation is regionally consistent, striking north-northwest and dipping 35-55° to the east-northeast. In any given local area the attitude of the lineation is uniform, although its trend changes from eastward in the southern part of the mylonite belt to ~N55°E in the San Jacinto Mountains and northern Santa Rosa Mountains (Todd et al., 1988). Deformational structures on both a microscopic and outcrop scale indicate east-over-west, but also down-to-the east sense of shear (Simpson, 1984; Erskine and Wenk, 1985; Erskine, 1986; O'Brien et al., 1987). Deformation took place under metamorphic conditions ranging from lower greenschist to upper amphibolite facies (Simpson, 1985b). Deeper structural levels are exposed in the SRMZ and CMMZ, where mylonites formed within the amphibolite to upper amphibolite facies. The western part of Coyote Mountain (i.e. CMMZ; Fig. 8) has been described as consisting of migmatitic gneisses (Theodore, 1970), and in the northern Santa Rosa Mountains (i.e. SRMZ; Fig. 7) Todd et al. (1988) observed common garnetiferous leucogranite anatexites in metasedimentary rocks and orthogneiss. In the BSMZ, deformation took place under predominantly upper greenschist facies pressures and temperatures. The timing of mylonitization in the SRMZ is presently constrained to between ~99 and 92 Ma, based on thermochronologic data from footwall rocks in the San Jacinto Mountains (George and Dokka, in review; chapter 2).

In the SRMZ at Palm Canyon between the southern end of the San Jacinto Mountains and the northern Santa Rosa Mountains, the contact between mylonites and plutonic footwall rocks dips 30-40° to the east (Fig. 7). Above, but not cutting the mylonite-footwall contact, are a number of imbricate low-angle faults that dip shallowly to the east (Erskine and Wenk, 1985; Erskine, 1986; Todd et al., 1988). The orientation

of these faults with respect to the mylonites has been interpreted as indicating kinematic linkage between low-angle faulting and mylonitization (Erskine and Wenk, 1985; Todd et al., 1988). It is not clear whether the faults are west-vergent thrusts, down-to-the-east normal faults, or have accommodated both during a history of reactivation (Todd et al., 1988). They do display brittle fault features reminiscent of Tertiary normal faults such has been described in the southern Santa Rosa Mountains by Wallace and English (1982). Imbricate low-angle faults, similar to those of the SRMZ, occur within and adjacent to the BSMZ to the south (Fig. 8; Engel and Schultejann, 1984; Schultejann, 1984). These faults also dip to the east and have brittle fault features, although there is some evidence of ductile deformation (Simpson, 1985a). They have been interpreted as forming during ENE-WSW extension and detachment faulting under greenschist facies conditions in Miocene(?) time (Schultejann, 1984).

The present positions of shear zones in the eastern Peninsular Ranges are the result of post-5.5 Ma right-lateral offsets along several faults of the San Andreas transform system. As will be presented later in the chapter, palinspastic reconstruction of the shear zones suggests they were part of a once-continuous, north-south trending, regional shear zone. Studies on metamorphic mineral assemblages from different parts of the mylonite belt (Theodore, 1970; Brown, 1981; Anderson, 1983; Simpson, 1985b; Erskine, 1986) also indicate differential vertical offsets between segments of the belt (i.e. between the SRMZ, CMMZ, and BSMZ). These offsets probably were the result of relatively recent (post-5.5 Ma) transpression and/or transtension between strike-slip faults of the San Andreas system, in a manner as described by Crowell (1974) and Christie-Blick and Biddle (1985).

METHODS

Thermobarometry

As discussed above, a primary purpose of this chapter is to test the hypothesis of major Late Cretaceous thrusting followed by regional extension. To accomplish this the Al-in-hornblende geobarometer is used to document any increases in pressure in pre- or syntectonic plutonic rock along the Santa Rosa mylonite belt resulting from thrusting. Relatively undeformed plutons that intruded the footwall rocks during extension have also been analyzed to determine their pressure histories.

The recent calibration by Schmidt (1992) of the Al-in-hornblende geobarometer originally proposed by Hammarstrom and Zen (1986) is employed here for calculating pressures. The geobarometer is based on the positive linear relationship between pressure and the aluminum content of hornblende in calc-alkaline granitoids buffered by the nine phase assemblage: quartz + plagioclase + K-feldspar + hornblende + biotite + titanite + Fe-Ti oxide + melt + fluid. Original calibrations were determined with pressures derived from metamorphic mineral assemblages in contact aureoles adjacent to calc-alkaline plutons (Hammarstrom and Zen, 1986; Hollister et al., 1987). These empirical calibrations are listed in Table 2 along with their respective uncertainties. The geobarometer was further calibrated by experimental studies (Johnson and Rutherford, 1989; Schmidt, 1992). Johnson and Rutherford (1989) performed reversed, f_{O_2}-buffered, vapor-present experiments over a range 2 to 8 kb at 740 -780°C on both volcanic and plutonic rocks using a mixed CO_2-H_2O fluid phase. Schmidt (1992) calibrated the geobarometer under water-saturated conditions at pressures of 2.5 to 13 kb and temperatures of 700-655°C.

Temperatures were calculated using the pressure-dependent geothermometer of Blundy and Holland (1990), which utilizes the tetrahedral aluminum content of calcic amphibole and the albite content of coexisting plagioclase (Table 2). It has a degree of

Table 2: Amphibole-Plagioclase Thermobarometry

Al-in-hornblende geobarometers;

$P (\pm 3 \text{ kb}) = -3.92 + 5.03\ Al_{total}$ $r^2 = 0.80$ (1)

$P (\pm 1 \text{ kb}) = -4.76 + 5.64\ Al_{total}$ $r^2 = 0.97$ (2)

$P (\pm 0.5 \text{ kb}) = -3.46 + 4.23\ Al_{total}$ $r^2 = 0.99$ (3)

$P (\pm 0.6 \text{ kb}) = -3.01 + 4.76\ Al_{total}$ $r^2 = 0.99$ (4)

amphibole-plagioclase geothermometer (Blundy and Holland, 1990);

$T = (0.677\ P - 48.98 + Y) / (-0.0429 - 0.008314 \ln K)$

Where $K = (Si - 4 / Si - 8)\ X_{Ab}$, Si is the number of atoms per formula unit in amphiboles, with P in kb and T in K; the term Y represents plagioclase nonideality. $Y = 0$ for $X_{Ab} > 0.5$ and $Y = -8.06 + 25.5(1 - X_{Ab})^2$ for $X_{Ab} < 0.5$.

(1) Hammarstrom and Zen (1986)
(2) Hollister et al. (1987)
(3) Johnson and Rutherford (1989)
(4) Schmidt (1992)

uncertainty of ± 75°C, and yields temperatures of equilibration of hornblende-plagioclase assemblages in the range of 500 to 1100°C. Its use is limited to rocks with plagioclase less calcic than An_{92}, amphibole with <7.8 Si atoms pfu, and the 500-1100°C temperature range (Blundy and Holland, 1990).

Analytical Procedures

Mineral analyses for samples PG 101, PG 102, PG 110, and PG 118 (Table 3) were done at Louisiana State University using a fully automated JOEL 733 electron microprobe. Minerals were imaged with back-scattered electrons (BSE) and quantitatively analyzed by wavelength-dispersion spectrometry (WDS). Analyses were obtained with an accelerating potential of 15 Kv and beam current of 10 nA. A beam size of 1-μm was used on the amphibole grains, but was defocused to a 10-μm spot for analysis of plagioclase to limit Na loss. Calibrations were accomplished using natural and synthetic silicate mineral standards, and the data were corrected on-line using the procedure of Bence and Albee (1968). Chemical formulas for amphibole were calculated assuming that cations sum to 13 (exclusive of Ca + Na + K + Ba), and Fe^{3+} was calculated by charge balance. Plagioclase compositions were normalized on the basis of 8 atoms of oxygen. Amphibole analyses of RA-26-E and RA-55-B from Anderson (1983) were recalculated based on the same normalization scheme.

RESULTS

Borrego Springs Area

The plutonic and metamorphic rocks of the BSMZ and CMMZ have been studied in terms of lithology, structure, and metamorphism (Theodore, 1970; Theodore and Sharp, 1975; Sharp, 1979; Christie and Ord, 1980; Anderson, 1983; Engel and Schultejann, 1984; Schultejann, 1984; Simpson, 1984, 1985b). Estimates of pressure and temperature conditions during mylonitization have been based on metamorphic mineral

Table 3: Location and Rock Type of Thermobarometry Samples from the San Jacinto Mountains, CA

Field #	Elev.(m)	Latitude	Longitude	7.5' Quadrangle	Rock Type
101	3293	33° 48' 53.2 "	116° 40' 42.2"	San Jacinto Peak	tonalite (1)
102	2365	33° 48' 07.0 "	116° 40' 52.6"	San Jacinto Peak	tonalite (1)
110	1353	33° 42' 18.8 "	116° 43' 50.3"	Idyllwild	tonalite (2)
118	811	33° 50' 10.6"	116° 36' 49.6"	Palm Springs	tonalite (3)

(1) youngest of three major, 94-93 Ma tonalitic plutons of San Jacinto Mountains (Hill, 1984)
(2) oldest of three major, 94-93 Ma tonalitic plutons of San Jacinto Mountains (Hill, 1984)
(3) ~99-94 Ma, early intrusive rocks of the San Jacinto Mountains (Hill et al., 1986)

assemblages (Theodore, 1970; Anderson, 1983) and the P-T requirements of the deformation mechanisms attributed to observed microstructures (Simpson, 1984, 1985b). Based on the stability field of sillimanite in association with K-feldspar + muscovite + quartz in samples from Coyote Mountains, Theodore (1970) estimated peak metamorphic conditions as upper amphibolite (~580-660°C and 3.4-7.0 kb) during mylonitization. Sillimanite is common in mylonites of the CMMZ, and occurs as either stout crystals with diamond-shaped cross sections or is fibrous and fine grained (Theodore, 1970). There is some textural evidence that suggests sillimanite was deformed during mylonitization, and the occurrence of fibrous crystals cutting across mylonitic foliation indicates that sillimanite continued to form after mylonitization. In the BSMZ Anderson (1983) suggested that metamorphic conditions ranged from andalusite-staurolite through sillimanite-muscovite grades, as defined for pelitic rocks. Based on the stability of muscovite + quartz in mylonitic rocks and a lack of evidence for remelting of granitic rocks, he estimated peak metamorphism at 650°C and 5 kb. On the basis of microstructural features in the BSMZ, Simpson (1985b) considered mylonitization as having occurred predominantly under upper greenschist facies conditions, with some local evidence of lowest greenschist to lowest amphibolite facies metamorphism. The complete absence of brittle deformation features in epidote-amphibolite and higher grade mylonites of the CMMZ, as well as the SRMZ, indicated to Simpson (1985b) that mylonitization took place in the 580-600°C range. In this section I present thermobarometry data based on microprobe analyses from Anderson (1983) of two samples from the mylonite zone. The results indicate maximum pressures and temperatures during mylonitization that exceed previous estimates.

Amphibole, biotite, and plagioclase in two samples from the Borrego Springs area were analyzed by Anderson (1983) using an electron microprobe. Sample RA-26-E is a strongly mylonitized diorite from the northeast side of Coyote Mountain (Fig. 8). Its

assemblage includes plagioclase, biotite, hornblende, quartz, apatite, epidote-allanite, ilmenite, sphene, and tourmaline. Sample RA-55-E is a mylonitic tonalite located just to the southwest of Borrego Springs in the BSMZ (Fig. 8). It has an assemblage of quartz, plagioclase, hornblende, epidote-allanite, sphene, alkali-feldspar, pyrite, and zircon. Amphibole in these samples consist of uniformly dark porphyroclast cores (pleochroic from brown to dark green) and discontinuous rims (pleochroic from green to blue-green). Representative amphibole analyses from both cores and rims are given in Table 4 (RA-55-B) and Table 5 (RA-26-E). Core compositions of RA-26-E are magnesio-hornblende, whereas the rims range from magnesio-hornblende to ferro-tschermakite (Fig. 16). RA-55-B has ferro-hornblende cores, and ferro-tschermakitic-hornblende rims. Plagioclase in RA-26-E occurs as two textural types with distinct compositions. Larger plagioclase grains (up to 2 mm in diameter) range in composition from An_{45}-An_{55}, and display angular patterns of zoned extinction that are typical of igneous plagioclase from the area. Smaller grains (0.1-0.2 mm) range in composition from An_{55}-An_{78}, and have zoned extinction but without the angular patterns. Biotite from the two samples also occurs as two distinct types. Biotite porphyroclasts, typically 0.5 to 2.0 mm in largest dimension, were partially reduced to aggregates of fine grained biotite, generally < 0.1 mm in largest diameter, and very fine-grained sphene or ilmenite. The fine-grained biotite is lower in TiO_2 and FeO than the larger porphyroclasts, and on average, slightly higher in MgO and Al_2O_3. Fine-grained biotite and plagioclase, and the discontinuous rims of amphibole formed during mylonitization in the BSMZ and CMMZ (Anderson, 1983). The larger grains of plagioclase, biotite, and amphibole are primary grains formed during initial crystallization of the plutonic rocks.

Pressure of crystallization for amphibole cores and rims are given in Table 6. They were determined using both the Al-in-hornblende geobarometer of Hollister et al. (1987)

Table 4: Representative Amphibole Analyses of RA-55-B from the Borrego Springs Mylonite Zone (Anderson,1983)

Sample No.	RA-55-B	RA-55-B	RA-55-B	RA-55-B	RA-55-B	RA-55-B	RA-55-B	RA-55-B
Analysis pt.	5201	5203	5203	5203	5201	5201	5203	5203
	9013	9012	9013	9018	9011	9015	9014	9015
Remarks	core	core	core	core	rim	rim	rim	rim
SiO_2	45.03	43.85	44.12	44.44	42.29	41.95	41.76	42.00
Al_2O_3	8.80	9.95	9.61	8.80	11.89	11.83	12.82	12.05
Cr_2O_3	0.03	0.02	0.01	0.03	0.03	0.02	0.05	0.02
Fe_2O_3 #	3.74	2.79	3.07	2.70	5.30	6.23	4.07	0.86
TiO_2	1.42	1.21	1.63	1.51	0.40	0.37	0.50	5.20
FeO	15.80	17.36	16.90	16.83	15.49	14.71	17.12	16.15
MnO	0.57	0.52	0.55	0.56	0.45	0.49	0.45	0.50
MgO	9.17	8.46	8.54	8.82	7.77	7.71	7.13	7.45
CaO	11.46	11.92	11.55	11.61	11.48	11.18	11.85	11.57
K_2O	0.93	1.08	1.07	0.88	0.93	1.00	1.09	1.13
Na_2O	1.13	1.18	1.21	1.17	1.34	1.32	1.31	1.22
F	0.06	0.008	0.09	0.08	0.08	0.07	0.05	0.07
Cl	0.02	0.01	0.03	0.04	0.00	0.01	0.01	0.02
Total	98.15	98.43	98.38	97.47	97.45	96.88	98.21	98.24
O=F,Cl	0.03	0.04	0.04	0.04	0.03	0.03	0.02	0.03
TOTAL	98.12	98.39	98.33	97.43	97.42	96.85	98.18	
	- - - Atomic proportions based on 13 cations (except Ca+Na+K+Ba) - - -							
Si	6.754	6.615	6.645	6.741	6.427	6.410	6.337	6.363
Al^{IV}	1.246	1.385	1.355	1.259	1.573	1.590	1.663	1.637
Al^{VI}	0.310	0.384	0.350	0.314	0.557	0.540	0.629	0.514
Cr	0.004	0.002	0.001	0.004	0.004	0.002	0.006	0.002
Fe^{3+} (calc)	0.422	0.317	0.348	0.308	0.606	0.716	0.464	0.098
Ti	0.016	0.137	0.185	0.172	0.046	0.043	0.057	0.592
Fe^{2+}	1.982	2.190	2.218	2.135	1.969	1.879	2.172	2.046
Mn^{2+}	0.072	0.066	0.070	0.072	0.058	0.063	0.058	0.064
Mg	2.050	1.903	1.917	1.995	1.760	1.756	1.613	1.682
C site (M1+M2+M3)	5.000	5.000	5.000	5.000	5.000	5.000	5.000	5.000
excess (M1+M2+M3)	0.000	0.000	0.000	0.000	0.000	0.000	0.000	0.000
Ca	1.842	1.927	1.864	1.887	1.869	1.830	1.927	1.878
Na (M4)	0.158	0.073	0.136	0.113	0.131	0.170	0.073	0.122
B site (M4) total	2.000	2.000	2.000	2.000	2.000	2.000	2.000	2.000
Na (A)	0.170	0.272	0.217	0.231	0.264	0.221	0.312	0.236
K	0.178	0.208	0.206	0.170	0.180	0.195	0.211	0.218
A site total	0.348	0.480	0.423	0.401	0.445	0.416	0.523	0.455
F	0.028	0.038	0.043	0.038	0.038	0.034	0.024	0.34
Cl	0.005	0.003	0.008	0.010	0.000	0.003	0.003	0.005
Mg/Fe (tot)	0.853	0.759	0.744	0.816	0.684	0.677	0.612	0.638
Mg/Fe^{2+}	1.035	0.869	0.901	0.934	0.894	0.935	0.742	0.822
Mg/Mg+Fe (tot)	0.460	0.431	0.436	0.449	0.406	0.404	0.380	0.389
$Mg/Mg+Fe^{2+}$	0.509	0.465	0.474	0.483	0.472	0.483	0.426	0.451
Fe^{3+}/Fe (tot)	0.176	0.126	0.141	0.126	0.235	0.276	0.176	0.225

Fe^{3+} calculated by charge balance

Table 5: Representative Amphibole Analyses of RA-26-E from the Borrego Springs Mylonite Zone (Anderson,1983)

Sample No.	RA-26-E	RA-26-E	RA-26-E	RA-26-E	RA-26-E	RA-26-E	RA-26-E	RA-26-E
Analysis pt.	5182	5182	5183	5183	5182	5183	5183	5183
	9051	9081	9061	9162	9021	9021	9022	9024
Remarks	core	core	core	core	rim	rim	rim	rim
SiO_2	45.58	45.67	46.21	46.93	41.02	44.21	44.40	42.06
Al_2O_3	10.45	10.21	9.30	9.48	17.83	14.60	11.85	15.99
Cr_2O_3	0.00	0.00	0.00	0.01	0.02	0.00	0.00	0.00
Fe_2O_3 #	5.48	3.10	5.03	3.20	2.74	2.20	2.16	3.84
TiO_2	0.96	0.99	1.10	1.02	0.11	0.07	0.45	0.06
FeO	12.69	13.53	12.35	13.46	14.95	14.79	14.82	14.07
MnO	0.52	0.38	0.47	0.45	0.30	0.37	0.39	0.37
MgO	9.62	10.12	10.53	10.40	6.49	8.19	9.26	7.09
CaO	11.18	11.76	11.43	11.60	11.68	11.98	12.22	11.39
K_2O	0.45	0.44	0.51	0.36	0.74	0.46	0.40	0.54
Na_2O	1.04	0.86	0.90	0.90	1.03	0.91	0.96	1.04
F	0.05	0.01	0.07	0.10	0.06	0.04	0.08	0.01
Cl	0.03	0.02	0.03	0.01	0.06	0.02	0.01	0.05
Total	98.05	97.09	97.93	97.92	97.02	97.84	97.00	96.50
O=F,Cl	0.03	0.01	0.04	0.04	0.04	0.02	0.04	0.02
TOTAL	98.02	97.08	97.90	97.88	96.99	97.82	96.96	96.49
	- - - Atomic proportions based on 13 cations (except Ca+Na+K+Ba) - - -							
Si	6.723	6.785	6.810	6.899	6.156	6.530	6.646	6.322
Al^{IV}	1.277	1.215	1.190	1.101	1.844	1.470	1.354	1.678
Al^{VI}	0.540	0.573	0.426	0.542	1.310	1.071	0.736	1.555
Cr	0.000	0.000	0.000	0.001	0.002	0.000	0.000	0.000
Fe^{3+} (calc)	0.608	0.346	0.558	0.354	0.309	0.245	0.243	0.434
Ti	0.106	0.111	0.122	0.113	0.012	0.008	0.051	0.007
Fe^{2+}	1.565	1.681	1.523	1.655	1.876	1.827	1.855	1.769
Mn^{2+}	0.065	0.048	0.059	0.056	0.038	0.046	0.049	0.047
Mg	2.115	2.241	2.313	2.279	1.452	1.803	2.066	1.589
C site (M1+M2+M3)	5.000	5.000	5.000	5.000	5.000	5.000	5.000	5.000
excess (M1+M2+M3)	0.000	0.000	0.000	0.000	0.000	0.000	0.000	0.000
Ca	1.767	1.872	1.805	1.827	1.878	1.896	1.960	1.834
Na (M4)	0.233	0.128	0.195	0.173	0.122	0.104	0.040	0.166
B site (M4) total	2.000	2.000	2.000	2.000	2.000	2.000	2.000	2.000
Na (A)	0.064	0.120	0.062	0.084	0.178	0.156	0.238	0.137
K	0.085	0.083	0.096	0.068	0.142	0.087	0.076	0.104
A site total	0.149	0.203	0.158	0.151	0.319	0.243	0.315	0.241
F	0.023	0.005	0.033	0.046	0.028	0.019	0.038	0.005
Cl	0.007	0.005	0.007	0.002	0.015	0.005	0.003	0.013
Mg/Fe (tot)	0.973	1.105	1.112	1.135	0.655	0.871	0.985	0.721
Mg/Fe^{2+}	1.352	1.333	1.519	1.377	0.774	0.987	1.114	0.898
Mg/Mg+Fe (tot)	0.493	0.525	0.527	0.532	0.399	0.465	0.496	0.419
$Mg/Mg+Fe^{2+}$	0.575	0.571	0.603	0.579	0.436	0.497	0.527	0.473
Fe^{3+}/Fe (tot)	0.280	0.171	0.268	0.176	0.141	0.118	0.116	0.197

Fe^{3+} calculated by charge balance

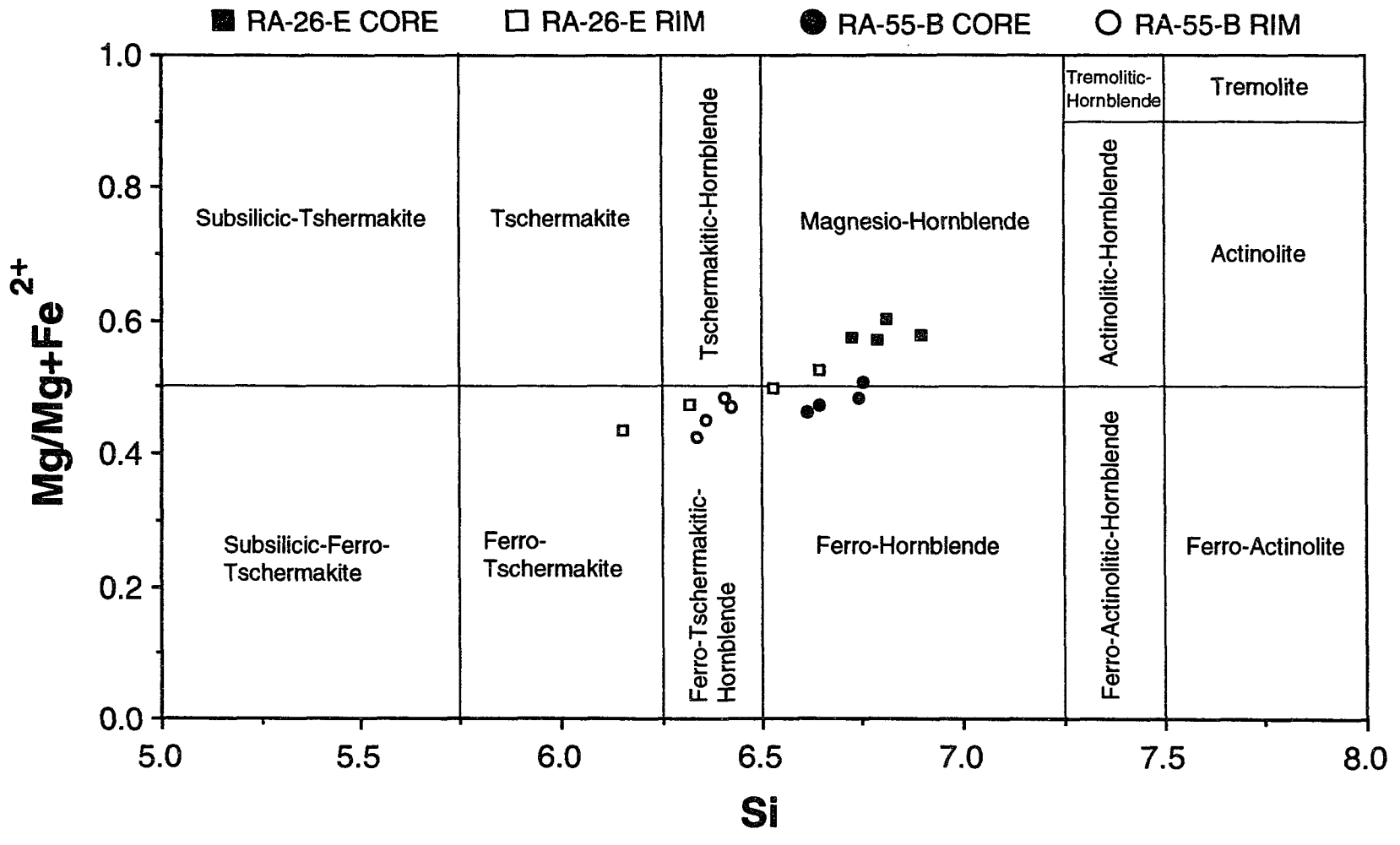

Figure 16. Amphibole compositions from mylonitic plutonic rocks in the Borrego Springs (RA-55-B) and Coyote Mountain (RA-26-E) mylonite zones. Analyses are from Anderson (1983). Atomic proportions are based on 13 cations (except Ca + Na + K + Ba), and Fe^{+3} was calculated by charge balance. See Figure 8 for sample locations.

Table 6: Selected Thermobarometry Results from the Santa Rosa mylonite belt near Borrego Springs, CA

Sample No. (remarks)	Amphibole ¢ Al total (analysis pt.)	Pressure* (Kb)	Pressure # (Kb)	X(Albite) ¢ maximum minimum	Temperature ^ (±75°C)
RA-26-E	1.817	5.49	5.64	0.55	748
(core)	(5182/9051)			0.45	796
RA-26-E	1.788	5.32	5.50	0.55	736
(core)	(5182/9081)			0.45	783
RA-26-E	1.652	4.56	4.85	0.55	741
(core)	(5183/9061)			0.45	788
RA-26-E	1.643	4.51	4.81	0.55	721
(core)	(5183/9162)			0.45	767
RA-26-E	3.154	13.03	12.00	0.45	824
(rim)	(5182/9021)			0.22	783
RA-26-E	2.541	9.57	9.09	0.45	786
(rim)	(5183/9021)			0.22	743
RA-26-E	2.09	7.03	6.94	0.45	794
(rim)	(5183/9022)			0.22	753
RA-26-E	2.833	11.22	10.48	0.45	811
(rim)	(5183/9024)			0.22	770
RA-55-B	1.556	4.02	4.40	§	§
(core)	(5201/9013)			§	§
RA-55-B	1.769	5.22	5.41	§	§
(core)	(5203/9012)			§	§
RA-55-B	1.705	4.86	5.11	§	§
(core)	(5203/9013)			§	§
RA-55-B	1.573	4.11	4.48	§	§
(core)	(5203/9018)			§	§
RA-55-B	2.13	7.25	7.13	§	§
(rim)	(5201/9011)			§	§
RA-55-B	2.13	7.25	7.13	§	§
(rim)	(5201/9015)			§	§
RA-55-B	2.292	8.17	7.90	§	§
(rim)	(5203/9014)			§	§
RA-55-B	2.151	7.37	7.23	§	§
(rim)	(5203/9015)			§	§

¢ from electron microprobe analyses of Anderson (1983)

* calculated using the geobarometer of Hollister et al. (1987)

calculated using the geobarometer of Schmidt (1992)

^ calculated with the geothermometer of Blundy and Holland (1990), using pressures determined with the Schmidt geobarometer

§ no available data

and Schmidt (1992) for comparison. The results show large increases in Al_{total}, and therefore pressure, from cores to rims. Using an average density of 2.72 g/cm^3 for granodiorites (Daly, 1966), these ~5-10 kb (RA-26-E) and ~5-7.5 kb (RA-55-B) core to rim increases in pressure equate to an ~18 km (RA-26-E) to 10 km (RA-55-B) increase in the depth of crystallization. A greater increase in pressure in the CMMZ, as opposed to the BSMZ, support the observation of Simpson (1985b) that the former area was deformed at deeper structural levels. Temperatures during crystallization of sample RA-26-E were determined with the geothermometer of Blundy and Holland (1990) using analyses from amphibole cores and the coarse-grained plagioclase (Table 6). Similar calculations were made using the analyses from the amphibole rims and the finer-grained plagioclase, which formed during mylonitization. Rim temperatures are slightly higher than those based on core compositions, although the increase is small and within the ± 75°C uncertainty of the geothermometer. Rim temperatures for RA-26-E range from ~740° to 820°C, and temperatures during crystallization of the core are from ~720° to 800°C.

Sample RA-55-B completely satisfies the mineral assemblage requirements for the Al-in-hornblende geobarometer (see *Methods*, this chapter). Anderson (1983) also presented evidence that indicates the presence of fluids and melt during mylonitization in the BSMZ. He described contact relations between mylonites and plutonic rocks that suggest the syntectonic emplacement of the latter. Sample RA-26-E is missing K-feldspar from the list of required minerals. This appears to be the only phase unaccounted for, since there is also evidence for the presence of fluids and melt in the CMMZ during mylonitization. Anderson (1983) noted that some of the mineral reactions accompanying mylonitization involved hydration, but that there is no evidence of dehydration reactions. He proposed that a large volume of water was introduced into the mylonite zone during deformation, and used whole rock chemical data to support

this notion. Theodore (1970) mapped the western part of Coyote Mountain, from which RA-26-E was collected, as consisting primarily of migmatitic gneiss. He described the gneisses as consisting of biotite-muscovite-(cordierite-garnet) assemblages that were partially replaced by sillimanite K-feldspar assemblages during metamorphism and concomitant migmitization. The absence of K-feldspar in RA-26-E means that pressures of crystallization determined for this sample, based on amphibole analyses, should be considered as limiting maximum values. .

Palm Springs Area

Representative analyses from electron microprobe traverses across amphibole and plagioclase in four tonalitic footwall rocks of the San Jacinto Mountains (Table 3; Fig 17; PG 101, PG 102, PG 110, and PG 118) are given in Tables 7 and 8, respectively (note that the complete data set from the analyses are given in appendix B). Si and Mg/(Mg + Fe) values from each of the samples are plotted separately on a calcic amphibole compositional scheme. Analyses from three of the four samples lie mainly within the magnesio-hornblende and ferro-hornblende fields, although some analyses indicate ferro-tschermakitic hornblende (Figs. 18, 19, and 20) Those of PG 118 are tightly clustered in the hastingsitic hornblende field (Fig 21). This separation between PG 118 and the other samples, in terms of composition, also appears in the plot of plagioclase analyses, where PG 118 is more albitic (Fig. 22). This reflects a distinctive bulk composition of the "early intrusives."

Al_{total} values from the representative analyses of Table 7 were inserted into the Al-in-hornblende geobarometer of Hollister et al. (1987) and Schmidt (1992), and their respective pressures and temperatures are given in Table 9. The highest pressures of ~6-7 kb were recorded in the oldest of the four samples (i.e. PG 118 lies in an area of ~99-94 Ma plutonic rocks as mapped by Hill, 1984; Fig. 17). Relatively lower pressures of ~4-5 kb were obtained from the three major tonalitic plutons of the San

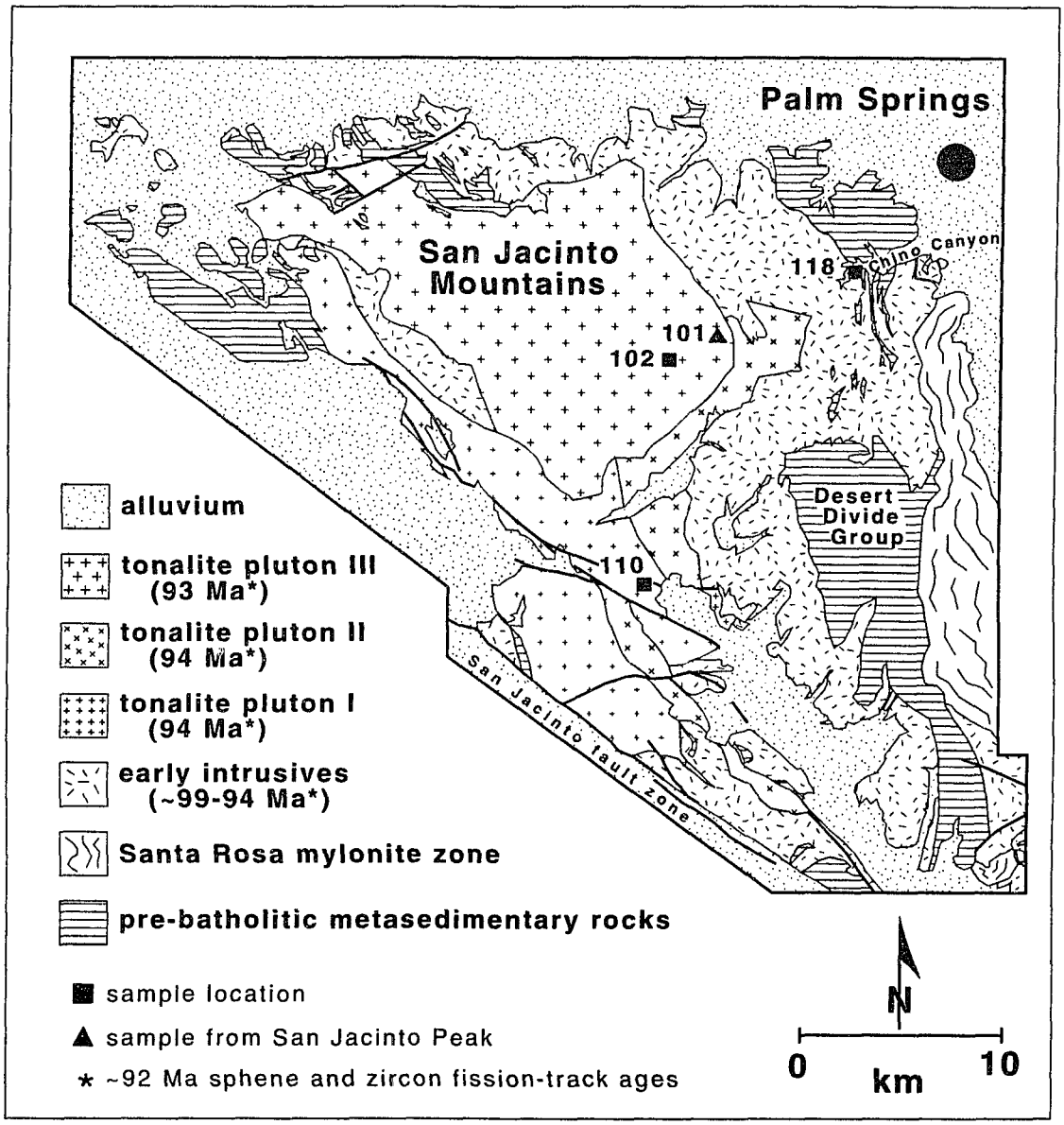

Figure 17. Geologic map of the San Jacinto Mountains, showing sample locations. U-Pb zircon ages from Hill et al. (1986) and Silver (1986) are also given. Modified from Hill et al. (1986).

Table 7: Representative Amphibole Analyses from the San Jacinto Mountains, CA

Sample No.	PG-101	PG-101	PG-102	PG-102	PG-110	PG-110	PG-118	PG-118
Analysis pt.	3	24	2	13	4	18	3	33
Remarks	rim	core	rim	core	rim	core	rim	core
SiO_2	43.46	43.70	42.91	44.71	45.08	45.20	40.24	40.76
Al_2O_3	1.59	1.19	1.52	1.30	1.62	1.31	1.38	1.34
Cr_2O_3	9.75	9.70	9.76	8.80	9.22	8.87	11.57	10.70
Fe_2O_3 #	0.00	0.01	0.00	0.00	0.06	0.01	0.07	0.00
TiO_2	3.58	4.42	4.47	4.22	3.50	4.51	5.33	6.35
FeO	17.91	16.83	16.74	15.62	16.64	15.69	23.59	22.95
MnO	0.57	0.51	0.56	0.49	0.40	0.44	0.76	0.88
MgO	7.91	8.18	8.26	9.42	8.84	9.30	2.57	2.67
CaO	11.57	11.45	11.45	11.60	11.39	11.48	10.54	10.22
Na_2O	1.33	1.21	1.48	1.26	1.19	1.16	1.63	1.68
K_2O	1.24	1.23	1.16	0.98	1.11	1.08	1.54	1.35
Total	98.91	98.43	98.31	98.40	99.05	99.04	99.21	98.90
	- - - Atomic proportions based on 13 cations (except Ca+Na+K+Ba) - - -							
Si	6.562	6.601	6.509	6.699	6.715	6.724	6.289	6.379
Ti	0.181	0.135	0.173	0.146	0.181	0.147	0.162	0.158
Al^{IV}	1.438	1.399	1.491	1.301	1.285	1.276	1.711	1.621
Al^{VI}	0.298	0.328	0.253	0.254	0.333	0.279	0.420	0.352
Cr	0.000	0.001	0.000	0.000	0.007	0.001	0.009	0.000
Fe^{3+} (calc)	0.407	0.502	0.510	0.476	0.393	0.504	0.627	0.748
Fe^{2+}	2.262	2.216	2.214	1.958	2.073	1.951	3.083	3.003
Mn^{2+}	0.073	0.065	0.072	0.062	0.050	0.055	0.101	0.117
Mg	1.781	1.842	1.868	2.104	1.963	2.062	0.599	0.623
C site (M1+M2+M3)	5.000	5.000	5.000	5.000	5.000	5.000	5.000	5.000
excess (M1+M2+M3)	0.000	0.000	0.000	0.000	0.000	0.000	0.000	0.000
Ca	1.872	1.853	1.861	1.862	1.818	1.830	1.765	1.714
Na (M4)	0.128	0.147	0.139	0.138	0.182	0.170	0.235	0.286
B site (M4) total	2.000	2.000	2.000	2.000	2.000	2.000	2.000	2.000
Na (A)	0.261	0.207	0.296	0.228	0.161	0.164	0.259	0.223
K	0.239	0.237	0.224	0.187	0.211	0.205	0.307	0.270
A site total	0.500	0.444	0.521	0.416	0.372	0.369	0.566	0.493
Mg/Fe (tot)	0.667	0.701	0.709	0.865	0.796	0.840	0.161	0.166
Mg/Fe^{2+}	0.787	0.866	0.879	1.075	0.947	1.057	0.194	0.207
Mg/Mg+Fe (tot)	0.400	0.412	0.415	0.464	0.443	0.456	0.139	0.142
$Mg/Mg+Fe^{2+}$	0.441	0.464	0.468	0.518	0.486	0.514	0.163	0.172
Fe^{3+}/Fe (tot)	0.152	0.191	0.194	0.196	0.159	0.205	0.169	0.199

Fe^{3+} calculated by charge balance

Table 8: Representative Plagioclase Analyses from the San Jacinto Mountains, CA

Sample No.	PG-101	PG-101	PG-102	PG-102	PG-110	PG-110	PG-118	PG-118
Analysis pt.	2	31	2	31	1	32	1	31
Remarks	rim	core	rim	core	rim	core	rim	core
SiO_2	61.27	59.16	61.43	59.34	59.88	58.58	63.25	63.54
Al_2O_3	24.10	25.67	24.02	25.16	25.86	26.32	23.51	24.08
FeO	0.09	0.05	0.03	0.04	0.09	0.02	0.13	0.05
CaO	5.99	7.41	5.63	6.96	6.99	7.99	4.69	4.89
BaO	0.08	0.06	0.00	0.01	0.04	0.11	0.00	0.02
Na_2O	7.84	7.00	8.29	7.52	7.50	6.89	9.08	8.72
K_2O	0.32	0.36	0.16	0.22	0.26	0.32	0.21	0.31
Total	99.69	99.71	99.56	99.25	100.62	100.23	100.87	101.61
	- - - Atomic proportions based on 8 oxygens - - -							
Si	2.731	2.648	2.738	2.666	2.654	2.615	2.778	2.769
Ti	1.266	1.354	1.262	1.332	1.351	1.385	1.217	1.237
Tet cations	3.997	4.002	3.999	3.998	4.005	4.000	3.995	4.005
Fe^{2+}	0.003	0.002	0.001	0.002	0.003	0.001	0.005	0.002
Ca	0.286	0.355	0.269	0.335	0.332	0.382	0.221	0.228
Ba	0.001	0.001	0.000	0.000	0.001	0.002	0.000	0.000
Na	0.678	0.608	0.716	0.655	0.645	0.596	0.773	0.737
K	0.018	0.021	0.009	0.013	0.015	0.018	0.012	0.017
A-site total	0.987	0.986	0.995	1.004	0.995	0.999	1.011	0.984
Anorthite	29.09	36.10	27.04	33.41	33.47	38.27	21.95	23.23
Albite	68.91	61.71	72.05	65.32	64.98	59.72	76.88	74.98
Orthoclase	1.85	2.09	0.91	1.26	1.48	1.82	1.17	1.75
Celsian	0.14	0.11	0.00	0.02	0.07	0.19	0.00	0.03

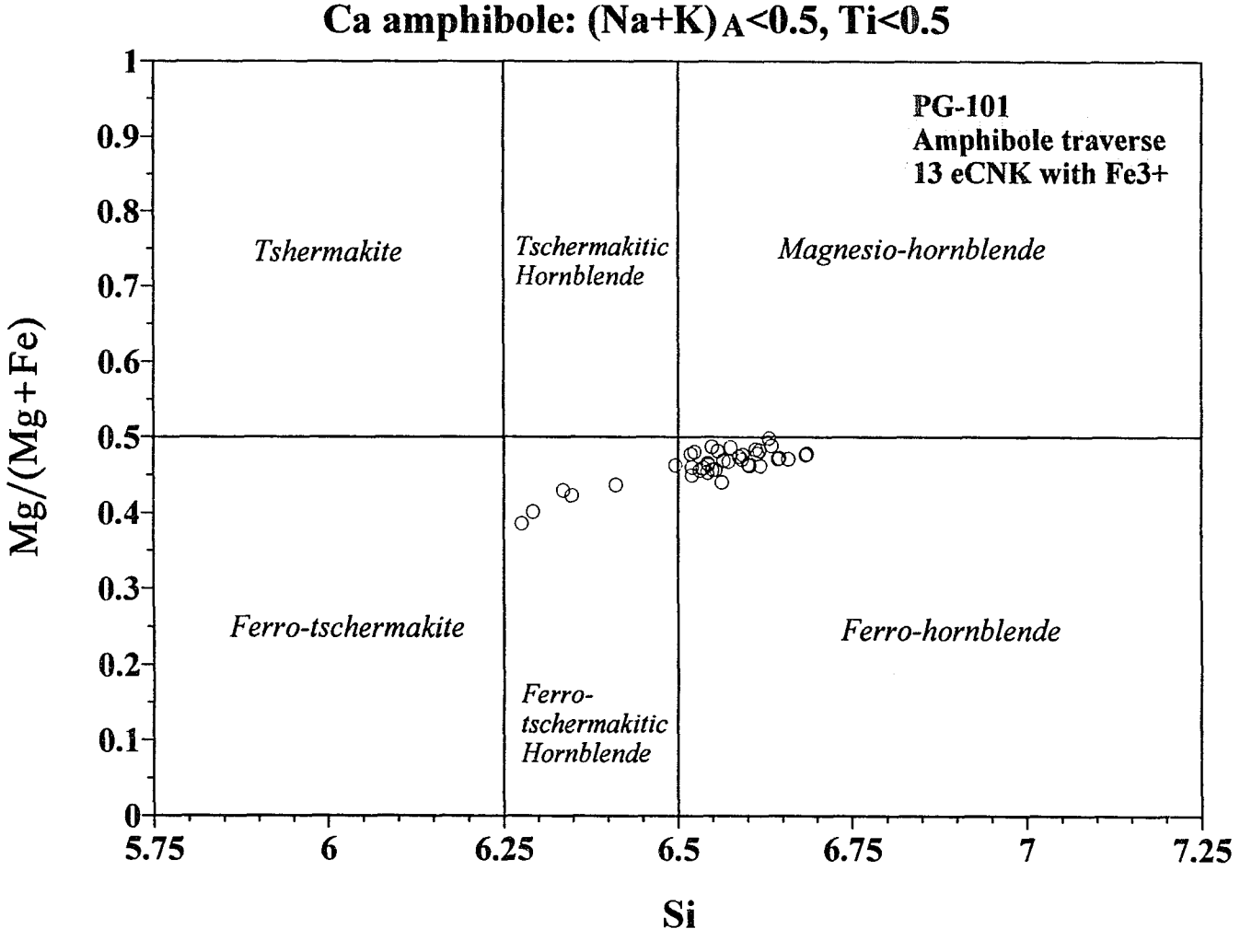

Figure 18. Compositions from electron microprobe traverse across amphibole of PG 101. Atomic proportions based on 13 cations (except Ca + Na + K + Ba), and Fe^{+3} was calculated by charge balance. See Figure 17 for sample location.

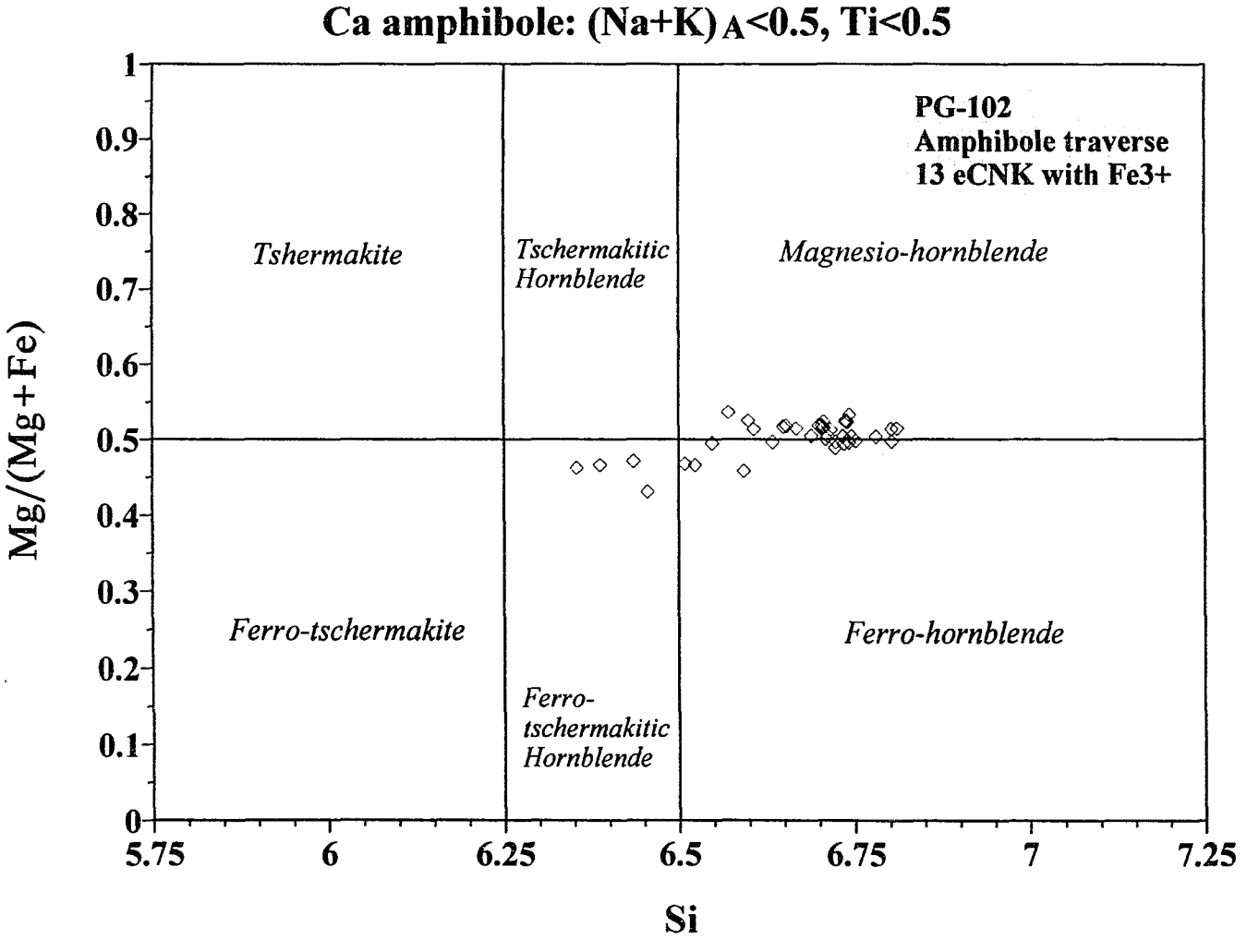

Figure 19. Compositions from electron microprobe traverse across amphibole of PG 102. Atomic proportions based on 13 cations (except Ca + Na + K + Ba), and Fe^{+3} was calculated by charge balance. See Figure 17 for sample location.

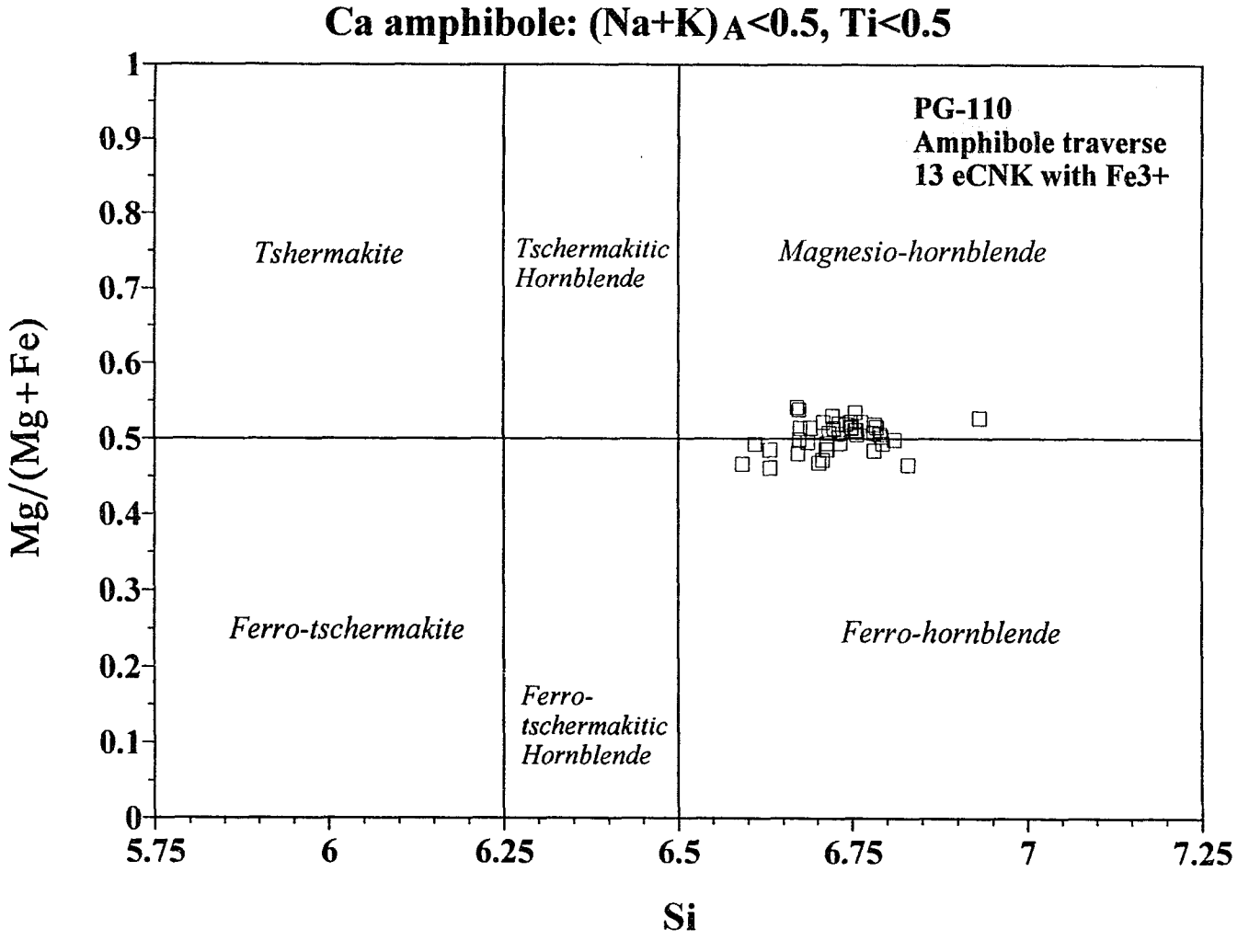

Figure 20. Compositions from electron microprobe traverse across amphibole of PG 110. Atomic proportions based on 13 cations (except Ca + Na + K + Ba), and Fe^{+3} was calculated by charge balance. See Figure 17 for sample location.

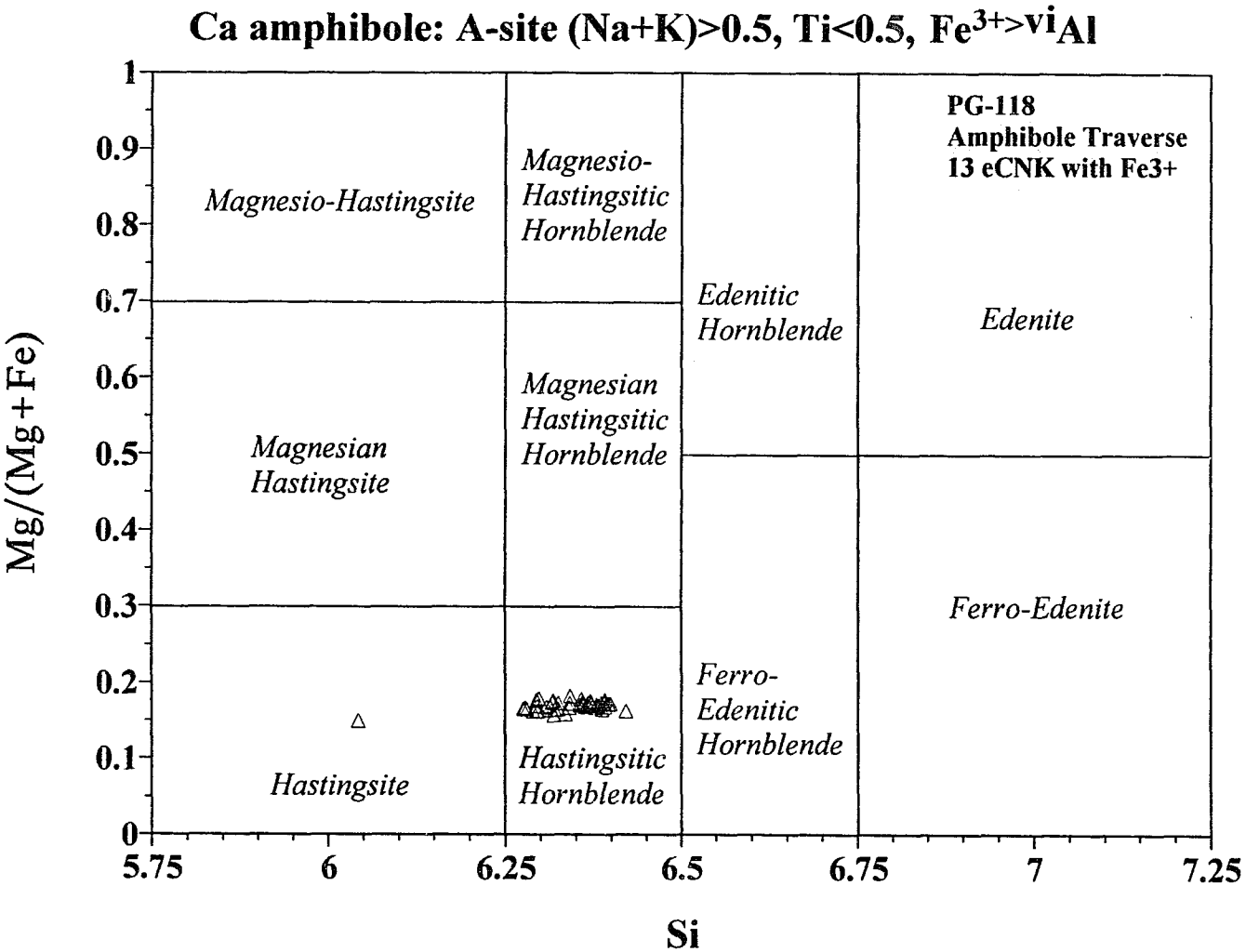

Figure 21. Compositions from electron microprobe traverse across amphibole of PG 118. Atomic proportions based on 13 cations (except Ca + Na + K + Ba), and Fe^{+3} was calculated by charge balance. See Figure 17 for sample location.

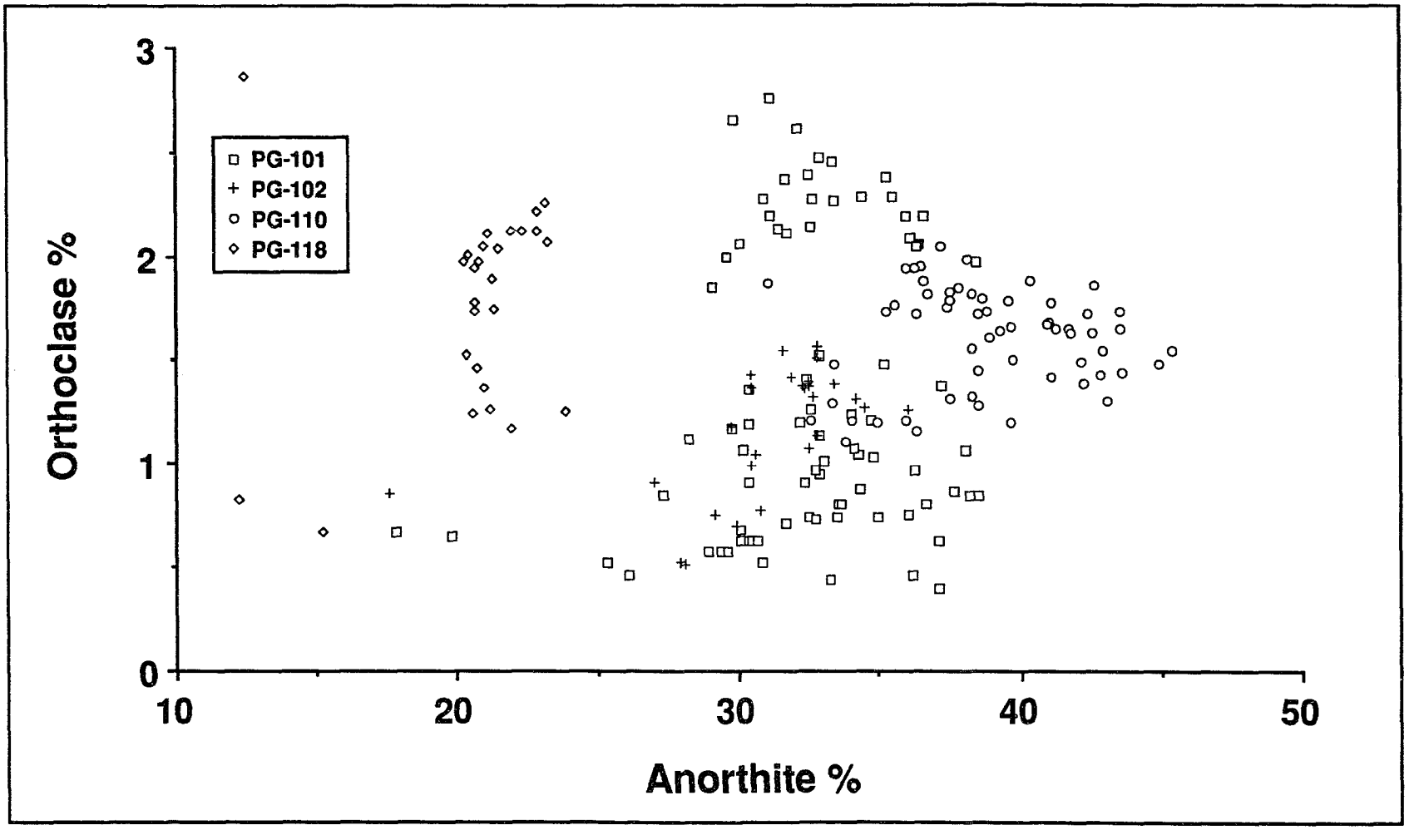

Figure 22. Compositions of plagioclase from tonalites in the San Jacinto Mountains. PG 101 data are from three traverses. PG 102 data are from one traverse in phenocryst next to k-feldspar. PG 110 data are from two traverses near amphibole, and PG 118 data are from one traverse near amphibole.

Table 9: Selected Thermobarometry Results from the San Jacinto Mountains, CA

Sample No. (remarks)	Amphibole Al total (analysis pt.)	Pressure* (Kb)	Pressure # (Kb)	Plagioclase X(Ab) (analysis pt.)	Temperature ^ (±75°C)
PG-101 (rim)	1.736 (pt. 3)	5.03	5.25	0.6891 (pt. 2)	745
PG-101 (core)	1.727 (pt. 24)	4.98	5.21	0.6171 (pt. 31)	759
PG-102 (rim)	1.744 (pt. 2)	5.08	5.29	0.7205 (pt. 2)	747
PG-102 (core)	1.555 (pt. 13)	4.01	4.39	0.6532 (pt. 31)	740
PG-110 (rim)	1.618 (pt. 4)	4.37	4.69	0.6498 (pt. 1)	733
PG-110 (core)	1.555 (pt. 18)	4.01	4.39	0.5972 (pt. 32)	751
PG-118 (rim)	2.131 (pt. 3)	7.26	7.13	0.7688 (pt. 1)	750
PG-118 (core)	1.973 (pt. 33)	6.37	6.38	0.7498 (pt. 31)	749

* calculated using the barometer of Hollister et al. (1987)

calculated using the barometer of Schmidt (1992)

^ calculated with the geothermometer of Blundy and Holland (1990), using pressures determined with the Schmidt geobarometer

Jacinto Mountains, which were emplaced approximately synchronously between 94 and 93 Ma (emplacement ages are U-Pb zircon dates from Hill et al., 1986 and Silver, 1986). In Figure 23 the differences in pressure, i.e. differences in Al_{total}, between the older and younger samples are shown on a plot of Ti/Fe and Si/Si + Al. Amphiboles in all four samples are weakly zoned with respect to Al content, and do not have compositionally distinct overgrowths (Fig. 24). Pressures, therefore, are slightly but consistently greater based on rim analyses compared with core pressure estimates.

Analyses from Tables 7 and 8 were inserted into the amphibole-plagioclase geothermometer of Blundy and Holland (1990), and are also given in Table 9. The results indicate temperatures close to expected solidus temperatures for a tonalite. Temperatures range from 730° to 760°C, and show no systematic variations with respect to sampling location. Given the ± 75°C uncertainty of the geothermometer, temperatures of crystallization for all four samples may be equivalent. Core to rim variations also show no systematic changes, and thus, indicate static temperatures (Table 9).

DISCUSSION

Thermobarometry studies from the Santa Rosa mylonite belt and footwall rocks in the San Jacinto Mountains, coupled with field and laboratory work, support the notion of regional west-vergent thrusting at ~99-94 Ma followed closely by major extension between ~94 and 92 Ma. Approximately 10 to 18 km of continental crust were thrust over the eastern margin of the Peninsular Ranges, which likely created an overthickened crustal welt. This crustal welt subsequently collapsed through extension, and thereby provided room for the emplacement of the voluminous tonalites and granodiorites of the eastern Peninsular Ranges. The following section is, in part, a discussion of the evidence for this proposed tectonic history.

This section also examines the possibility that the Santa Rosa mylonite belt was part of a much larger west-directed ductile thrust system. This has previously been

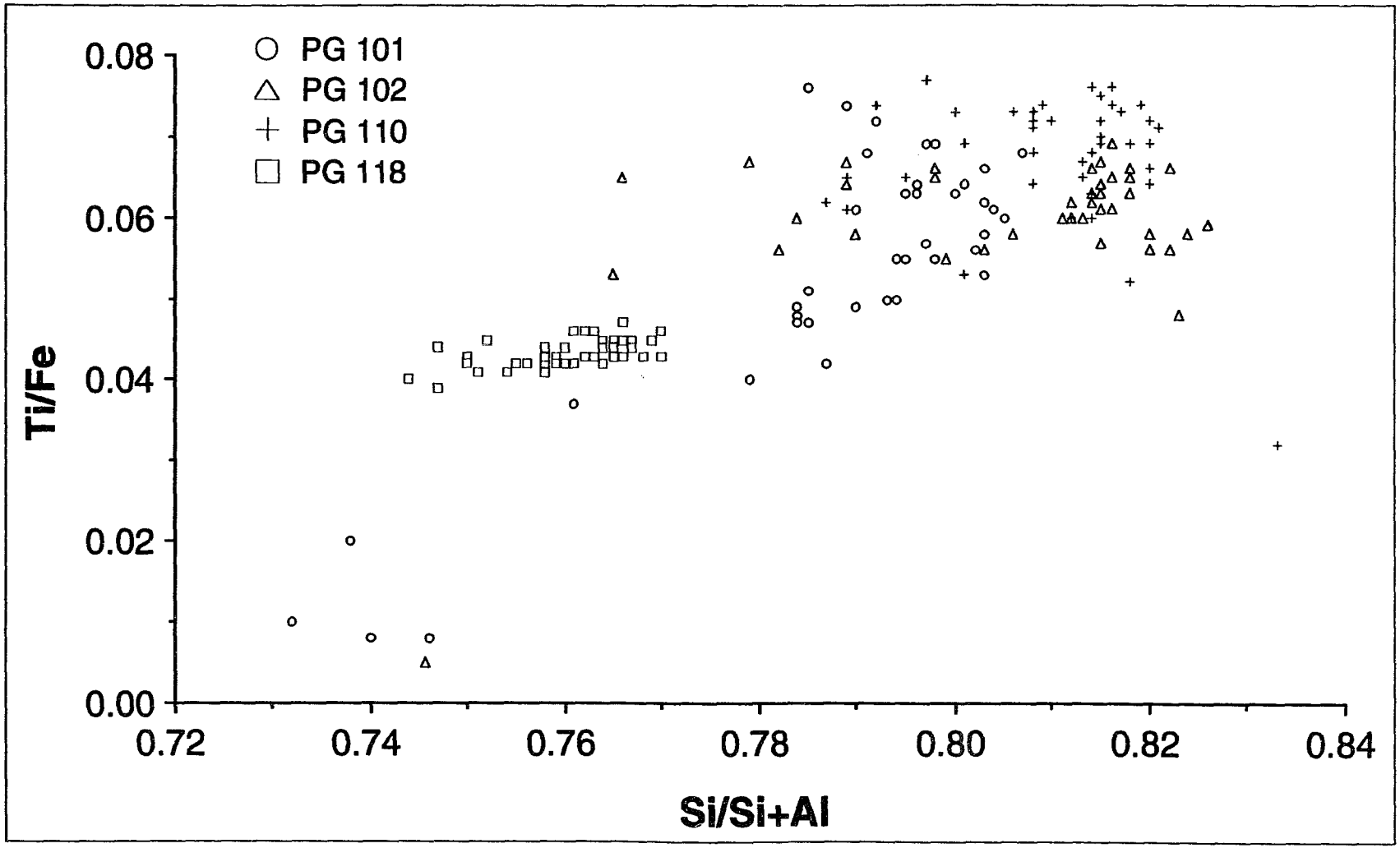

Figure 23. Ti/Fe is plotted here against Si/Si+Al for amphibole analyses from PG 101, 102, 110, and 118 from the San Jacinto Mountains. Note the correlation between Si/Si+Al and sample location (i.e. Si/Si+Al decreases from west to east).

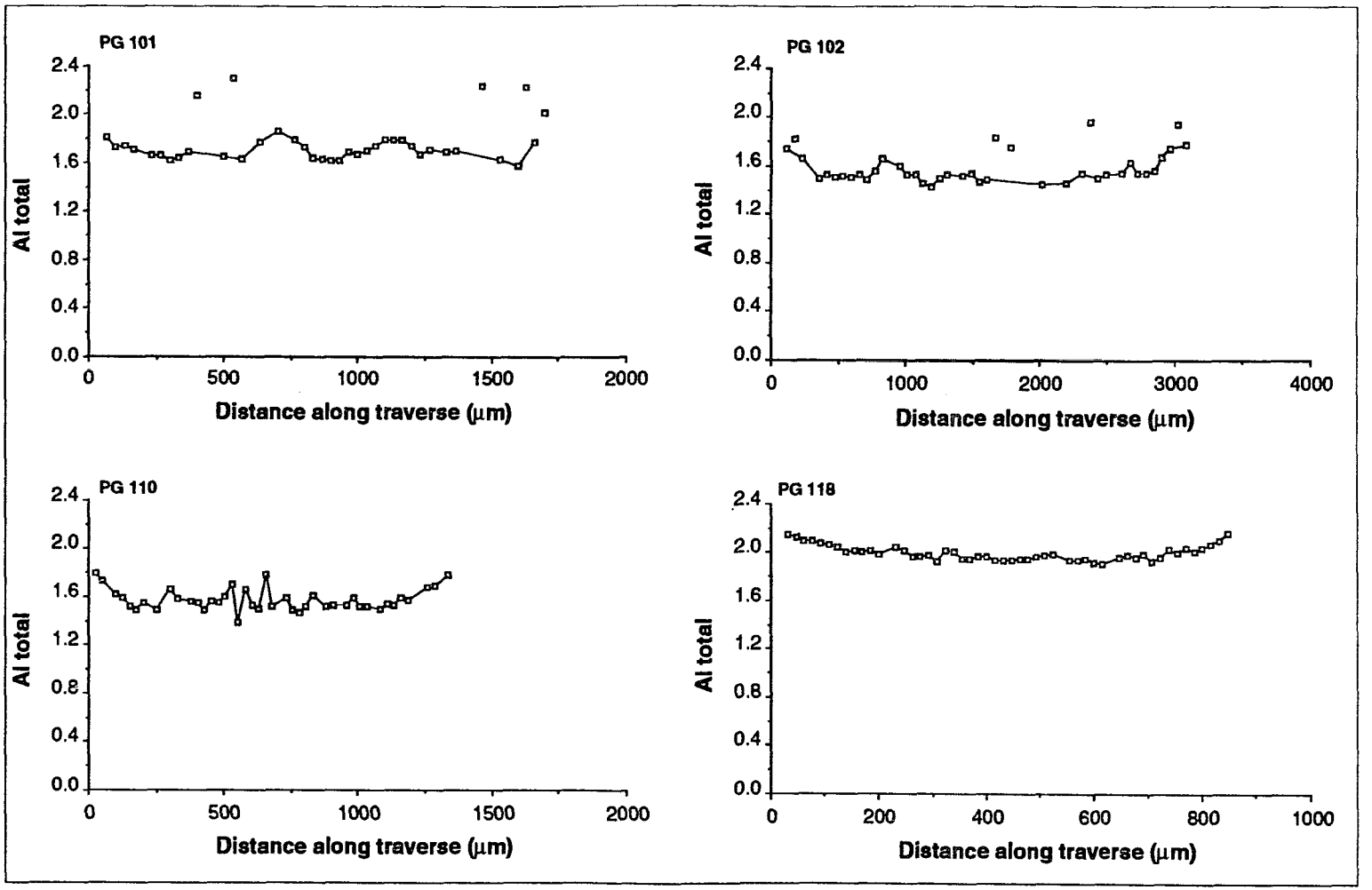

Figure 24. Al_{total} is plotted here with distance along amphibole traverses for samples PG 101, 102, 110, and 118. The amphiboles are weakly zoned with respect to Al content, and do not have crystallographically distinct rims.The anomaously high Al_{total} points represent minor amphibole exsolution.

suggested by Sharp (1979), who described an eastern Peninsular Ranges mylonite zone extending from the San Jacinto Mountains to perhaps as far south as Baja California Sur. May (1989) proposed the existence a semi-continuous belt of mylonitic rock that trends approximately north-south through a palinspastically restored Transverse and Peninsular Ranges. A similar restoration is presented here, specifically involving the Santa Rosa mylonite belt and the Cuyamaca-Laguna Mountains shear zone.

Evidence for West-Vergent Thrusting in the Borrego Springs Area

Abundant microstructural and field evidence in the BSMZ indicate ductile shearing with an east-over-west sense of movement (Simpson, 1984). There are common S and C planes, with the C planes dipping ~35° to the east, as well as shear bands in the granodiorites west of Borrego Springs. In the CMMZ sillimanite-bearing mylonites generally are well foliated, with foliation dipping to the east. The mylonites are characterized by prominent linear structures, small- and large-scale folds, and a strong preferred orientation of minerals (Theodore, 1967). Engel and Schultejann (1984) and Schultejann (1984) described structures indicating west and NNW-vergent thrusting in the BSMZ, at Coyote Mountain, and in the southern Santa Rosa Mountains (Figs. 15 and 8). They include overthrusts and associated drag folds and nappes that form imbricate stacks of metasediments, plutonic rocks, and mylonites. The orientation, vergence, and detachment of both large and small folds, as well as the displacements of crosscutting pegmatites and stratigraphic reconstructions also indicate east-over-west thrusting. Similar microstructural and field evidence for west-vergent thrusting are also found in the SRMZ (Simpson and Schmid, 1983; Erskine and Wenk, 1985; Erskine, 1986; O'Brien et al., 1987; chapter 2).

Thermobarometry from mylonites of the CMMZ and BSMZ support the notion of major Late Cretaceous west-vergent thrusting in the eastern Peninsular Ranges (Table 6). The results from sample RA-55-B indicate that the BSMZ segment of the Santa

Rosa mylonite belt was buried by an additional ~10 km of rock as a result of thrusting. Its total depth of burial during mylonitization was ~ 28 km. In the samples from Coyote Mountain (RA-26-E) core to rim variations in Al_{total} indicate that this part of the mylonite belt was buried to ~36 km, with ~18 km attributed to tectonic burial. Core to rim variations in estimated temperature for amphibole in sample RA-26-E increase only slightly, if at all. The ~760° to 780°C average increase in temperature is less than the ± 75°C degree of uncertainty of the geothermometer. The absence of a large core to rim increase in estimated temperature appears to contradict the geobarometry results indicating a large increase in depth of burial during mylonitization. One might expect that thrusting of ~10 to 18 km of crust over midcrustal rock (already at ~18 km) would have ultimately raised temperatures significantly in the vicinity of the mylonite belt. This apparent contradiction can be explained by having the thrusting event followed closely in time by extension, tectonic denudation, and exhumation of the mylonite belt. In this scenario the mylonites would not have been at the greater depths long enough to thermally equilibrate, but would have retained the effects of an essentially instantaneous increase in pressure. A similar sequence of tectonic events has been described for the Waterman Metamorphic Complex in the central Mojave Desert (Henry and Dokka, 1992).

Evidence for Major Late Cretaceous Extension in the Palm Springs Area

The age of the Santa Rosa mylonite belt in the Palm Springs area is constrained between ~99-92 Ma, based on thermochronologic data presented in Chapter 2. Initially, this east-dipping shear zone developed as a west-vergent thrust fault. In the San Jacinto Mountains ~99-94 Ma "early intrusives," as defined by Hill (1984), were deformed by west-vergent thrusting (Fig. 17; Simpson and Schmid, 1983; Erskine and Wenk, 1985; Erskine, 1986; O'Brien et al., 1987). Erskine (1986) described these older rocks as syntectonic and as having been emplaced during thrusting. He based this on a

concordance of foliation and lineation in the mylonite belt with primary foliation, lineation, and strained mafic inclusion fabrics in sheeted plutonic rocks just below the SRMZ. This notion is supported by crystallization pressures of sample PG 118, which is from the "early intrusives" unit. Pressures are from 6-7 kb (Table 9), which is approximately equal to those based on rim compositions of RA-55-B from the Borrego Springs mylonite zone (~7-8 kb, Table 6).

In contrast to the early intrusives, thermochronologic and thermobarometric data support the notion that the voluminous 94-93 Ma tonalites of the San Jacinto Mountains were emplaced following thrusting in an extensional environment. This is also indicated by field and microstructural studies in the San Jacinto Mountains and SRMZ. The voluminous tonalites of the San Jacinto Mountains have amphiboles that are weakly zoned with respect to Al_{total} (Fig. 24), unlike those from samples RA-55-B and RA-26-E (Table 6) near Borrego Springs. This suggests that they were emplaced following thrusting, since they sit in the footwall of the SRMZ but do not have high Al_{total} rims. Thermobarometry data from the major tonalitic plutons indicate crystallization at 730°-760°C and ~4-5 kb (samples PG 101, 102, and 110). Given their ~92 Ma sphene and zircon fission-track ages (George and Dokka, in review; chapter 2) with closure temperatures of ~285°C and ~235°C (Zeitler et al., 1982), respectively, these rocks cooled some 510°C in less than 1 to 2 m.y. To account for this rapid cooling, as well as the room which would have been necessary to accommodate the emplacement of the voluminous tonalitic plutons, it is proposed that these rocks were intruded and subsequently exhumed following thrusting during a period of extension (George et al., 1991). Based on their thermochronology (chapter 2), and assuming paleogeothermal gradients of ~35° to 45°C as indicated by pressure-temperature data (Table 9), the tonalites were exhumed ~10-14.5 km during synextensional emplacement (note that these are disturbed geothermal gradients due to the intrusions).

In the San Jacinto Mountains deformational structures in and adjacent to the major tonalites suggest emplacement along an active shear zone. The three major tonalitic plutons of the San Jacinto Mountains (Fig. 17) have large length to width ratios (Hill, 1984), which would be expected of plutons intruding into an actively extending shear zone. Internal and external foliations in these plutons are parallel or subparallel with contacts with metasedimentary and/or older igneous wall rocks (Hill, 1988). Hill (1988) interpreted the external structures as forming during emplacement of the plutons. He interpreted the internal structures including banding, schlieren, and mafic inclusion trains, as being produced during emplacement by magmatic flow within a semi-lithified tonalitic magma.

Microstructural evidence from the SRMZ, in part, supports extension during the later stages of mylonitization along the shear zone. However, as previously discussed in Chapter 2 (see *Age and Origin of the Santa Rosa Mylonite Belt*) there also is microstructural evidence of noncoaxial deformation with an east-over-west sense of shear. To account for both, extensional deformation was probably superimposed upon previous structures formed during west-vergent thrusting. The microstructural evidence for extension includes pole figures of calcite from mylonitic marbles of the Palm Canyon Complex, as well as those from quartz bands in the lower plate mylonitic plutonic rocks of the SRMZ (Kmg, Fig. 7; Erskine and Wenk, 1985). Both sets of data display similar orthorhombic symmetry that is characteristic of coaxial extension. Erskine and Wenk (1985) interpreted the pole figures as indicating flattening normal to the foliation of the SRMZ (striking NNW, and dipping 20-55° ENE) and stretching along a well developed lineation that trends about N55°E. Because extension in the mylonitic plutonic rocks included crystal-plastic deformation of quartz, it had to have occurred before ~92 Ma. This is because deformation of quartz requires temperatures greater than ~300°C (Sibson, 1977), and based on fission-track ages from footwall rocks in the San Jacinto

Mountains (George and Dokka, in review; chapter 2) the SRMZ was cooler than ~235°C by ~92 Ma.

The occurrence of low-angle, east-dipping imbricate faults in the SRMZ was cited by Erskine and Wenk (1985) as supporting evidence for coaxial extension along the mylonite belt. (Fig. 7). Their geometry with respect to the underlying Palm Canyon fault was seen as similar to that of metamorphic core complexes, such as are exposed in southeastern California and southern Arizona (eg. Davis et al., 1980; Dokka, 1989; and Spencer and Reynolds, 1990). The faults generally are shallower than mylonitic foliation, and do not cut across the Palm Canyon fault. Erskine and Wenk (1985) described the Palm Canyon fault as a basal décollement to the structurally higher low-angle faults, and considered both to be kinematically related. The surfaces of the low-angle faults commonly have a well developed chloritic breccia zone, and linear slip-related structures are subparallel to extensional lineations in the SRMZ (Erskine and Wenk, 1985). Some of the faults also display northeast-directed drag folds.

Todd et al. (1988) noted the similarity between the low-angle faults in the SRMZ with other low-angle, brittle normal faults to the south. Specifically, they cited the Yaqui Ridge detatchment fault of Schultejann (1984), which also occurs within the Santa Rosa mylonite belt (Fig. 8). The detachment fault dips 10-40° to the northeast and separates a lower core of mylonitic granodiorite of the BSMZ from an unconsolidated, unmetamorphosed megabreccia of Miocene(?) age (Schultejann, 1984). The fault is smooth and planar with striations that indicate movement parallel and subparallel to the northeast dip of the fault. Directly below the fault surface is a band of intensely sheared cataclasite, and below that is a chlorite-breccia zone of intense brecciation and chloritization. Schultejann (1984) attributed these structures to a "mid-Cenozoic low temperature episode of ENE-WSW extension and detachment faulting accompanied by lower greenschist facies metamorphism and brittle deformation." Todd et al (1988)

proposed that the low-angle faults in the SRMZ may also have been active in mid-Cenozoic time, since they display evidence of greenschist facies metamorphism and brittle deformation. They further proposed that this later Tertiary deformation may have occurred along reactivated Late Cretaceous, low-angle, normal faults in the SRMZ.

A Proposed Tectonic History for the Santa Rosa Mylonite Belt

The Santa Rosa mylonite belt is a regional feature that extends some 80 km along the eastern Peninsular Ranges. As will be discussed below, it may also be part of a much larger eastern Peninsular Ranges mylonite zone extending from the eastern Transverse Ranges to the Cuyamaca-Laguna Mountains shear zone, and perhaps as far south as Baja California Sur. The data presented here and in Chapter 2 suggest a tectonic history for the eastern Peninsular Ranges that involved creation of an overthickened crustal welt in Late Cretaceous time, that subsequently collapsed by major extensional faulting (Fig. 25). The Santa Rosa mylonite belt is the regional, ductile shear zone along which west-vergent thrusting, and later extensional collapse took place.

The majority of pluton emplacement and formation of the Peninsular Ranges batholith occurred along an active Andean-type plate margin between ~120-89 Ma (Silver et al., 1979; Silver and Chappell, 1988; Walawender et al., 1990). Subduction was continuous but variable during this period, and the rate of convergence between the Farallon and North American plates was moderately high (50-100 km/m.y., Engebretson et al., 1985). At ~100 Ma there was a major change in the direction and increase in the rate of convergence (Fig. 26). Hotspot plate reconstructions indicate that convergence increased from 60 km/m.y. to greater than 100 km/m.y. and the direction of convergence shifted from approximately east-west to a northeast-southwest direction (Engebretson et al., 1985). This change in Farallon-North America plate motion likely affected regional geological events in the Peninsular Ranges batholith. At ~100 Ma the locus of magmatism shifted from a static arc located along the western half of the

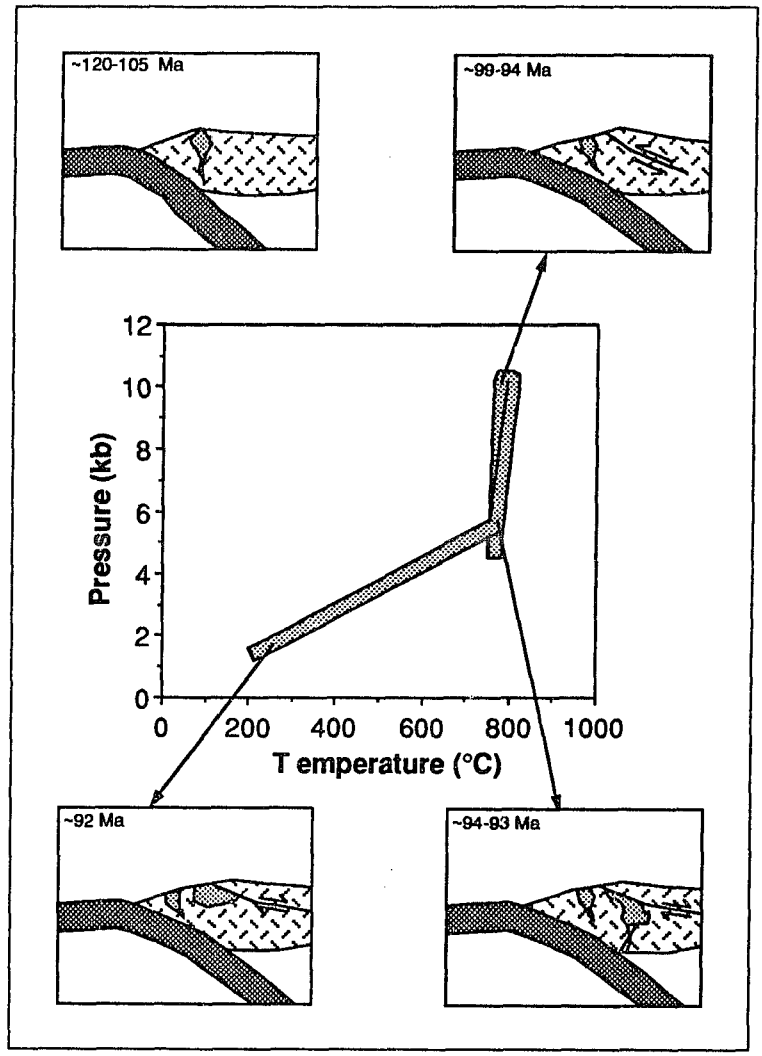

Figure 25. P-T-t diagram illustrating a proposed tectonic history for the Santa Rosa mylonite belt. Between ~120 and 105 Ma magmatism was concentrated in the western Peninsular Ranges. At ~100 Ma a change in plate motions was coincident with a shift in the locus of magmatism into the east, which may have been the result of a decrease in the subduction angle of the Farallon plate beneath North America. Thermal weakening of the crust in the eastern Peninsular Ranges due to the addition of magmatic heat, along with shear stresses between the Farallon and North American plates, may have facilitated thrusting along the mylonite belt between ~99 and 94 Ma. Approximately 10 to 18 km of crust were thrust over the eastern margin of the batholith, which thickened the lithosphere and increased pressures in rocks of the Santa Rosa mylonite belt by ~3-5 kb. Subsequent extensional collapse of the overthickened crust may have caused the rapid decompression and cooling of the area, as seen in the San Jacinto Mountains. Crustal extension was accompanied by emplacement of tonalites into footwall rocks of the mylonite belt from 94 to 93 Ma in the San Jacinto Mountains. Between 94-93 Ma and ~92 Ma the tonalites were exhumed some 10-14.5 km as they cooled from temperatures of 733°-759°C to below ~235°C.

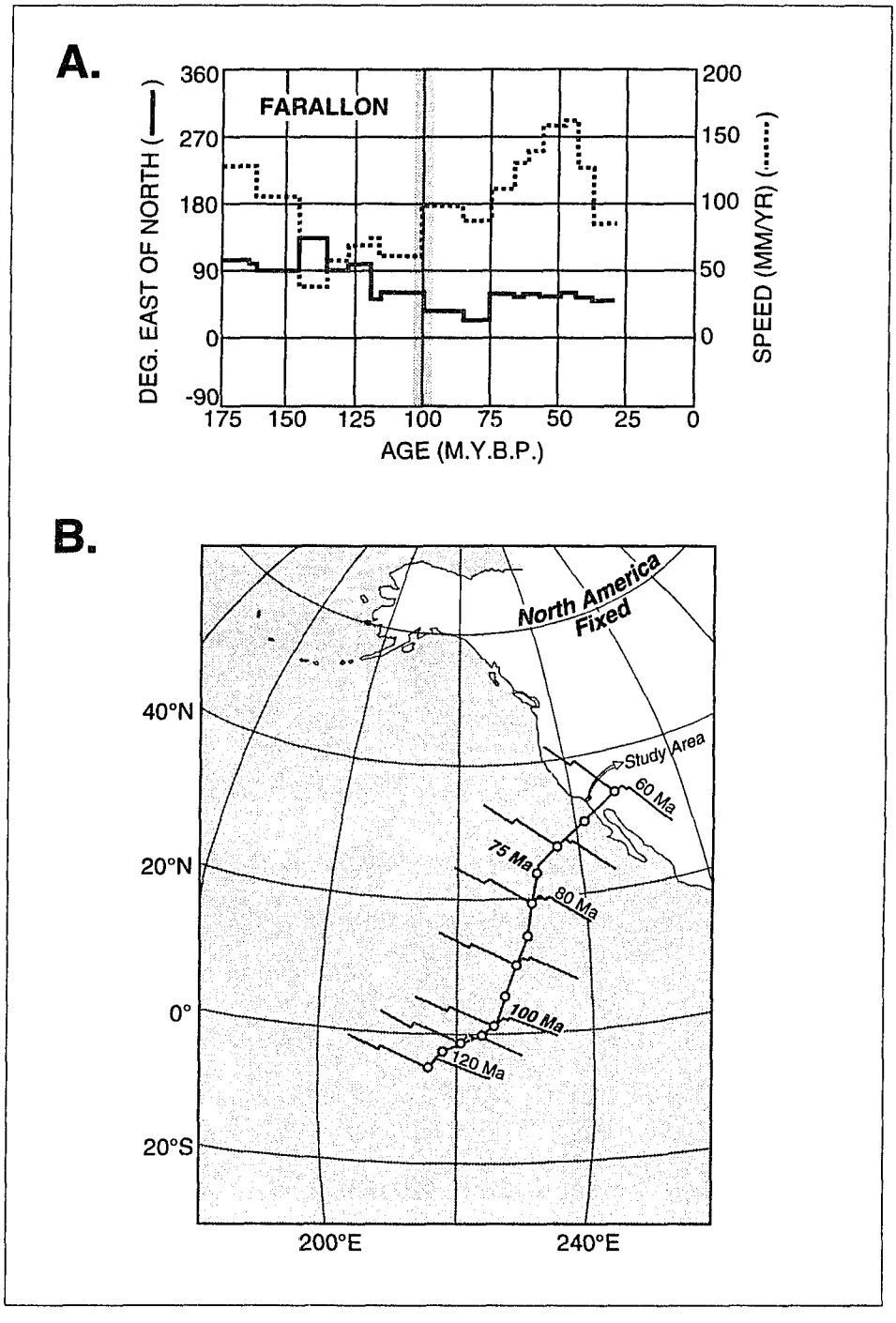

Figure 26. a) Azimuth and speed of linear velocities of the Farallon and Kula plates relative to North America at Baja, California (site coordinates of Lat. 26°, Long. 248°; from Engebretson et al., 1985). Shaded area highlights a major change in the rate of convergence at ~100 Ma. b) Sequence of circles shows the trajectory of a point on the Farallon plate as it moves across the Pacific basin. The point is located on anomaly M29 (164 Ma). Note the changes in direction of convergence at 100 and 75 Ma. From Engebretson et al. (1985).

batholith into the eastern Peninsular Ranges where voluminous tonalites and granodiorites were intruded and emplaced between ~99 and 89 Ma (Silver et al., 1979; Silver, 1986; Silver and Chappell, 1988; Walawender et al., 1991). This shift in magmatism has been attributed to an inferred shallowing in the angle of subduction at ~105 Ma (Walawender et al., 1991). In turn, this shallowing in the subduction angle may have been due to the increase in in plate convergence at ~100 Ma, although as Atwater (1989) points out plate-motion reconstructions of that age are very uncertain both with respect to timing and rates. Therefore, these possible cause and effect relationships remain equivocal.

West-vergent thrusting along the Santa Rosa mylonite belt in the Palm Springs area occurred between ~99 and 94 Ma, and was approximately coincident with the shift of magmatism into the eastern Peninsular Ranges. The two events may be related, and both due to the inferred shallowing in the subduction angle. Hamilton (1988) proposed a model for development of the mylonite belt that involves low-angle subduction, tectonic erosion, and underplating beneath the arc. Underplating of low-density sediments and continental crust beneath the eastern Peninsular Ranges during subduction is seen as increasing drag against the overriding continental plate, which ultimately produces west-vergent ductile thrusting at mid-crustal levels. Another possible factor in forming the mylonite belt, in addition to the inferred shallowing in the angle of subduction, may have been the addition of heat into the area with the eastward shift in the locus of magmatism. Arrival of magmatism into the eastern Peninsular Ranges may have thermally weakened the crust and facilitated ductile thrusting. This latter notion was previously proposed by Burchfiel and Davis (1975) to explain certain Mesozoic and early Cenozoic deformational features along the Cordilleran orogen.

Whatever the underlying controls were that resulted in west-vergent thrusting, the thermobarometry data presented here indicate that ~10 to 18 km of crust were thrust over

the eastern Peninsular Ranges in Late Cretaceous time. Thrusting was soon followed by major extension and exhumation of the mylonite belt, which was also accompanied by voluminous synextensional intrusions of tonalite and granodiorite. The extension and exhumation of the mylonite belt may represent the gravitational collapse of an overthickened crustal welt formed during the previous thrusting, in a manner as proposed by Coney and Harms (1984).

A Palinspastic Reconstruction of the Eastern Peninsular Ranges Mylonite Zone

Mylonitization along the SRMZ segment of the Santa Rosa mylonite belt was previously constrained to between ~99 and 62 Ma. The 99 Ma value is the oldest known U-Pb age for zircon from deformed plutonic rocks adjacent to the SRMZ (Hill et al., 1986; Silver, 1986), and the younger constraint is based on concordant sphene, zircon, and apatite ages from hanging wall rocks in the northern Santa Rosa Mountains (Dokka, 1984). As discussed in Chapter 2, sphene and zircon fission-track ages from footwall rocks in the San Jacinto Mountains have further narrowed the period of ductile deformation along the SRMZ to between ~99 and 92 Ma. Mylonitization along the Cuyamaca-Laguna Mountains shear zone located south-southeast of the Santa Rosa mylonite belt (Fig. 27a) is, at present, constrained to between ~118 and 93-90 Ma (Todd and Shaw, 1979; Leeson, 1989; Walawender et al, 1991; Grove and Harrison, 1992). The younger age is based on biotite $^{40}Ar/^{39}Ar$ dates from footwall rocks of the shear zone (Grove and Harrison, 1992), and the ~118 Ma value is based on the U-Pb zircon age of the Pine Valley granite (Walawender et al., 1991) that is deformed along the shear zone (Todd, 1979; Leeson, 1989). The older age constraints from this shear zone, as well as that from the SRMZ, are based on a limited number of U-Pb zircon ages and should be considered less definite than the younger constraints based on thermochronologic evidence. In any case, it is possible that both shear zones were active at approximately the same time as part of a much larger eastern Peninsular Ranges

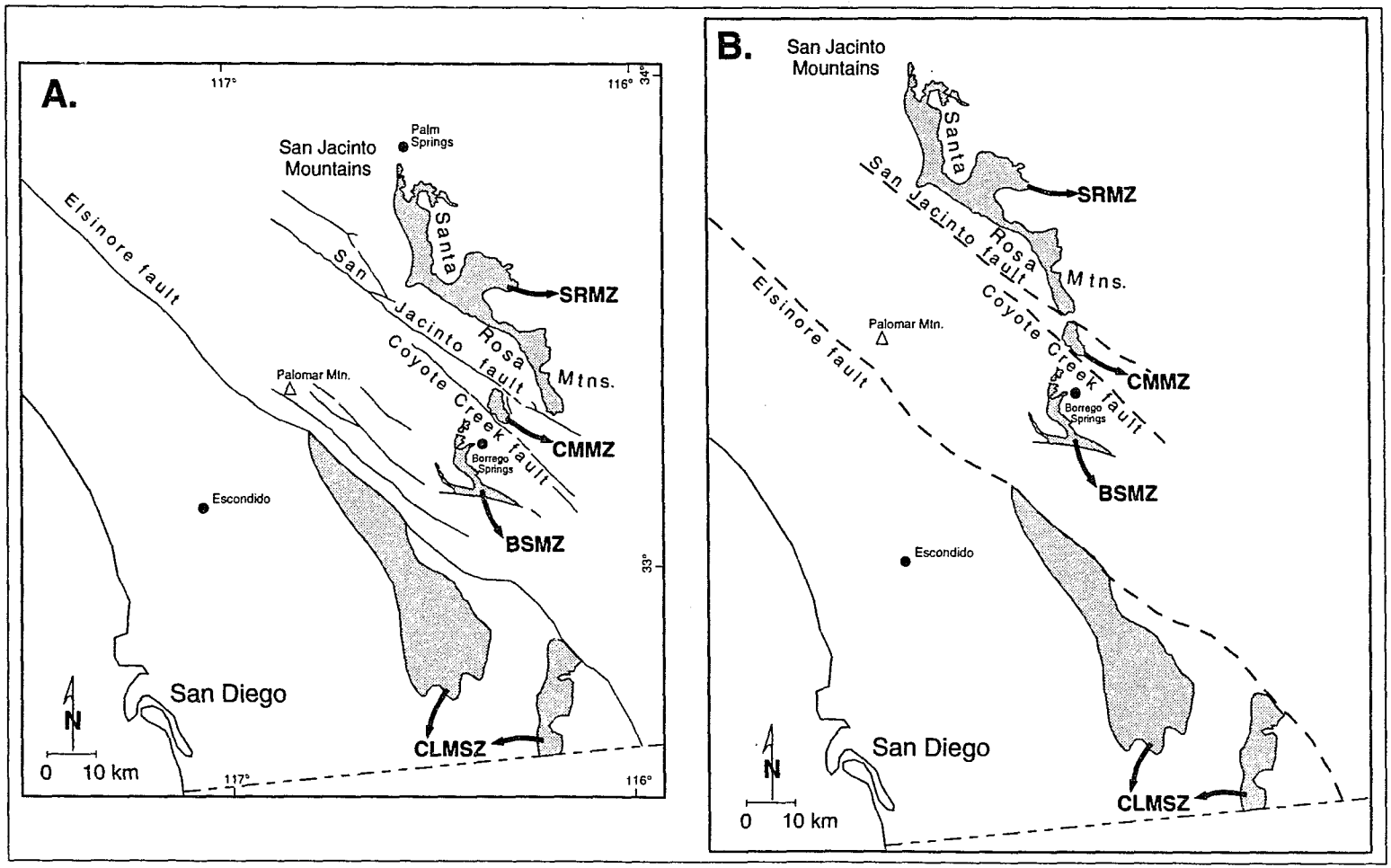

Figure 27. a) Present distribution of major ductile shear zones in the eastern Peninsular Ranges of southern California (stippled pattern). b) Palinspastic reconstruction of the shear zones after removing right-lateral separations along the Elsinore fault (~30 km, Sage, 1973), the San Jacinto fault (~19 km, Sharp, 1967), and the Coyote Creek fault (~5 km, Sharp, 1967). Abbreviations are as follows: SRMZ, Santa Rosa mylonite zone; CMMZ, Coyote Mountain mylonite zone; BSMZ, Borrego Springs mylonite zone; and CLMSZ, Cuyamaca Laguna Mountain shear zone. Modified from Sharp, 1967, Simpson, 1984, and Todd et al., 1988.

mylonite zone. Besides the overlapping timing relations, the two shear zones are also very similar in terms of lithology and structure. As with the SRMZ, there is evidence for east-over-west sense of movement along the Cuyamaca-Laguna Mountains shear zone (Grove, 1986; Clinkenbeard, 1987; Todd et al., 1988). There is also microstructural and mesoscopic structural data from an S-C mylonite that indicate down-to-the-east extension (Leeson, 1989; Leeson et al., 1989; Walawender et al., 1991). Both shear zones display evidence of ductile and brittle deformation that suggests emplacement into an evolving shear zone near the brittle-ductile transition (Hill, 1984, 1988; Todd et al., 1988). Also, the Cuyamaca-Laguna Mountains shear zone is bordered by the voluminous tonalites and granodiorites of the La Posta pluton (~1400 km^2), which are alike in terms of lithology, structure, and age (94 ± 2 Ma) to the 94-93 Ma tonalites and granodiorites in the San Jacinto Mountains. Walawender et al. (1991) speculated that the La Posta pluton was emplaced into a synbatholithic extensional zone (i.e. the Cuyamaca-Laguna Mountains shear zone), similar to the SRMZ.

Figure 27b shows a palinspastic map that restores the two major shear zones of the eastern Peninsular Ranges. After removing 30 km of late Neogene dextral slip along the Elsinore fault (Sage, 1973) and 24 km of dextral slip along the San Jacinto and Coyote Creek faults (Sharp, 1967), the Santa Rosa mylonite belt and the Cuyamaca-Laguna Mountains shear zone are oriented ~north-south. This strongly supports the notion that the two shear zones were kinematically related. These shear zones may be part of the larger mylonite belt, described by May (1989) as extending from the Transverse Ranges into the eastern Peninsular Ranges (Fig. 28). In turn this larger shear zone may extend northward into the Mojave Desert (May, 1989) and southward, as suggested by Sharp (1979), towards the tip of Baja California. Shown in Figure 28, taken from May (1989), is the distribution of basement terranes in southern California after palinspastic reconstruction of the San Andreas and older fault systems. Also shown in dark stippled

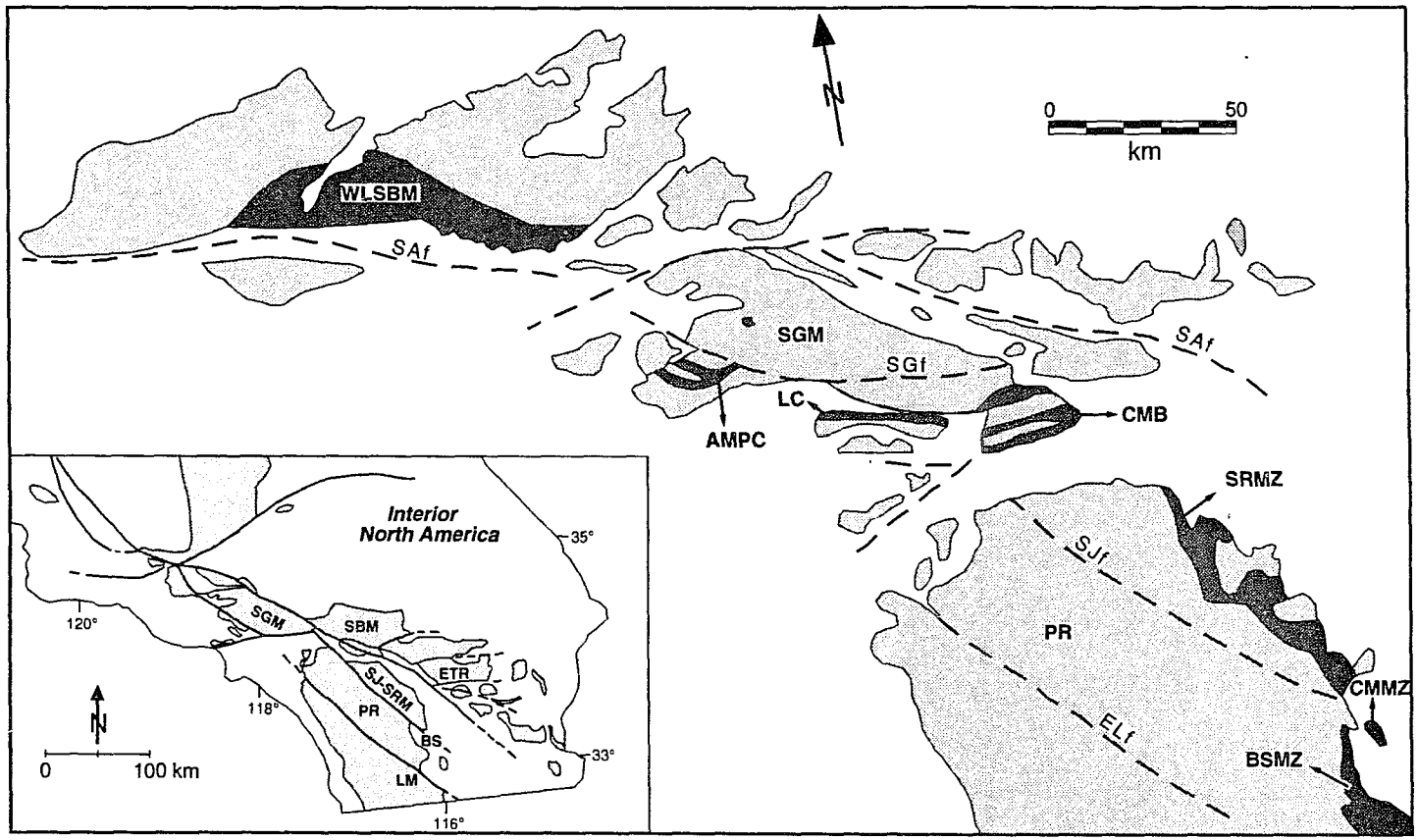

Figure 28: Palinspastic reconstruction of basement terranes (light stipple) and major ductile shear zones (dark stipple) in southern California (from May, 1989). Inset map shows the present locations of crystalline terranes and Cenozoic faults used in the reconstruction by May (1989). Abbreviations are as follows: SGM, San Gabriel Mountains; SBM, San Bernardino Mountains; ETR, eastern Transverse Ranges; PR, northern Peninsular Ranges; SJ-SRM, San Jacinto and Santa Rosa Mountains; BS, Borrego Springs; CLM, Cuyamaca-Laguna Mountains; WLSBM, mylonitic and cataclastic rocks of the western Little San Bernardino Mountains; AMPC, Alamo Mountain and Piru Creek shear zones; CMB, mylonitic belts in the Cucamonga region; LC, Limerock complex; SRMZ, Santa Rosa mylonite zone; CMMZ, Coyote Mountain mylonite zone; BSMZ, Borrego Springs mylonite zone; SAf, San Andreas fault; SGf, San Gabriel fault; ELf , Elsinore fault; and SJf, San Jacinto fault.

pattern is the distribution of the Late Cretaceous age mylonite zones, including the Santa Rosa mylonite belt. Deformation in all of these mylonites occurred under similar conditions and produced similar structures (May, 1989). Ductile deformation generally occurred under upper greenschist to amphibolite facies conditions, although commonly there is evidence for late-stage brittle deformation. Mylonitization was coeval with emplacement of upper Cretaceous granitic rocks, and locally post-dates intrusion. After the removal of net rotations of fault-bounded blocks in the Transverse Ranges, as indicated by studies of Luyendyk et al. (1980) and Hornafius et al. (1986), foliations and lineations from the various mylonites indicate west-vergent thrusting in directions from 270 to 235° (May, 1989, the latter value being the Santa Rosa mylonite belt). In the Cucamonga region (CMB) and in the Limerock Complex (LC) in the San Gabriel Mountains mylonitization occurred within major sinistral transcurrent shear zones along directions from 260 to 250° (May and Walker, 1989). These transcurrent fault systems have been interpreted as left-slip tear faults that offset major ductile thrusts in the Transverse Ranges from those in the eastern Peninsular Ranges (May, 1989; May and Walker, 1989).

CONCLUSIONS

1. Mylonites from the Borrego Springs mylonite zone (BSMZ) and Coyote Mountain mylonite zone (CMMZ) have amphibole that are strongly zoned with respect to Al_{total} (i.e. RA-26-E and RA-55-B). Core to rim increases in Al_{total}, when employing the Al-in-hornblende geobarometer of Schmidt (1992), indicate increased pressures of ~3 to 5 kb during mylonitization. This implies that ~10 to 18 km of crust were thrust to the west over the eastern margin of the Peninsular Ranges in Late Cretaceous time.

2. Application of the geothermometer of Blundy and Holland (1990) to the amphibole and plagioclase compositional data of a mylonite from Coyote Mountain (RA-26-E), indicate that temperature increased only slightly, if at all, during mylonitization. Amphibole rim temperatures, which represent conditions during mylonitization, range from ~740°-820°C, as opposed to core temperatures of ~720°-800°C. The absence of a large temperature increase during mylonitization is attributed to exhumation of the mylonite belt by extensional tectonic denudation following thrusting.

3. Thermobarometry results from the 94-93 Ma tonalites in the San Jacinto Mountains (i.e. footwall rocks of the Santa Rosa mylonite zone, SRMZ) suggest that they were emplaced following thrusting during extension and exhumation of the mylonite belt. They were emplaced at temperatures of 733°-759°C and pressures of ~4-5 kb, and were subsequently exhumed ~10-14.5 km.

4. A palinspastic reconstruction of major mylonite zones in the eastern Peninsular Ranges suggests a regional, Late-Cretaceous, north-south trending shear zone that includes both the Santa Rosa mylonite zone and the Cuyamaca-Laguna Mountains shear zone.

CHAPTER 4

FISSION-TRACK EVIDENCE FOR TILTING OF THE PENINSULAR RANGES BATHOLITH OF SOUTHERN CALIFORNIA: AN ALTERNATIVE TO LONG-DISTANCE NORTHWARD TRANSPORT

INTRODUCTION

Paleomagnetic directions from Mesozoic plutonic rocks of the Peninsular Ranges batholith of southern California are discordant with the expected Cretaceous magnetic field direction (Teissere and Beck, 1973; Hagstrum et al., 1985). Two models have been proposed to explain the difference between expected and observed directions. The model proposed by Teissere and Beck (1973) and Hagstrum et al. (1985) explain the data as indicative of ~25° of clockwise vertical-axis rotation and ~11° (~1200 km) of northward translation of the batholith with respect to cratonic North America during late Mesozoic and early Cenozoic time. This, however, is based on the assumption that present horizontal approximates paleohorizontal. Butler et al. (1991) questioned the validity of this assumption and proposed instead that the discordant directions are due to the tilting of the batholith. They argue, based on various geological evidence from previous studies, that the batholith has been tilted a minimum of 12°-15° to the southwest. They also stated the need for geochronologic data to define the tilt more accurately. The purpose of this study is to test this model by constraining the tilt.

REGIONAL SETTING

The study area is located in the northwestern Peninsular Ranges between Palomar Mountain and Escondido, California (Figs. 29 and 30). It includes a great diversity of plutonic rocks ranging from undersaturated gabbros to leucogranites (Miller, 1937; Larsen, 1948; Walawender and Smith, 1980; Gastil, 1983; Baird and Miesch, 1984; Silver and Chappell, 1988). Tonalites are the most abundant rock type, and low-K granodiorites the second most common (Larsen, 1948; Silver and Chappell, 1988).

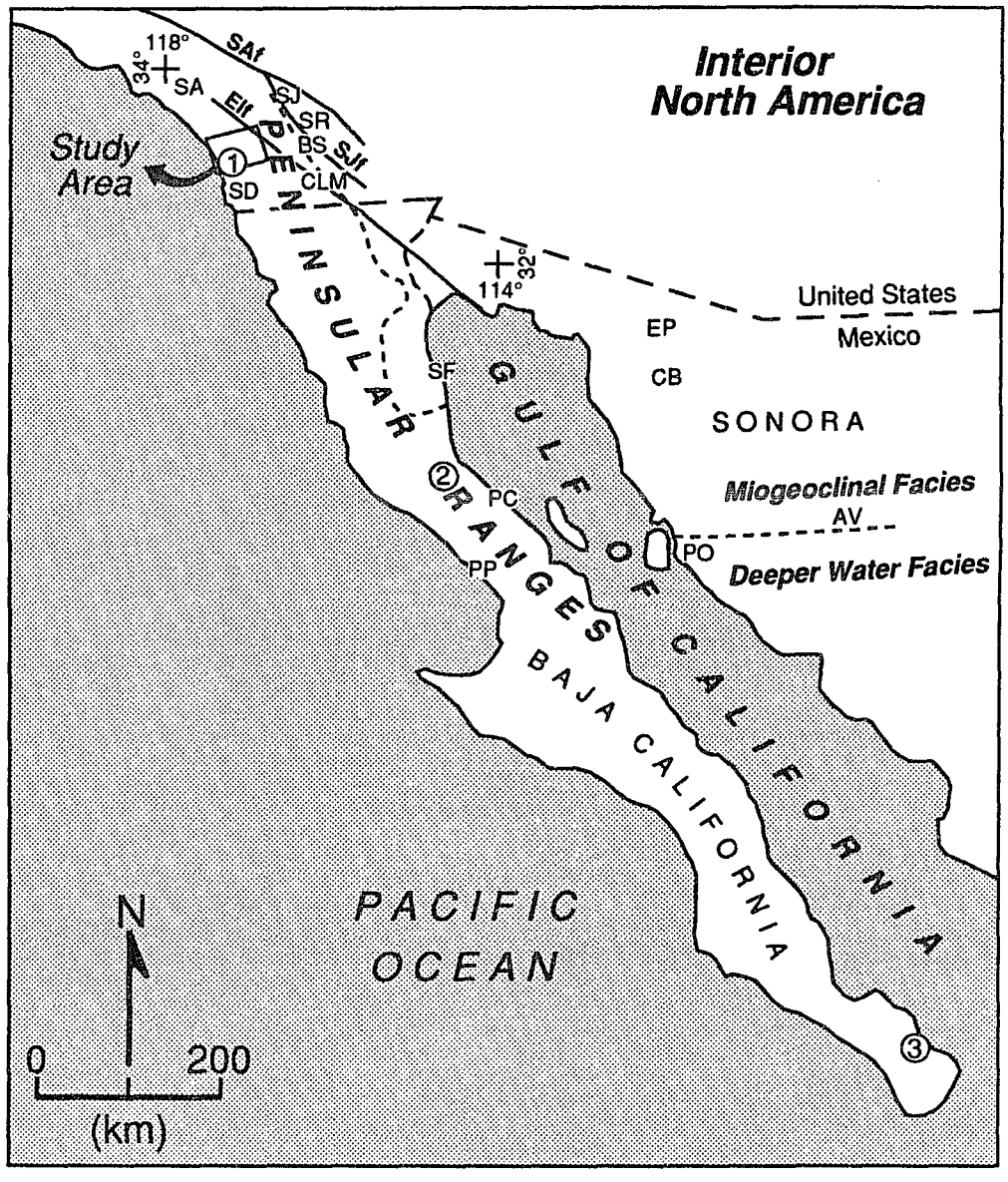

Figure 29. Map of of Baja and southern California showing location of the study area. Modified from Butler et al. (1991) and Gastil et al. (1991). Areas 1, 2, and 3 are paleomagnetic site locations of Hagstrum et al. (1985) and Teissere and Beck (1973) from the Peninsular Ranges batholith. The dashed line separates Paleozoic miogeoclinal facies from deeper water facies. The abbreviations are locations discussed in the text. They are as follows: SAf, San Andreas fault; SJf, San Jacinto fault; ELf, Elsinore fault; SA, Santa Ana Mountains; SJ, San Jacinto Mountains; SR, Santa Rosa Mountains; BS, Borrego Springs; CLM, Cuyamaca-Laguna Mountains (Coyote Mountains are just to the south); SD, San Diego; SF, San Felipe; EP, El Plomo; CB, Caborca; PC, Puerto Calamujue; PP, Punta Prieta; AV, Sierra Agua Verde; and PO, Punta Onah.

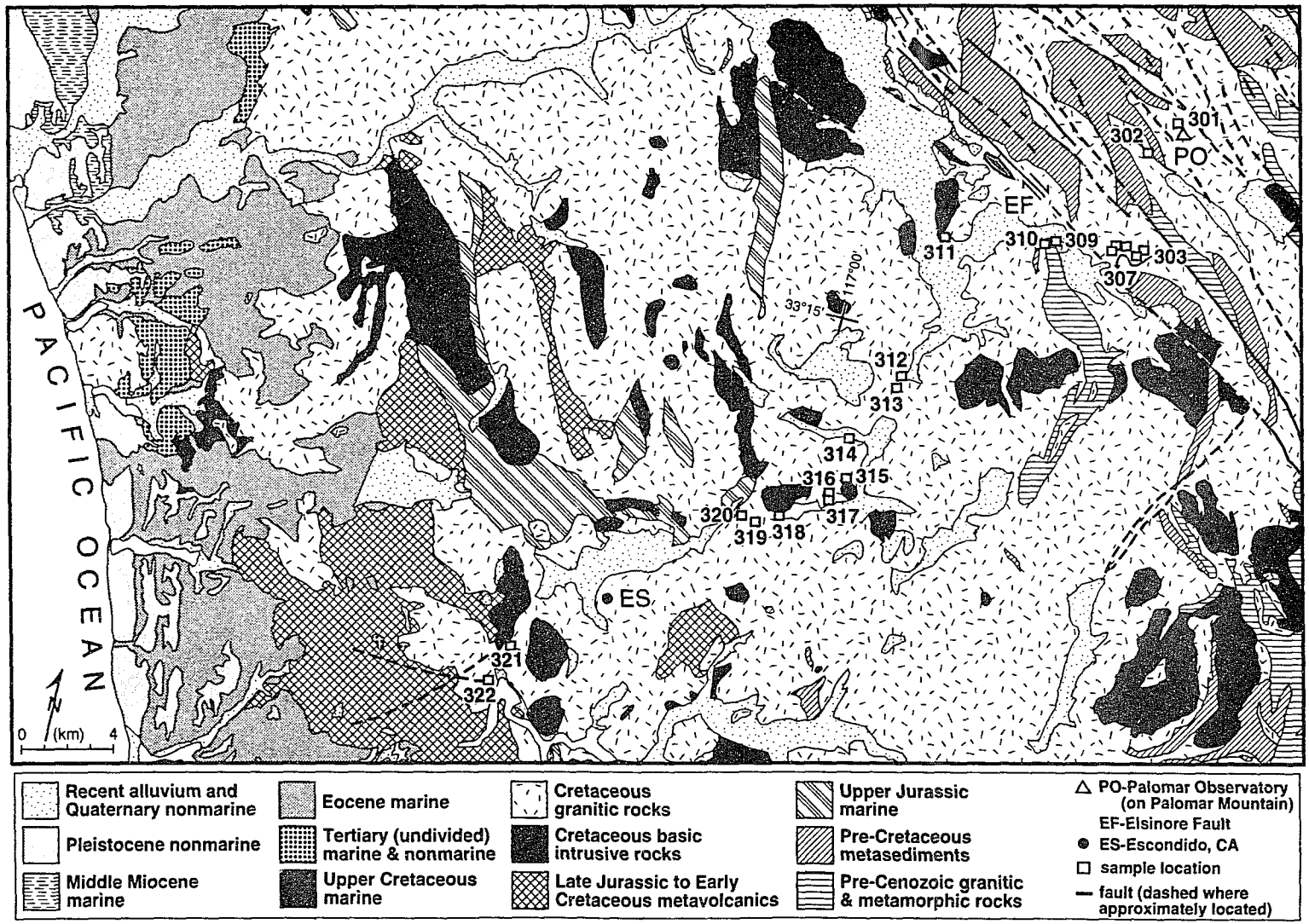

Figure 30. Geologic map of the study area shown in Figures 1 and 29. Modified from the Geologic Map of California, Santa Ana Sheet (Rodgers, 1965).

Samples collected for this study are tonalites and granodiorites (Table 10). Paleomagnetic data of Teissere and Beck (1973) and Hagstrum et al. (1985) in the vicinity of the study area are primarily from samples of the San Marcos gabbro (Fig. 29, location 1). Rocks of the San Marcos gabbro are widely variable in terms of composition and texture (Miller, 1937; Larsen, 1948; Walawender and Smith, 1980). They range in composition from gabbro norite to calcic olivine norite or quartz biotite norite.

Silver et al. (1979) divided the Peninsular Ranges batholith into *western* and *eastern* parts separated by a boundary that trends northwest to southeast along its center. This division is based on the distribution of emplacement ages for plutonic rocks. U-Pb zircon ages from the *western* batholith range from 140 to 105 Ma, with the majority between 120 and 105 Ma (Silver and Chappell, 1988; Silver et al., 1979). They are randomly distributed without any apparent west to east age gradient (Silver et al., 1979). Silver and Chappell (1988) interpreted this distribution as representing a static magmatic arc. The study area crosses the entire width of this western arc, and its eastern border is approximately coincident with the boundary between the *western* and *eastern* batholiths. A progressive decrease of the U-Pb zircon ages across the *eastern* batholith indicated to Silver et al. (1979) a transgressing arc that moved eastward between 105 Ma and 80 Ma. Walawender et al. (1990, 1991) presented an alternative static-arc model for development of the *eastern* batholith that occurs over a shorter time interval of between 98 Ma and 89 Ma. They base their model on additional age and isotopic data, and a slight repositioning of the age boundary of Silver et al. (1979).

Metamorphic grade generally increases from greenschist to upper amphibolite facies eastward across the northern Peninsular Ranges (Todd et al., 1988; Schwarcz, 1969; Todd and Shaw, 1979; Simpson, 1985). In the western part of the batholith the Santiago Peak Volcanics have undergone greenschist facies metamorphism that varies

Table 10: Location and Rock Type of Samples from Palomar Mountain-Escondido Study Area

Field #	Latitude	Longitude	Rock Type
301	33° 21' 32.4"	116° 52' 09.1"	tonalite
302	33° 20' 40.4"	116° 52' 44.2"	tonalite
303	33° 18' 22.9"	116° 52' 09.6"	tonalite
304	33° 18' 11.3"	116° 52' 16.8"	tonalite
305	33° 18' 18.1"	116° 52' 39.4"	tonalite
306	33° 18' 15.1"	116° 53' 00.3"	tonalite
307	33° 18' 10.4"	116° 53' 06.6"	tonalite
308	33° 18' 01.3"	116° 52' 59.7"	tonalite
309	33° 18' 05.7"	116° 54' 43.7"	tonalite
310	33° 17' 53.5"	116° 54' 55.0"	tonalite
311	33° 17' 24.2"	116° 57' 58.3"	tonalite
312	33° 14' 03.4"	116° 57' 54.4"	tonalite
313	33° 13' 43.4"	116° 57' 58.3"	tonalite
314	33° 12' 20.9"	116° 59' 01.0"	tonalite
315	33° 11' 20.7"	116° 58' 45.3"	granodiorite
316	33° 10' 50.1"	116° 59' 08.3"	granodiorite
317	33° 10' 41.0"	116° 59' 07.1"	granodiorite
318	33° 10' 07.3"	117° 00' 21.6"	granodiorite *
319	33° 09' 49.4"	117° 00' 57.0"	granodiorite *
320	33° 09' 50.6"	117° 01' 29.4"	granodiorite *
321	33° 05' 24.6"	117° 06' 49.3"	tonalite ¢
322	33° 04' 27.9"	117° 07' 14.9"	granodiorite $

Rock types of Larsen (1948); *Lake Wolford granodiorite,
¢ Green Valley tonalite, $ Escondido Creek leucogranodiorite

from the lowest to slightly higher-grade parts of the chlorite zone (Larsen, 1948; Jahns and Lance, 1950; Adams, 1979). The westernmost samples from this study are near a transition from greenschist to amphibolite facies. However, the majority of the samples lie within an andalusite + sillimanite-bearing amphibolite facies (Schwarcz, 1969; Berggren and Walawender, 1977; Todd and Shaw, 1979; Germinario, 1982). Studies on metamorphic reactions in the amphibolite facies rocks indicate peak temperatures and pressures of 600°-700°C and ~2-4 kb. Samples located to the east of the Elsinore fault (i.e. samples 301-308, see Fig. 30) may extend into a sillimanite-bearing amphibolite facies that continues into the eastern Peninsular Ranges (Todd et al., 1988).

Progressive changes in texture and deformational style eastward across the northern part of the batholith, in addition to the increase in metamorphic grade, indicated to Gastil (1975) an increase in depth of pluton emplacement from "shallow" in the west to "deep" in the east. The samples from the study area are located primarily within an "intermediate-depth" zone. Some of the westernmost samples fall in the shallow zone and those to the east of the Elsinore fault are located in the deep zone. Gastil (1975) observed that host rocks change progressively eastward across the batholith from fine-grained hornfels, slate, and phyllite to coarse-grained schist, gneiss, and amphibolite . The latter commonly show multiple foliations, and little preservation of premetamorphic fabric. In the west plutons have irregular outlines, crosscutting relationships, and textures that indicate shallow emplacement. Plutons of the intermediate-depth zone are subcircular in outline with concentric internal structures, and are 5-10 km in exposed diameter. Plutons of the eastern Peninsular Ranges, such as those in the San Jacinto Mountains or the La Posta pluton in the Cuyamaca-Laguna Mountains area, are larger and have internal and external foliations that are concordant with adjacent metamorphic screens (Gastil, 1975; Todd and Shaw, 1979; Hill, 1984; Walawender et al., 1990).

Recent geobarometry studies on amphibole from plutonic rocks sampled across the batholith support the proposed eastward increase in the depth of exposure. The geobarometer is based on an empirical calibration of the variation in aluminum content of amphibole with pressure in calc-alkaline rocks (Hammarstrom and Zen, 1986; Hollister et al., 1987; Johnson and Rutherford, 1989; Schmidt, 1992). Pressures calculated using the geobarometer are pressures of crystallization, and in the northern Peninsular Ranges they vary systematically from west to east. Ague and Brimhall (1988) reported a 1.0 to >6.0 kb progressive increase in pressure across the batholith, corresponding to an increase in depth of crystallization of 4 to >23 km. Smith et al. (1991) found several more local gradients, but still their reported pressures are low in the west and higher in the east. From the western edge of the batholith to the Elsinore fault they found that pressures averaged 3 kb (11 km). From the Elsinore fault zone to the San Jacinto fault pressures increased from 3-4 kb (11-15 km) to 6.0 kb (23 km). East of the San Jacinto fault pressures were lower at 4 kb (15 km) but again increased to 5 kb (19 km) in the southern San Jacinto Mountains. George et al. (1991) determined similar pressures of 4-7 kb (15-26 km) across the San Jacinto Mountains in an east-west direction (chapter 3). In the region between San Diego, California and the Laguna Mountains to the east, Todd et al. (1991) found that pressures increased from ~2 kb in the Early Cretaceous volcano-plutonic complex in the west to ~6 kb for Late Cretaceous plutons in the east.

The distribution of K-Ar ages across the northern Peninsular Ranges batholith has been interpreted as indicating southwest tilting of the batholith (Butler et al., 1991). The ages generally become younger to the east, which indicated to Butler et al. (1991) that tilting uplifted the more deep-seated granitic rocks of the eastern Peninsular Ranges after earlier cooling in the western part of the batholith. K-Ar ages from the northern Peninsular Ranges have been reported in studies by Morten (1969), Everden and Kistler (1970), Armstrong and Suppe (1973), Krummenacher et al. (1975), Dalrymple (1976),

and Smith et al. (1991). The majority of the ages are for hornblende and biotite, which have closure temperatures of 530° ± 40°C (Harrison and McDougall, 1980) and 345°C (Harrison et al., 1985, cooling at 100°C/Ma), respectively. The K-Ar ages from these studies, excluding Smith et al. (1991), were determined before introduction of a set of decay constants by Steiger (1977). Therefore, in the following review of K-Ar ages the original values are followed in parentheses by converted ages corrected according to Dalrymple (1979). Biotite K-Ar ages, as reported in Krummenacher et al. (1975), decrease eastward in a regular manner from ~115 to 65 Ma (~118 to 67 Ma) across the Peninsular Ranges in southern California. In the study by Smith et al. (1991) biotite ages decrease from 128 Ma on the west side of the batholith to 60 Ma east of the Santa Rosa mylonite belt in the Palm Springs area. They observed a steepening of the age gradient eastward from the western edge of the batholith to the central Perris block; the Perris block is bounded by the San Jacinto and Elsinore fault zones (Fig. 29). From the central Perris block into the western San Jacinto Mountains the gradient is gentle, but then steepens eastward towards the Santa Rosa mylonite belt. Hornblende K-Ar ages also decrease across the batholith, but in a less regular manner (Krummenacher et al., 1975). They range from ~140 Ma in the west to 65 Ma along the eastern margin of the batholith (~143 to 67 Ma).

$^{40}Ar/^{39}Ar$ K-feldspar ages have been reported for samples along the boundary separating the *western* and *eastern* batholiths of the Peninsular Ranges, as defined by Silver et al. (1979). The ages range from 87 to 95 Ma for plutonic rocks of the *western* batholith in the Cuyamaca and Laguna Mountains (Grove and Harrison, 1992). In nearby plutons of the *eastern* batholith, the ages are tightly clustered at 72-78 Ma. K-feldspar, $^{40}Ar/^{39}Ar$ age closure temperatures (300°-120°C, McDougall and Harrison, 1988) are comparable to those of fission-track ages for common minerals (350°-70°C, see *Interpretation of Fission-Track Data*, this chapter).

Fission-track age data for the northern Peninsular Ranges, not including this study, are limited to the northeastern part of the batholith. Studies in the San Jacinto Mountains (George and Dokka, in review; chapter 2) and Santa Rosa Mountains (Dokka, 1984) indicate major cooling events in the eastern Peninsular Ranges at ~92 Ma, ~76 Ma, and ~62 Ma. The oldest event is interpreted as representing cooling during synextensional emplacement of tonalitic plutons, and the latter two as rapid cooling during regional uplift and erosion.

The distribution of U-Pb and K-Ar ages across the batholith indicates an eastward increase in discordance between emplacement and cooling ages (Krummenacher et al., 1975; Silver et al., 1979; Gastil, 1983). Discordance of 20-30 m.y. occurs along the central and eastern portions of the batholith in the northern Peninsular Ranges, and has been interpreted as a region of maximum uplift and erosion (Krummenacher et al., 1975; Gastil, 1983). Regional uplift and erosion of the ancestral Peninsular Ranges during Late Cretaceous time resulted in the deposition of large volumes of coarse unroofing debris into the adjacent forearc basin to the west (Minch, 1979). In the westernmost part of the study area and in the vicinity of San Diego to the south the unroofing debris rests unconformably on the metavolcanic and plutonic rocks of the batholith. These coarse sediments, designated the Lusardi Formation, are considered alluvial fan deposits of Turonian(?) age (Nordstrom, 1970; Peterson, 1971). Stratigraphically overlying the Lusardi Formation are shelf and deep-marine fan deposits of the Point Loma and Cabrillo Formations of Campanian to Maastrichtian age (Peterson and Nordstrom, 1970; Nilsen and Abbott, 1981; Girty, 1987; Bannon et al., 1989). Near San Diego and in the western part of the study area Eocene fluvial and submarine fan sediments overlie the Late Cretaceous sediments forming a low-angle unconformity (Kennedy and Moore, 1971; Link et al., 1979; Lohmar et al., 1979). The unconformity is characterized by a thick weathering profile at a number of localities in peninsular California (Abbott et al.,

1976). Basal Eocene conglomerates above the unconformity contain distinctive clast types derived from northwestern Sonora (Merriam, 1979; Minch, 1979; Abbott and Smith, 1978, 1989).

Between 28 and 26 Ma the ridge crest separating the Pacific and North American plates arrived at the trench at some location off southern California or northern Baja California (Atwater, 1970; Stock and Molnar, 1988; Atwater, 1989). From the first arrival of the ridge crest until about 5.5 Ma the southern California and northernmost Baja California region, including the study area, was a "connection zone" between a southern offshore boundary of the North American and Pacific plates and onshore motion of the San Andreas transform system (Atwater, 1989). This connection zone was a right step in a right-lateral system, i.e. an extensional "releasing bend" as defined by Crowell (1974). Extension related to the San Andreas transform system in Miocene time was concentrated to the north and west of the study area (Atwater, 1989). To the east and southeast, extension along the western edge of the Basin and Range province was taking place in the eastern Peninsular Ranges (Wallace and English, 1982) and in northeastern Baja and coastal Sonora (Karig and Jensky, 1972; Gastil and Krummenacher, 1977; Gastil et al., 1979; Dokka and Merriam, 1982; Stock and Hodges, 1989). At ~5.5 Ma the locus of deformation along the San Andreas system shifted inland to the present-day Gulf of California as Baja California was transferred to the Pacific plate (Atwater, 1989). It was at this time, with the opening of the Gulf of California, that the northern Peninsular Ranges began the 300 ± 10 km NNW translation along the San Andreas system to their present positions (Crowell, 1962; Atwater, 1970; Atwater, 1989). Figure 31 is a pre-Neogene, palinspastic tectonic restoration by Gastil et al. (1991) that shows the location of the Peninsular Ranges prior to translation.

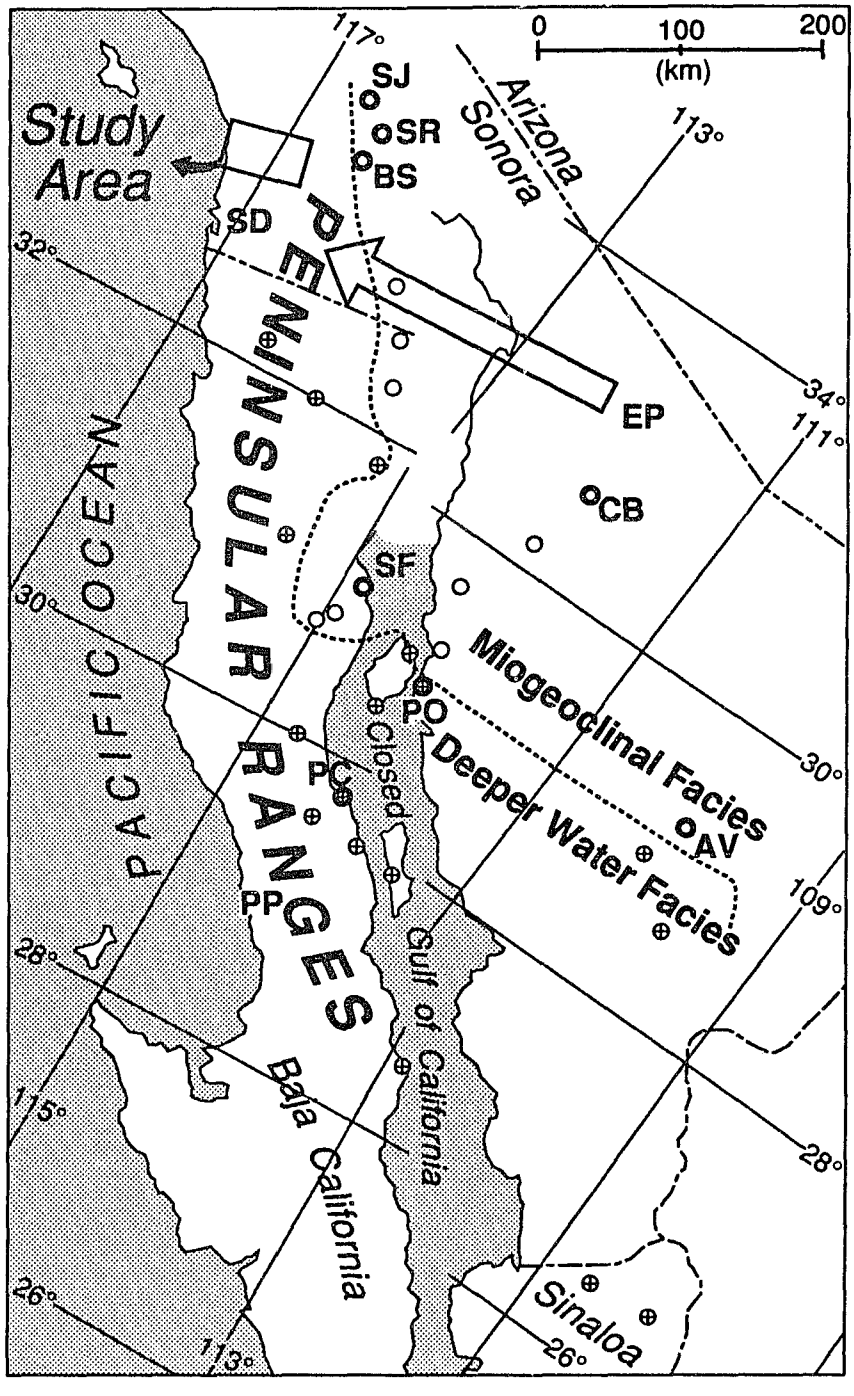

Figure 31. Map of peninsular California and adjacent Sonora after removing 300 km of right-lateral motion along the San Andreas system. Open circles are exposures of Paleozoic miogeoclinal strata, and those with crosses represent outcrops of deeper water facies. Location names are abbreviated, and are listed in the explanation for Figure 1. The large arrow indicates the transport direction of Poway Conglomerates from Sonora into the San Diego area in Eocene time. Modified from Gastil et al. (1991).

ANALYTICAL PROCEDURES

Samples of tonalite and granodiorite were collected for fission-track analysis along a northeast to southwest transect between Palomar Mountain and Escondido, California over a distance of ~40 km. Sample locations are given in Table 10 and shown in Figure 30. Separates of apatite and zircon, and in some cases sphene, in the size range of 62-250 μm were recovered from crushed and pulverized rock using a concentration table, non-toxic heavy liquids (sodium polytungstate and lithium metatungstate), and a Frantz magnetic separator (see appendix A for a more detailed description of methods used in this study). All minerals were dated using the external detector method (Naeser, 1976), following procedures described in Dokka et al. (1986). Apatite samples were also prepared for track length measurements according to methods outlined by Green (1981) and Laslett et. al. (1982). Track lengths were measured using an optical microscope (1500x) linked by way of a camera lucida to a digitizing pad and microcomputer. Ages were calculated by the "zeta" method of Hurford and Green (1983) using National Bureau of Standards Fission-track Glasses 962 and 963a and coupled muscovite detectors; these standards have been calibrated using apatite and zircon from the Fish Canyon tuff. Statistical uncertainty for all age determinations was calculated by the method of Johnson et al. (1979). A chi-square test at the 5% level was applied to all age data as proposed by Galbraith (1981).

INTERPRETATION OF FISSION-TRACK DATA

Fission-track thermochronology can closely constrain the timing of tectonic events that involve rapid cooling due to uplift and erosion or tectonic denudation (Dodge and Naeser, 1968; Wagner et al., 1977; Dokka and Lingrey, 1979; Harrison et al., 1979; Zeitler et al., 1982; Parrish, 1983; Dokka, 1984; Dokka et al., 1986; Fitzgerald and Stump, 1991; Hurford et al., 1991; George and Dokka, in review). As a rock is displaced towards the earth's surface, i.e. exhumed, it cools through a series of specific

temperatures where individual mineral systems dated by the fission-track method become stable (Dodson, 1973). The closure temperature concept is typically employed in the interpretation of fission-track data (Dodson, 1973, 1979; Wagner et al., 1979)

Fission-track closure temperatures are mineral specific and positively correlated to cooling rates (Dodson, 1973). For sphene it is believed to be between 250° and 350°C (Naeser and Faul, 1969). Estimates of the closure temperature for zircon range from 175°C (Harrison et al., 1979) to 240° ± 50°C (Hurford, 1986). Zeitler et al. (1982) estimated closure temperatures of ~285° and ~235°C for sphene and zircon, respectively, from rocks of the northwestern Himalaya that were rapidly uplifted and cooled (at rates of ~10 to 100°C/Ma). Laboratory studies and data from deep boreholes indicate that for apatite annealing takes place over a wide range of time-temperature conditions (Naeser and Faul, 1969; Wagner and Reimer, 1972; Mark et al., 1973; Naeser and Forbes, 1976; Zimmerman and Gaines, 1978; Gleadow and Duddy, 1981; Watt and Durrani, 1985; Green et al., 1986; Donelick et al., 1990), and is supported by mathematical modeling of track annealing (Zimmerman and Gaines, 1978; Bertagnolli et al., 1983; Crowley, 1985; Laslett et al., 1987; Duddy et al., 1988; Jones and Dokka, 1990). However, for geologically significant time periods (>10^5 yr.) complete annealing occurs between ~100° and 150°C (Naeser, 1979; Naeser, 1981). A closure temperature of ~120°C from Dokka et al. (1986), based on a cooling rate of 40°C/Ma, is used in this study.

A crustal block that cools through a set of horizontal isotherms will have fission-track ages distributed as a series of horizontal "apparent age surfaces" (Wagner et al., 1977; Jones and Dokka, 1986). If cooling is gradual, such as in a case of slow uplift, the distance between age surfaces will be small. In contrast, if cooling is rapid the distance between age surfaces will be large; if very rapid, ages will be concordant within a vertical column of rock, the thickness of which depends on the amount of exhumation.

Rapid episodic uplift, with each event affecting a relatively thick section of crust, will produce similar ages within each crustal section. Any post-cooling deformation of the apparent age surfaces or crustal slabs will be superimposed on the initial distribution of the fission-track ages. For example, curviplanar age surfaces suggest post-cooling folding, inclined age surfaces suggest structural tilting, and large age differences between nearby samples may indicate faulting (Jones and Dokka, 1986).

RESULTS

Fission-Track Ages

Sample locations from Figure 30 were projected onto a N36.5°E line and are plotted with respect to elevation in Figure 32. The maximum relief along the 40 km sampling transect is 1520 m. Fission-track age data for apatite are given in Table 11 and displayed in Figures 32 and 33. In the northeast, samples 301 to 313 have similar mean ages that range from 73.9 to 81.9 Ma. To the southwest of sample 313, the mean ages increase gradually from 82.3 to 88.8 Ma for samples 314 to 318. Apatite ages are oldest in the southwest at 95.8 and 95.2 Ma for samples 320 and 322, respectively. Fission-track age data for zircon are given in Table 12, and show the same pattern as the apatite ages with equivalent ages in the northeast and a progressive increase beyond sample 313 to the southwest (Figs. 32 and 33). In the northeast zircon ages range from 74.8 to 79.9 Ma, and southwest of sample 313 they increase from 82.8 to 89.6 Ma for samples 314 to 319. Sample 318 (Zr = 92.2 Ma) deviates from this regular increase, however, and is closer in age to sample 322 (Zr = 93.0 Ma) farthest to the west. A limited amount of fission-track age data for sphene are given in Table 13 and shown in Figures 32 and 33. The ages range from 100.3 to 95.1 Ma, and become older to the west.

The combined distribution of the fission-track ages, along with their 2 σ error bars, are plotted with respect to distance in Figure 33. The ages of zircon and apatite mineral pairs for each sample are concordant. This indicates that each sample experienced rapid

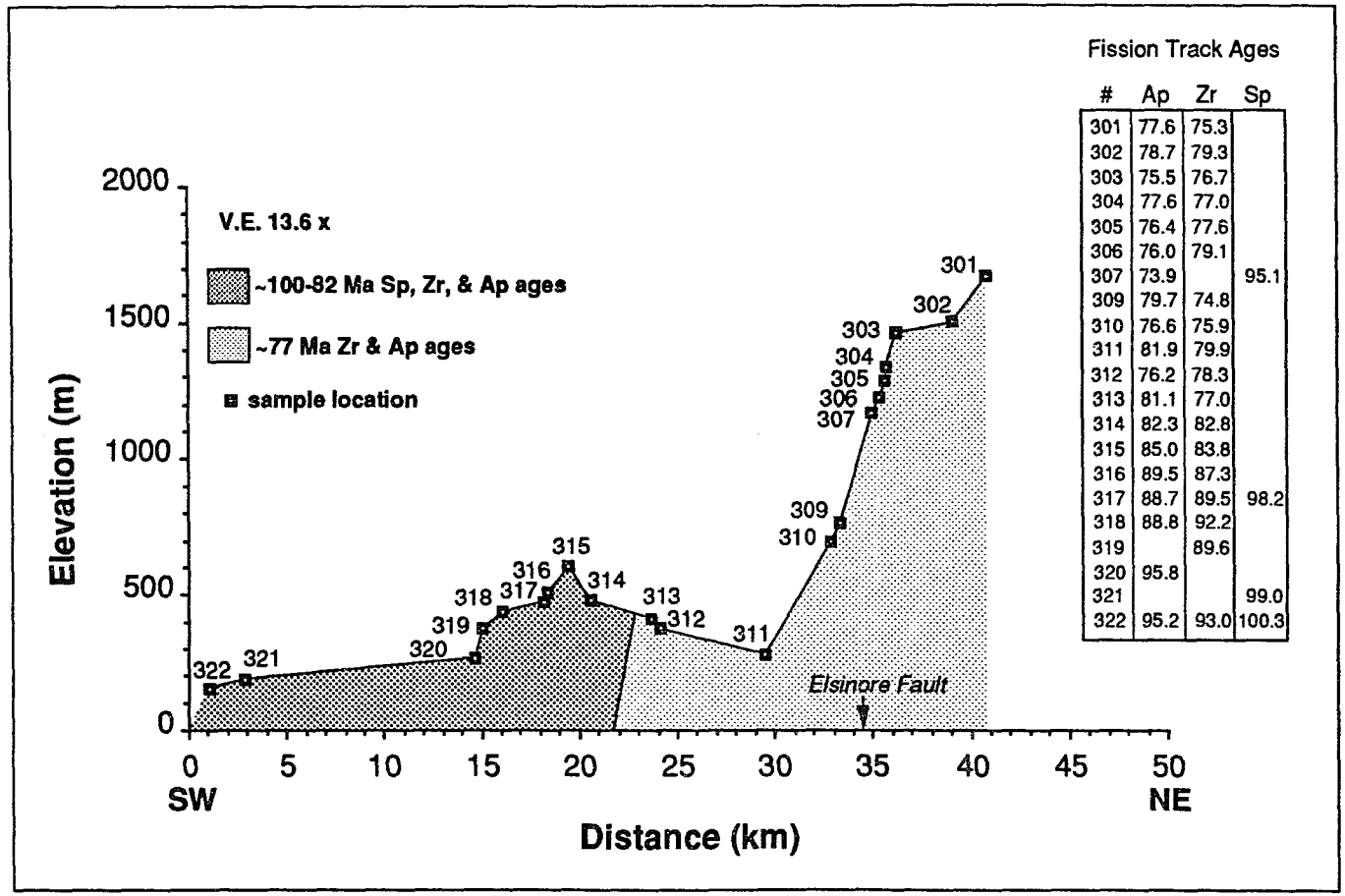

Figure 32. Sphene, zircon, and apatite fission-track ages are given here along with their respective sample locations, which have been projected onto a N36.5°E line between Palomar Mountain and Escondido, California. The line separating ~77 Ma ages from ~100-82 Ma ages dips to the southwest at 21°, with a vertical exaggeration of ~13.6. Also shown is the position of the Elsinore fault (between samples 307 and 309), along which there has been both right-lateral (~30 km, Sage, 1973) and vertical separation (Larsen, 1948).

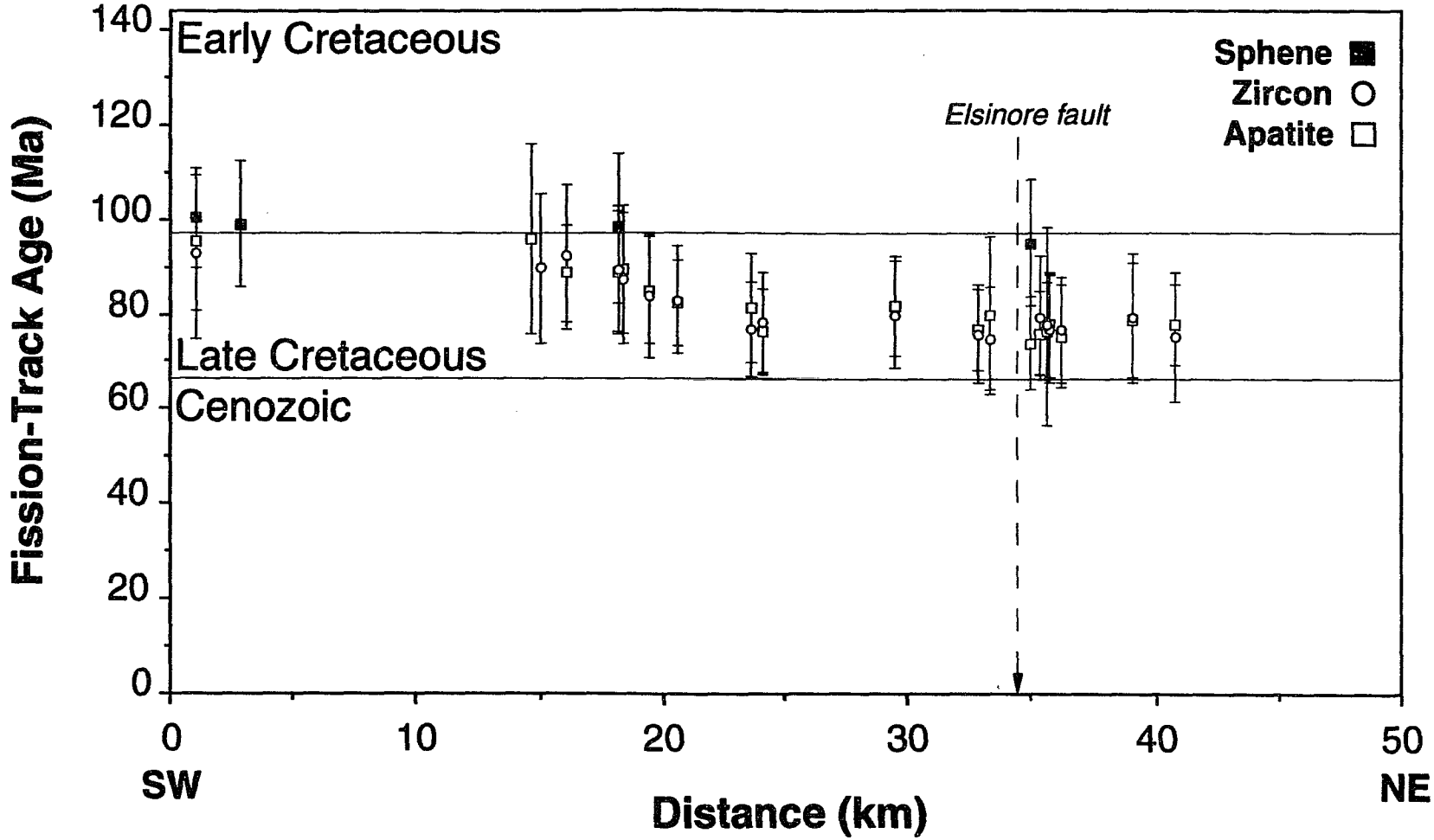

Figure 33. The fission-track ages, along with their respective 2 sigma error bars, are plotted here against distance along the N36.5°E line of sampling. Ages to the northeast indicate a major cooling event at ~77 Ma. Those towards the southwest progressively increase to ~100 Ma, suggesting that fission-track age surfaces are tilted to the southwest.

Table 11. Apatite Fission-Track Data from Palomar Mtn. to Escondido, CA

Field # [Lab #]	Elevation meters	Spontaneous Track Density tracks/cm2 [tracks counted]	Induced Track Density tracks/cm2 [tracks counted]	Standard Track Density tracks/cm2 [tracks counted]	Grains Counted	Chi-Square Statistic [X2]$	Correlation Coefficient*	Age [Ma]#	±1 sigma [Ma]
301 [910044]	1672	2.495E+06 [534]	7.229E+06 [1547]	4.231E+04 [2009]	6	3.002	0.970	77.6	4.3
302 [910074]	1506	1.006E+06 [310]	2.812E+06 [866]	4.140E+04 [2015]	7	3.340	0.991	78.7	5.5
303 [910030]	1463	1.610E+06 [301]	4.802E+06 [898]	4.239E+04 [2009]	6	1.052	0.973	75.5	5.3
304 [910024]	1341	1.080E+06 [298]	3.116E+06 [860]	4.215E+04 [2009]	5	2.065	0.954	77.6	5.5
305 [910035]	1289	8.444E+05 [331]	2.480E+06 [972]	4.223E+04 [2009]	7	2.756	0.963	76.4	5.2
306 [910041]	1228	2.479E+06 [481]	7.330E+06 [1422]	4.228E+04 [2009]	7	4.022	0.938	76.0	4.4
307 [910040]	1170	1.650E+06 [340]	4.903E+06 [1010]	4.130E+04 [2015]	6	0.596	0.989	73.9	4.9
309 [910028]	765	8.397E+05 [131]	2.327E+06 [363]	4.154E+04 [2015]	4	1.805	0.877	79.7	8.3
310 [910032]	695	1.620E+06 [512]	4.759E+06 [1504]	4.236E+04 [2009]	8	8.017	0.926	76.6	4.3
311 [910042]	280	2.824E+06 [384]	7.713E+06 [1049]	4.213E+04 [2009]	6	1.868	0.990	81.9	5.2
312 [910039]	375	2.276E+06 [446]	6.679E+06 [1309]	4.210E+04 [2009]	6	4.696	0.914	76.2	4.5
313 [910025]	411	2.021E+06 [295]	5.582E+06 [815]	4.218E+04 [2009]	6	1.559	0.970	81.1	5.8
314 [910037]	482	2.248E+06 [517]	6.035E+06 [1388]	4.158E+04 [2015]	7	5.002	0.990	82.3	4.6
315 [910029]	604	2.445E+06 [357]	6.336E+06 [925]	4.145E+04 [2015]	6	2.654	0.968	85.0	5.6
316 [910038]	506	7.354E+05 [264]	1.836E+06 [659]	4.207E+04 [2009]	10	5.374	0.824	89.5	6.8
317 [910026]	472	2.119E+06 [284]	5.246E+06 [703]	4.135E+04 [2015]	5	2.084	0.995	88.7	6.5
318 [910033]	442	3.897E+06 [491]	9.619E+06 [1212]	4.126E+04 [2015]	7	0.922	0.988	88.8	5.1
320 [910043]	268	1.229E+06 [134]	2.862E+06 [312]	4.204E+04 [2009]	5	1.261	0.995	95.8	10.1
322 [910034]	152	1.781E+06 [276]	4.135E+06 [641]	4.167E+04 [2015]	7	1.802	0.939	95.2	7.2

$ X2 value according to Galbraith (1981) for n degrees of freedom (n is number of grains minus 1); all samples pass at 5% level

* comparison between individual crystal track counts

calculated according to Hurford and Green (1983) using a zeta value of 10692

Table 12. Zircon Fission-Track Data from Palomar Mtn. to Escondido, CA

Field # [Lab #]	Elevation meters	Spontaneous Track Density tracks/cm2 [tracks counted]	Induced Track Density tracks/cm2 [tracks counted]	Standard Track Density tracks/cm2 [tracks counted]	Grains Counted	Chi-Square Statistic [X2]$	Correlation Coefficient*	Age [Ma]#	±1 sigma [Ma]
301 [910008]	1672	1.247E+07 [449]	5.000E+06 [180]	1.815E+05 [2116]	5	0.767	0.984	75.3	6.8
302 [910010]	1506	1.182E+07 [532]	4.533E+06 [204]	1.829E+05 [2116]	6	1.291	0.909	79.3	6.8
303 [910011]	1463	4.571E+06 [736]	1.807E+06 [291]	1.823E+05 [2116]	7	2.997	0.977	76.7	5.6
304 [910015]	1341	8.384E+06 [721]	3.291E+06 [283]	1.817E+05 [2116]	7	0.808	0.969	77.0	5.7
305 [910016]	1289	1.347E+07 [202]	5.333E+06 [80]	1.848E+05 [2116]	4	0.453	0.998	77.6	10.4
306 [910004]	1228	1.217E+07 [572]	4.723E+06 [222]	1.846E+05 [2116]	7	0.655	0.981	79.1	6.5
309 [910022]	765	6.151E+06 [732]	2.462E+06 [293]	1.800E+05 [2116]	8	1.116	0.995	74.8	5.4
310 [910018]	695	3.549E+06 [834]	1.434E+06 [337]	1.844E+05 [2116]	6	1.072	0.955	75.9	5.2
311 [910007]	280	8.489E+06 [798]	3.245E+06 [305]	1.835E+05 [2116]	6	0.655	0.965	79.9	5.6
312 [910009]	375	5.889E+06 [901]	2.275E+06 [348]	1.819E+05 [2116]	6	0.899	0.976	78.3	5.2
313 [910021]	411	6.038E+06 [942]	2.346E+06 [366]	1.798E+05 [2116]	6	0.704	0.995	77.0	5.0
314 [910005]	482	5.890E+06 [907]	2.123E+06 [327]	1.796E+05 [2116]	6	0.368	0.996	82.8	5.6
315 [910017]	604	1.240E+07 [657]	4.453E+06 [236]	1.811E+05 [2116]	7	0.681	0.963	83.8	6.6
316 [910006]	506	8.309E+06 [673]	2.889E+06 [234]	1.827E+05 [2116]	5	0.605	0.992	87.3	6.9
317 [910020]	472	1.458E+07 [802]	4.964E+06 [273]	1.833E+05 [2116]	7	1.601	0.883	89.5	6.6
318 [910013]	442	7.888E+06 [631]	2.650E+06 [212]	1.864E+05 [2116]	7	0.891	0.993	92.2	7.6
319 [910003]	378	8.903E+06 [552]	2.984E+06 [185]	1.806E+05 [2116]	6	0.720	0.994	89.6	7.9
322 [910014]	152	7.377E+06 [450]	2.426E+06 [148]	1.842E+05 [2116]	8	2.241	0.853	93.0	9.0

$ X2 value according to Galbraith (1981) for n degrees of freedom (n is number of grains minus 1); all samples pass at 5% level

* comparison between individual crystal track counts

calculated according to Hurford and Green (1983) using a zeta value of 335

Table 13. Sphene Fission-Track Data from Palomar Mtn. to Escondido, CA

Field # [Lab #]	Elevation meters	Spontaneous Track Density tracks/cm2 [tracks counted]	Induced Track Density tracks/cm2 [tracks counted]	Standard Track Density tracks/cm2 [tracks counted]	Grains Counted	Chi-Square Statistic [X2]$	Correlation Coefficient*	Age [Ma]#	±1 sigma [Ma]
307 [910049]	1170	6.500E+06 [923]	2.113E+06 [300]	1.860E+05 [2116]	6	1.673	0.968	95.1	6.6
317 [910055]	472	3.849E+06 [689]	1.207E+06 [216]	1.854E+05 [2116]	6	1.146	0.954	98.2	8.0
321 [910054]	189	9.817E+06 [1070]	3.000E+06 [327]	1.821E+05 [2116]	7	1.402	0.967	99.0	6.6
322 [910060]	152	8.114E+06 [1858]	2.424E+06 [555]	1.804E+05 [2116]	9	12.528	0.860	100.3	5.3

$ X2 value according to Galbraith (1981) for n degrees of freedom (n is number of grains minus 1); all samples pass at 5% level

* comparison between individual crystal track counts

calculated according to Hurford and Green (1983) using a zeta value of 335

cooling from above the closure temperature of zircon (240° ± 50°C) to below that for apatite (~120°C). As discussed, zircon and apatite ages increase together southwest of sample 313. However, in the northeastern half of the study area samples 301 to 313 show no correlation of apatite and zircon ages with respect to location. The distribution of some 23 ages has a mean of 77.5 Ma with a standard deviation of 2.0 Ma. Also, the overlap of their 2 σ error bars is between 71.5 Ma and 83.8 Ma, with a midpoint at 77.6 Ma. The relatively narrow distribution of ages suggests that these rocks experienced a common cooling event at ~77.5 Ma. The occurrence of a major cooling event in the northern Peninsular Ranges at this time is supported by other fission-track ages ~50 km to the east in the San Jacinto Mountains (Figs. 29 and 3). There a minimum of 2.3 km of crust was rapidly cooled at ~76 Ma due to surface uplift. This uplift is correlated with an increase in plate convergence at the onset of the Laramide Orogeny (George and Dokka, in review; chapter 2). $^{40}Ar/^{39}Ar$ K-feldspar ages of 72-78 Ma from the Cuyamaca-Laguna Mountains area (Grove and Harrison, 1992) add additional support to the notion of regional cooling in the Peninsular Ranges at ~77-76 Ma.

In the southwestern half of the study area the systematic variation of zircon and apatite ages suggests rapid cooling in the study area between ~95 and 82 Ma. Sphene ages from the westernmost part of the study area indicate that cooling may have begun as early as ~100 Ma.

As discussed in Wagner et al. (1977) and Wagner and Reimer (1972), the expected distribution of fission-track ages for a coherent crustal block that has been slowly exhumed is to have the oldest ages at the highest elevations with a systematic decrease towards lower elevations. If exhumation is large, and also rapid enough, then all the ages will be the same (e.g. George and Dokka, in review; chapter 2). In this study ages increase, rather than decrease, with decreasing elevation. This enigma can be explained

by a westward tilting of the batholith, whereby samples 301 to 313 are part of a thick west-dipping crustal slab of rocks with a thermal history common to that of the San Jacinto Mountains to the east. Lying structurally above, and also dipping to the west, are a series of apparent age surfaces representing the older, ~100 to 82 Ma period of cooling discussed above.

Apatite Track-Length Distributions

The size distribution of fission tracks in apatite provides an independent measure of the cooling history of a sample (Fleischer et al., 1965; Nand Lal et al., 1976). For example, in slowly cooled granitic terranes track-length distributions are negatively skewed with mean track-lengths of 12-13μm and standard deviations of 1.2-2.0μm (Gleadow et al., 1986). In contrast, rapidly cooled granitic terranes have normal to positively skewed distributions with mean lengths >14.0μm and standard deviations between 0.8 and 1.2μm. The difference in these types of distributions is a function of the amount of time spent at temperatures where annealing takes place. In apatite this is a temperature interval between ~70 and 130°C (Naeser, 1979; 1981). Track-length distributions from the study area have mean lengths that range from 13.7 to 14.4μm with standard deviations between 0.7 and 1.0μm (Fig. 34). These values are comparable to those of rapidly cooled granitic terranes (Dokka et al., 1986; Gleadow et al., 1986), including those from the San Jacinto Mountains to the east (George and Dokka, in review; chapter 2). Mean track-lengths show no correlation with respect to elevation or distance along the sampling transect (Fig. 35) These results support the interpretation of the fission-track age data by providing independent evidence of rapid cooling of the batholith in the study area in Late Cretaceous time.

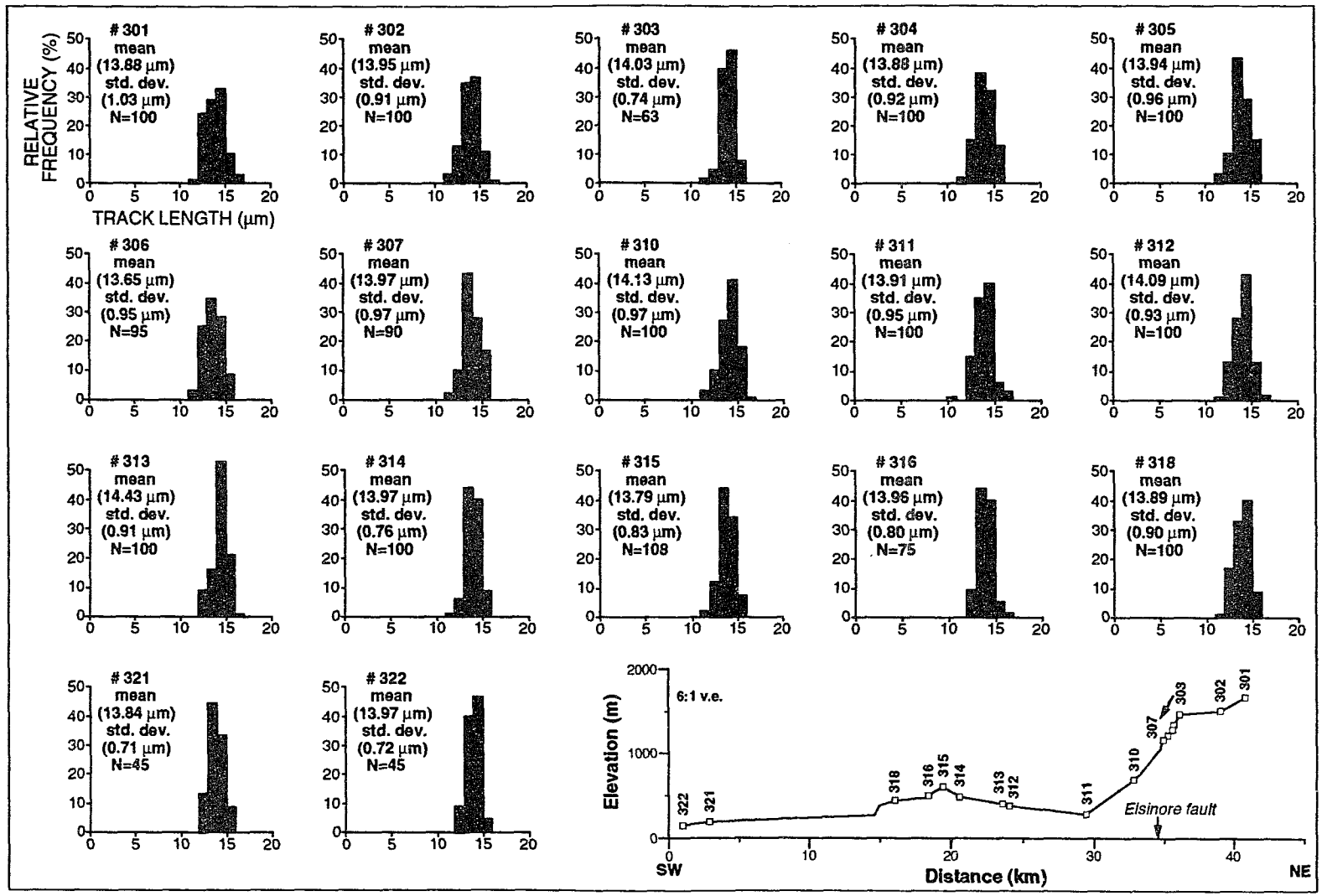

Figure 34. Frequency distributions of confined fission-tracks in apatite from samples in the study area have means of 13.7 to 14.4 μm with standard deviations of 0.7 to 1.0 μm, which are typical of those from rapidly cooled basement terranes. Their respective sample locations along the line of sampling are given in the inset.

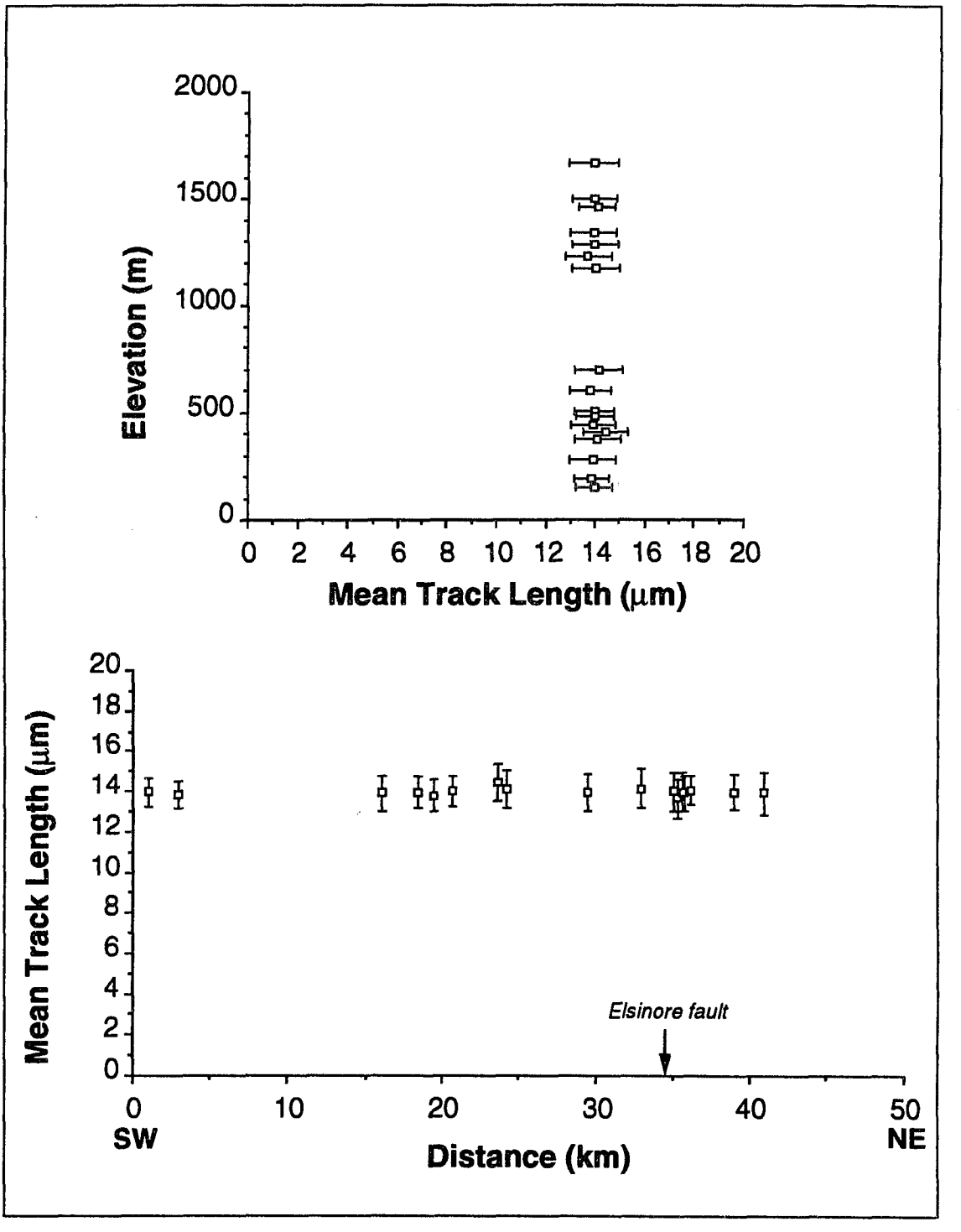

Figure 35. Mean-track lengths of apatite plotted against elevation and distance along the line of sampling show no correlation, suggesting that all of the samples experienced rapid cooling in Late Cretaceous time.

DISCUSSION

Discordant paleomagnetic directions from the Peninsular Ranges batholith have been interpreted as indicating long-distance northward translation of batholith with respect to cratonic North America (Teissere and Beck, 1973; Hagstrum et al., 1985). However, geologic correlations across the Gulf of California, involving Late Precambrian to Eocene age rocks, indicate that peninsular California was adjacent to Sonora until the development of the San Andreas transform system (Gastil et al., 1991). This is supported by paleomagnetic data from Eocene sedimentary rocks (Flynn et al., 1989) and Miocene volcanic rocks (Hagstrum et al., 1987) of Baja, California. The distribution of fission-track ages across the study area indicates that the batholith is tilted to the southwest. Southwest tilting, as proposed by Butler et al. (1991), explains the discordant paleomagnetic data without invoking long-distance northward translation of the peninsula. The following is a discussion of the geologic data from this study and previous work that support tilting.

Paleomagnetic Data from the Peninsular Ranges Batholith

The first study to report discordant paleomagnetic directions for peninsular California was that of Teissere and Beck (1973) from plutonic rocks of the Peninsular Ranges batholith. The majority of the directions were from the San Marcos Gabbro, which crops out in the western part of the batholith, although some sample sites were in tonalites and granodiorites (Fig. 29, location 1). Their results from 18 stable sites yielded an average direction of magnetization of 49.5°, and 3.0° (inclination, declination) and a mean paleomagnetic pole of 85.5°N, 22.5°E (latitude, longitude). Teissere and Beck (1973) found no correlation between magnetic directions and sample locations, meaning that sample sites have not been significantly rotated relative to one another. Also, the site-mean directions form a tight circular group, indicating that no significant movement of the pole relative to the sampling area occurred during magnetization

(Teissere and Beck, 1973). Teissere and Beck (1973) reported an 11.5° and 26° difference in inclination and declination, respectively, between their directions and the expected Cretaceous direction of Beck and Noson (1972). They accounted for these results by clockwise vertical-axis rotation and lateral translation during transform faulting between the North American and Pacific plates.

Hagstrum et al. (1985) reported paleomagnetic directions from 14 sites in the San Marcos Gabbro (Fig. 29, location 1), some of which were site locations of Teissere and Beck (1973). They also sampled mafic and felsic plutonic rocks from the Baja California Peninsula (locations 2 and 3). Their results indicated a stable high-T_b (blocking temperature) component of magnetization for these rocks, which was inferred to be a primary thermoremanent magnetization. The average direction of magnetization is 49.2°, and 8.3° (inclination, declination). Site-mean directions for the sample sites, when plotted, also show no significant difference between their paleomagnetic poles (Hagstrum et al., 1985). Hagstrum et al (1985) interpreted their results as indicating ~11° of post-Cretaceous (but pre-15 Ma) northward latitudinal transport of peninsular California relative to interior North America.

Butler et al. (1991) combined the paleomagnetic data of Teissere and Beck (1973) and Hagstrum et al. (1985) from a total of 32 sites, and determined a mean direction of 48.7°, and 5.9° (inclination, declination) with a 95% confidence limit of 3.0°. The revised expected Cretaceous magnetic field direction for peninsular California, based on the mid-Cretaceous paleomagnetic pole for North America (Globerman and Irving, 1988), is 60.8 ± 4.2°, and 340.5 ± 6.6° (inclination, declination). Assuming that the structural attitude of the batholith has not changed through time, the difference between expected and observed paleomagnetic directions indicates ~11° northward translation and ~25° clockwise vertical-axis rotation of the batholith relative to cratonic North America (Butler et al., 1991).

Geologic Correlations Between Peninsular California and Mainland Mexico

The proposed long-distance northward translation and accompanying rotation of peninsular California conflicts with geologic correlations between mainland Mexico and the peninsula (Butler et al., 1991; Gastil et al., 1991). Lithologic and paleontologic correlations in rocks ranging in age from Precambrian to Eocene are more compatible with the post ~5.5 Ma, 300 ± 10 km of north-northwest translation along the San Andreas transform system (Figs. 29 and 31; Gastil et al., 1991). Paleozoic and older correlations include Precambrian(?) to lower Ordovician shallow-water carbonates and siliciclastic strata in the northeastern Peninsular Ranges and similar rocks of Precambrian to Mississippian age in northwestern Sonora (Gastil et al., 1986). Anderson (1982) correlated ultrapure quartzite, carbonate rocks, and fine grained siliciclastics from the east coast of Baja California near San Felipe (SF) with the upper Precambrian-lower Cambrian section of the Caborca (CB) in Sonora. Both areas also include basalts at the base of the Cambrian section (Anderson, 1982). In the Coyote Mountains (CLM) of southern California Early Ordovician carbonate rocks have been correlated to strata of similar age in the Sierra Agua Verde (AV) of central Sonora (Miller and Dockum, 1983; Gastil et al., 1986). In the eastern part of the peninsula near Puerto Calamujue (PC) deep-water siliceous strata of Devonian to Carboniferous age can be correlated across the gulf island-by-island onto the coast of Sonora immediately south Punta Onah (PO, Gastil and Miller, 1984). Also shown in Figures 29 and 31 is the boundary that separates the Paleozoic miogeoclinal rock from deep-water slope and basinal strata to the south and west (Gastil et al., 1986). The boundary is offset by ~300 km in a right lateral sense, which is consonant with slip attributed to the San Andreas transform system. Any larger latitudinal displacements, such as suggested by the paleomagnetic data from plutonic rocks of the batholith, would involve a large post-

Paleozoic translation to the south followed by a large post-Early Cretaceous returning displacement to the north.

Deep-water siliciclastics of upper Triassic to middle Cretaceous age crop out in the western and central parts of the peninsula, and are composed of both volcanic and non-volcanic, cratonic detritus (Gastil and Miller, 1984). They were deposited in a northwest-southeast trending basin bordered on the west by the Alistos arc and the North American craton to the east. Probable source areas for the volcaniclastic sediments are the Alistos arc (Gastil and Miller, 1984) and scattered volcanic terranes in coastal Sonora (Anderson and Silver, 1969) and eastern Sonora (King, 1939; Rangin, 1982). Recognizable non-volcanic detritus in Triassic and Jurassic strata were derived from cratonic rocks to the east (Gastil and Miller, 1984). A palinspastic restoration of post-Miocene offsets along the San Andreas transform system by Gastil and Miller (1984) places these flysch deposits adjacent to Sonoran source rocks. This supports the notion that peninsular California was adjacent to Sonora in the Mesozoic, as it was during Paleozoic time. Additional support comes from the trends of compositional belts and the distribution of isotopic ages for Mesozoic and early Cenozoic granitic rocks of peninsular California and northwestern Mexico. After restoring the peninsula to its pre-Gulf of California position, Gastil (1983) observed that magmatic rocks from six north-northwest trending compositional belts extend continuously from peninsular California into coastal Mexico. He found a similar continuous distribution of K-Ar isochrons. U-Pb isotopic ages for zircon from the batholith also display an apparent continuous distribution from southern California into northwestern Sonora. (Silver et al., 1975; Silver et al., 1979).

The northern Peninsular Ranges were adjacent to Sonora in Eocene time, based on provenance studies of exotic clasts in conglomerates from the Poway Group of southern California (Abbott and Smith, 1978, 1989; Merriam, 1979; Minch, 1979). Rhyolite

clasts from fluvial and alluvial fan conglomerates of the Poway Group are chemically and petrographically similar to the Jurassic-age Imuris Volcanics of northwestern Sonora (Woodford et al., 1968; Merriam, 1972; Abbott and Smith, 1978; Minch, 1979). Specifically, Late Jurassic rhyolites exposed 13 km west of El Plomo (EP, Figs. 29 and 31) in Sonora have identical trace element compositions as clasts from an alluvial fan of the Poway group in San Diego County, California (Abbott and Smith, 1989). Palinspastic restoration of peninsular California to its pre-Gulf of California position places the alluvial fan deposits directly west of the Sonoran source area (Minch, 1979; Abbott and Smith, 1989). The two areas are connected by a linear exposure of the Ballena Gravels, which contain a high percentage of the exotic Poway-type clasts (Minch, 1979). An ~300 km long Ballena river transported the exotic clasts from Sonora to fluvial and alluvial fan systems in the San Diego area (see large arrow, Fig. 31).

Paleomagnetic Data from Tertiary Sedimentary and Volcanic Rocks of Baja, California

Paleomagnetic data from early Eocene marine and continental strata in central Baja California (Flynn et al., 1989), and Miocene volcanic rocks from the Baja California Sur (Hagstrum et al., 1987) also indicate that peninsular California was next to Sonora in Eocene and Miocene time. Paleomagnetic inclinations of intertonguing marine (Bateque Formation) and continental (Las Tetas de Cabra Formation) strata of middle Early Eocene age from the Punta Prieta area (PP, Figs. 29 and 31) are very close to the expected inclination (± 47.8°) for the present site latitude (Flynn et al., 1989). Flynn et al. (1989) interpreted the concordant inclinations as indicating that there has been no significant post-Early Eocene northward translation of Baja California. This is supported by their study of mammalian fauna from the Las Tetas de Cabra Formation, that is "remarkably similar" to other United States Wasatchian faunas and unlike those of Central America. Also, the majority of the molluscan taxa (82%) from the marine

sediments are equivalent to others found along the North American west coast (Flynn et al., 1989). Paleomagnetic data from volcanic rocks of Baja California Sur, which span Miocene time, indicate that the Baja Peninsula was in its pre-Gulf of California position adjacent to mainland Mexico from at least early Miocene time until the Pliocene opening of the Gulf (Hagstrum et al., 1987). A paleomagnetic pole based on 64 virtual geomagnetic poles for these rocks (86.1°N, and 142.6°E, with a 95% confidence limit of 3.9°) is similar to a reference pole for the North American craton (87.4°N, and 129.7°E, with a 95% confidence limit of 3.0°), and therefore indicates that peninsular California was just west of Sonora during Miocene time.

In summary, numerous geologic correlations across the Gulf of California, as well as concordant Eocene and Miocene paleomagnetic data, place peninsular California adjacent to Sonora from Late Precambrian to Miocene time. It appears that the peninsula has only experienced ~2° of northward translation and ~8° of clockwise vertical-axis rotation in conjunction with the opening of the Gulf of California (Larsen, 1972; Mammerickx and Klitgord, 1982). Therefore, the discordant paleomagnetic directions from the plutonic rocks of the batholith need to be reconciled with this evidence, and an alternative mechanism to explain the former is required.

Geologic Evidence for Southwest Tilting of the batholith

Butler et al. (1991) presented an alternative interpretation of the paleomagnetic data from the batholith that does not involve long-distance northward transport of peninsular California. They showed that southwest tilting of the batholith by 21° about an axis with an azimuth of 320° causes observed paleomagnetic directions to become parallel with the expected Cretaceous direction for the peninsula. There is abundant geological evidence that support this proposed tilting of the batholith. As discussed in *Regional Setting* metamorphic grade and depth of pluton crystallization increase west to east across the northern Peninsular Ranges. Also, K-Ar ages for both biotite and hornblende decrease

eastward across the batholith. These trends can be explained by a southwesterly tilt of the batholith that exposes progressively greater structural levels towards the east (Butler et al., 1991). Butler et al. (1991) estimated a tilt of 12-15° about a NNW axis, based on pressures of crystallization from Ague and Brimhall (1988). Using pressures from only the western part of the batholith, they further estimated a tilt of 16 ± 4° about an axis of 340 ± 10°. The areal distributions of U-Pb and K-Ar ages from the western half of the batholith were also used by Butler et al. (1991) to estimate a tilt for the batholith. They calculated a minimum tilt of 12-15° assuming a paleogeothermal gradient of 30°-35°C/km and K-Ar closure temperatures of 250°C for biotite and 525°C for hornblende.

Ague and Brandon (1992) estimated tilts of 19 ± 5.4° about an axis of 340 ± 5.5° for the western half of the batholith, and 15 ± 3.3° about an axis of 341 ± 7.9° in the eastern Peninsular Ranges. These estimates are based on Al-in-hornblende geobarometry of Ague and Brimhall (1988), supplemented by additional crystallization pressures. They consider the western and eastern parts of the batholith to have been tilted as two separate, but coherent crustal blocks. They further state that the data imply the existence of a major NW-SE trending fault with 7 km of dip separation cutting through the central part of the batholith. The proposed fault corresponds to the boundary that defines the *western* and *eastern* batholiths of Silver et al. (1979), as well as with various other structural and compositional discontinuities (Todd et al., 1988).

For the plutons in the vicinity of the study area total Al for amphibole increases by 0.5 formula units over a distance of 25 km to the northeast (Ague and Brimhall, 1988). Using the recent experimental calibration by Schmidt (1992) of the Al-in-hornblende barometer, this equates to an increase in pressure of crystallization of 2.4 (± 0.6 kb). Assuming a crustal density of 2.7 g/cm^3 this corresponds to an increase in the depth of emplacement of 9.0 ± 2 km. To bring those plutons to a common, approximately horizontal plane (i.e. the present erosional surface) requires a tilt of 20 ± 5° to the

southwest about an axis of 330°, which is in close agreement with the amount of tilt needed to achieve statistical concordance between observed and expected paleomagnetic directions in the batholith (i.e. 21 ± 5° about an axis of 320 ± 10°; Butler et al., 1991).

Evidence for Tilting of the Batholith based on Fission-Track Data from the Study Area

The fission-track ages from the study area, as discussed in *Results*, generally increase to the west. Also, instead of the ages becoming younger with decreasing elevation, as expected for a crustal block that is vertically uplifted, they are progressively older (Figs. 32 and 33). These data imply that the fission-track apparent age surfaces have been tilted to the southwest. The amount of tilt, however, can not be precisely determined. A wide range of possible attitudes for the age surfaces can be drawn based on the data in Figure 32. In addition, the relatively large errors characteristic of fission-track analysis add to the uncertainty. What can be said is that the tilts estimated by other independent geological data are compatible with the distribution of the fission-track ages.

The interpretation of southwest tilting of the batholith, based on the distribution of fission-track ages across the study area, assumes that the apparent age surfaces were initially horizontal; i.e. they formed during exhumation through a series of approximately horizontal isotherms. The fission-track ages indicate cooling of the study area through the closure temperatures of sphene, zircon, and apatite between ~100 and 77 Ma. During this period magmatism was located in the eastern Peninsular Ranges (i.e. between ~99 and 89 Ma; Silver et al., 1979; Walawender et al., 1990, 1991), and the western portion of the batholith is considered to have been inactive (Silver and Chappell, 1988). Therefore, in the absence of magmatic activity, the isotherms were assumed to be approximately horizontal during exhumation of the study area in Late Cretaceous time.

Possible Thermal and Paleomagnetic Consequences of Tilting a Batholith; Arguments Against Southwest Tilting

A recent study by Beck (1992) considers the thermal and paleomagnetic consequences of tilting a batholith. He argues that the tilting of a large batholith would necessarily produce unequal paleomagnetic directions from rocks sampled parallel to the direction of tilt. This is based on geometrical constraints that place the rocks currently exposed at the surface at progressively greater depths, and therefore temperatures, towards the region of maximum uplift prior to tilting (Fig. 36). Rocks closest to the hinge region, i.e. an area of minimum uplift, would lie above the critical isotherm for acquisition of thermoremanent magnetism (i.e. lie within zone M). Rocks located at increasingly greater depths away from the hinge region would lie within a zone of partial magnetization (zone P), and finally in a zone where temperatures are too high to permit magnetization (zone U). Samples from zone M acquire their primary paleomagnetic directions prior to tilting, those from zone P have remnant magnetizations acquired prior to and during tilting, and samples from zone U are magnetized as they pass through zone P until reaching the M/P boundary. As a consequence of tilting, samples from different initial depths become magnetized at different times, and as a result paleomagnetic directions across the batholith are unequal (Beck, 1992). The positions of the critical isotherms that delimit the M/P and P/U boundaries are partly a function of cooling and uplift rates. Slow cooling is considered to significantly lower magmatic blocking temperatures in igneous rocks (T_B) and batholiths typically cool slowly (Beck, 1992). This moves the M/P boundary closer to the surface, and increases the width of zone P to an estimated 300-650°C interval (Beck, 1992). With the M/P boundary closer to the surface, there is a greater probability for unequal magnetizations across the batholith. The effect of rapid uplift and denudation associated with tilting is to raise the temperature of the upper crust, which moves critical isotherms closer together and nearer

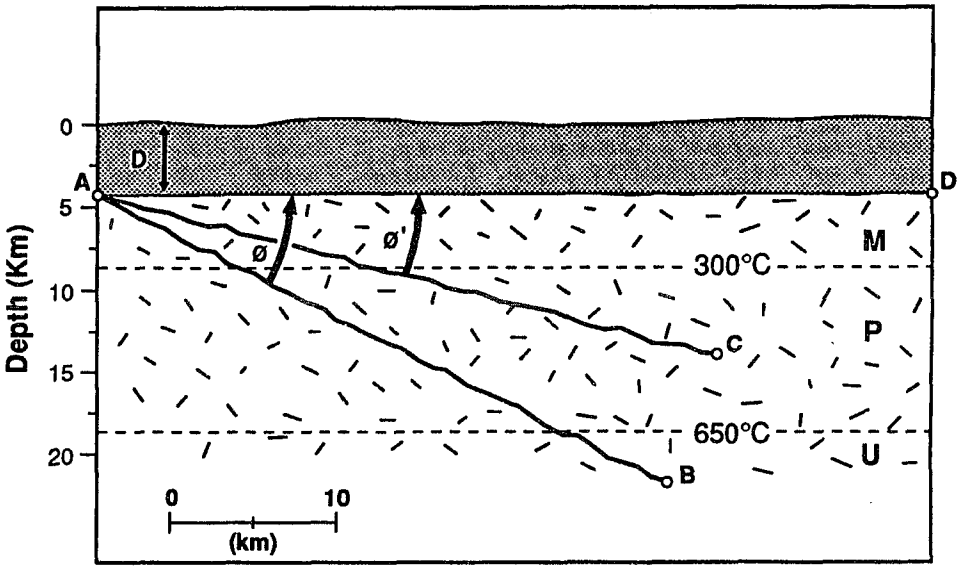

Figure 36. Possible thermal and paleomagnetic consuquences of tilting a batholith. A model by Beck (1992) showing that tilting of a batholith produces unequal paleomagnetic directions in rocks sampled parallel to the direction of tilt. D is overburden, U is a zone in which temperatures are too high to permit magnetization (i.e. above the Curie temperature), in zone P rocks are partially magnetized, and in zone M rocks are magnetized. Lines AB, AC, and AD represent a surface that is progressively rotated during tilting (e.g. from ø to ø').

to the surface. This delays acquisition of magnetization until tilting is nearly complete and, again, increases the likelihood that paleomagnetic directions will differ across the batholith (Beck, 1992).

It is proposed here that the geobarometry and thermochronology data from the western part of the batholith indicate these rocks were above the M/P boundary before tilting occurred. As discussed in *Regional Setting* the majority of the U-Pb ages for the *western* batholith are between 120 and 105 Ma (Silver et al., 1979; Silver and Chappell, 1988). This includes several ages (119, 111, and 104 Ma) from quartz gabbros located to the east of San Diego. Similar quartz gabbros of the San Marcos Gabbro have been described by Larsen (1948) in the study area, and are probably time equivalent to these in the south. Although no U-Pb zircon ages for the type "San Marcos Gabbro" in the study area have been published, Dalrymple (1976) reported hornblende and biotite K-Ar ages of ~113 to 108 Ma (corrected according to Dalrymple, 1979). For all samples with hornblende and biotite mineral pairs, ages are concordant and indicate rapid cooling from above 530° ± 40°C to below ~345°C (Dalrymple, 1976). Silver et al. (1979) also reported several concordant hornblende and biotite K-Ar ages, in their study of gabbroic to tonalitic plutons east of San Diego. Cooling was especially rapid in the western part of the study area where contact relations and metamorphic mineral assemblages indicate shallow emplacement (Gastil, 1975; Todd et al., 1988). Therefore, there is evidence that the San Marcos Gabbro, from which the majority of the discordant paleomagnetic directions for the northern Peninsular Ranges batholith are derived, cooled rapidly soon after emplacement. Because of this rapid cooling, the critical temperature defining the M/P boundary must have been greater than the estimate of Beck (1992). Instead of the boundary being located at the 300°C isotherm, the rocks must have been magnetized nearer the 580°C Curie temperature for magnetite (titanomagnetite is the dominant magnetic mineral in the *western* batholith; Hagstrum et al., 1985). In support of a

higher blocking temperature, Hagstrum et al. (1985) found that samples of the San Marcos Gabbro have a single component of magnetization that is removed between 10 and 100 mT, or primarily between 500 and 590°C. Assuming a paleogeothermal gradient of 35°C/km (typical of active orogenic belts), the 580°C isotherm would have been at a depth of ~16.5 km. The geobarometry data of Ague and Brimhall (1988) indicate that rocks of the *western* batholith crystallized at progressively greater depths from ~8 to 17 km across the study area to the east (recalculated using the geobarometer of Schmidt, 1992). This places all rocks very near or above the M/P boundary at the time of crystallization. In addition, the K-Ar cooling ages of Dalrymple (1976) place the San Marcos Gabbro well within zone M at ~113-108 Ma. Primary magnetization must have occurred relatively soon after crystallization, and before tilting, as a result of rapid cooling through the blocking temperature of titanomagnetite based on these data. Finally, perhaps the strongest evidence for the rocks currently exposed at the surface being within zone M prior to tilting is the paleomagnetic data itself. As noted by Beck (1992) site mean-directions from the plutonic rocks in the batholith have essentially circular distributions (i.e. are not streaked), and their orthogonal demagnetization diagrams show no signs of systematic curvature. Both attributes may be interpreted as indicating that rocks of the *western* batholith were in zone M prior to tilting, and subsequently were tilted together by the same amount.

Constraints on the Timing of Tilting

Late Cretaceous and Tertiary sedimentary rocks overlap the batholith along its western edge. Ideally, the attitudes of the overlying sedimentary rocks should be a function of the amount of tilting of the underlying batholith, and an analysis of their dips should also allow a determination of the timing and amount of regional tilting. However, post-depositional deformation attributed to strike-slip faulting along the San Andreas transform system makes such an analysis difficult in this case. For example, in

the San Diego area motion along the Rose Canyon fault zone has resulted in folding and faulting of rocks ranging in age from Late Cretaceous (Point Loma Formation) to Late Pleistocene (Bay Point Formation; Kennedy, 1975). In the northern Santa Ana Mountains, Late Cretaceous to Late Pleistocene age strata are complexly folded and faulted (Fig. 29; Schoellhamer et al., 1981). Between these two areas Late Cretaceous and Tertiary strata generally dip to the west although in some areas folding and faulting of Eocene strata has occurred (Kennedy, 1975). To the northeast of San Diego, but south of the study area (in La Mesa, Poway, and Escondido quadrangles), the middle to late Eocene Friars Formation dips 3° to the southwest and the Late Eocene Mission Valley Formation consistently dips 2° in the same direction (Kennedy and Peterson, 1975). Sandstones and siltstones located ~25 km to the northwest of Escondido dip from 5° to 10° to the WSW, and have been correlated to the middle Eocene Santiago Formation of the Santa Ana Mountains (Elliott, 1985). Along the west coast of Baja California the amount of southwest dip also generally decreases upsection. The Late Cretaceous Rosario Group, which is equivalent to the Point Loma and Cabrillo Formations near San Diego, dips from 5° to 10° to the WSW. Paleocene strata dip from 2° to 6° WSW, and Miocene and Pliocene sedimentary rocks dip 2° to 3° (Gastil et al., 1975). Assuming that these attitudes are the result of southwest tilting of the underlying batholith, no more than ~10° of tilting has occurred since deposition of Turonian age strata along the western margin of the batholith (i.e. since deposition of the Trabuco Formation of Popenoe, 1941; the Lusardi Formation of Nordstrom, 1970; and the Redondo Formation of Flynn, 1970). This leaves ~9-11° of southwest tilting to be accounted for, based on previous estimates of total tilt (~19°, Ague and Brandon, 1992; 21°, Butler et al., 1991). The ~9-11° of tilting must have occurred after rocks of the *western* batholith cooled below the blocking temperature for acquisition of TRM, and before deposition of Turonian-age sediments along the western margin of the batholith.

The concordant hornblende and biotite K-Ar ages for the San Marcos Gabbro (~113-108 Ma; Dalrymple, 1976), from which most of the paleomagnetic data of Teissere and Beck (1973) and Hagstrum et al. (1985) are derived, indicate acquisition of TRM in the gabbros by the beginning of Albian time. This implies that the initial ~9-11° of tilting occurred during Albian and/or Cenomanian time (i.e. between ~113-108 Ma to ~91 Ma). The batholith, therefore, was probably not tilted by a single tectonic event, but rather experienced incremental tilting over a prolonged time interval. This notion is supported by fission-track data from the study area, as well as from similar data in the San Jacinto Mountains (chapter 2) and the northern Santa Rosa Mountains (Dokka, 1984).

The fission-track data from across the batholith, including the study area and the San Jacinto-Santa Rosa Mountains area (George and Dokka, in review; chapter 2), indicate that a series of episodic cooling events affected the region between Late Cretaceous and Paleocene time (~100 to 62 Ma). Cooling is attributed primarily to episodic *surface uplift* of the batholith. "Surface uplift," as defined by England and Molnar (1990), is the displacement of the earth's surface on a regional scale (at least 10^3-10^4 km^2) with respect to the geoid. It is proposed that greater amounts of total surface uplift in the eastern and central parts of the batholith produced tilting about a hinge line located west of the study area.

There is abundant evidence in the Late Cretaceous and Tertiary stratigraphic record along the western margin of the batholith for regional surface uplift in the Peninsular Ranges, as implied by the fission-track data. The absence of unroofing debris older than Turonian in age at the base of the section, and the deeply weathered surface separating plutonic and metamorphic rocks of the batholith from overlying sediments indicates post-Early Cretaceous, pre-Turonian age surface uplift (Peterson, 1970; Kennedy, 1975; Kennedy and Peterson, 1975). In Turonian time coarse unroofing debris of the Lusardi Formation (Nordstrom, 1970), and equivalent strata to the north

(Trabuco Fm., Popenoe, 1941) and south (Redondo Fm., Flynn, 1970) were transported to the west down deeply incised canyons to a narrow shelf following, or during, continued surface uplift in the batholith to the east (Peterson, 1971; Minch, 1979; Nilsen and Abbott, 1981). Beginning at the Campanian-Maastrichtian boundary (74.4 ± 4.0 Ma) major reorganization of marine facies followed by progradation of a Late Cretaceous fan system of the Point Loma Formation near San Diego is approximately coincident with regional surface uplift in the Peninsular Ranges at ~77-76 Ma (George and Dokka, in review; chapter 2). The general absence of Paleocene age strata (Nilsen and McKee, 1979) in the vicinity of the batholith also suggests regional uplift, erosion, or nondeposition in the early Tertiary (Dokka, 1984). The notion of surface uplift during Paleocene time is supported by the presence of angular unconformities of Paleocene(?) age along the western edge of the batholith. Slight angular discordance between the Maastrichtian Cabrillo Formation and the Eocene La Jolla Formation in the western part of the study area, and to the south near San Diego, were interpreted by Peterson and Nordstrom (1970) as representing uplift, erosion, and southwest tilting. Southwestward tilting of the ancestral Santa Ana Mountains to the north of the study area is indicated by the northeastward transgression of the Paleocene Silverado Formation onto successively older members of the upper Cretaceous section, and finally onto basement rocks (Schoellhamer et al., 1981). The fission-track ages from the Santa Rosa Mountains in the eastern Peninsular Ranges (Dokka, 1984) support the notion of Paleocene age surface uplift.

In addition to the angular unconformities of probable Paleocene age, there are widespread erosional surfaces along the axis of the batholith in southern California and northern Baja California (Gastil, 1961; Minch, 1979). These features probably began forming in late Mesozoic time, and were well developed by middle Eocene time (Minch, 1979). In northern Baja California during Paleocene and Eocene time the surfaces were

characterized by low rolling relief. Both Gastil (1961) and Minch (1979) suggested that these surfaces formed together as one larger surface. This once continuous erosion surface is perhaps the strongest evidence for uplift on a regional scale during Late Cretaceous-early Tertiary time. Fission-track data from the northern Peninsular Ranges (Dokka, 1984; George and Dokka, in review; chapter 2) imply that it formed primarily due to major surface uplift with associated tilting at ~77-76 Ma, and again at ~62 Ma.

CONCLUSIONS

1. Fission-track ages and apatite track-length distributions from the western half of the Peninsular Ranges batholith between Palomar Mountain and Escondido, California indicate a series of cooling events in the area in Late Cretaceous time (~100 to 77 Ma). The cooling events are attributed to episodic surface uplift of the batholith. It is proposed that greater amounts of surface uplift in the eastern and central parts of the batholith produced tilting about a hinge line located west of the study area.

2. The distribution of the fission-track ages from the study area is compatible with the notion of southwest tilting of the batholith, as well as with previous estimates of the total amount of tilting based on thermobarometric and thermochronologic data.

3. It is proposed that the batholith was tilted incrementally over a prolonged time interval in Late Cretaceous time. This is supported by the fission-track ages from the study area, by similar data in the San Jacinto-Santa Rosa Mountains area in the eastern Peninsular Ranges (Dokka, 1984; George and Dokka, in review), and by the stratigraphy of the Late Cretaceous and Tertiary sedimentary rocks in the region.

CHAPTER 5

SUMMARY AND CONCLUSIONS

Fission-track and thermobarometry data from the northern Peninsular Ranges presented here have significant implications for local, regional, and Cordilleran tectonics. The following is a summary of the findings of this study, as they relate to the Cretaceous tectonic history of the batholith.

Between ~120 and 89 Ma, the majority of the Peninsular Ranges batholith formed along an Andean-type plate margin where the Farallon plate was continuously subducting beneath the North American plate (Silver et al., 1979; Silver and Chappell, 1988; Walawender et al., 1990). The rate of convergence was moderately high (50-100 km/m.y.) and variable during this period (Engebretson et al., 1985). A major change in direction and increase in the rate of convergence occurred at ~100 Ma. The direction of convergence shifted from approximately east-west to a northeast-southwest direction, and the rate of convergence increased from 60 km/m.y. to greater than 100 km/m.y. This change in plate motions likely affected the geological history of the Cretaceous magmatic arc of peninsular California (i.e. the Peninsular Ranges batholith). At ~100 Ma the locus of magmatism shifted from a static arc located along the western half of the batholith into the eastern Peninsular Ranges, in response to a probable shallowing of the angle of subduction (Walawender et al., 1991). Resultant heating of the lithosphere along the eastern half of the batholith may have weakened the crust (chapter 3), and in a manner described by Burchfiel and Davis (1975), produced a ductility contrast with the more rigid and cooler western arc. West-vergent thrusting along the Santa Rosa mylonite belt resulted in ~10 to 18 km of crustal thickening in the eastern Peninsular Ranges between ~99 and 94 Ma (chapters 2 and 3). Thrusting may have been facilitated by magmatic heating and weakening of the crust, and perhaps was driven by the subduction of a buoyant Farallon plate and underplated low density rock. This event

may have occurred along a Late Cretaceous ductile shear zone that extended from the Transverse Ranges to perhaps as far south as the Laguna Mountains, near the international border with Mexico (May, 1989; chapter 3).

West-vergent thrusting along the Santa Rosa mylonite belt at ~99-94 Ma likely produced thickened crust that seems to have collapsed through major extensional faulting. Extension resulted in tectonic denudation and exhumation of the mylonite belt between ~94 and 92 Ma in the Palm Springs area (chapters 2 and 3). Tectonic denudation and exhumation were accompanied by the synextensional intrusion of large tonalitic plutons into footwall rocks of the mylonite belt. These plutons were emplaced at ~4-5 kb (15-19 km) into an evolving shear zone, and subsequently cooled during exhumation. Emplacement temperatures are estimated at 730-760°C (chapter 3), using amphibole-plagioclase thermobarometry. The tonalites were emplaced during a short time interval, based on U-Pb dating of multiple zircon fractions (94 and 93 Ma; Hill et al., 1986; Silver, 1986). Sphene and zircon fission-track ages from these same rocks indicate they had cooled to below ~235°C by ~92 Ma (George and Dokka, in review; chapter 2). Therefore, the rocks cooled from crystallization temperatures to below ~235°C in ~1 to 2 m.y. The geobarometry data, coupled with the thermochronologic constraints, suggest that cooling occurred during ~10-14.5 km of exhumation. Ductile deformation along the Santa Rosa Mylonite belt was over by ~92 Ma. This is because temperatures of >300°C are needed for the crystal-plastic deformation of quartz (Sibson, 1977), and the fission-track ages from the San Jacinto Mountains have established that footwall rocks were below this temperature by ~92 Ma.

Concurrent with extension and exhumation in the eastern Peninsular Ranges batholith, the western and central portions of the batholith experienced numerous cooling events that continued into Campanian time. Fission-track ages from the western batholith (chapter 4) indicate a series of rapid cooling events between ~100 and 82 Ma.

The stratigraphy of upper Cretaceous rocks along the western margin of the batholith supports the notion that cooling was the result of surface uplift and attendant erosion. The absence of unroofing debris older than Turonian in age at the base of the section, and a deeply weathered surface separating plutonic and metamorphic rocks of the batholith from overlying sediments indicate post-Early Cretaceous, pre-Turonian age surface uplift (Peterson, 1970; Kennedy, 1975; Kennedy and Peterson, 1975). During surface uplift in Turonian time, coarse unroofing debris of the Lusardi Formation (Nordstrom, 1970), and equivalent strata to the north and south were transported down deeply incised canyons to a narrow continental shelf.

Apatite fission-track ages and track-length distributions from the San Jacinto Mountains, and apatite and zircon fission-track ages and apatite track-length distributions from the eastern half of the Palomar Mountain to Escondido study area indicate a major cooling event in the Peninsular Ranges at ~77-76 Ma (chapters 2 and 4). In the San Jacinto Mountains, 2.3 km of exposed vertical section have indistinguishable apatite ages (~76 Ma) and apatite track-length distributions (13.9-14.4μm, with standard deviations of 0.8-1.2 μm); this thickness is a minimum because it is not known how much rock with the same cooling history has been removed from above the present erosion surface. The apatite fission-track ages also indicate a minimum of 4.5 km of exhumation in conjunction with the cooling event, assuming a reasonable range of geothermal gradients (20°-40°C/km). Exhumation was the result of regional surface uplift and accompanying erosion, and coincided with several important changes in North American and Farallon (or Kula) plate motions at ~75 Ma. These changes include an increase in the convergence rate, an increase in the absolute velocity of the North American plate, and a change in the direction of convergence between the plates (Coney, 1972, 1976; Cross and Pilger, 1978; Engebretson et al., 1985). Changes in plate motions are thought to have initiated low-angle subduction that, in turn, was responsible

for the Laramide deformation of the Cordilleran foreland. Low-angle subduction beneath the Late Cretaceous magmatic arc also is thought to have resulted in tectonic erosion of the lithospheric mantle of the North American plate (Bird, 1988). This would have produced changes in the density distribution of the North American plate and resulted in isostatic rise of crust and surface uplift of the Peninsular Ranges batholith. It is estimated that the lithosphere beneath the eastern Peninsular Ranges experienced ~2-3 km of "uplift of rocks" (uplift of rocks = surface uplift + exhumation). The estimate is based, in part, on models of Bird (1979, 1988), which consider the regional geologic and geophysical effects of vertical separation or "delamination" of the lithospheric mantle from the continental crust during Laramide deformation of the North America plate. The estimate also takes into account the substantial uplift of rocks that takes place during isostatic rebound due to the erosion of a topographic uplift (Nunn, 1990). Also, an additional feature of the model by Bird (1988) and the geological model of Hamilton (1988) is called upon to explain the 4-5 km of exhumation, as indicated by the apatite fission-track data from the San Jacinto Mountains. This feature is underplating of low density rocks, such as continental margin sediments and lower crustal rocks, beneath North America during low-angle subduction. Underplating would have contributed to the buoyancy of the plate and, in conjunction with tectonic erosion of the mantle lithosphere, help explain the of exhumation of the San Jacinto Mountains.

Low-angle subduction and accompanying erosion and underplating likely produced regional uplift, affecting central parts of the batholith and areas to the south of the San Jacinto Mountains and northern Santa Rosa Mountains. Fission-track ages and apatite track-length distributions from the eastern half of the Palomar Mountain to Escondido sample transect indicate major cooling at ~77 Ma (chapter 4). Concordant zircon and apatite fission-track ages range from 73.9 to 81.9 Ma and 74.8 to 79.9 Ma, respectively. Apatite track-length distributions range from 13.8 to 14.4 μm with standard deviations

of 0.7 to 1.0 μm (for samples 301-313), and are typical of rapidly cooled granitic terranes (e.g. the San Jacinto Mountains). The ages and track-length distributions are essentially identical on either side of the Elsinore fault, along which there has been considerable lateral (~30 km of right-lateral separation, Sage, 1973) as well as vertical displacement (Larsen, 1948). Grove and Harrison (1992) documented rapid cooling between 78 and 72 Ma in an region including the Cuyamaca-Laguna Mountains, the southern Santa Rosa Mountains, and Fish Creek Mountains to the south of the San Jacinto Mountains, based on $^{40}Ar/^{39}Ar$ ages of K-feldspars from batholithic rocks.

At ~62 Ma the eastern Peninsular ranges experienced an additional major cooling event, based on concordant sphene, zircon, and apatite fission-track ages from the northern Santa Rosa Mountains (Dokka, 1984). This event has also been attributed to regional surface uplift (Dokka, 1984), since Paleocene-age strata are generally missing throughout southern and Baja California (Nilsen and McKee, 1979). Paleocene age surface uplift may have been caused by the same tectonic mechanisms that produced regional uplift at ~77-76 Ma.

Regional unconformities that are exposed today throughout northern Baja California and southern California (Gastil, 1961; Minch, 1979) are attributed to surface uplift in the Peninsular Ranges at ~77-76 Ma (George and Dokka, in review; chapter 2). These unconformities are erosional surfaces cut into the granitic and metamorphic rocks of the batholith. Cutting of the unconformities produced a large amount of unroofing debris that was shed west to the adjacent forearc basin. The debris was transported ~50-100 km to the southwest and deposited in the San Diego area as shelf and deep marine fan deposits of the Point Loma Formation (Nilsen and Abbott, 1981; Girty, 1987; Bannon et al., 1989). The sediments were deposited near the Campanian-Maastrichtian boundary (74.4 ± 4.0 Ma) at the same time the batholith was undergoing regional surface uplift to the east.

Following a Paleocene hiatus, alluvial fan conglomerates (eg. Poway Conglomerates) and coarse marine turbidites were deposited in the forearc basin to the west in Eocene time (Link et al., 1979). The source area for the Poway conglomerates is in Sonora, which in Eocene time was adjacent to the northern Peninsular Ranges (Merriam, 1979; Minch, 1979; Abbott and Smith, 1989). The eastern ancestral Peninsular Ranges, therefore, were the site of west flowing streams that connected Sonoran source regions with areas of deposition in the forearc basin to the west (e.g. the present San Diego area). In Tertiary (Miocene?) time the eastern Peninsular Ranges were again affected by regional deformation. In the southern Santa Rosa Mountains, along the Santa Rosa mylonite belt near Borrego Springs, and probably along the mylonite belt in the Palm Springs area, extensional detachment faulting and concomitant greenschist facies metamorphism were taking place (Wallace and English, 1982; Schultejann, 1984; Todd et al., 1988; chapters 2 and 3). In northwestern Baja and coastal Sonora there is also evidence of Miocene extension, which is considered the western extent of deformation in the Basin and Range province (Karig and Jensky, 1972; Gastil and Krummenacher, 1977; Gastil et al., 1979; Dokka and Merriam, 1982; Stock and Hodges, 1989).

The northern Peninsular ranges began the 300 ± 10 km of NNW translation along the San Andreas transform system to their present positions with the opening of the Gulf of California at ~5.5 Ma (Atwater, 1989). Since that time the batholith has been broken into a numerous crustal blocks that have been uplifted and/or down-dropped, as well as tilted, in response to transpression and transtension between right-lateral transform faults (Larsen, 1948; Crowell, 1974; Christie-Blick and Biddle, 1985).

The northern Peninsular Ranges, therefore, have experienced repeated regional tectonic events since the batholith formed (i.e. between ~120 Ma and the present). Teissere and Beck (1973) and Hagstrum et al. (1985) proposed that one such event was

the long distance northward translation (~11°) and clockwise vertical-axis rotation (~25°) of peninsular California with respect to cratonic North America. They based this on paleomagnetic directions of plutonic rocks from the Peninsular Ranges batholith, which are discordant with the expected Cretaceous magnetic field direction. However, the discordant directions may also be due to tilting of the batholith to the southwest (Butler et al., 1991). The general east-to-west increase in fission-track ages across the western half of the batholith between Palomar Mountain and Escondido, California support the notion of southwest tilting, as does an abundance of geologic evidence from across the batholith (chapter 4). Apatite and zircon fission-track ages in the northeastern part of the study area are concordant at ~77 Ma, but increase towards the southwest from 82 to 96 Ma and 83 to 93 Ma, respectively. Sphene fission-track ages also increase west of the Elsinore fault (chapter 4), from ~95 to 100 Ma. This distribution of ages may be explained by tilting of the batholith and its fission-track age surfaces to the southwest. It is proposed here that tilting was the result of several surface uplift events that affected the interior portions of the batholith in Late Cretaceous and early Tertiary time (~100 to 62 Ma, based on fission-track data from the northern Peninsular Ranges; Dokka, 1984; George and Dokka , in review; chapters 2 and 4).

REFERENCES

Abbott, P. L., Minch, J. A., and Peterson, G. L., 1976, Pre-Eocene paleosol south of Tijuana, Baja California, Mexico: Journal of Sedimentary Petrology, v. 46, p. 355-361.

Abbott, P. L., and Smith, T. E., 1978, Trace-element comparison of clasts in Eocene conglomerates, southwestern California and northwestern Mexico: Journal of Geology, v. 86, p. 753-762.

_____, and _____, 1989, Sonora, Mexico, source for the Eocene Poway Conglomerate of southern California: Geology, v. 17, p. 329-332.

Adams, M. A., 1979, Stratigraphy and petrology of the Santiago Peak Volcanics east of Rancho Santa Fe, California [M.S. thesis]: San Diego, California, San Diego State University, 123 p.

Ague, J. J., and Brimhall, G. H., 1988, Magmatic arc asymmetry and distribution of anomalous plutonic belts in the batholiths of California: effects of assimilation, crustal thickness, and depth of crystallization: Geological Society of America Bulletin, v. 100, p. 912-927.

Ague, J. J., and Brandon, M. T., 1992, Tilt and northward offset of Cordilleran batholiths resolved using igneous barometry: Nature, v. 360, p. 146-149.

Anderson, J. R., 1983, Petrology of a portion of the Eastern Peninsular Ranges mylonite zone: Contributions to Mineralogy and Petrology, v. 84, p. 253-271.

Anderson, P. V., 1982, Prebatholithic stratigraphy of the San Felipe area, Baja California, Mexico [M.S. thesis]: San Diego, California, San Diego State University, 100 p.

Anderson, T. H., and Silver, L. T., 1969, Mesozoic magmatic events of the northern Sonora coastal region, Mexico: Geological Society of America Abstracts with Programs, v. 1, p. 3.

Armstrong, R. L., 1968, Sevier orogenic belt in Nevada and Utah: Geological Society of America Bulletin, v. 79, p. 429-458.

Armstrong, R. L., and Suppe, J., 1973, Potassium-argon geochronometry of Mesozoic igneous rocks, in Nevada, Utah, and southern California: Geological Society of America Bulletin, v. 84, p. 1375-1392.

Atwater, T., 1970, Implications of plate tectonics for the Cenozoic tectonic evolution of western North America: Geological Society of America Bulletin, v. 81, p. 3513-3535.

_____, 1989, Plate tectonic history of the northeast Pacific and western North America, *in* E. L. Winterer, D. M. Hussong and R. W. Decher eds., The Eastern Pacific Ocean and Hawaii: Geological Society of America, The Geology of North America, v. N, p. 21-72.

Baird, A. K., and Miesch, A. T., 1984, Batholithic rocks of southern California-a model for the petrochemical nature of source materials: United States Geological Society Professional Paper 1284, 42 p.

Bannon, J. L., Bottjer, D. J., Lund, S. P., and Saul, L. R., 1989, Campanian/Maastrichtian stage boundary in southern California: Resolution and implications for large-scale depositional patterns: Geology, v. 17, p. 80-83.

Bartling, W. A., and Abbott, P. L., 1984, Upper Cretaceous Sedimentation and tectonics with reference to the Eocene, San Miguel Island, and San Diego area, California, *in* Abbott, P. L. ed., Upper Cretaceous depositional systems, southern California-northern Baja California: Pacific Section, Society of Economic Paleontologists and Mineralologists, volume and guidebook no. 36, p. 85-102.

Beck, M. E., Jr., 1992, Some thermal and paleomagnetic consequences of tilting a batholith: Tectonics, v. 11, p. 297-302.

Beck, M. E., Jr., and Noson, L., 1972, Anomalous paleolatitudes in Cretaceous granitic rocks: Nature Phys. Sci., v. 235, p. 11.

Bence, A. E., and Albee, A. L., 1968, Empirical correction factors for the electron microanalysis of silicates and oxides: Journal of Geology, v. 76, p. 382-403.

Berggreen, R. G., and Walawender, M. J., 1977, Morena Reservoir roof pendant, southern California: California Division of Mines and Geology Special Report 129, v. p. 61-65.

Bertagnolli, E., Kiel, R., and Pahl, M., 1983, Thermal history and length distribution of fission tracks in apatite: part 1: Nuclear Tracks and Radiation Measurements, v. 4, p. 163-177.

Bird, P., 1979, Continental delamination and the Colorado Plateau: Journal of Geophysical Research, v. 84, p. 7561-7571.

_____, 1984, Laramide crustal thickening event in the Rocky Mountain foreland and Great Plains: Tectonics, v. 3, p. 741-758.

_____, 1988, Formation of the Rocky Mountains, western United States: Science, v. 239, p. 1501-1507.

Blundy, J. D., and Holland, T. J. B., 1990, Calcic amphibole equilibria and a new amphibole-plagioclase geothermometer: Contributions to Mineralogy and Petrology, v. 104, p. 208-224.

Brown, A. R., 1981, Structural history of the metamorphic, granitic, and cataclastic rocks in the southeastern San Jacinto Mountains, *in* Brown, A. R. and Ruff, R. W. eds., Geology of the San Jacinto Mountains: South Coast Geological Society, Annual Field Trip Guidebook No. 9, p. 100-138.

Bryant, B., and Naeser, C. W., 1980, The significance of fission-track ages of apatite in relation to the tectonic history of the Front and Sawatch Ranges, Colorado: Geological Society of America Bulletin, v. 91, p. 156-164.

Burchfiel, B. C., and Davis, G. H., 1972, Structural framework and evolution of the southern part of the Cordilleran orogen, western United States: American Journal of Science, v. 272, p. 97-118.

_____, and _____, 1975, Nature and controls of Cordilleran orogenesis, western United States; extensions of an earlier synthesis: American Journal of Science, v. 275-A, p. 363-396.

Burchfiel, B. C., and Royden, L. H., 1985, North-south extension within the convergent Himalayan region: Geology, v. 13, p. 679-682.

Butler, R. F., Dickinson, W. R., and Gehrels, G. E., 1991, Paleomagnetism of coastal California and Baja California: alternatives to large scale northward transport: Tectonics, v. 10, p. 561-576.

Callahan, J., 1980, A nontoxic heavy liquid and inexpensive filters for separation of mineral grains: Journal of Sedimentary Petrology, v. 57, p. 765-766.

Christie, J. M., and Ord, A. V., 1980, Flow stress from microstructures of mylonites: examples and current assessment: Journal of Geophysical Research, v. 85, p. 6253-6262.

Christie-Blick, N., and Biddle, K. T., 1985, Deformation and basin formation along strike-slip faults, *in* K. T. Biddle and N. Christie-Blick eds., Strike-slip deformation, basin formation, and sedimentation: Society of Economic Paleontologists and Mineralogists, Special Publication 37, p. 1-34

Clinkenbeard, J. P., 1987, The mineralogy, geochemistry, and geochronology of the La Posta pluton, San Diego and Imperial counties, California [M.S. thesis]: San Diego State University, 215 p.

Coney, P. J., 1972, Cordilleran tectonics and North American plate motion: American Journal of Science, v. 272, p. 603-628.

_____, 1976, Plate tectonics and the Laramide orogeny: New Mexico Geological Society Special Publication 6, p. 5-10.

Coney, P. J., and Reynolds, S. J., 1977, Cordilleran Benioff zones: Nature, v. 270, p. 403-406.

Coney, P. J., Jones, D. L., and Monger, J. W. H., 1980, Cordilleran suspect terranes: Nature, v. 288, p. 329-333.

Coney, P. J., and Harms, T. A., 1984, Cordilleran metamorphic core complexes: Cenozoic extensional relics of Mesozoic compression: Geology, v. 12, p. 550-554.

Cross, T., and Pilger, R. H., 1978, Constraints on absolute motion and plate interaction inferred from Cenozoic igneous activity in the western United States: American Journal of Science, v. 278, p. 865-902.

_____, and _____, 1982, Controls on subduction geometry, location of magmatic arcs, and tectonics of arc and back-arc regions: Geological Society of America Bulletin, v. 93, p. 545-562.

Crowell, J. C., 1962, Displacement along the San Andreas fault, California: Geological Society of America Special Paper 71, 61 p.

_____, 1974, Origin of the Late Cenozoic basins of southern California: Society of Economic Paleontologists and Mineralogists Special Publication 22, v. p. 190-204.

Crowley, K. D., 1985, Thermal significance of fission-track length distributions: Nuclear Tracks and Radiation Measurements, v. 10, p. 311-332.

Crowley, K. D., Naeser, C. W., and Naeser, N. D., 1989, Short course manual on fission-track analysis: theory and applications: St. Louis, Missouri, Geological Society of America.

Dalrymple, G. B., 1976, K-Ar ages of the San Marcos Gabbro and related rocks of the southern California batholith: Isochron/West, No. 15, p. 35-36.

_____, 1979, Critical tables for conversion of K-Ar ages from old to new constants, research note: Geology, v. 7, p. 558-560.

Daly, R. A., Manger, G. E., and Clark, S. P., Jr., 1966, Density of rocks, *in* S. P. Clark Jr. ed., Handbook of physical constants: Geological Society of America Memoir 97, p. 19-26.

Davis, G. A., Anderson, J. L., Frost, E. G., and Shackelford, T. J., 1980, Mylonitization and detachment faulting in the Whipple-Buckskin-Rawhide Mountains terrane, southeastern California and western Arizona, *in* Cittenden, M. D., Jr., Coney, P. J., and Davis, G. H. eds., Cordilleran metamorphic core complexes: Geological Society of America Memoir 153, p. 79-129.

Davis, J. C., 1973, Statistics and data analysis in geology: New York, Wiley, 550 p.

Debiche, M. G., Cox, A., Engebretson, D. C., 1987, The motion of allochthonous terranes across the North Pacific basin: Geological Society of America Special Paper 207, 49 p.

Dewey, J. F., 1988, Extensional collapse of orogens: Tectonics, v. 7, p. 1123-1139.

Dibblee, T. W., Jr., 1971, Regional geologic map of San Andreas and related faults in eastern San Gabriel, San Bernadino, and San Jacinto Mountains, California: United States Geological Survey Open-Filed Map, scale 1:125,000.

_____, 1981, Geology of the San Jacinto Mountains and adjacent areas, *in* Brown, A. R. and Ruff, R. W. eds., Geology of the San Jacinto Mountains: South Coast Geological Society, Annual Field Trip Guidebook No. 9, p. 1-47.

Dickinson, W. R., and Synder, W. S., 1978, Plate tectonics of the Laramide orogeny, *in* Matthews, V., III eds., Laramide folding associated with basement block faulting in the western United States: Geological Society of America Memoir 151, p. 355-366.

Dickinson, W. R., Klute, M. A., Hayes, M. J., Janecke, S. U., Lundin, E. R., McKittrick, M. A., and Olivares, M. D., 1988, Paleogeographic and paleotectonic setting of Laramide sedimentary basins in the central Rocky Mountain region: Geological Society of America Bulletin, v. 100, p. 1023-1039.

Dodge, F. C. W., and Naeser, C. W., 1968, Fission-track ages of apatites from granitic rocks of the Sierra Nevada Batholith: American Geophysical Union, Transactions, v. 49, p. 348.

Dodson, M. H., 1973, Closure temperature in cooling geochronological and petrological systems: Contributions to Mineralogy and Petrology, v. 40, p. 259-274.

_____, 1979, Theory of cooling ages, *in* E. Jäger and J. C. Hunziker eds., Lectures in Isotope Geology: Springer-Verlag, New York, p. 195-202.

Dokka, R. K., 1984, Fission-track geochronologic evidence for the Late Cretaceous mylonitization and early Paleocene uplift of the northeastern Peninsular Ranges, California: Geophysical Research Letters, v. 11, p. 46-49.

_____, 1989, The Mojave Extensional Belt of southern California: Tectonics, v. 8, p. 363-390.

Dokka, R. K., and Lingrey, S. H., 1979, Fission-track evidence for a Miocene cooling event, Whipple Mountains, southeastern California, *in* J. M. Armentrout, M. R. Cole, and H. Terbert Jr. eds., Cenozoic Paleogeography of the western United States: Pacific Section, Society of Economic Paleontologists and Mineralologists, Pacific Coast Paleogeography Symposium 3, p. 195-202.

Dokka, R. K., and Merriam, R. H., 1982, Late Cenozoic extension of northeastern Baja California, Mexico: Geological Society of America Bulletin, v. 93, p. 371-378.

Dokka, R. K., and Lingrey, S. H., 1979, Late Cenozoic extension of northeastern Baja California, Mexico: Geological Society of America Bulletin, v. 93, p. 371-378.

Dokka, R. K., Mahaffie, M. J., and Snoke, A. W., 1986, Thermochronologic evidence of major tectonic denudation associated with detachment faulting, northern Rubey Mountains-East Humboldt Range, Nevada: Tectonics, v. 5, p. 995-1006.

Donelick, R. A., Roden, M. K., Moores, J. D., Carpenter, B. S., and Miller, D. S., 1990, Etchable length reduction of induced fission tracks in apatite at room temperature (23°C): Crystallographic effects and "initial" mean lengths: Nuclear Tracks, v. 17, p. 261-265.

Duddy, I. R., Green, P. F., and Laslett, G. M., 1988, Thermal annealing of fission tracks in apatite, 3. Variable temperature behavior: Chemical Geology, v. 73, p. 25-38.

Elliott, W. J., 1985, Geology of the Morro Hill area, northwestern San Diego County, California, *in* P. L. Abbott ed., On the manner of deposition of the Eocene strata in northern San Diego County: San Diego Association of Geologists, p. 85.

Engebretson, D. C., Cox, A., and Gorden, R. G., 1985, Relative motions between oceanic and continental plates in the Pacific Basin: Geological Society of America Special Paper 206, 59 p.

Engel, A. E. J., and Schultejann, P. A., 1984, Late Mesozoic and Cenozoic tectonic history of south central California: Tectonics, v. 3, p. 659-675.

England, P. C., and Houseman, D. P., 1988, The mechanics of the Tibetan Plateau: Philosophical Transactions of the Royal Society of London, v. A326, p. 301-320.

England, P., and Molnar, P., 1990, Surface uplift, uplift of rocks, and exhumation of rocks: Geology, v. 18, p. 1173-1176.

Erskine, B. G., 1986, Syn-tectonic granitic intrusion and mylonitic deformation along the eastern margin of the northern Peninsular Ranges batholith, southern California: Geological Society of America Abstracts with Programs, v. 18, p. 105.

Erskine, B. G., and Wenk, H. R., 1985, Evidence for Late Cretaceous crustal thinning in the Santa Rosa mylonite zone, southern California: Geology, v. 13, p. 274-276.

Everden, J. F., and Kistler, R. W., 1970, Chronology of emplacement of Mesozoic batholithic complexes in California and western Nevada: U.S. Geological Survey Professional Paper 623, 49 p.

Fitzgerald, P. G., and Stump, E., 1991, Early Cretaceous uplift in the Ellsworth Mountains of West Antarctica: Science, v. 254, p. 92-94.

Fleischer, R. L., Price, R. L., and Walker, R. M., 1965, Effects of temperature, pressure, and ionization of the formation and stability of fission tracks in minerals and glasses: Journal Geophysical Research, v. 70, p. 1497-1502.

_____, _____, and _____, 1975, Nuclear tracks in solids; principles and applications: University of California Press, Berkeley, 605 p.

Flynn, C. J., 1970, Post batholithic geology of the La Gloria-Presa Rodriquez area, Baja California, Mexico: Geological Society of America Bulletin, v. 81, p. 1789-1806.

Flynn, J. J., Cipolletti, R. M., and Novacek, M. J., 1989, Chronology of early Eocene marine and terrestrial strata, Baja California, Mexico: Geological Society of America Bulletin, v. 101, p. 1182-1196.

Galbraith, R. F., 1981, On statistical models for fission track counts: Journal of Mathematical Geology, v. 13, p. 471-478.

Gastil, R. G., 1961, The elevated erosion surfaces, *in* Blakemore, E. T. ed., Guidebook for field trips, Geological Society of America, Cordilleran Section: San Diego, California, San Diego State College, p. 1-3.

_____, 1975, Plutonic zones in the Peninsular Ranges of southern California and northern Baja California: Geology, v. 3, p. 361-363.

_____, 1983, Mesozoic and Cenozoic rocks of southern California and western Mexico: Geological Society of America Memoir 159, p. 265-275.

_____, 1985, Terranes of Peninsular California and adjacent Sonora, in Howell, D. G., ed., Tectonostratigraphic terranes of the Circum-Pacific region: Circum-Pacific Council for Energy and Mineral Resources, Earth Science Series, no. 1,p. 273-284.

Gastil, R. G., Phillips, R. P., and Allison, E. C., 1975, Reconnaissance geology of the state of Baja California: Geological Society of America Memoir 140, 170 p.

Gastil, R. G., and Krummenacher, D., 1977, Reconnaissance geology of coastal Sonora between Puerto Lobos and Bahia Kino: Geological Society of America Bulletin, v. 88, p. 189-198.

Gastil, R. G., Krummenacher, D., and Minch, J., 1979, The record of Cenozoic volcanism around the Gulf of California: Geological Society of America Bulletin, v. 90, p. 839-857.

Gastil, R. G., and Miller, R., 1984, Prebatholithic paleogeography of peninsular California and adjacent Mexico, *in* V. A. Frizzell Jr. eds., Geology of the Baja California Peninsula: Pacific Section, Society of Economic Paleontologists and Mineralogists, p. 9-16.

Gastil, R. G., Miller, R. H., and Uranga, M. C., 1986, The Cretaceous paleogeography of peninsular California and adjacent Mexico, *in* P. L. Abbott ed., Cretaceous stratigraphy, western North America: Pacific Section, Society of Economic Paleontologists and Mineralogists, p. 41-50.

Gastil, R. G., Miller, R., Anderson, P., Crocker, J., Campbell, M., Buch, P., Lothringer, C., Engelhardt, P. L., DeLattre, M., Hobbs, J., Roldán-Quivtana, J., 1991, The relation between Paleozoic strata on opposite sides of the Gulf of California, *in* Efrén Pérez-Segura and César Jacques-Ayala eds., Studies in Sonoran geology: Geological Society of America Special Paper 254, p. 7-18.

George, P. G., Dokka, R. K., and Henry, D. J., 1991, Major Late Cretaceous thrusting and subsequent extension in the eastern Peninsular Ranges of southern California: Geological Society of America Abstracts with Programs, v. 23, p. 480.

George, P. G., and Dokka, R. K., 1992, Fission-track evidence for tilting of the Peninsular Ranges batholith of southern California: an alternative to long-distance northward transport: Geological Society of America Abstracts with Programs, v. 24, p. A64.

_____, and _____, in review., Major Late Cretaceous cooling events in the eastern Peninsular Ranges, California and their implications for Cordilleran tectonics (Geological Society of America Bulletin).

Germinario, M. P., 1982, The depositional and tectonic environments of the Julian Schist, Julian, California [M.S. thesis]: San Diego, California, San Diego State University, 95 p.

Girty, G. H., 1987, Sandstone provenance, Point Loma formation, San Diego, California: evidence for the uplift of the Peninsular Ranges during the Laramide Orogeny: Journal of Sedimentary Petrology, v. 57, p. 839-844.

Gleadow, A. J. W., and Duddy, I. R., 1981, A natural long-term annealing experiment for apatite: Nuclear Tracks and Radiation Measurements, v. 5, p. 169-174.

Gleadow, A. J. W., Duddy, I. R., Green, P. F., and Lovering, J. F., 1986, Confined fission track lengths in apatite: a diagnostic tool for thermal history analysis: Contributions to Mineralogy and Petrology, v. 94, p. 405-415.

Globerman, B. R., and Irving, E., 1988, Mid-Cretaceous paleomagnetic reference field for North America: restudy of 100 Ma intrusive rocks from Arkansas: Journal of Geophysical Research, v. 93, p. 11,721-11,733.

Green, P. F., 1981, "Track-in-track" length measurements in annealed apatites: Nuclear Tracks, v. 5, p. 121-128.

Green, P. F., Duddy, I. R., Gleadow, A. J. W., Tingate, P. R., and Laslett, G. M., 1986, Thermal annealing of tracks in apatite, 1. A qualitative description: Chemical Geology, v. 59, p. 237-253.

Gregory, M. R., and Johnston, K. A., 1987, A nontoxic substitute for hazardous heavy liquids - aqueous sodium polytungstate ($3Na_2WO_4.9WO_3.H_2O$) (Note): New Zealand Journal of Geology and Geophysics, v. 30, p. 317-320.

Grove, M., 1986, Metamorphism and deformation in the Box Canyon area, eastern Peninsular Ranges, San Diego County, California [M. S. thesis]: Los Angeles, California, University of California, 118 p.

Grove, M., and Harrison, T. M., 1992, Thermal evolution of the eastern Peninsular Ranges batholith, California: Geological Society of America Abstracts with Programs, v. 24, p. A65.

Hagstrum, J. T., McWilliams, M., Howell, D. G., and Grommé, S., 1985, Mesozoic paleomagnetism and northward translation of the Baja California Peninsula: Geological Society of America Bulletin, v. 96, p. 1077-1090.

Hagstrum, J. T., Sawlan, M. G., Hausback, B. P., Smith, J. G., and Grommé, C. S., 1987, Miocene Paleomagnetism and tectonic setting of the Baja California Peninsula: Journal of Geophysical Research, v. 92, p. 2627-2639.

Hamilton, W. B., 1969, Mesozoic California and the underflow of the Pacific mantle: Geological Society of America Bulletin, v. 80, p. 2409-2430.

_____, 1978, Mesozoic tectonics of the western United States, *in* Howell, D. G. and McDougall, K. A. eds., Mesozoic paleogeography of the western United States: Pacific Section, Society of Economic Paleontologists and Mineralologists, Los Angeles, California, p. 33-70.

_____, 1988, Laramide crustal shortening, *in* C. J. Schmidt and W. J. Perry Jr. eds., Interaction of the Rocky Mountain foreland and the Cordilleran thrust belt: Geological Society of America Memoir 171, p. 27-39.

_____, 1989, Crustal geologic processes of the continental United states, *in* Parker, L. C., and Mooney, W. D., eds., Geophysical framework of the continental United States: Geological Society of America Memoir 172, p. 743-781.

Hammarstrom, J. M., and Zen, E., 1986, Aluminum in hornblende: an empirical igneous geobarometer: American Mineralogist, v. 71, p. 1297-1313.

Haq, B. U., Hardenbol, J., and Vail, P. R., 1987, Chronology of fluctuating sea levels since the Triassic: Science, v. 235, p. 1156-1166.

Harrison, T. M., and McDougall, I., 1980, Investigations of an intrusive contact, northwest Nelson, New Zealand-I. Thermal, chronological, and isotopic constraints: Geochimica Cosmochimica Acta, v. 44, p. 1985-2003.

Harrison, T. M., Duncan, I., and McDougall, I., 1985, Diffusion of ^{40}Ar in biotite: temperature, pressure and compositional effects: Geochimica Cosmochimica Acta, v. 49, p. 2461-2468.

Henderson, L. J., Gorden, R. G., and Engebretson, D. C., 1984, Mesozoic aseismic ridges of the Farallon plate and southward migration of shallow subduction during the Laramide orogeny: Tectonics, v. 3, p. 121-132.

Henry, D. J., and Dokka, R. K., 1992, Metamorphic evolution of exhumed middle to lower crustal rocks in the Mojave Extensional Belt, southern California: Journal of Metamorphic Geology, v. 10, p. 347-364.

Hill, R. I., 1984, Petrology and petrogenesis of batholithic rocks, San Jacinto Mountains, southern California [Ph. D. thesis]: Pasadena, California Institute of Technology, 660 p.

_____, 1988, San Jacinto intrusive complex 1. Geology and mineral chemistry, and a model for intermittent recharge of tonalitic magma chambers: Journal of Geophysical Research, v. 93, p. 10325-10348.

Hill, R. I., and Silver, L. T., 1979, Strontium isotopic variability in the pluton of San Jacinto Peak, southern California: EOS (American Geophysical Union Transactions), v. 61, p. 411.

Hill, R. I., Silver, L. T., and Taylor, H. P., 1986, Coupled Sr-O isotope variations as an indicator of source heterogeneity for the northern Peninsular Ranges batholith: Contributions to Mineralogy and Petrology, v. 92, p. 351-361.

Hollister, L. S., Grissom, G. C., Peters, E. K., Stowell, H. H., and Sisson, V. B., 1987, Confirmation of the empirical correlation of Al in hornblende with pressure of solidification of calc-alkaline plutons: American Mineralogist, v. 72, p. 231-239.

Holm, D. K., and Dokka, R. K., 1991, Major Late Miocene cooling of the middle crust associated with extensional orogenesis in the Funeral Mountains, California: Geophysical Research Letters, v. 18, p. 1759-1768.

Hornafius, J. W., Luyendyk, B. P., Terress, R. R., and Kamerling, M. J., 1986, Timing and extent of Neogene tectonic rotations in the western Transverse Ranges, California: Geological Society of America Bulletin, v. 97, p. 211-217.

Hurford, A. J., 1986, Cooling and uplift patterns in the Leopontine Alps, south central Switzerland and an age of vertical movement on the Insubric fault line: Contributions to Mineralogy and Petrology, v. 92, p. 413-427.

Hurford, A. J., and Green, P. F., 1983, The zeta age calibration of fission-track dating: Isotope Geoscience, v. 1, p. 285-317.

Hurford, A. J., Hunziker, J. C., and Stockhert, B., 1991, Constraints on the late thermotectonic evolution of the western Alps: evidence for episodic rapid uplift: Tectonics, v. 10, p. 758-769.

Jahns, R. H., and Lance, J. F., 1950, Geology of the San Dieguito pyrophyllite area, San Diego County, California: California Division of Mines Special Report, No. 4, 32 p.

Johnson, M. C., and Rutherford, M. J., 1989, Experimental calibration of the aluminum-in-hornblende geobarometer with applications to Long Valley caldera (California) volcanic rocks: Geology, v. 17, p. 837-841.

Johnson, N. M., McGee, V. E., and Naeser, C. W., 1979, A practical method of estimating standard error of age in the fission-track dating method: Nuclear Tracks, v. 3, p. 93-99.

Jones, S. M., and Dokka, R. K., 1986, Effects of time and temperature on the length distribution of fission tracks: implications for thermal history studies of orogenic belts and basins: Geological Society of America Abstracts with Programs, v. 18, p. 506.

_____, and _____, 1990, Modeling fission track annealing in apatite: an assessment of the uncertainties: Nuclear Tracks and Radiation Measurements: v. 17, p. 255-260.

Karig, D. E., and Jensky, W., 1972, The proto-Gulf of California: Earth and Planetary Science Letters, v. 17, p. 169-174.

Keith, S. B., 1978, Paleosubduction geometries inferred from Cretaceous and Tertiary magmatic patterns in southwestern North America: Geology, v. 6, p. 516-521.

Kennedy, M. P., 1975, Geology of the San Diego metropolitan area; Section A, western San Diego metropolitan area: California Division of Mines and Geology Bulletin 200, p. 9-39.

Kennedy, M. P., and Moore, G. W., 1971, Stratigraphic relations of upper Cretaceous and Eocene formations, San Diego coastal area, California: American Association of Petroleum Geologists Bulletin, v. 55, p. 709-722.

Kennedy, M. P., and Peterson, G. L., 1975, Geology of the San Diego metropolitan area; Section B, eastern San Diego metropolitan area: California Division of Mines and Geology Bulletin 200, p. 43-56.

King, R. E., 1939, Geological Reconnaissance in northern Sierra Madre Occidental of Mexico: Geological Society of America Bulletin, v. 50, p. 1625-1727.

Krummenacher, D., Gastil, R. G., Bushee, J., and Doupont, J., 1975, K-Ar apparent ages, Peninsular Ranges batholith, southern California and Baja California: Geological Society of America Bulletin, v. 86, p. 760-768.

Larsen, E. S., Jr., 1948, Batholith and associated rocks of Corona, Elsinore, and San Luis Rey quadrangles, southern California: Geological Society of America Memoir 29, 182 p.

Larsen, R. L., 1972, Bathymetry, magnetic anomalies, and plate tectonic history of the mouth of the Gulf of California: Geological Society of America Bulletin, v. 83, p. 3345-3360.

Laslett, G. M., Kendall, W. S., Gleadow, A. J. W., and Duddy, I. R., 1982, Bias in measurement of fission track length distributions: Nuclear Tracks, v. 6, p. 79-85.

Laslett, G. M., Green, P. F., Duddy, I. R., and Gleadow, A. J. W., 1987, Thermal annealing of fission tracks in apatite, 2. A quantitative analysis: Chemical Geology, v. 65, p. 1-13.

Leeson, R. T., Jr., 1989, Fabric analysis of the Cuyamaca-Laguna Mountains shear zone [M.S. thesis]: San Diego, California, San Diego State University, 136 p.

Leeson, R. T., Jr., Girty, G. H., Wardlaw, M. S., and Meier, D. B., 1989, Harper Creek gneiss, Peninsular Ranges, southern California: Geological Society of America Abstracts with Programs, v. 21, p. 105.

Link, M. H., Peterson, G. L., and Abbott, P. L., 1979, Eocene depositional systems, San Diego, California, *in* P. L. Abbott ed., Eocene depositional systems, San Diego, California: Pacific Section, Society of Economic Paleontologists and Mineralogists, p. 1-8.

Lipman, P. W., Prostka, H. J., and Christiansen, R. L., 1971, Evolving subduction zones in the western United States, as interpreted from igneous rocks: Science, v. 174, p. 821-825.

Livaccari, R. F., Burke, K., and Sengor, A. M. C., 1981, Was the Laramide orogeny related to the subduction of an oceanic plateau?: Nature, v. 289, p. 276-278.

Lohmar, J. M., May, J. A., Boyer, J. E., and Warme, J. E., 1979, Shelf edge deposits of the San Diego Embayment, *in* P. L. Abbott ed., Eocene depositional systems, San Diego, California: Pacific Section, Society of Economic Paleontologists and Mineralogists, p. 15-34.

Luyendyk, B. P., Kamerling, M. J., and Terress, R. R., 1980, Geometric model for Neogene crustal rotations in southern California: Geological Society of America Bulletin, v. 91, p. 1476-1487.

Mammerickx, J., and Klitgord, K. D., 1982, Northern East Pacific Rise; evolution from 25 m.y.b.p. to the present: Journal of Geophysical Research, v. 87, p. 6751-6759.

Mark, E., Pahl, M., Purtscheller, F., and Mark, T. D., 1973, Therische Ausheilung von Uran-Spaltspuren in Apatiten, Alterskorrekturen und Beitrage zur Geothermochonologie: Tschermaks Mineralogische und Petrographische Mitteilungen, v. 20, p. 131-154.

Matti, J. C., Cox, B. F., Powell, R. E., Oliver, H. W., and Kuizon, L., 1983, Mineral resource potential of the Cactus Springs Roadless Area, California: United States Geological Survey Miscellaneous Field Studies Map MF-1650-A, 10 p.

May, D. J., 1989, Late Cretaceous intra-arc thrusting in southern California: Tectonics, v. 8, p. 1159-1173.

May, D. J., and Walker, N. W., 1989, Late Cretaceous juxtaposition of metamorphic terranes in the southeastern San Gabriel Mountains, California: Geological Society of America Bulletin, v. 101, p. 1246-1267.

McDougall, I., and Harrison, T. M., 1988, Geochronology and thermochronology by the $^{40}Ar/^{39}Ar$ method: New York, Oxford University Press, 212 p.

Merriam, R., 1972, Reconnaissance geologic map of the Sonoyta quadrangle, Sonora, Mexico: Geological Society of America Bulletin, v. 83, p. 3533-3536.

_____, 1979, Petrographic evidence of a Sonoran source for upper Paleogene conglomerates in southern California, *in* P. L. Abbott ed., Eocene depositional systems, San Diego, California: Pacific Section, Society of Economic Paleontologists and Mineralogists, p. 119-120.

Miller, F. S., 1937, Petrology of the San Marcos gabbro, southern California: Geological Society of America Bulletin, v. 48, p. 1397-1426.

Miller, R. H., and Dockum, M. S., 1983, Ordovician conodonts from metamorphosed carbonates of the Salton Trough, California: Geology, v. 11, p. 410-412.

Minch, J. A., 1979, The late Mesozoic-early Tertiary framework of continental sedimentation, northern Peninsular Ranges, Baja California, Mexico, *in* Abbott, P. L. ed., Eocene depositional systems, San Diego: Pacific Section, Society of Economic Paleontologists and Mineralogists, p. 43-68.

Morten, D. M., 1969, The Lakeview Mountains pluton, Southern California batholith-Pt.1, Petrology and structure: Geological Society of America Bulletin, v. 80, p. 1539-1551.

Naeser, C. W., 1976, Fission-track dating: United States Geological Survey Open File Report, 76-190, 65 p.

_____, 1979, Fission-Track dating and geologic annealing of fission tracks, *in* E. Jager, and J. C. Hunziker eds., Lectures in isotope geology: New York, Springer-Verlag, p. 154-169.

_____, 1981, The fading of fission tracks in the geologic environment-Data from deep drill holes: Nuclear Tracks, v. 5, p. 248-250.

Naeser, C. W., and Faul, H., 1969, Fission track annealing in apatite and sphene: Journal of Geophysical Research, v. 74, p. 705-710.

Naeser, C. W., and Forbes, R. B., 1976, Variation of fission track ages with depth in two deep drill holes: EOS (American Geophysical Union Transactions), v. 57, p. 363.

Naeser, C. W., Zimmerman, R. A., and Cebula, G. T., 1981, Fission-track dating of apatite and zircon: an interlaboratory comparison: Nuclear Tracks, v. 5, p. 65-72.

Nand Lal, Saini, H. S., Nagpaul, K. K., and Sharma K. K., 1976, Tectonic and cooling history of the Bihar Mica Belt, India, as revealed by fission-track analysis: Tectonophysics, v. 34, p. 163-180.

Nilsen, T. H., and McKee, E. H., 1979, Paleogene Paleogeography of the western United States, *in* J. M. Armentrout, M. R. Cole, and H. Terbert Jr. eds., Cenozoic Paleogeography of the western United States: Pacific Section, Society of Economic Paleontologists and Mineralologists, Pacific Coast Paleogeography Symposium 3, p. 257-276.

Nilsen, T. H., and Abbott, P. L., 1981, Paleogeography and sedimentology of upper Cretaceous turbidites, San Diego, California: American Association of Petroleum Geologists Bulletin, v. 65, p. 1256-1284.

Nordstrom, C. E., 1970, Lusardi formation: a post-batholithic Cretaceous conglomerate north of San Diego: Geological Society of America Bulletin, v. 81, p. 601-606.

Nunn, J. A., 1990, Relaxation of continental lithosphere: an explanation for Late Cretaceous reactivation of the Sabine uplift of Louisiana-Texas: Tectonics, v. 9, p. 341-359.

O'Brien, D. K., Wenk, H., Ratschbacher, L., and You, Z., 1987, Preferred orientation of phyllosilicates in phyllonites and ultramylonites: Journal of Structural geology, v. 9, p. 719-730.

Page, B. M., and Engebretson, D. C., 1984, Correlation between the geologic record and computed plate motions for central California: Tectonics, v. 3, p. 133-155.

Parrish, R. R., 1983, Cenozoic thermal evolution and tectonics of the Coast Mountains of British Columbia 1. Fission track dating, apparent uplift rates, and patterns of uplift: Tectonics, v. 2, p. 601-631.

Peterson, G. L., 1971, Stratigraphy of the Poway area, southwestern California: San Diego Society of Natural History, v. 16, p. 225-236.

Peterson, G. L., and Nordstrom, C. E., 1970, Sub-La Jolla unconformity in vicinity of San Diego, California: American Association of Petroleum Geologists Bulletin, v. 54, p. 265-274.

Popenoe, W. P., 1941, The Trabuco and Baker conglomerates of the Santa Ana Mountains: Journal of Geology, v. 49, p. 738-752.

Rangin, C., 1982, Contribution al'etude geologique du systeme Cordillerain du nord-quest du Mexique: Memores des Sciences de la Terre, Academie de Paris, Universite Pierre et Marie Curie, 588 p.

Roberts, J. H., Gold, R., and Armani, R. J., 1968, Spontaneous fission decay constant of ^{238}U: Physical Review, v. 174, p.1482-1484.

Rodgers, T. H., 1965, Geologic map of California, Santa Ana sheet: California Division of Mines and Geology, scale 1:250,000.

Sage, O., Jr., 1973, Paleocene geography of the Los Angeles region: Stanford University Publication of Geological Science, v. 13, p. 348-357.

Schmidt, M. W., 1992, Amphibole composition in tonalite as a function of pressure: an experimental calibration of the Al-in-hornblende: Contributions to Mineralogy and Petrology, v. 110, p. 304-310.

Schoellhamer, J. E., Kinney, D. M., Yerkes, R. F., and Vedder, J. G., 1981, Geology of the northern Santa Ana Mountains, California: United States Geological Survey Professional Paper, v. 420-D, p. D1-D109.

Schultejann, P. A., 1984, The Yaqui Ridge antiform and detachment fault: mid-Cenozoic extensional terrane west of the San Andreas fault: Tectonics, v. 3, p. 676-691.

Schwarcz, H. P., 1969, Pre-Cretaceous sedimentation and metamorphism in the Winchester area, northern Peninsular Ranges, California: Geological Society of America Special Paper 100, 61 p.

Sharp, R. V., 1966, Ancient mylonite zone and fault displacements in the Peninsular Ranges of southern California: Geological Society of America Special Paper 101, p. 333.

_____, 1967, San Jacinto fault zone in the Peninsular Ranges of southern California: Geological Society of America Bulletin, v. 78, p. 705-730.

_____, 1979, Some characteristics of the eastern Peninsular Ranges mylonite zone: Proceedings on conference VIII, analysis of actual fault zones in bedrock: United States Geological Survey Open-file Report, 79-1239, p. 258-267.

Sibson, R. H., 1977, Fault rocks and fault mechanisms: Journal of the Geological Society of London: v. 133, p. 191-213.

Silver, L. T., 1986, U-Th-Pb microdiscordance in young zircons; a case study in the San Jacinto Mountains, California: EOS (American Geophysical Union Transactions), v. 67, p. 399-400.

Silver, L. T., Early, T. O., and Anderson, T. H., 1975, Petrological, geochemical, and geochronological asymmetries of the Peninsular Ranges batholith: Geological Society of America Abstracts with Programs, v. 7, p. 375-376.

Silver, L. T., Taylor, H. P., Jr., and Chappell, B., 1979, Some petrological, geochemical and geochronological observations in the Peninsular Ranges batholith near the International Border of the U.S.A., and Mexico: Guidebook Geological Society of America Annual Meeting, San Diego, *in* P. L. Abbott and V. R. Todd eds., Mesozoic crystalline rocks: Peninsular Ranges Batholith and pegmatites, Point Sal Ophiolite: Department of Geological Sciences, San Diego State University, p. 83-110.

Silver, L. T., and Chappell, B. W., 1988, The Peninsular Ranges batholith: an insight into the evolution of the Cordilleran batholiths of southwestern North America: Transactions of the Royal Society of Edinburgh: Earth Sciences, v. 79, p. 105-121.

Simpson, C., 1984, Borrego Springs-Santa Rosa mylonite zone: A Late Cretaceous west-directed thrust in southern California: Geology, v. 12, p. 8-11.

_____, 1985a, Comment on "Late Mesozoic and Cenozoic tectonic history of south central California" by A. E. J. Engel and P. A. Schultejann and on " The Yaqui Ridge antiform and detachment fault: mid-Cenozoic extensional terrane west of the San Andreas fault" by Patricia A. Schultejann: Tectonics, v. 4, p. 595-596.

_____, 1985b, Deformation of granitic rocks across the brittle-ductile transition: Journal of Structural Geology, v. 7, p. 503-511.

Simpson, C., and Schmid, S. M., 1983, An evaluation of criteria to deduce the sense of movement in sheared rocks: Geological Society of America Bulletin, v. 94, p. 1281-1280.

Sliter, W. V., 1979, Cretaceous foraminifers from La Jolla, California, *in* Abbott, P. L., ed., Geological excursions in the southern California area: San Diego State University, Department of Geological Sciences, San Diego, California, p. 171-172.

Smith, D. K., Morten, D. M., and Miller, F. K., 1991, Hornblende geobarometry and biotite K-Ar ages from the northern part of the Peninsular Ranges batholith, southern California: Geological Society of America Abstracts with Programs, v. 23, p. 273.

Smith, M. J., and Leigh-Jones, P., 1991, An automated microscope scanning stage system for fission track dating: Nuclear Tracks.

Spencer, J. E., and Reynolds, S. J., 1990, Relationship between Mesozoic and Cenozoic tectonic features in west central Arizona and adjacent southeastern California: Journal of Geophysical Research, v. 95, p. 539-555.

Steiger, R. H., and Jager, E., 1977, Subcommission on geochronology: convention on the use of decay constants in geo- and cosmochronology: Earth and Planetary Science Letters, v. 36, p. 359-362.

Stock, J., and Molnar, P., 1988, Uncertainties and implications of the Late Cretaceous and Tertiary position of North America relative to the Farallon, Kula, and Pacific plates: Tectonics, v. 7, p. 1339-1384.

Stock, J., and Hodges, K. V., 1989, Pre-Pliocene extension around the Gulf of California and the transfer of Baja California to the Pacific Plate: Tectonics, v. 8, p. 99-115.

Sundberg, F. A., 1979, Upper Cretaceous macro-fossils of San Diego, *in* Abbott, P. L., ed., Geological excursions in the southern California area: San Diego State University, Department of Geological Sciences, San Diego, California, p. 173-176.

Teissere, R. F., and Beck, M. E., Jr., 1973, Divergent Cretaceous paleomagnetic pole position for the Southern California Batholith, U.S.A.: Earth and Planetary Science Letters, v. 18, p. 296-300.

Theodore, T. G., 1967, Structure and petrology of the gneisses and mylonites at Coyote Mountain, Borrego Springs, California [Ph. D. thesis]: University of California, Los Angeles, 268 p.

_____, 1970, Petrogenesis of mylonites of high metamorphic grade in the Peninsular ranges of southern California: Geological Society of America Bulletin, v. 81, p. 435-450.

Theodore, T. G., and Sharp, R. V., 1975, Geologic map of the Clark Lake quadrangle, San Diego County, California: United States Geological Survey Miscellaneous Field Study map, No. MF-644, geologic map 1:24,000.

Todd, V. R., 1979, Geologic map of the Mount Laguna quadrangle, San Diego County, California: United States Geological Survey Open File Report 79-862.

Todd, V. R., and Shaw, S. E., 1979, Structural, metamorphic, and intrusive framework of the Peninsular Ranges Batholith in southern San Diego County, California, *in* Abbott, P. L.and Todd, V. R., eds., Mesozoic crystalline rocks: Geological Society of America Annual Meeting Field Trip Guidebook, San Diego, San Diego State University, p. 176-231.

Todd, V. R., Erskine, B. G., and Morten, D. M., 1988, Metamorphic and tectonic evolution of the northern Peninsular Ranges Batholith, southern California, *in* W. G. Ernst ed., Metamorphism and crustal evolution of the western United States, Rubey Volume VII: Engelwood Cliffs, New Jersey, Prentice-Hall, p. 894-937.

Todd, V. R., Shaw, S. E., Jachens, R. C., Kimbrough, D. L., Girty, G. H., and Hammarstrom, J. M., 1991, The El Cajon 30' X 60" quadrangle, southern California: a geologic history from early Mesozoic continental growth to modern rift-transform tectonics: Geological Society of America Abstracts with Programs, v. 23, p. 479.

Tweto, O., 1975, Laramide (Late Cretaceous-early Tertiary) orogeny in the southern Rocky Mountains: Geological Society of America Memoir 144, p. 1-44.

Wagner, G. A., and Reimer, G. M., 1972, Fission track tectonics: The tectonic interpretation of fission track ages: Earth and Planetary Science Letters, v. 45, p. 355-360.

Wagner, F., Wenk, H. -R., Kern, H., Van Houtte, P., and Esling, C., 1982, Development of preferred orientation in plane strain deformed limestone: Experiment and theory: Contributions to Mineralogy and Petrology, v. 80, p. 132-139.

Wagner, G. A., Reimer, G. M., and Jager, E., 1977, Cooling ages derived by apatite fission-track, mica Rb-Sr, and K-Ar dating: the uplift and cooling history of the central Alps: Memorie degli Instuti di Geologia e Mineralogia dell'Universita di Padova, 28 p.

Walawender, M. J., and Smith, T. E., 1980, Geochemical and petrologic evolution of the basic plutons of the Peninsular Ranges batholith, southern California: Journal of Geology, v. 88, p. 233-242.

Walawender, M. J., Gastil, R. G., Clinkenbeard, J. P., McCormick, W. V., Eastman, B. G., Wernicke, R. S., Wardlaw, M. S., Gunn, S. H., and Smith, B. M., 1990, Origin and evolution of the zoned La Posta-type plutons, eastern Peninsular Ranges batholith, southern and Baja California, in Anderson, J. L., ed., The nature and origin of Cordilleran magmatism: Geological Society of America Memoir 174, p. 1-18.

Walawender, M. J., Girty, G. H., Lombardi, M. R., Kimbrough, D., Girty, M. S., and Anderson, C., 1991, A synthesis of recent work in the Peninsular Ranges batholith, *in* M. J. Walawender and B. B. Hanan eds., Geological excursions in southern California and Mexico: Geological Society of America Annual Meeting Field Trip Guidebook, San Diego State University, San Diego, California, p. 297-312.

Wallace, R. D., and English, D. L., 1982, Evaluation of possible detachment faulting west of the San Andreas, southern Santa Rosa Mountains, California, *in* E. G. Frost and D. L. Martin eds., Mesozoic-Cenozoic tectonic evolution of the Colorado River region, California, Arizona, and Nevada: Cordilleran Publishers, p. 503-509.

Watt, S., and Durrani, S. A., 1985, Thermal stability of fission tracks in apatite and sphene: Using confined-track-length measurements: Nuclear Tracks and Radiation Measurements, v. 10, p. 200-215.

Weber, F. H., Jr., 1963, Geology and mineral resources of San Diego County, California: California Division of Mines and Geology County Report 3, 309 p.

Woodford, A. O., Welday, E. E., and Merriam, R. H., 1968, Siliceous tuff clasts in the Upper Paleogene of southern California: Geological Society of America Bulletin, v. 79, p. 1461-1486.

Zeitler, P. K., Tahirkeli, A. K., Naeser, C. W., and Johnson, N. M., 1982, Unroofing history of a suture zone in the Himalaya of Pakistan by means of fission-track annealing ages: Earth and Planetary Science Letters, v. 57, p. 227-240.

Zimmerman, R. A., and Gaines, A. M., 1978, A new approach to the study of fission track dating: United States Geological Survey Open-file Report 78-701, p. 467-468.

APPENDIX A

METHODS FOR FISSION-TRACK ANALYSIS

The following is a description of methods for fission-track analysis used in this study. It includes procedures followed for sample preparation, as well as those for fission-track dating and determining apatite track-length distributions.

Samples of 9-14 kg (20-30 lbs.) were collected, generally along road cuts. These samples were then broken into "plum-sized" pieces and run through a jaw crusher. "Pea-sized" rock fragments from the jaw crusher were passed through a Bico pulverizer and broken down into very fine to medium-grained sand (1-4 ϕ, or .0625-0.5 mm). This material was then sieved to remove any coarse material.

The samples were initially concentrated on a Wilfley concentration table, which generally produced ~0.5 kg of heavy mineral concentrate. This 0.5 kg of sample was then air dried, and its magnetic fraction removed with a hand magnet. A vertically-oriented Frantz magnetic separator can also be used for the same purpose. The material was further concentrated using sodium polytungstate (sp. gr. = 2.85) and standard heavy liquid separation techniques. Sodium polytungstate was used instead of bromoform because it is non-toxic. The majority of quartz and feldspar floated in the liquid, although some samples required two passes to completely remove the light mineral fraction. Complete descriptions on the use of sodium polytungstate in mineral separations has been reported by Callahan (1987) and Gregory and Johnston (1987). The heavy fraction was then run through a Frantz magnetic separator at progressively increasing amperage (up to ~1.6 amps), which produced final nonmagnetic fractions of apatite + zircon. Sphene was recovered at an intermediate step (i.e. between ~1.0 and 1.5 amps) in the magnetic separation. The apatite and zircon were finally separated from one another using methylene iodide (sp. gr. = 3.33). Lithium metatungstate (sp. gr. =

3.2) can also be used to separate the two, as it was for the Palomar Mountain-Escondido samples, if the apatite has a specific gravity less than 3.2.

After separation, the minerals were mounted and polished before etching. In the case of apatite, the grains were mounted in epoxy, ground with silicon carbide abrasive paper (400 and 600 grit), and polished with diamond polishing compound (6 and 1μm paste). Zircon and sphene were mounted in FEP teflon® on a hot plate at ~315°C. They were then ground and polished using the same procedures as for apatite. A more complete description of these sample preparation techniques can be found in Naeser (1976).

Fission tracks are too small to be seen unless they are enlarged with a chemical etchant. Apatite mounts used for age determinations in this study were etched with 7% HNO_3 for 30-40 seconds at 25°C (see Naeser, 1976; Crowley et al., 1989). Apatite mounts used for measuring track lengths were etched with 5 M HNO_3 for 20 seconds, also at 25°C, as described in Green (1981). Zircon mounts were etched anywhere from 6 to 18 hours in a eutectic melt of KOH and NaOH at ~220°C in an oven. Sphene mounts were etched from 1 to 3 hours with 50 M HNO_3 at ~130°C.

All grain ages from this study were dated using the external detector method (see Naeser, 1976; Crowley et al., 1989). This method involves covering each grain mount with a clean piece of low uranium (< 10 ppb) muscovite after etching. The mounts are stacked vertically between two pieces of uranium glass (National Bureau of Standards Fission-Track Glasses 962 and 963a were used in this study), which also are covered with muscovite, and the entire stack is placed inside a plastic irradiation tube. Four separate tubes of apatite or zircon + sphene were prepared in this study, which were then sent to the Triga nuclear reactor at the United States Geological Survey in Denver, Colorado. After irradiation, the muscovite detectors from the grain mounts were removed and etched in 48% HF at 25°C for 11 minutes. The detectors from the glasses

were etched under similar conditions for 1 hour. The grain mounts and their respective muscovite detectors were affixed, side by side, on a glass microscope slide in order to be counted using the Autoscan(TM) microcomputer-controlled automated stage (see Smith and Leigh-Jones, 1985 for a description of the Autoscan(TM) system).

There are three measurements that must be made in order to calculate a fission-track age for an individual grain mount using the "zeta" method (this method is described in the following paragraph). They are the fossil track density, induced track density, and the track densities of the detectors covering the standard glasses. Track densities were determined for each grain mount and detector by counting at x1500 magnification under oil. Fossil tracks were counted within a reticle grid of known area covering some part of a grain, and a number of grains were counted in each mount (see Fission-Track Data Tables in chapters 2 and 4 for the exact number). The induced tracks were counted on the mirror image of these grains over exactly the same area of the grain counted for fossil tracks. Induced tracks form during bombardment of the grains in the reactor by thermal neutrons (i.e. by slow, or low-energy neutrons). This causes ^{235}U contained in the mineral grains to fission, and the uranium that fissions near the surface of the grains will send fragments into the adjacent muscovite detector (i.e. will form induced fission tracks). By counting the density of induced fission tracks in the detectors, the uranium concentration of the areas counted for fossil tracks can be determined. Determining uranium concentration is a necessary step in dating a mineral, since fossil-track densities are a function of time and the amount of uranium in a mineral grain. Track densities of induced fission tracks are also counted in the muscovite detectors covering the glass standards. The glasses used in this study were National Bureau of Standards Fission-Track Glasses 962 and 963a. These standards were previously calibrated using apatite and zircon of known age from the Fish Canyon Tuff (see Naeser et al., 1981). The

specifics of counting are described in greater detail in Naeser (1976), Crowley et al. (1989), and Smith and Leigh-Jones (1985).

The conventional fission-track age equation is:

$$t = \frac{1}{\lambda_d} \ln\left[1 + \frac{\rho_s}{\rho_i}\left(\frac{\lambda_d \phi \sigma I}{\lambda_f}\right)\right] \quad (1)$$

where

λ_d = total decay constant for ^{238}U (λ_α , alpha decay + λ_f , spontaneous decay)

= 1.551×10^{-10} yr^{-1}

λ_f = spontaneous fission decay constant for ^{238}U

= 7.03×10^{-17} yr^{-1} (Roberts et al., 1968)

ρ_s = spontaneous fission-track density

ρ_i = induced fission-track density

ϕ = thermal neutron dose (neutrons / cm^2)

I = atomic ratio of ^{235}U / ^{238}U

= 7.25×10^{-3}

σ = cross-section for neutron induced fission of ^{235}U

= 580.2×10^{-24} cm^{-2}

Fission-track ages determined using equation (1) are subject to errors due to the uncertainty of the decay constant for spontaneous fission , and are also prone to difficulties with measurements of the neutron dose . To avoid these problems Hurford and Green (1983) recommended the "zeta" method of age calculation. This was the method used in age determinations in this study. The zeta method involves the

calibration of glass dosimeters (NBS 962 and 963a were used here) with minerals of known age (apatite and zircon of the Fish Canyon Tuff, t = 27.5 Ma). The first step of the zeta method is the determination of zeta factors (ζ) for apatite and zircon. Zeta factors for both apatite and zircon using the Fish Canyon Tuff were determined by irradiating these minerals along with NBS glass dosimeters 962 and 963a. They were calculated by the following equation of Hurford and Green (1983):

$$\zeta = \frac{\exp(\lambda_d t_{std}) - 1}{\lambda_d \left[\left(\frac{\rho_s}{g} \right) \rho_i \right]_{std} \rho_d} \qquad (2)$$

where

t_{std} = the age of the mineral standard (Fish Canyon Tuff = 27.5 Ma)

$\left(\frac{\rho_s}{\rho_i} \right)_{std}$ = the ratio of fossil- and induced-track densities in the age standard

ρ_d = track density in the neutron dose monitor

g = geometry factor

= 2 (external detector method)

Once the zeta factors have been determined (in this study ζ apatite = 10692, and ζ zircon = 335), a mineral can be dated using the following equation of Hurford and Green (1983):

$$t_{unk} = \frac{1}{\lambda_d} \ln \left[1 + \left(\frac{\rho_s}{\rho_i} \right) \zeta \rho_d \lambda_d \right] \qquad (3)$$

where

t_{unk} = age of the unknown mineral

ρ_s = fossil-track density in unknown

ρ_i = induced-track density in unknown

Radioactive decay, including the formation of fission tracks, can be treated with Poissonian statistics (Johnson et al., 1979; Galbraith, 1981; Green, 1981). Poissonian statistics are based on the Poisson frequency distribution, which assumes that events occur independently (Davis, 1973). The probability of a event occurring, in this case the decay of a uranium nucleus by fission, is directly proportional to the length of time preceding the event. In Poissonian statistics the mean is equal to the variance, and variance is equal to the standard deviation squared. Therefore, basic fission-track counting data lends itself to calculating standard errors based on the Poisson distribution. The standard error of an age is the sum of the standard errors of the fossil count, $\sigma(\rho_s)$, the induced count, $\sigma(\rho_i)$, and the counts used for neutron dose determinations, $\sigma(\phi)$. These errors are:

$$\sigma(\rho_s) = \frac{(N_s)^{0.5}}{A};\ \sigma(\rho_i) = \frac{(N_i)^{0.5}}{A};\ \sigma(\phi) = \frac{(N_d)^{0.5}}{A} \qquad (4)$$

where

N_s = total number of spontaneous tracks counted

N_i = total number of induced tracks counted

N_d = total number of tracks counted in the dosimeter

A = total area counted

The total error of an age, t, determined using the external detector method is:

$$\frac{\sigma(t)}{t} = C\left(\left[\frac{\sigma(\rho_s)}{\rho_s}\right]^2 + \left[\frac{\sigma(\rho_i)}{\rho_i}\right]^2 + \left[\frac{\sigma(\phi)}{\phi}\right]^2\right)^{0.5} \qquad (5)$$

C is an age-dependent correction factor from Johnson et al. (1979) in which:

$$C = \frac{1}{t\,\lambda_\alpha}\left(1 - e^{-t\,\lambda_\alpha}\right) \tag{6}$$

where

t = calculated fission-track age

λ_α = the decay constant for ^{238}U

Galbraith (1981) suggested a chi squared (χ^2) test to determine whether or not age data conform to the Poissonian distribution. For *n* number of grains counted per grain mount, the χ^2 statistic is calculated by:

$$\chi^2 = \sum_{j=1}^{n} \frac{\left(N_{sj} - \hat{N_{sj}}\right)}{\hat{N_{sj}}} + \sum_{j=1}^{n} \frac{\left(N_{ij} - \hat{N_{ij}}\right)}{\hat{N_{ij}}} \tag{7}$$

where

N_{sj} = the number of spontaneous tracks counted on the *j* th grain

N_{ij} = the number of induced tracks counted on the *j* th grain

The expected values, $\hat{N}_{sj}$ and $\hat{N}_{ij}$ are determined by:

$$\hat{N_{sj}} = \frac{N_s}{N_s + N_i}(N_{sj} + N_{ij}); \; \hat{N_{ij}} = \frac{N_i}{N_s + N_i}(N_{sj} + N_{ij}) \tag{8}$$

A 5% probability cutoff is accepted as determining whether or not a distribution is Poissonian. If the χ^2 value is less than the critical value for (n-1) degrees of freedom at the 5% level (i.e. passed the test), then the standard error of the age, t, can be determined using equation (5). If value is larger than the critical value (i.e. failed the test), then equation (5) is not acceptable for determining the standard error. In this study all values passed the χ^2 test (see Fission-Track Data Tables in chapters 2 and 4).

Apatite track-lengths were measured for the majority of samples in this study. They were prepared for track-length measurements according to the methods of Green (1981) and Laslett et al. (1982). Only horizontal confined fission tracks located on prismatic surfaces were measured (i.e. parallel to the c-axis). Track lengths were measured "dry" using an optical microscope (x1500) linked by way of a camera lucida to a digitizing pad and microcomputer. Generally 100 tracks per sample were measured, although this was not always possible. Track-length distributions were constructed using standard statistical software (Statview®) and mean track lengths and standard deviations were determined. These distributions are presented in figures in chapters 2 and 4.

APPENDIX B

ELECTRON MICROPROBE COMPOSITIONAL DATA FOR AMPHIBOLE AND PLAGIOCLASE OF SAMPLES FROM THE SAN JACINTO MOUNTAINS

AMPHIBOLE TRAVERSE ACROSS PHENOCRYST IN SAN JACINTO MTNS (10804') PG-101

Sample name	PG-101									
Analysis pt	2	3	4	5	7	8	9	10	11	12
Remark	33.3 um int									
SiO2	43.56	43.46	43.36	43.02	43.45	43.51	44.24	43.98	43.51	41.92
TiO2	1.15	1.59	1.71	1.63	1.59	1.57	1.53	1.47	1.43	0.21
Al2O3	10.21	9.75	9.82	9.59	9.37	9.33	9.20	9.31	9.48	12.10
Cr2O3	0.00	0.00	0.00	0.00	0.00	0.00	0.01	0.02	0.05	0.01
Fe2O3 @	5.34	3.58	4.99	4.82	5.07	4.79	4.88	5.12	4.61	7.25
FeO	16.42	17.91	16.26	16.13	16.11	16.07	16.43	16.46	16.45	16.24
MnO	0.55	0.57	0.54	0.69	0.56	0.68	0.54	0.56	0.51	0.47
MgO	7.96	7.91	8.35	8.37	8.59	8.53	8.59	8.42	8.33	6.87
CaO	11.36	11.57	11.20	11.31	11.41	11.28	11.22	11.31	11.40	11.47
Na2O	1.21	1.33	1.46	1.40	1.34	1.41	1.47	1.38	1.21	1.33
K2O	1.21	1.24	1.25	1.19	1.18	1.14	1.19	1.17	1.16	1.02
Total	98.96	98.91	98.94	98.15	98.67	98.31	99.30	99.20	98.13	98.89
---Atomic proportions based on 13 cations (except Ca+Na+K+Ba)---										
Si	6.544	6.562	6.518	6.524	6.549	6.575	6.617	6.593	6.587	6.335
Ti	0.130	0.181	0.193	0.186	0.180	0.178	0.172	0.166	0.163	0.024
Al(iv)	1.456	1.438	1.482	1.476	1.451	1.425	1.383	1.407	1.413	1.665
Al(vi)	0.352	0.298	0.258	0.237	0.213	0.237	0.239	0.238	0.279	0.490
Cr	0.000	0.000	0.000	0.000	0.000	0.000	0.001	0.002	0.006	0.001
Fe3+ (calc)	0.604	0.407	0.564	0.550	0.575	0.545	0.550	0.578	0.525	0.825
Fe2+	2.062	2.262	2.045	2.046	2.031	2.031	2.055	2.064	2.082	2.052
Mn2+	0.070	0.073	0.069	0.089	0.071	0.087	0.068	0.071	0.065	0.060
Mg	1.783	1.781	1.871	1.892	1.930	1.922	1.915	1.882	1.880	1.548
C site (M1+M2+M3)	5.000	5.000	5.000	5.000	5.000	5.000	5.000	5.000	5.000	5.000
excess (M1+M2+M3)	0.000	0.000	0.000	0.000	0.000	0.000	0.000	0.000	0.000	0.000
Ca	1.828	1.872	1.804	1.838	1.842	1.826	1.798	1.817	1.849	1.857
Na(M4)	0.172	0.128	0.196	0.162	0.158	0.174	0.202	0.183	0.151	0.143
B site (M4) total	2.000	2.000	2.000	2.000	2.000	2.000	2.000	2.000	2.000	2.000
Na(A)	0.181	0.261	0.229	0.249	0.234	0.240	0.224	0.218	0.204	0.247
K	0.232	0.239	0.240	0.230	0.227	0.220	0.227	0.224	0.224	0.197
A site total	0.413	0.500	0.469	0.479	0.461	0.459	0.451	0.441	0.428	0.444
Mg/Fe(tot)	0.669	0.667	0.717	0.729	0.741	0.746	0.735	0.712	0.721	0.538
Mg/Fe2+	0.864	0.787	0.915	0.925	0.950	0.946	0.932	0.912	0.903	0.754
Mg/Mg+Fe(tot)	0.401	0.400	0.418	0.422	0.426	0.427	0.424	0.416	0.419	0.350
Mg/Mg+Fe2+	0.464	0.441	0.478	0.481	0.487	0.486	0.482	0.477	0.474	0.430
Fe3+/Fe(tot)	0.226	0.152	0.216	0.212	0.221	0.212	0.211	0.219	0.201	0.287
Cation charge	44.793	45.186	44.872	44.899	44.851	44.910	44.901	44.845	44.951	44.351

@ Fe3+ calculated by charge balance

AMPHIBLOE TRAVERSE ACROSS PHENOCRYST IN SAN JACINTO MTNS (10804') PG-101

Sample name Analysis pt Remark	15	16	17	19	21	23	24	25	26	27
SiO2	44.03	41.45	43.94	43.20	43.16	43.09	43.70	44.14	44.36	44.46
TiO2	1.46	0.26	1.21	0.98	0.93	1.13	1.19	1.28	1.35	1.38
Al2O3	9.31	12.89	9.14	9.90	10.41	10.07	9.70	9.24	9.21	9.14
Cr2O3	0.00	0.05	0.00	0.00	0.00	0.01	0.01	0.03	0.02	0.03
Fe2O3 @	4.20	6.48	4.16	4.61	4.58	4.70	4.42	5.27	4.84	4.86
FeO	16.79	17.46	16.84	17.01	16.84	16.85	16.83	15.98	16.69	16.26
MnO	0.41	0.40	0.48	0.46	0.50	0.52	0.51	0.48	0.52	0.52
MgO	8.39	6.15	8.42	8.05	7.84	8.07	8.18	8.55	8.38	8.36
CaO	11.40	11.48	11.60	11.69	11.55	11.70	11.45	11.30	11.48	11.26
Na2O	1.18	1.29	1.11	1.20	1.10	1.19	1.21	1.25	1.17	1.02
K2O	1.13	1.25	1.08	1.13	1.28	1.18	1.23	1.06	1.08	1.14
Total	98.30	99.16	97.98	98.23	98.19	98.51	98.43	98.58	99.11	98.44
---Atomic proportions based on 13 cations (except Ca+Na+K+Ba)---										
Si	6.644	6.276	6.658	6.554	6.542	6.520	6.601	6.634	6.645	6.685
Ti	0.166	0.030	0.138	0.112	0.106	0.129	0.135	0.145	0.152	0.156
Al(iv)	1.356	1.724	1.342	1.446	1.458	1.480	1.399	1.366	1.355	1.315
Al(vi)	0.299	0.576	0.291	0.324	0.401	0.316	0.328	0.271	0.271	0.305
Cr	0.000	0.006	0.000	0.000	0.000	0.001	0.001	0.004	0.002	0.004
Fe3+ (calc)	0.477	0.738	0.474	0.527	0.523	0.535	0.502	0.596	0.546	0.550
Fe2+	2.118	2.211	2.134	2.158	2.134	2.132	2.126	2.009	2.091	2.045
Mn2+	0.052	0.051	0.062	0.059	0.064	0.067	0.065	0.061	0.066	0.066
Mg	1.887	1.388	1.902	1.821	1.772	1.820	1.842	1.916	1.871	1.874
C site (M1+M2+M3)	5.000	5.000	5.000	5.000	5.000	5.000	5.000	5.000	5.000	5.000
excess (M1+M2+M3)	0.000	0.000	0.000	0.000	0.000	0.000	0.000	0.000	0.000	0.000
Ca	1.843	1.862	1.883	1.900	1.876	1.897	1.853	1.820	1.843	1.814
Na(M4)	0.157	0.138	0.117	0.100	0.124	0.103	0.147	0.180	0.157	0.186
B site (M4) total	2.000	2.000	2.000	2.000	2.000	2.000	2.000	2.000	2.000	2.000
Na(A)	0.188	0.241	0.209	0.253	0.199	0.246	0.207	0.184	0.182	0.111
K	0.218	0.241	0.209	0.219	0.248	0.228	0.237	0.203	0.206	0.219
A site total	0.406	0.482	0.418	0.472	0.446	0.474	0.444	0.387	0.389	0.330
Mg/Fe(tot)	0.727	0.471	0.729	0.678	0.667	0.682	0.701	0.736	0.710	0.722
Mg/Fe2+	0.891	0.628	0.891	0.844	0.830	0.854	0.866	0.954	0.895	0.916
Mg/Mg+Fe(tot)	0.421	0.320	0.422	0.404	0.400	0.406	0.412	0.424	0.415	0.419
Mg/Mg+Fe2+	0.471	0.386	0.471	0.458	0.454	0.461	0.464	0.488	0.472	0.478
Fe3+/Fe(tot)	0.184	0.250	0.182	0.196	0.197	0.201	0.191	0.229	0.207	0.212
Cation charge	45.045	44.523	45.052	44.946	44.955	44.929	44.995	44.809	44.908	44.899

@ Fe3+ calculated by charge balance

AMPHIBLDE TRAVERSE ACROSS PHENOCRYST IN SAN JACINTO MTNS (10804') PG-101

Sample name Analysis pt Remark	28	29	30	31	32	33	34	35	36	37
SiO2	44.02	44.05	44.14	43.39	43.45	43.47	43.34	43.24	43.28	43.64
TiO2	1.45	1.48	1.28	1.17	1.17	1.12	1.13	1.20	1.44	1.33
Al2O3	9.14	9.56	9.47	9.55	9.82	10.13	10.10	10.02	9.79	9.41
Cr2O3	0.00	0.04	0.00	0.01	0.00	0.00	0.01	0.00	0.05	0.00
Fe2O3 @	4.99	3.83	5.43	5.76	5.37	4.95	4.84	4.93	5.14	4.55
FeO	16.48	17.19	16.04	15.94	16.58	16.95	17.25	16.74	16.70	16.77
MnO	0.55	0.51	0.55	0.52	0.53	0.54	0.55	0.46	0.53	0.49
MgO	8.48	8.30	8.43	8.31	8.10	7.99	7.91	7.90	7.96	8.37
CaO	11.50	11.56	11.41	11.42	11.43	11.72	11.64	11.37	11.36	11.66
Na2O	1.20	1.21	1.14	1.19	1.32	1.13	1.29	1.21	1.21	1.15
K2O	1.10	1.17	1.11	1.12	1.17	1.19	1.24	1.20	1.24	1.10
Total	98.91	98.90	98.99	98.38	98.94	99.20	99.29	98.27	98.69	98.47
---Atomic proportions based on 13 cations (except Ca+Na+K+Ba)---										
Si	6.614	6.618	6.611	6.557	6.543	6.531	6.519	6.549	6.536	6.592
Ti	0.164	0.167	0.144	0.133	0.132	0.127	0.128	0.137	0.164	0.151
Al(iv)	1.386	1.382	1.389	1.443	1.457	1.469	1.481	1.451	1.464	1.408
Al(vi)	0.232	0.311	0.283	0.258	0.285	0.325	0.310	0.338	0.278	0.267
Cr	0.000	0.005	0.000	0.001	0.000	0.000	0.001	0.000	0.006	0.000
Fe3+ (calc)	0.564	0.434	0.612	0.655	0.609	0.560	0.548	0.562	0.584	0.517
Fe2+	2.071	2.160	2.009	2.014	2.088	2.130	2.169	2.120	2.109	2.118
Mn2+	0.070	0.065	0.070	0.067	0.068	0.069	0.070	0.059	0.068	0.063
Mg	1.899	1.859	1.882	1.872	1.818	1.790	1.774	1.784	1.792	1.885
C site (M1+M2+M3)	5.000	5.000	5.000	5.000	5.000	5.000	5.000	5.000	5.000	5.000
excess (M1+M2+M3)	0.000	0.000	0.000	0.000	0.000	0.000	0.000	0.000	0.000	0.000
Ca	1.851	1.861	1.831	1.849	1.844	1.887	1.876	1.845	1.838	1.887
Na(M4)	0.149	0.139	0.169	0.151	0.156	0.113	0.124	0.155	0.162	0.113
B site (M4) total	2.000	2.000	2.000	2.000	2.000	2.000	2.000	2.000	2.000	2.000
Na(A)	0.201	0.213	0.162	0.198	0.229	0.216	0.252	0.200	0.192	0.224
K	0.211	0.224	0.212	0.216	0.225	0.228	0.238	0.232	0.239	0.212
A site total	0.412	0.438	0.374	0.414	0.454	0.444	0.490	0.432	0.431	0.436
Mg/Fe(tot)	0.721	0.717	0.718	0.701	0.674	0.665	0.653	0.665	0.666	0.715
Mg/Fe2+	0.917	0.861	0.937	0.930	0.871	0.840	0.818	0.841	0.850	0.890
Mg/Mg+Fe(tot)	0.419	0.418	0.418	0.412	0.403	0.399	0.395	0.399	0.400	0.417
Mg/Mg+Fe2+	0.478	0.463	0.484	0.482	0.466	0.457	0.450	0.457	0.459	0.471
Fe3+/Fe(tot)	0.214	0.167	0.233	0.245	0.226	0.208	0.202	0.210	0.217	0.196
Cation charge	44.872	45.133	44.777	44.690	44.783	44.880	44.904	44.875	44.833	44.966

@ Fe3+ calculated by charge balance

AMPHIBLOE TRAVERSE ACROSS PHENOCRYST IN SAN JACINTO MTNS (10804') PG-101

Sample name Analysis pt Remark	38	40	41	44	46	48	49	50	51
SiO2	43.65	43.50	44.09	42.54	44.55	44.40	41.73	42.78	42.56
TiO2	1.31	1.31	1.47	0.20	1.38	1.56	0.52	1.74	0.88
Al2O3	9.62	9.49	9.62	12.71	9.22	8.99	12.56	9.92	11.35
Cr2O3	0.00	0.02	0.00	0.00	0.02	0.02	0.04	0.06	0.01
Fe2O3 @	5.09	5.37	4.38	6.93	4.59	5.69	6.54	4.07	5.14
FeO	16.60	16.49	17.04	16.43	16.40	15.63	17.09	16.88	17.06
MnO	0.52	0.49	0.55	0.50	0.62	0.65	0.54	0.50	0.57
MgO	8.19	8.18	8.23	6.76	8.38	8.70	6.43	8.17	7.43
CaO	11.50	11.39	11.45	11.60	11.19	11.11	11.57	11.32	11.59
Na2O	1.16	1.25	1.30	1.20	1.25	1.41	1.28	1.51	1.36
K2O	1.17	1.15	1.16	1.00	1.10	1.06	1.07	1.21	1.26
Total	98.81	98.65	99.29	99.86	98.70	99.22	99.38	98.16	99.22
---Atomic proportions based on 13 cations (except Ca+Na+K+Ba)---									
Si	6.573	6.565	6.602	6.348	6.683	6.630	6.292	6.496	6.411
Ti	0.148	0.149	0.166	0.022	0.156	0.175	0.059	0.199	0.100
Al(iv)	1.427	1.435	1.398	1.652	1.317	1.370	1.708	1.504	1.589
Al(vi)	0.280	0.254	0.300	0.583	0.313	0.212	0.524	0.272	0.426
Cr	0.000	0.002	0.000	0.000	0.002	0.002	0.005	0.007	0.001
Fe3+ (calc)	0.577	0.610	0.493	0.778	0.518	0.640	0.743	0.465	0.583
Fe2+	2.090	2.082	2.134	2.050	2.057	1.952	2.155	2.144	2.150
Mn2+	0.066	0.063	0.070	0.063	0.079	0.082	0.069	0.064	0.073
Mg	1.838	1.840	1.837	1.504	1.874	1.937	1.445	1.850	1.668
C site (M1+M2+M3)	5.000	5.000	5.000	5.000	5.000	5.000	5.000	5.000	5.000
excess (M1+M2+M3)	0.000	0.000	0.000	0.000	0.000	0.000	0.000	0.000	0.000
Ca	1.855	1.842	1.837	1.855	1.799	1.777	1.869	1.842	1.870
Na(M4)	0.145	0.158	0.163	0.145	0.201	0.223	0.131	0.158	0.130
B site (M4) total	2.000	2.000	2.000	2.000	2.000	2.000	2.000	2.000	2.000
Na(A)	0.194	0.208	0.214	0.202	0.162	0.186	0.243	0.286	0.268
K	0.225	0.221	0.222	0.190	0.211	0.202	0.206	0.234	0.242
A site total	0.419	0.429	0.436	0.392	0.373	0.388	0.449	0.521	0.510
Mg/Fe(tot)	0.689	0.684	0.699	0.532	0.728	0.747	0.499	0.709	0.611
Mg/Fe2+	0.880	0.884	0.861	0.734	0.911	0.992	0.671	0.863	0.776
Mg/Mg+Fe(tot)	0.408	0.406	0.412	0.347	0.421	0.428	0.333	0.415	0.379
Mg/Mg+Fe2+	0.468	0.469	0.463	0.423	0.477	0.498	0.401	0.463	0.437
Fe3+/Fe(tot)	0.216	0.227	0.188	0.275	0.201	0.247	0.256	0.178	0.213
Cation charge	44.846	44.779	45.013	44.444	44.963	44.721	44.515	45.071	44.835

@ Fe3+ calculated by charge balance

TRAVERSE ACROSS AMPHIBOLE PHENOCRYST FROM SAN JACINTO (8960') PG-102

Sample name	PG-102									
Analysis pt	2	3	4	6	7	8	9	10	11	12
Remark	59.3 um int									
SiO2	42.91	42.25	43.94	45.13	44.70	44.40	45.23	45.16	44.84	45.73
TiO2	1.52	1.54	1.54	1.45	1.41	1.49	1.36	1.45	1.35	1.24
Al2O3	9.76	10.15	9.44	8.54	8.63	8.48	8.68	8.62	8.65	8.50
Cr2O3	0.00	0.00	0.02	0.06	0.10	0.05	0.00	0.00	0.00	0.00
Fe2O3 @	4.47	4.65	5.60	4.74	3.82	3.54	4.55	4.02	3.69	3.73
FeO	16.74	16.46	15.91	15.77	16.56	16.14	15.88	16.45	16.47	15.95
MnO	0.56	0.51	0.52	0.57	0.53	0.62	0.47	0.58	0.58	0.56
MgO	8.26	8.24	8.75	9.35	8.89	9.23	9.37	9.27	9.03	9.45
CaO	11.45	11.57	11.40	11.37	11.28	11.42	11.49	11.59	11.44	11.34
Na2O	1.48	1.38	1.43	1.49	1.47	1.44	1.32	1.45	1.34	1.39
K2O	1.16	1.23	1.15	0.99	1.03	1.02	1.06	1.01	1.07	1.02
Total	98.31	97.99	99.70	99.46	98.42	97.82	99.41	99.60	98.46	98.91
---Atomic proportions based on 13 cations (except Ca+Na+K+Ba)---										
Si	6.509	6.435	6.547	6.704	6.723	6.712	6.716	6.709	6.735	6.803
Ti	0.173	0.176	0.173	0.162	0.159	0.169	0.152	0.162	0.152	0.139
Al(iv)	1.491	1.565	1.453	1.296	1.277	1.288	1.284	1.291	1.265	1.197
Al(vi)	0.253	0.257	0.205	0.199	0.252	0.223	0.235	0.218	0.266	0.293
Cr	0.000	0.000	0.002	0.007	0.012	0.006	0.000	0.000	0.000	0.000
Fe3+ (calc)	0.510	0.533	0.628	0.530	0.432	0.403	0.508	0.450	0.417	0.418
Fe2+	2.124	2.097	1.982	1.960	2.083	2.040	1.971	2.044	2.069	1.984
Mn2+	0.072	0.066	0.066	0.072	0.068	0.079	0.059	0.073	0.074	0.071
Mg	1.868	1.871	1.944	2.071	1.993	2.080	2.074	2.053	2.022	2.096
C site (M1+M2+M3)	5.000	5.000	5.000	5.000	5.000	5.000	5.000	5.000	5.000	5.000
excess (M1+M2+M3)	0.000	0.000	0.000	0.000	0.000	0.000	0.000	0.000	0.000	0.000
Ca	1.861	1.888	1.820	1.810	1.818	1.850	1.828	1.845	1.841	1.807
Na(M4)	0.139	0.112	0.180	0.190	0.182	0.150	0.172	0.155	0.159	0.193
B site (M4) total	2.000	2.000	2.000	2.000	2.000	2.000	2.000	2.000	2.000	2.000
Na(A)	0.296	0.296	0.233	0.239	0.246	0.272	0.208	0.262	0.231	0.208
K	0.224	0.239	0.219	0.188	0.198	0.197	0.201	0.191	0.205	0.194
A site total	0.521	0.534	0.452	0.426	0.444	0.468	0.409	0.454	0.436	0.402
Mg/Fe(tot)	0.709	0.711	0.745	0.832	0.792	0.852	0.836	0.823	0.813	0.872
Mg/Fe2+	0.879	0.892	0.981	1.057	0.957	1.020	1.052	1.005	0.977	1.056
Mg/Mg+Fe(tot)	0.415	0.416	0.427	0.454	0.442	0.460	0.455	0.452	0.449	0.466
Mg/Mg+Fe2+	0.468	0.472	0.495	0.514	0.489	0.505	0.513	0.501	0.494	0.514
Fe3+/Fe(tot)	0.194	0.203	0.241	0.213	0.172	0.165	0.205	0.180	0.168	0.174
Cation charge	44.981	44.934	44.743	44.940	45.135	45.195	44.983	45.101	45.166	45.164

@ Fe3+ calculated by charge balance

TRAVERSE ACROSS AMPHIBOLE PHENOCRYST FROM SAN JACINTO (8960') PG-102

Sample name										
Analysis pt	13	14	16	17	18	19	20	21	22	24
Remark										
SiO2	44.71	43.89	44.44	45.13	44.25	45.18	44.93	45.08	45.14	44.64
TiO2	1.30	1.20	1.26	1.25	1.30	1.21	1.28	1.34	1.26	1.35
Al2O3	8.80	9.38	9.06	8.68	8.63	8.28	8.05	8.52	8.70	8.59
Cr2O3	0.00	0.00	0.00	0.06	0.16	0.06	0.08	0.09	0.05	0.05
Fe2O3 @	4.22	4.50	4.76	3.44	3.84	4.82	4.24	4.28	3.82	3.96
FeO	15.62	15.53	15.44	16.52	15.91	15.15	15.71	15.44	16.26	15.54
MnO	0.49	0.50	0.60	0.51	0.54	0.53	0.56	0.54	0.58	0.54
MgO	9.42	9.20	9.27	9.20	9.46	9.70	9.67	9.52	9.26	9.58
CaO	11.60	11.69	11.52	11.54	11.63	11.47	11.61	11.52	11.48	11.70
Na2O	1.26	1.29	1.34	1.34	1.48	1.35	1.42	1.25	1.50	1.22
K2O	0.98	1.01	1.06	1.06	1.02	0.94	0.92	0.94	0.96	0.97
Total	98.40	98.19	98.75	98.72	98.21	98.69	98.47	98.52	99.01	98.14
---Atomic proportions based on 13 cations (except Ca+Na+K+Ba)---										
Si	6.699	6.607	6.649	6.752	6.668	6.743	6.740	6.738	6.733	6.707
Ti	0.146	0.136	0.142	0.141	0.147	0.136	0.144	0.151	0.141	0.153
Al(iv)	1.301	1.393	1.351	1.248	1.332	1.257	1.260	1.262	1.267	1.293
Al(vi)	0.254	0.271	0.247	0.282	0.200	0.199	0.163	0.238	0.263	0.228
Cr	0.000	0.000	0.000	0.007	0.019	0.007	0.009	0.011	0.006	0.006
Fe3+ (calc)	0.476	0.509	0.536	0.387	0.435	0.541	0.479	0.482	0.429	0.447
Fe2+	1.958	1.956	1.932	2.066	2.005	1.891	1.971	1.930	2.028	1.953
Mn2+	0.062	0.064	0.076	0.065	0.069	0.067	0.071	0.068	0.073	0.069
Mg	2.104	2.065	2.068	2.052	2.125	2.158	2.162	2.121	2.059	2.146
C site (M1+M2+M3)	5.000	5.000	5.000	5.000	5.000	5.000	5.000	5.000	5.000	5.000
excess (M1+M2+M3)	0.000	0.000	0.000	0.000	0.000	0.000	0.000	0.000	0.000	0.000
Ca	1.862	1.885	1.847	1.850	1.878	1.834	1.866	1.845	1.835	1.883
Na(M4)	0.138	0.115	0.153	0.150	0.122	0.166	0.134	0.155	0.165	0.117
B site (M4) total	2.000	2.000	2.000	2.000	2.000	2.000	2.000	2.000	2.000	2.000
Na(A)	0.228	0.262	0.235	0.238	0.310	0.225	0.279	0.207	0.269	0.239
K	0.187	0.194	0.202	0.202	0.196	0.179	0.176	0.179	0.183	0.186
A site total	0.416	0.456	0.438	0.441	0.506	0.404	0.455	0.386	0.451	0.425
Mg/Fe(tot)	0.865	0.838	0.838	0.836	0.871	0.887	0.883	0.880	0.838	0.894
Mg/Fe2+	1.075	1.056	1.070	0.993	1.060	1.141	1.097	1.099	1.015	1.099
Mg/Mg+Fe(tot)	0.464	0.456	0.456	0.455	0.466	0.470	0.469	0.468	0.456	0.472
Mg/Mg+Fe2+	0.518	0.514	0.517	0.498	0.515	0.533	0.523	0.524	0.504	0.524
Fe3+/Fe(tot)	0.196	0.207	0.217	0.158	0.178	0.222	0.195	0.200	0.175	0.186
Cation charge	45.048	44.981	44.929	45.226	45.130	44.918	45.043	45.037	45.141	45.106

@ Fe3+ calculated by charge balance

TRAVERSE ACROSS AMPHIBOLE PHENOCRYST FROM SAN JACINTO (8960') PG-102

Sample name										
Analysis pt	25	26	27	28	30	34	37	39	40	41
Remark										
SiO2	44.75	45.18	45.07	44.05	44.28	44.78	45.47	44.39	42.67	44.77
TiO2	1.33	1.43	1.24	1.17	1.24	1.24	1.03	1.36	1.22	1.44
Al2O3	8.70	8.30	8.42	10.43	9.96	8.11	8.28	8.71	11.11	8.47
Cr2O3	0.00	0.00	0.02	0.04	0.00	0.01	0.00	0.03	0.00	0.00
Fe2O3 @	4.37	3.15	5.50	4.99	4.75	2.92	3.38	4.23	4.35	4.09
FeO	15.53	16.50	14.96	14.24	14.93	16.59	16.15	15.80	16.90	15.98
MnO	0.60	0.50	0.60	0.52	0.48	0.57	0.48	0.50	0.47	0.46
MgO	9.38	9.39	9.29	9.25	9.26	9.22	9.61	9.53	8.29	9.49
CaO	11.51	11.55	11.31	11.31	11.58	11.52	11.73	11.74	11.95	11.72
Na2O	1.26	1.37	1.09	1.38	1.24	1.31	1.25	1.34	1.48	1.24
K2O	1.06	0.94	1.05	0.96	0.97	0.97	0.92	1.08	1.25	1.00
Total	98.50	98.31	98.55	98.34	98.70	97.23	98.31	98.71	99.70	98.66
---Atomic proportions based on 13 cations (except Ca+Na+K+Ba)---										
Si	6.704	6.780	6.738	6.571	6.599	6.803	6.811	6.653	6.387	6.704
Ti	0.150	0.161	0.139	0.131	0.139	0.142	0.116	0.153	0.137	0.162
Al(iv)	1.296	1.220	1.262	1.429	1.401	1.197	1.189	1.347	1.613	1.296
Al(vi)	0.240	0.248	0.222	0.405	0.349	0.255	0.272	0.192	0.347	0.199
Cr	0.000	0.000	0.002	0.005	0.000	0.001	0.000	0.004	0.000	0.000
Fe3+ (calc)	0.493	0.356	0.618	0.560	0.533	0.333	0.381	0.478	0.490	0.461
Fe2+	1.946	2.070	1.871	1.777	1.861	2.107	2.024	1.980	2.116	2.001
Mn2+	0.076	0.064	0.076	0.066	0.061	0.073	0.061	0.063	0.060	0.058
Mg	2.095	2.101	2.071	2.057	2.057	2.088	2.146	2.129	1.850	2.119
C site (M1+M2+M3)	5.000	5.000	5.000	5.000	5.000	5.000	5.000	5.000	5.000	5.000
excess (M1+M2+M3)	0.000	0.000	0.000	0.000	0.000	0.000	0.000	0.000	0.000	0.000
Ca	1.847	1.857	1.812	1.808	1.849	1.875	1.882	1.885	1.916	1.880
Na(M4)	0.153	0.143	0.188	0.192	0.151	0.125	0.118	0.115	0.084	0.120
B site (M4) total	2.000	2.000	2.000	2.000	2.000	2.000	2.000	2.000	2.000	2.000
Na(A)	0.213	0.256	0.128	0.207	0.207	0.261	0.245	0.275	0.346	0.240
K	0.203	0.180	0.200	0.183	0.184	0.188	0.176	0.207	0.239	0.191
A site total	0.416	0.436	0.328	0.389	0.392	0.449	0.421	0.481	0.585	0.431
Mg/Fe(tot)	0.859	0.866	0.832	0.880	0.859	0.856	0.892	0.866	0.710	0.860
Mg/Fe2+	1.076	1.015	1.107	1.158	1.105	0.991	1.060	1.075	0.874	1.059
Mg/Mg+Fe(tot)	0.462	0.464	0.454	0.468	0.462	0.461	0.472	0.464	0.415	0.463
Mg/Mg+Fe2+	0.518	0.504	0.525	0.537	0.525	0.498	0.515	0.518	0.466	0.514
Fe3+/Fe(tot)	0.202	0.147	0.248	0.240	0.223	0.137	0.159	0.194	0.188	0.187
Cation charge	45.014	45.288	44.763	44.880	44.934	45.333	45.237	45.045	45.020	45.078

@ Fe3+ calculated by charge balance

TRAVERSE ACROSS AMPHIBOLE PHENOCRYST FROM SAN JACINTO (8960') PG-102

Sample name Analysis pt Remark	42	44	45	46	47	48	49	50	51	52
SiO2	45.00	45.06	44.21	44.89	44.95	44.63	43.56	43.39	41.94	42.38
TiO2	1.37	1.34	1.24	1.44	1.46	1.32	1.50	1.57	1.53	1.41
Al2O3	8.70	8.72	9.21	8.72	8.68	8.83	9.38	9.84	10.90	10.39
Cr2O3	0.13	0.00	0.01	0.00	0.00	0.00	0.00	0.00	0.00	0.00
Fe2O3 @	4.81	3.12	3.73	3.36	3.44	4.37	3.47	4.49	5.50	3.46
FeO	15.53	16.46	16.50	16.63	16.50	16.00	17.53	16.87	16.31	18.14
MnO	0.51	0.47	0.47	0.44	0.48	0.46	0.54	0.58	0.43	0.47
MgO	9.27	9.38	9.14	9.21	9.12	9.16	8.33	8.27	7.87	7.71
CaO	11.37	11.62	11.84	11.50	11.37	11.48	11.44	11.33	11.23	11.65
Na2O	1.31	1.38	1.36	1.46	1.45	1.34	1.59	1.61	1.57	1.53
K2O	1.00	0.99	1.04	1.02	0.98	1.03	1.18	1.19	1.37	1.29
Total	98.99	98.54	98.75	98.68	98.43	98.62	98.53	99.14	98.65	98.43
---Atomic proportions based on 13 cations (except Ca+Na+K+Ba)---										
Si	6.706	6.745	6.634	6.724	6.742	6.689	6.593	6.523	6.354	6.455
Ti	0.154	0.151	0.140	0.162	0.165	0.149	0.171	0.177	0.174	0.162
Al(iv)	1.294	1.255	1.366	1.276	1.258	1.311	1.407	1.477	1.646	1.545
Al(vi)	0.234	0.284	0.262	0.263	0.277	0.248	0.266	0.266	0.300	0.320
Cr	0.015	0.000	0.001	0.000	0.000	0.000	0.000	0.000	0.000	0.000
Fe3+ (calc)	0.539	0.352	0.421	0.379	0.388	0.492	0.396	0.508	0.627	0.397
Fe2+	1.935	2.060	2.071	2.083	2.070	2.006	2.219	2.121	2.067	2.310
Mn2+	0.064	0.060	0.060	0.056	0.061	0.058	0.069	0.074	0.055	0.061
Mg	2.059	2.093	2.045	2.056	2.039	2.047	1.879	1.853	1.777	1.751
C site (M1+M2+M3)	5.000	5.000	5.000	5.000	5.000	5.000	5.000	5.000	5.000	5.000
excess (M1+M2+M3)	0.000	0.000	0.000	0.000	0.000	0.000	0.000	0.000	0.000	0.000
Ca	1.815	1.864	1.903	1.845	1.827	1.843	1.855	1.825	1.823	1.901
Na(M4)	0.185	0.136	0.097	0.155	0.173	0.157	0.145	0.175	0.177	0.099
B site (M4) total	2.000	2.000	2.000	2.000	2.000	2.000	2.000	2.000	2.000	2.000
Na(A)	0.194	0.264	0.299	0.269	0.249	0.233	0.322	0.294	0.284	0.353
K	0.190	0.189	0.199	0.195	0.188	0.197	0.228	0.228	0.265	0.251
A site total	0.384	0.453	0.498	0.464	0.436	0.430	0.549	0.522	0.549	0.604
Mg/Fe(tot)	0.832	0.868	0.820	0.835	0.829	0.819	0.719	0.705	0.660	0.647
Mg/Fe2+	1.064	1.016	0.987	0.987	0.985	1.020	0.847	0.874	0.860	0.758
Mg/Mg+Fe(tot)	0.454	0.465	0.451	0.455	0.453	0.450	0.418	0.413	0.398	0.393
Mg/Mg+Fe2+	0.516	0.504	0.497	0.497	0.496	0.505	0.459	0.466	0.462	0.431
Fe3+/Fe(tot)	0.218	0.146	0.169	0.154	0.158	0.197	0.151	0.193	0.233	0.147
Cation charge	44.922	45.296	45.158	45.242	45.223	45.015	45.209	44.983	44.747	45.207

@ Fe3+ calculated by charge balance

TRAVERSE ACROSS AMPHIBOLE PHENOCRYST IN SAN JACINTO (4400') PG-110

Sample name	PG-110									
Analysis pt	1	2	4	5	6	7	8	10	12	13
Remark	25.2 um int									
SiO2	44.05	44.03	45.08	44.67	45.18	45.71	45.54	45.80	45.34	45.50
TiO2	1.35	1.67	1.62	1.48	1.16	1.47	1.45	1.43	1.47	1.56
Al2O3	10.12	9.83	9.22	8.99	8.53	8.49	8.85	8.53	9.55	9.08
Cr2O3	0.00	0.04	0.06	0.07	0.01	0.03	0.00	0.02	0.07	0.11
Fe2O3 @	2.60	3.34	3.50	2.98	2.60	3.61	4.87	3.23	5.52	4.03
FeO	17.42	17.25	16.64	16.89	17.62	16.01	14.79	16.61	14.30	15.94
MnO	0.41	0.43	0.40	0.42	0.40	0.46	0.39	0.40	0.42	0.42
MgO	8.38	8.47	8.84	8.96	8.62	9.55	9.54	9.43	9.48	9.19
CaO	11.77	11.62	11.39	11.69	11.59	11.62	11.30	11.74	11.32	11.42
Na2O	1.06	1.25	1.19	1.18	1.06	1.14	1.04	1.18	1.13	1.17
K2O	1.23	1.23	1.11	1.02	1.01	0.98	0.98	0.92	0.89	1.01
Total	98.39	99.16	99.05	98.35	97.78	99.07	98.75	99.29	99.49	99.42
---Atomic proportions based on 13 cations (except Ca+Na+K+Ba)---										
Si	6.631	6.592	6.715	6.712	6.830	6.785	6.755	6.792	6.671	6.731
Ti	0.153	0.188	0.181	0.167	0.132	0.164	0.162	0.159	0.163	0.174
Al(iv)	1.369	1.408	1.285	1.288	1.170	1.215	1.245	1.208	1.329	1.269
Al(vi)	0.427	0.326	0.333	0.305	0.350	0.270	0.302	0.283	0.327	0.314
Cr	0.000	0.005	0.007	0.008	0.001	0.004	0.000	0.002	0.008	0.013
Fe3+ (calc)	0.294	0.376	0.393	0.337	0.296	0.403	0.544	0.361	0.611	0.448
Fe2+	2.193	2.160	2.073	2.123	2.228	1.988	1.834	2.060	1.760	1.972
Mn2+	0.052	0.055	0.050	0.053	0.051	0.058	0.049	0.050	0.052	0.053
Mg	1.881	1.890	1.963	2.007	1.943	2.113	2.109	2.085	2.079	2.027
C site (M1+M2+M3)	5.000	5.000	5.000	5.000	5.000	5.000	5.000	5.000	5.000	5.000
excess (M1+M2+M3)	0.000	0.000	0.000	0.000	0.000	0.000	0.000	0.000	0.000	0.000
Ca	1.898	1.864	1.818	1.882	1.877	1.848	1.796	1.865	1.784	1.810
Na(M4)	0.102	0.136	0.182	0.118	0.123	0.152	0.204	0.135	0.216	0.190
B site (M4) total	2.000	2.000	2.000	2.000	2.000	2.000	2.000	2.000	2.000	2.000
Na(A)	0.208	0.227	0.161	0.226	0.188	0.176	0.095	0.205	0.107	0.146
K	0.236	0.235	0.211	0.196	0.195	0.186	0.185	0.174	0.167	0.191
A site total	0.444	0.462	0.372	0.421	0.383	0.362	0.280	0.379	0.274	0.336
Mg/Fe(tot)	0.756	0.745	0.796	0.816	0.770	0.884	0.887	0.861	0.877	0.838
Mg/Fe2+	0.857	0.875	0.947	0.946	0.872	1.063	1.150	1.012	1.181	1.028
Mg/Mg+Fe(tot)	0.431	0.427	0.443	0.449	0.435	0.469	0.470	0.463	0.467	0.456
Mg/Mg+Fe2+	0.462	0.467	0.486	0.486	0.466	0.515	0.535	0.503	0.542	0.507
Fe3+/Fe(tot)	0.118	0.148	0.159	0.137	0.117	0.169	0.229	0.149	0.258	0.185
Cation charge	45.412	45.247	45.215	45.326	45.409	45.194	44.912	45.279	44.778	45.104

@ Fe3+ calculated by charge balance

TRAVERSE ACROSS AMPHIBOLE PHENOCRYST IN SAN JACINTO (4400') PG-110

Sample name Analysis pt Remark	15	16	17	18	19	20	21	22	23	24
SiO2	45.24	45.21	45.39	45.20	45.12	44.85	44.38	46.93	44.32	45.50
TiO2	1.39	1.46	1.37	1.31	1.28	1.40	1.46	0.70	1.20	1.38
Al2O3	8.81	8.80	8.43	8.87	8.73	9.05	9.69	7.97	9.33	8.79
Cr2O3	0.02	0.02	0.00	0.01	0.00	0.00	0.00	0.00	0.00	0.00
Fe2O3 @	2.12	3.23	3.13	4.51	2.86	3.50	4.54	4.94	3.57	5.00
FeO	17.31	16.79	16.50	15.69	16.59	16.49	16.11	15.31	16.95	15.38
MnO	0.44	0.46	0.50	0.44	0.49	0.45	0.45	0.41	0.47	0.47
MgO	9.12	9.21	9.20	9.30	9.07	9.04	8.80	9.59	8.38	9.36
CaO	11.72	11.81	11.56	11.48	11.54	11.69	11.54	11.53	11.52	11.48
Na2O	1.20	1.16	1.12	1.16	1.13	1.06	1.15	0.87	1.08	1.10
K2O	1.11	1.02	0.96	1.08	1.02	1.10	1.21	0.78	1.06	0.99
Total	98.48	99.17	98.15	99.04	97.84	98.63	99.33	99.04	97.88	99.45
---Atomic proportions based on 13 cations (except Ca+Na+K+Ba)---										
Si	6.781	6.733	6.810	6.724	6.794	6.713	6.609	6.931	6.702	6.731
Ti	0.157	0.164	0.155	0.147	0.145	0.158	0.164	0.078	0.136	0.154
Al(iv)	1.219	1.267	1.190	1.276	1.206	1.287	1.391	1.069	1.298	1.269
Al(vi)	0.338	0.278	0.301	0.279	0.343	0.310	0.310	0.319	0.365	0.264
Cr	0.002	0.002	0.000	0.001	0.000	0.000	0.000	0.000	0.000	0.000
Fe3+ (calc)	0.240	0.362	0.353	0.504	0.325	0.395	0.509	0.549	0.406	0.556
Fe2+	2.170	2.091	2.070	1.951	2.089	2.064	2.007	1.892	2.143	1.903
Mn2+	0.056	0.058	0.064	0.055	0.062	0.057	0.057	0.051	0.060	0.059
Mg	2.038	2.045	2.058	2.062	2.036	2.017	1.954	2.112	1.889	2.064
C site (M1+M2+M3)	5.000	5.000	5.000	5.000	5.000	5.000	5.000	5.000	5.000	5.000
excess (M1+M2+M3)	0.000	0.000	0.000	0.000	0.000	0.000	0.000	0.000	0.000	0.000
Ca	1.882	1.884	1.858	1.830	1.862	1.875	1.841	1.825	1.866	1.820
Na(M4)	0.118	0.116	0.142	0.170	0.138	0.125	0.159	0.175	0.134	0.180
B site (M4) total	2.000	2.000	2.000	2.000	2.000	2.000	2.000	2.000	2.000	2.000
Na(A)	0.231	0.219	0.184	0.164	0.192	0.182	0.173	0.074	0.183	0.135
K	0.212	0.194	0.184	0.205	0.196	0.210	0.230	0.147	0.204	0.187
A site total	0.443	0.413	0.368	0.369	0.387	0.392	0.403	0.221	0.388	0.322
Mg/Fe(tot)	0.846	0.833	0.849	0.840	0.843	0.821	0.777	0.865	0.741	0.839
Mg/Fe2+	0.939	0.978	0.994	1.057	0.974	0.977	0.973	1.116	0.881	1.085
Mg/Mg+Fe(tot)	0.458	0.455	0.459	0.456	0.458	0.451	0.437	0.464	0.426	0.456
Mg/Mg+Fe2+	0.484	0.494	0.499	0.514	0.494	0.494	0.493	0.527	0.469	0.520
Fe3+/Fe(tot)	0.099	0.148	0.146	0.205	0.134	0.161	0.202	0.225	0.159	0.226
Cation charge	45.521	45.276	45.294	44.991	45.351	45.210	44.982	44.902	45.187	44.887

@ Fe3+ calculated by charge balance

TRAVERSE ACROSS AMPHIBOLE PHENOCRYST IN SAN JACINTO (4400') PG-110

Sample name										
Analysis pt	25	26	27	29	30	31	32	33	35	36
Remark										
SiO2	44.51	45.47	45.33	45.14	45.69	45.35	45.39	45.10	45.08	45.68
TiO2	1.49	1.37	1.50	1.60	1.56	1.55	1.56	1.50	1.58	1.55
Al2O3	8.43	10.30	8.72	9.12	8.52	8.40	8.64	9.07	8.63	8.81
Cr2O3	0.01	0.05	0.10	0.08	0.00	0.02	0.06	0.00	0.00	0.00
Fe2O3 @	3.81	5.28	4.35	4.37	3.53	4.37	3.80	4.21	3.54	4.54
FeO	16.07	14.10	15.60	15.74	16.29	15.55	15.84	15.35	15.90	15.35
MnO	0.47	0.42	0.54	0.47	0.42	0.54	0.51	0.37	0.50	0.46
MgO	9.30	9.24	9.56	9.33	9.35	9.52	9.45	8.87	9.33	9.71
CaO	11.65	11.15	11.65	11.62	11.46	11.47	11.53	10.86	11.48	11.48
Na2O	1.13	1.07	1.22	1.16	1.22	1.28	1.21	1.11	1.15	1.30
K2O	1.02	0.90	0.99	1.03	0.97	0.88	0.96	1.00	0.97	1.02
Total	97.89	99.35	99.56	99.66	99.01	98.93	98.95	97.44	98.16	99.89
---Atomic proportions based on 13 cations (except Ca+Na+K+Ba)---										
Si	6.717	6.674	6.709	6.675	6.790	6.748	6.750	6.781	6.757	6.722
Ti	0.169	0.151	0.167	0.178	0.174	0.173	0.174	0.170	0.178	0.172
Al(iv)	1.283	1.326	1.291	1.325	1.210	1.252	1.250	1.219	1.243	1.278
Al(vi)	0.216	0.455	0.230	0.265	0.282	0.221	0.264	0.388	0.281	0.250
Cr	0.001	0.006	0.012	0.009	0.000	0.002	0.007	0.000	0.000	0.000
Fe3+ (calc)	0.433	0.583	0.484	0.486	0.395	0.489	0.425	0.477	0.400	0.503
Fe2+	2.028	1.731	1.930	1.946	2.024	1.935	1.970	1.930	1.993	1.888
Mn2+	0.060	0.052	0.068	0.059	0.053	0.068	0.064	0.047	0.063	0.057
Mg	2.092	2.022	2.109	2.057	2.071	2.112	2.095	1.988	2.085	2.130
C site (M1+M2+M3)	5.000	5.000	5.000	5.000	5.000	5.000	5.000	5.000	5.000	5.000
excess (M1+M2+M3)	0.000	0.000	0.000	0.000	0.000	0.000	0.000	0.000	0.000	0.000
Ca	1.884	1.753	1.847	1.841	1.825	1.828	1.837	1.749	1.843	1.810
Na(M4)	0.116	0.247	0.153	0.159	0.175	0.172	0.163	0.251	0.157	0.190
B site (M4) total	2.000	2.000	2.000	2.000	2.000	2.000	2.000	2.000	2.000	2.000
Na(A)	0.214	0.058	0.197	0.174	0.176	0.198	0.186	0.073	0.178	0.181
K	0.196	0.169	0.187	0.194	0.184	0.167	0.182	0.192	0.185	0.191
A site total	0.411	0.226	0.384	0.368	0.360	0.365	0.368	0.265	0.363	0.372
Mg/Fe(tot)	0.850	0.874	0.873	0.846	0.856	0.871	0.875	0.826	0.871	0.891
Mg/Fe2+	1.032	1.168	1.093	1.057	1.023	1.091	1.063	1.030	1.046	1.128
Mg/Mg+Fe(tot)	0.460	0.466	0.466	0.458	0.461	0.466	0.467	0.452	0.466	0.471
Mg/Mg+Fe2+	0.508	0.539	0.522	0.514	0.506	0.522	0.515	0.507	0.511	0.530
Fe3+/Fe(tot)	0.176	0.252	0.201	0.200	0.163	0.202	0.177	0.198	0.167	0.210
Cation charge	45.134	44.834	45.031	45.028	45.210	45.021	45.150	45.046	45.201	44.995

@ Fe3+ calculated by charge balance

TRAVERSE ACROSS AMPHIBOLE PHENOCRYST IN SAN JACINTO (4400') PG-110

Sample name										
Analysis pt	38	39	40	41	43	44	45	46	47	50
Remark										
SiO2	45.11	44.95	45.49	45.09	45.95	45.15	45.54	44.41	44.48	44.58
TiO2	1.57	1.56	1.58	1.57	1.59	1.62	1.52	1.58	1.62	1.57
Al2O3	8.68	9.08	8.68	8.62	8.59	8.74	8.77	8.97	8.89	9.48
Cr2O3	0.01	0.00	0.00	0.00	0.00	0.01	0.05	0.01	0.04	0.03
Fe2O3 @	3.20	3.98	3.55	3.74	3.77	3.60	3.87	3.64	3.70	2.41
FeO	16.09	15.77	15.65	15.70	15.90	15.86	16.13	16.40	16.38	17.18
MnO	0.44	0.45	0.55	0.48	0.41	0.36	0.42	0.31	0.41	0.47
MgO	9.43	9.36	9.60	9.50	9.61	9.40	9.26	9.03	9.13	8.63
CaO	11.54	11.63	11.52	11.52	11.45	11.56	11.52	11.51	11.62	11.40
Na2O	1.21	1.15	1.23	1.20	1.29	1.07	1.12	1.19	1.20	1.29
K2O	1.00	1.00	0.94	0.97	0.95	0.94	1.01	1.07	1.09	1.15
Total	98.28	98.93	98.79	98.39	99.51	98.31	99.21	98.11	98.56	98.19
---Atomic proportions based on 13 cations (except Ca+Na+K+Ba)---										
Si	6.754	6.690	6.763	6.742	6.782	6.749	6.757	6.686	6.673	6.707
Ti	0.177	0.175	0.177	0.177	0.176	0.182	0.170	0.179	0.183	0.178
Al(iv)	1.246	1.310	1.237	1.258	1.218	1.251	1.243	1.314	1.327	1.293
Al(vi)	0.286	0.283	0.284	0.261	0.277	0.289	0.290	0.277	0.245	0.388
Cr	0.001	0.000	0.000	0.000	0.000	0.001	0.006	0.001	0.005	0.004
Fe3+ (calc)	0.360	0.446	0.397	0.421	0.419	0.405	0.432	0.412	0.418	0.273
Fe2+	2.015	1.962	1.946	1.964	1.962	1.983	2.001	2.064	2.055	2.162
Mn2+	0.056	0.057	0.069	0.061	0.051	0.046	0.053	0.040	0.052	0.060
Mg	2.105	2.077	2.128	2.117	2.115	2.095	2.048	2.027	2.042	1.936
C site (M1+M2+M3)	5.000	5.000	5.000	5.000	5.000	5.000	5.000	5.000	5.000	5.000
excess (M1+M2+M3)	0.000	0.000	0.000	0.000	0.000	0.000	0.000	0.000	0.000	0.000
Ca	1.851	1.855	1.835	1.845	1.811	1.851	1.831	1.857	1.868	1.838
Na(M4)	0.149	0.145	0.165	0.155	0.189	0.149	0.169	0.143	0.132	0.162
B site (M4) total	2.000	2.000	2.000	2.000	2.000	2.000	2.000	2.000	2.000	2.000
Na(A)	0.203	0.187	0.190	0.193	0.180	0.162	0.153	0.204	0.217	0.214
K	0.191	0.190	0.178	0.185	0.179	0.179	0.191	0.206	0.209	0.221
A site total	0.394	0.376	0.368	0.378	0.359	0.341	0.345	0.409	0.426	0.435
Mg/Fe(tot)	0.886	0.862	0.908	0.888	0.888	0.877	0.842	0.818	0.826	0.795
Mg/Fe2+	1.045	1.058	1.094	1.078	1.078	1.056	1.023	0.982	0.993	0.895
Mg/Mg+Fe(tot)	0.470	0.463	0.476	0.470	0.470	0.467	0.457	0.450	0.452	0.443
Mg/Mg+Fe2+	0.511	0.514	0.522	0.519	0.519	0.514	0.506	0.495	0.498	0.472
Fe3+/Fe(tot)	0.152	0.185	0.169	0.176	0.176	0.169	0.177	0.166	0.169	0.112
Cation charge	45.280	45.108	45.206	45.158	45.163	45.191	45.136	45.176	45.165	45.454

@ Fe3+ calculated by charge balance

TRAVERSE ACROSS AMPHIBOLE PHENOCRYST IN SAN JACINTO (4400') PG-110

Sample name		
Analysis pt	51	53
Remark		
SiO2	44.44	44.78
TiO2	1.71	1.31
Al2O3	9.61	10.14
Cr2O3	0.05	0.01
Fe2O3 @	3.69	2.66
FeO	16.55	16.86
MnO	0.42	0.44
MgO	8.76	8.76
CaO	11.38	11.69
Na2O	1.36	1.17
K2O	1.11	1.12
Total	99.08	98.94

---Atomic proportions based on 13 cations (except Ca+Na+K+Ba)---

Si	6.631	6.672
Ti	0.192	0.147
Al(iv)	1.369	1.328
Al(vi)	0.321	0.452
Cr	0.006	0.001
Fe3+ (calc)	0.415	0.298
Fe2+	2.065	2.100
Mn2+	0.053	0.056
Mg	1.949	1.946
C site (M1+M2+M3)	5.000	5.000
excess (M1+M2+M3)	0.000	0.000
Ca	1.819	1.866
Na(M4)	0.181	0.134
B site (M4) total	2.000	2.000
Na(A)	0.213	0.204
K	0.211	0.213
A site total	0.424	0.417
Mg/Fe(tot)	0.786	0.811
Mg/Fe2+	0.944	0.926
Mg/Mg+Fe(tot)	0.440	0.448
Mg/Mg+Fe2+	0.486	0.481
Fe3+/Fe(tot)	0.167	0.124
Cation charge	45.170	45.404

@ Fe3+ calculated by charge balance

TRAVERSE ACROSS AMPHIBOLE PHENOCRYST IN SAN JACINTO (2660') PG-118

Sample name	PG-118									
Analysis pt	2	3	4	5	6	7	8	9	10	11
Remark	15.4 um int									
SiO2	40.93	40.24	40.33	40.31	40.40	40.07	40.70	40.74	40.73	40.40
TiO2	1.25	1.38	1.33	1.36	1.43	1.44	1.37	1.34	1.41	1.40
Al2O3	11.77	11.57	11.41	11.39	11.30	11.19	11.22	10.91	10.93	10.90
Cr2O3	0.07	0.07	0.10	0.03	0.08	0.11	0.07	0.00	0.00	0.02
Fe2O3 @	4.59	5.33	6.31	5.88	5.86	5.85	6.22	6.19	5.74	5.31
FeO	24.27	23.59	23.18	23.41	23.25	23.35	23.51	23.42	23.42	24.29
MnO	0.72	0.76	0.84	0.79	0.90	0.82	0.99	0.88	0.80	0.82
MgO	2.57	2.57	2.58	2.55	2.66	2.63	2.58	2.64	2.66	2.55
CaO	10.86	10.54	10.55	10.46	10.50	10.51	10.63	10.54	10.47	10.76
Na2O	1.52	1.63	1.61	1.68	1.72	1.69	1.69	1.66	1.56	1.70
K2O	1.47	1.54	1.47	1.47	1.40	1.47	1.42	1.33	1.40	1.38
Total	100.02	99.21	99.71	99.33	99.50	99.14	100.40	99.65	99.11	99.53
---Atomic proportions based on 13 cations (except Ca+Na+K+Ba)---										
Si	6.335	6.289	6.275	6.294	6.295	6.278	6.296	6.340	6.363	6.318
Ti	0.145	0.162	0.156	0.160	0.168	0.170	0.159	0.157	0.166	0.165
Al(iv)	1.665	1.711	1.725	1.706	1.705	1.722	1.704	1.660	1.637	1.682
Fe3+(iv)	0.000	0.000	0.000	0.000	0.000	0.000	0.000	0.000	0.000	0.000
Al(vi)	0.482	0.420	0.368	0.391	0.370	0.344	0.342	0.342	0.375	0.328
Cr	0.009	0.009	0.012	0.004	0.010	0.014	0.009	0.000	0.000	0.002
Fe3+ (calc)	0.534	0.627	0.739	0.690	0.687	0.690	0.725	0.724	0.674	0.625
Fe2+	3.142	3.083	3.017	3.058	3.029	3.060	3.041	3.049	3.059	3.177
Mn2+	0.094	0.101	0.111	0.104	0.119	0.109	0.130	0.116	0.106	0.109
Mg	0.593	0.599	0.598	0.594	0.618	0.614	0.595	0.613	0.619	0.595
C site (M1+M2+M3)	5.000	5.000	5.000	5.000	5.000	5.000	5.000	5.000	5.000	5.000
excess (M1+M2+M3)	0.000	0.000	0.000	0.000	0.000	0.000	0.000	0.000	0.000	0.000
Ca	1.801	1.765	1.759	1.750	1.753	1.764	1.762	1.757	1.752	1.803
Na(M4)	0.199	0.235	0.241	0.250	0.247	0.236	0.238	0.243	0.248	0.197
B site (M4) total	2.000	2.000	2.000	2.000	2.000	2.000	2.000	2.000	2.000	2.000
Na(A)	0.257	0.259	0.244	0.259	0.272	0.278	0.269	0.258	0.225	0.319
K	0.290	0.307	0.292	0.293	0.278	0.294	0.280	0.264	0.279	0.275
A site total	0.547	0.566	0.536	0.551	0.551	0.571	0.549	0.522	0.504	0.594
Mg/Fe(tot)	0.161	0.161	0.159	0.158	0.166	0.164	0.158	0.162	0.166	0.156
Mg/Fe2+	0.189	0.194	0.198	0.194	0.204	0.201	0.196	0.201	0.202	0.187
Mg/Mg+Fe(tot)	0.139	0.139	0.137	0.137	0.143	0.141	0.136	0.140	0.142	0.135
Mg/Mg+Fe2+	0.159	0.163	0.166	0.163	0.169	0.167	0.164	0.167	0.168	0.158
Fe3+/Fe(tot)	0.145	0.169	0.197	0.184	0.185	0.184	0.192	0.192	0.181	0.164
Cation charge	44.931	44.747	44.523	44.619	44.626	44.620	44.551	44.551	44.651	44.749

@ Fe3+ calculated by charge balance

TRAVERSE ACROSS AMPHIBOLE PHENOCRYST IN SAN JACINTO (2660') PG-118

Sample name Analysis pt Remark	12	13	14	15	16	17	18	19	20	21
SiO2	40.26	40.34	34.32	41.34	41.31	40.39	40.73	40.79	41.24	40.87
TiO2	1.42	1.36	1.37	1.34	1.37	1.38	1.43	1.39	1.43	1.41
Al2O3	10.89	10.75	9.07	11.34	11.11	10.68	10.66	10.83	10.53	11.09
Cr2O3	0.04	0.00	0.00	0.00	0.04	0.10	0.17	0.03	0.08	0.06
Fe2O3 @	6.13	5.88	7.79	7.25	6.38	7.25	5.58	6.88	6.11	6.43
FeO	23.30	23.72	21.50	22.34	23.13	22.57	23.60	23.05	23.22	23.32
MnO	0.87	0.83	0.92	0.85	0.86	0.83	0.91	0.85	1.15	0.92
MgO	2.65	2.63	2.13	2.80	2.76	2.68	2.68	2.78	2.72	2.68
CaO	10.49	10.55	10.35	10.09	10.40	10.09	10.42	10.51	10.44	10.55
Na2O	1.68	1.73	1.30	1.85	1.74	1.78	1.77	1.68	1.63	1.73
K2O	1.40	1.40	1.29	1.30	1.30	1.44	1.37	1.35	1.36	1.34
Total	99.12	99.19	90.04	100.51	100.40	99.20	99.33	100.14	99.90	100.40
---Atomic proportions based on 13 cations (except Ca+Na+K+Ba)---										
Si	6.308	6.325	6.042	6.341	6.359	6.316	6.363	6.317	6.395	6.313
Ti	0.167	0.160	0.181	0.155	0.159	0.162	0.168	0.162	0.167	0.164
Al(iv)	1.692	1.675	1.882	1.659	1.641	1.684	1.637	1.683	1.605	1.687
Fe3+(iv)	0.000	0.000	0.075	0.000	0.000	0.000	0.000	0.000	0.000	0.000
Al(vi)	0.319	0.311	0.000	0.391	0.375	0.285	0.326	0.294	0.320	0.331
Cr	0.005	0.000	0.000	0.000	0.005	0.012	0.021	0.004	0.010	0.007
Fe3+ (calc)	0.722	0.693	0.956	0.837	0.739	0.854	0.657	0.802	0.713	0.747
Fe2+	3.053	3.110	3.166	2.866	2.977	2.952	3.084	2.985	3.011	3.013
Mn2+	0.115	0.110	0.137	0.110	0.112	0.110	0.120	0.112	0.151	0.120
Mg	0.619	0.615	0.559	0.640	0.633	0.625	0.624	0.642	0.629	0.617
C site (M1+M2+M3)	5.000	5.000	5.000	5.000	5.000	5.000	5.000	5.000	5.000	5.000
excess (M1+M2+M3)	0.000	0.000	0.075	0.000	0.000	0.000	0.000	0.000	0.000	0.000
Ca	1.761	1.772	1.952	1.658	1.715	1.691	1.744	1.744	1.735	1.746
Na(M4)	0.239	0.228	0.000	0.342	0.285	0.309	0.256	0.256	0.265	0.254
B site (M4) total	2.000	2.000	1.952	2.000	2.000	2.000	2.000	2.000	2.000	2.000
Na(A)	0.271	0.298	0.444	0.208	0.235	0.230	0.280	0.248	0.225	0.264
K	0.280	0.280	0.290	0.254	0.255	0.287	0.273	0.267	0.269	0.264
A site total	0.551	0.578	0.734	0.463	0.490	0.518	0.553	0.515	0.494	0.528
Mg/Fe(tot)	0.164	0.162	0.133	0.173	0.170	0.164	0.167	0.169	0.169	0.164
Mg/Fe2+	0.203	0.198	0.177	0.223	0.213	0.212	0.202	0.215	0.209	0.205
Mg/Mg+Fe(tot)	0.141	0.139	0.118	0.147	0.146	0.141	0.143	0.145	0.144	0.141
Mg/Mg+Fe2+	0.169	0.165	0.150	0.183	0.175	0.175	0.168	0.177	0.173	0.170
Fe3+/Fe(tot)	0.191	0.182	0.246	0.226	0.199	0.224	0.176	0.212	0.191	0.199
Cation charge	44.555	44.613	43.936	44.325	44.521	44.293	44.687	44.396	44.575	44.505

@ Fe3+ calculated by charge balance

TRAVERSE ACROSS AMPHIBOLE PHENOCRYST IN SAN JACINTO (2660') PG-118

Sample name Analysis pt Remark	22	23	24	25	26	27	28	29	30	31
SiO2	40.66	41.06	40.93	40.97	40.75	40.74	40.71	40.59	40.75	40.62
TiO2	1.44	1.40	1.43	1.40	1.42	1.45	1.39	1.45	1.39	1.48
Al2O3	10.86	10.68	10.58	10.75	10.66	10.62	10.52	10.48	10.51	10.54
Cr2O3	0.06	0.07	0.01	0.00	0.00	0.06	0.00	0.04	0.00	0.00
Fe2O3 @	4.89	6.05	5.24	5.78	5.91	7.71	6.43	6.63	5.65	6.27
FeO	23.86	23.68	23.71	23.68	23.29	22.80	23.17	22.73	23.62	22.86
MnO	0.76	0.96	0.91	0.79	0.87	0.91	0.96	0.94	0.93	1.04
MgO	2.69	2.73	2.77	2.78	2.69	2.76	2.72	2.78	2.71	2.70
CaO	10.44	10.57	10.32	10.59	10.41	10.45	10.50	10.33	10.60	10.31
Na2O	1.76	1.78	1.93	1.71	1.65	1.76	1.63	1.65	1.63	1.67
K2O	1.34	1.33	1.29	1.28	1.27	1.28	1.29	1.28	1.26	1.25
Total	98.76	100.31	99.13	99.73	98.92	100.54	99.31	98.90	99.05	98.74
---Atomic proportions based on 13 cations (except Ca+Na+K+Ba)---										
Si	6.378	6.355	6.399	6.367	6.378	6.294	6.358	6.357	6.382	6.370
Ti	0.170	0.163	0.168	0.164	0.167	0.168	0.163	0.171	0.164	0.175
Al(iv)	1.622	1.645	1.601	1.633	1.622	1.706	1.642	1.643	1.618	1.630
Fe3+(iv)	0.000	0.000	0.000	0.000	0.000	0.000	0.000	0.000	0.000	0.000
Al(vi)	0.386	0.303	0.348	0.335	0.345	0.227	0.295	0.291	0.322	0.318
Cr	0.007	0.009	0.001	0.000	0.000	0.007	0.000	0.005	0.000	0.000
Fe3+ (calc)	0.577	0.704	0.617	0.676	0.697	0.896	0.755	0.781	0.666	0.740
Fe2+	3.130	3.065	3.100	3.077	3.048	2.946	3.026	2.978	3.093	2.998
Mn2+	0.101	0.126	0.120	0.104	0.115	0.119	0.127	0.125	0.123	0.138
Mg	0.629	0.630	0.646	0.644	0.628	0.636	0.633	0.649	0.633	0.631
C site (M1+M2+M3)	5.000	5.000	5.000	5.000	5.000	5.000	5.000	5.000	5.000	5.000
excess (M1+M2+M3)	0.000	0.000	0.000	0.000	0.000	0.000	0.000	0.000	0.000	0.000
Ca	1.755	1.753	1.729	1.763	1.746	1.730	1.757	1.733	1.779	1.732
Na(M4)	0.245	0.247	0.271	0.237	0.254	0.270	0.243	0.267	0.221	0.268
B site (M4) total	2.000	2.000	2.000	2.000	2.000	2.000	2.000	2.000	2.000	2.000
Na(A)	0.290	0.287	0.314	0.278	0.247	0.257	0.251	0.234	0.273	0.240
K	0.268	0.263	0.257	0.254	0.254	0.252	0.257	0.256	0.252	0.250
A site total	0.558	0.550	0.571	0.532	0.500	0.509	0.508	0.490	0.525	0.490
Mg/Fe(tot)	0.170	0.167	0.174	0.172	0.168	0.165	0.167	0.173	0.168	0.169
Mg/Fe2+	0.201	0.206	0.208	0.209	0.206	0.216	0.209	0.218	0.205	0.211
Mg/Mg+Fe(tot)	0.145	0.143	0.148	0.146	0.144	0.142	0.143	0.147	0.144	0.144
Mg/Mg+Fe2+	0.167	0.170	0.172	0.173	0.171	0.177	0.173	0.179	0.170	0.174
Fe3+/Fe(tot)	0.156	0.187	0.166	0.180	0.186	0.233	0.200	0.208	0.177	0.198
Cation charge	44.846	44.591	44.766	44.649	44.607	44.208	44.490	44.437	44.669	44.520

@ Fe3+ calculated by charge balance

TRAVERSE ACROSS AMPHIBOLE PHENOCRYST IN SAN JACINTO (2660') PG-118

Sample name Analysis pt Remark	32	33	34	36	37	38	39	40	42	43
SiO2	40.36	40.76	40.82	40.65	40.75	41.10	41.18	41.01	40.97	40.92
TiO2	1.47	1.34	1.46	1.43	1.43	1.40	1.47	1.39	1.44	1.43
Al2O3	10.66	10.70	10.82	10.49	10.49	10.59	10.46	10.39	10.67	10.73
Cr2O3	0.02	0.00	0.00	0.00	0.00	0.04	0.02	0.02	0.00	0.00
Fe2O3 @	6.62	6.35	6.16	6.45	5.85	5.17	6.09	5.81	6.03	5.43
FeO	22.89	22.95	23.16	23.32	23.64	23.95	23.49	23.77	23.43	23.78
MnO	0.92	0.88	0.87	0.85	0.83	0.86	0.94	0.90	0.90	0.88
MgO	2.69	2.67	2.69	2.68	2.78	2.62	2.77	2.79	2.74	2.64
CaO	10.44	10.22	10.45	10.41	10.50	10.46	10.53	10.57	10.47	10.48
Na2O	1.59	1.68	1.60	1.67	1.73	1.70	1.67	1.75	1.72	1.69
K2O	1.32	1.35	1.27	1.35	1.37	1.26	1.25	1.30	1.28	1.32
Total	98.98	98.90	99.30	99.30	99.38	99.15	99.87	99.70	99.64	99.29
---Atomic proportions based on 13 cations (except Ca+Na+K+Ba)---										
Si	6.324	6.379	6.361	6.355	6.366	6.421	6.390	6.386	6.371	6.387
Ti	0.173	0.158	0.171	0.168	0.168	0.164	0.172	0.163	0.168	0.168
Al(iv)	1.676	1.621	1.639	1.645	1.634	1.579	1.610	1.614	1.629	1.613
Fe3+(iv)	0.000	0.000	0.000	0.000	0.000	0.000	0.000	0.000	0.000	0.000
Al(vi)	0.293	0.352	0.349	0.288	0.298	0.370	0.303	0.292	0.326	0.361
Cr	0.002	0.000	0.000	0.000	0.000	0.005	0.002	0.002	0.000	0.000
Fe3+ (calc)	0.781	0.748	0.722	0.759	0.688	0.608	0.711	0.681	0.705	0.638
Fe2+	3.000	3.003	3.018	3.049	3.089	3.128	3.048	3.095	3.047	3.103
Mn2+	0.122	0.117	0.115	0.113	0.110	0.114	0.124	0.119	0.119	0.116
Mg	0.628	0.623	0.625	0.625	0.647	0.610	0.641	0.648	0.635	0.614
C site (M1+M2+M3)	5.000	5.000	5.000	5.000	5.000	5.000	5.000	5.000	5.000	5.000
excess (M1+M2+M3)	0.000	0.000	0.000	0.000	0.000	0.000	0.000	0.000	0.000	0.000
Ca	1.753	1.714	1.745	1.744	1.758	1.751	1.751	1.763	1.744	1.753
Na(M4)	0.247	0.286	0.255	0.256	0.242	0.249	0.249	0.237	0.256	0.247
B site (M4) total	2.000	2.000	2.000	2.000	2.000	2.000	2.000	2.000	2.000	2.000
Na(A)	0.236	0.223	0.228	0.250	0.282	0.266	0.253	0.292	0.263	0.264
K	0.264	0.270	0.252	0.269	0.273	0.251	0.247	0.258	0.254	0.263
A site total	0.500	0.493	0.481	0.519	0.555	0.517	0.500	0.550	0.517	0.527
Mg/Fe(tot)	0.166	0.166	0.167	0.164	0.171	0.163	0.170	0.171	0.169	0.164
Mg/Fe2+	0.209	0.207	0.207	0.205	0.210	0.195	0.210	0.209	0.208	0.198
Mg/Mg+Fe(tot)	0.143	0.142	0.143	0.141	0.146	0.140	0.146	0.146	0.145	0.141
Mg/Mg+Fe2+	0.173	0.172	0.172	0.170	0.173	0.163	0.174	0.173	0.173	0.165
Fe3+/Fe(tot)	0.207	0.199	0.193	0.199	0.182	0.163	0.189	0.180	0.188	0.170
Cation charge	44.438	44.505	44.556	44.483	44.624	44.784	44.577	44.638	44.590	44.725

@ Fe3+ calculated by charge balance

TRAVERSE ACROSS AMPHIBOLE PHENOCRYST IN SAN JACINTO (2660') PG-118

Sample name Analysis pt Remark	44	45	46	47	48	49	50	51	52	53
SiO2	40.94	40.99	40.98	40.73	40.81	40.53	41.02	40.28	40.94	40.47
TiO2	1.45	1.37	1.38	1.38	1.36	1.40	1.29	1.35	1.33	1.31
Al2O3	10.61	10.81	10.52	10.59	11.04	10.84	11.09	10.86	11.12	11.23
Cr2O3	0.00	0.00	0.00	0.00	0.00	0.00	0.00	0.00	0.00	0.00
Fe2O3 @	5.51	6.89	6.73	6.22	5.89	6.39	5.59	6.70	5.69	5.65
FeO	23.82	22.66	23.01	23.27	23.14	22.92	23.08	22.82	23.27	23.53
MnO	0.76	0.89	0.94	0.93	0.86	0.89	0.85	0.90	0.87	0.88
MgO	2.71	2.67	2.76	2.69	2.72	2.69	2.79	2.80	2.67	2.61
CaO	10.55	10.28	10.39	10.51	10.43	10.37	10.39	10.51	10.47	10.69
Na2O	1.63	1.58	1.69	1.59	1.64	1.62	1.61	1.65	1.59	1.57
K2O	1.29	1.26	1.28	1.32	1.32	1.36	1.36	1.40	1.32	1.36
Total	99.26	99.40	99.68	99.23	99.21	99.01	99.07	99.27	99.27	99.30
---Atomic proportions based on 13 cations (except Ca+Na+K+Ba)---										
Si	6.391	6.372	6.370	6.365	6.360	6.341	6.390	6.297	6.373	6.319
Ti	0.170	0.160	0.161	0.162	0.159	0.165	0.151	0.159	0.156	0.154
Al(iv)	1.609	1.628	1.630	1.635	1.640	1.659	1.610	1.703	1.627	1.681
Fe3+(iv)	0.000	0.000	0.000	0.000	0.000	0.000	0.000	0.000	0.000	0.000
Al(vi)	0.343	0.352	0.297	0.315	0.388	0.339	0.427	0.298	0.414	0.386
Cr	0.000	0.000	0.000	0.000	0.000	0.000	0.000	0.000	0.000	0.000
Fe3+ (calc)	0.647	0.805	0.787	0.731	0.691	0.752	0.656	0.788	0.667	0.664
Fe2+	3.109	2.946	2.991	3.041	3.016	2.999	3.006	2.984	3.030	3.072
Mn2+	0.100	0.117	0.124	0.123	0.114	0.118	0.112	0.119	0.115	0.116
Mg	0.631	0.619	0.640	0.627	0.632	0.627	0.648	0.653	0.620	0.608
C site (M1+M2+M3)	5.000	5.000	5.000	5.000	5.000	5.000	5.000	5.000	5.000	5.000
excess (M1+M2+M3)	0.000	0.000	0.000	0.000	0.000	0.000	0.000	0.000	0.000	0.000
Ca	1.764	1.712	1.730	1.760	1.742	1.738	1.734	1.760	1.746	1.788
Na(M4)	0.236	0.288	0.270	0.240	0.258	0.262	0.266	0.240	0.254	0.212
B site (M4) total	2.000	2.000	2.000	2.000	2.000	2.000	2.000	2.000	2.000	2.000
Na(A)	0.258	0.188	0.240	0.241	0.237	0.230	0.221	0.260	0.226	0.264
K	0.257	0.250	0.254	0.263	0.262	0.271	0.270	0.279	0.262	0.271
A site total	0.515	0.438	0.493	0.505	0.500	0.501	0.491	0.540	0.488	0.535
Mg/Fe(tot)	0.168	0.165	0.169	0.166	0.170	0.167	0.177	0.173	0.168	0.163
Mg/Fe2+	0.203	0.210	0.214	0.206	0.210	0.209	0.216	0.219	0.205	0.198
Mg/Mg+Fe(tot)	0.144	0.142	0.145	0.142	0.146	0.143	0.150	0.147	0.144	0.140
Mg/Mg+Fe2+	0.169	0.174	0.176	0.171	0.173	0.173	0.177	0.179	0.170	0.165
Fe3+/Fe(tot)	0.172	0.215	0.208	0.194	0.186	0.200	0.179	0.209	0.180	0.178
Cation charge	44.707	44.389	44.425	44.537	44.618	44.496	44.688	44.424	44.667	44.673

@ Fe3+ calculated by charge balance

TRAVERSE ACROSS AMPHIBOLE PHENOCRYST IN SAN JACINTO (2660') PG-118

Sample name		
Analysis pt	54	55
Remark		
SiO2	40.46	40.65
TiO2	1.30	1.28
Al2O3	11.37	11.84
Cr2O3	0.00	0.04
Fe2O3 @	5.57	5.45
FeO	23.50	23.67
MnO	0.88	0.86
MgO	2.59	2.63
CaO	10.75	10.95
Na2O	1.50	1.44
K2O	1.35	1.48
Total	99.27	100.30

---Atomic proportions based on 13 cations (except Ca+Na+K+Ba)---

Si	6.315	6.280
Ti	0.153	0.149
Al(iv)	1.685	1.720
Fe3+(iv)	0.000	0.000
Al(vi)	0.407	0.436
Cr	0.000	0.005
Fe3+ (calc)	0.654	0.634
Fe2+	3.067	3.058
Mn2+	0.116	0.113
Mg	0.603	0.606
C site (M1+M2+M3)	5.000	5.000
excess (M1+M2+M3)	0.000	0.000
Ca	1.798	1.812
Na(M4)	0.202	0.188
B site (M4) total	2.000	2.000
Na(A)	0.252	0.244
K	0.269	0.292
A site total	0.521	0.535
Mg/Fe(tot)	0.162	0.164
Mg/Fe2+	0.196	0.198
Mg/Mg+Fe(tot)	0.139	0.141
Mg/Mg+Fe2+	0.164	0.165
Fe3+/Fe(tot)	0.176	0.172
Cation charge	44.691	44.732

@ Fe3+ calculated by charge balance

PLAGIOCLASE TRAVERSES FRON SAN JACINTO (SAMPLE PG-101) 3 TRAVERSES

Sample name	PG101									
Analysis pt	1	2	3	4	5	6	7	8	9	11
Remark	37.8 um									
SiO2	61.54	61.27	61.28	60.92	60.51	60.23	61.20	60.83	60.53	60.49
Al2O3	24.63	24.10	24.75	24.73	24.76	25.12	25.17	24.69	24.81	24.56
FeO	0.10	0.09	0.09	0.10	0.08	0.16	0.13	0.12	0.14	0.12
CaO	5.73	5.99	6.16	6.26	6.24	6.65	6.62	6.46	6.28	6.53
BaO	0.10	0.08	0.08	0.06	0.06	0.05	0.07	0.09	0.02	0.05
Na2O	8.30	7.84	7.85	7.78	7.36	7.31	7.61	7.69	7.83	7.49
K2O	0.15	0.32	0.35	0.36	0.37	0.39	0.37	0.40	0.47	0.41
Total	100.55	99.69	100.56	100.21	99.38	99.91	101.17	100.28	100.08	99.65
--Atomic proportions on the basis of 8 oxygens--										
Si	2.720	2.731	2.711	2.705	2.705	2.685	2.694	2.702	2.695	2.703
Al	1.283	1.266	1.290	1.294	1.305	1.320	1.306	1.293	1.302	1.293
Tet cations	4.002	3.997	4.001	4.000	4.010	4.004	4.000	3.995	3.997	3.996
Fe2+	0.004	0.003	0.003	0.004	0.003	0.006	0.005	0.004	0.005	0.004
Ca	0.271	0.286	0.292	0.298	0.299	0.318	0.312	0.307	0.300	0.313
Ba	0.002	0.001	0.001	0.001	0.001	0.001	0.001	0.002	0.000	0.001
Na	0.711	0.678	0.673	0.670	0.638	0.632	0.649	0.662	0.676	0.649
K	0.008	0.018	0.020	0.020	0.021	0.022	0.021	0.023	0.027	0.023
A-site total	0.996	0.987	0.990	0.993	0.962	0.978	0.988	0.999	1.008	0.990
Anorthite	27.33	29.09	29.60	30.11	31.17	32.66	31.74	30.93	29.88	31.71
Albite	71.64	68.91	68.26	67.72	66.52	64.97	66.03	66.63	67.42	65.83
Orthoclase	0.85	1.85	2.00	2.06	2.20	2.28	2.11	2.28	2.66	2.37
Celsian	0.17	0.14	0.14	0.11	0.11	0.09	0.12	0.16	0.03	0.09

PLAGIOCLASE TRAVERSES FRON SAN JACINTO (SAMPLE PG-101) 3 TRAVERSES

Sample name										
Analysis pt	12	13	14	15	16	17	18	21	22	23
Remark										
SiO2	59.72	60.05	59.42	58.76	59.53	59.41	58.34	60.44	59.71	59.31
Al2O3	25.21	25.61	25.87	25.76	25.62	26.21	26.12	25.45	24.84	25.73
FeO	0.13	0.10	0.13	0.13	0.16	0.08	0.12	0.10	0.12	0.07
CaO	6.64	7.15	7.38	7.54	7.41	7.59	7.85	6.79	6.45	7.06
BaO	0.06	0.03	0.06	0.01	0.03	0.03	0.03	0.02	0.06	0.04
Na2O	7.12	7.26	7.12	6.96	7.03	7.07	6.71	7.22	7.55	6.89
K2O	0.93	0.40	0.40	0.38	0.38	0.36	0.34	0.42	0.48	0.40
Total	99.81	100.60	100.38	99.54	100.16	100.75	99.51	100.44	99.21	99.50
--Atomic proportions on the basis of 8 oxygens--										
Si	2.673	2.663	2.644	2.637	2.653	2.634	2.621	2.679	2.684	2.655
Al	1.330	1.338	1.357	1.363	1.346	1.369	1.383	1.329	1.316	1.358
Tet cations	4.003	4.001	4.001	4.000	3.999	4.003	4.003	4.008	4.000	4.013
Fe2+	0.005	0.004	0.005	0.005	0.006	0.003	0.005	0.004	0.005	0.003
Ca	0.318	0.340	0.352	0.363	0.354	0.361	0.378	0.322	0.311	0.339
Ba	0.001	0.001	0.001	0.000	0.001	0.001	0.001	0.000	0.001	0.001
Na	0.618	0.624	0.614	0.606	0.607	0.608	0.584	0.620	0.658	0.598
K	0.053	0.023	0.023	0.022	0.022	0.020	0.019	0.024	0.028	0.023
A-site total	0.995	0.991	0.995	0.995	0.989	0.992	0.987	0.971	1.002	0.963
Anorthite	32.15	34.42	35.54	36.62	35.98	36.45	38.46	33.34	31.15	35.27
Albite	62.38	63.24	62.06	61.17	61.77	61.44	59.50	64.16	65.98	62.28
Orthoclase	5.36	2.29	2.29	2.20	2.20	2.06	1.98	2.46	2.76	2.38
Celsian	0.11	0.05	0.11	0.02	0.05	0.05	0.05	0.04	0.11	0.07

PLAGIOCLASE TRAVERSES FRON SAN JACINTO (SAMPLE PG-101) 3 TRAVERSES

Sample name									pg101	
Analysis pt	24	25	26	27	28	29	30	31	1/2	3
Remark									40 um int	
SiO2	59.88	59.16	59.09	60.94	60.46	59.76	60.14	59.16	60.51	61.42
Al2O3	25.32	25.52	25.97	25.30	25.13	25.10	25.60	25.67	25.12	24.72
FeO	0.06	0.04	0.06	0.06	0.12	0.12	0.09	0.05	0.06	0.12
CaO	7.02	7.35	7.62	6.71	6.75	6.81	6.81	7.41	6.52	6.01
BaO	0.02	0.07	0.04	0.06	0.01	0.02	0.05	0.06	0.03	0.00
Na2O	7.44	7.30	7.12	7.42	7.56	7.38	7.51	7.00	7.60	8.30
K2O	0.40	0.26	0.36	0.37	0.46	0.43	0.42	0.36	0.37	0.20
Total	100.14	99.70	100.26	100.86	100.49	99.62	100.62	99.71	100.21	100.77
	--Atomic proportions on the basis of 8 oxygens--									
Si	2.668	2.650	2.634	2.689	2.683	2.675	2.666	2.648	2.688	2.711
Al	1.329	1.347	1.364	1.316	1.314	1.324	1.337	1.354	1.315	1.286
Tet cations	3.997	3.997	3.999	4.005	3.997	3.999	4.003	4.002	4.003	3.997
Fe2+	0.002	0.001	0.002	0.002	0.004	0.004	0.003	0.002	0.002	0.004
Ca	0.335	0.353	0.364	0.317	0.321	0.327	0.323	0.355	0.310	0.284
Ba	0.000	0.001	0.001	0.001	0.000	0.000	0.001	0.001	0.001	0.000
Na	0.643	0.634	0.615	0.635	0.650	0.640	0.645	0.608	0.655	0.710
K	0.023	0.015	0.020	0.021	0.026	0.025	0.024	0.021	0.021	0.011
A-site total	1.003	1.004	1.003	0.976	1.002	0.996	0.997	0.986	0.989	1.010
Anorthite	33.48	35.18	36.38	32.57	32.17	32.92	32.55	36.10	31.46	28.26
Albite	64.21	63.22	61.51	65.18	65.20	64.57	64.97	61.71	66.36	70.62
Orthoclase	2.27	1.48	2.05	2.14	2.61	2.48	2.39	2.09	2.13	1.12
Celsian	0.03	0.12	0.07	0.11	0.02	0.04	0.09	0.11	0.05	0.00

PLAGIOCLASE TRAVERSES FRON SAN JACINTO (SAMPLE PG-101) 3 TRAVERSES

Sample name										
Analysis pt	4	5	7	8	9	10	12	13	14	16
Remark										
SiO2	61.40	60.74	60.59	61.10	62.00	60.08	60.21	58.94	58.99	60.48
Al2O3	24.83	24.77	24.96	24.98	24.16	25.44	25.45	26.01	25.99	25.59
FeO	0.01	0.02	0.02	0.04	0.02	0.10	0.17	0.10	0.11	0.12
CaO	6.03	6.22	6.35	6.38	5.23	6.78	7.01	7.61	6.99	6.94
BaO	0.00	0.00	0.00	0.00	0.00	0.00	0.01	0.02	0.02	0.00
Na2O	7.94	7.92	7.95	7.84	8.48	7.68	7.77	7.26	7.27	7.78
K2O	0.10	0.11	0.11	0.09	0.09	0.13	0.17	0.17	0.15	0.13
Total	100.31	99.78	99.98	100.43	99.98	100.21	100.79	100.11	99.52	101.04
	--Atomic proportions on the basis of 8 oxygens--									
Si	2.715	2.704	2.694	2.702	2.746	2.670	2.665	2.630	2.641	2.668
Al	1.294	1.300	1.308	1.302	1.261	1.332	1.328	1.368	1.372	1.330
Tet cations	4.009	4.004	4.002	4.004	4.008	4.003	3.993	3.999	4.013	3.998
Fe2+	0.000	0.001	0.001	0.001	0.001	0.004	0.006	0.004	0.004	0.004
Ca	0.286	0.297	0.303	0.302	0.248	0.323	0.332	0.364	0.335	0.328
Ba	0.000	0.000	0.000	0.000	0.000	0.000	0.000	0.000	0.000	0.000
Na	0.681	0.684	0.685	0.672	0.728	0.662	0.667	0.628	0.631	0.665
K	0.006	0.006	0.006	0.005	0.005	0.007	0.010	0.010	0.009	0.007
A-site total	0.972	0.987	0.995	0.981	0.982	0.996	1.015	1.006	0.980	1.005
Anorthite	29.39	30.07	30.43	30.86	25.29	32.54	32.95	36.31	34.38	32.78
Albite	70.03	69.29	68.94	68.62	74.20	66.71	66.08	62.69	64.71	66.49
Orthoclase	0.58	0.63	0.63	0.52	0.52	0.74	0.95	0.97	0.88	0.73
Celsian	0.00	0.00	0.00	0.00	0.00	0.00	0.02	0.03	0.04	0.00

PLAGIOCLASE TRAVERSES FRON SAN JACINTO (SAMPLE PG-101) 3 TRAVERSES

Sample name Analysis pt Remark	17	18	19	20	21	22	23	24	25	26
SiO2	59.98	63.44	59.99	62.51	61.82	59.82	59.87	60.73	60.10	59.70
Al2O3	25.30	22.75	24.82	22.83	23.91	25.46	25.12	25.05	25.36	25.77
FeO	0.10	0.00	0.23	0.00	0.00	0.08	0.04	0.03	0.01	0.12
CaO	7.04	3.80	7.12	3.98	5.37	6.38	6.92	6.88	6.82	7.21
BaO	0.00	0.02	0.06	0.01	0.06	0.02	0.01	0.00	0.02	0.05
Na2O	7.62	9.60	7.83	8.81	8.33	7.53	7.47	7.61	7.61	7.32
K2O	0.13	0.12	0.08	0.11	0.08	0.12	0.14	0.20	0.17	0.18
Total	100.17	99.73	100.13	98.25	99.57	99.41	99.57	100.50	100.09	100.35
--Atomic proportions on the basis of 8 oxygens--										
Si	2.669	2.811	2.676	2.805	2.750	2.674	2.677	2.689	2.673	2.653
Al	1.327	1.188	1.305	1.208	1.254	1.342	1.324	1.307	1.330	1.350
Tet cations	3.996	3.999	3.981	4.013	4.004	4.016	4.000	3.997	4.003	4.003
Fe2+	0.004	0.000	0.009	0.000	0.000	0.003	0.001	0.001	0.000	0.004
Ca	0.336	0.180	0.340	0.191	0.256	0.306	0.331	0.326	0.325	0.343
Ba	0.000	0.000	0.001	0.000	0.001	0.000	0.000	0.000	0.000	0.001
Na	0.657	0.825	0.677	0.767	0.719	0.653	0.648	0.653	0.656	0.631
K	0.007	0.007	0.005	0.006	0.005	0.007	0.008	0.011	0.010	0.010
A-site total	1.004	1.012	1.032	0.964	0.980	0.969	0.989	0.992	0.992	0.990
Anorthite	33.55	17.82	33.26	19.84	26.12	31.65	33.58	32.94	32.79	34.85
Albite	65.71	81.47	66.19	79.49	73.31	67.60	65.59	65.92	66.20	64.03
Orthoclase	0.74	0.67	0.44	0.65	0.46	0.71	0.81	1.14	0.97	1.04
Celsian	0.00	0.03	0.10	0.02	0.11	0.04	0.02	0.00	0.04	0.09

PLAGIOCLASE TRAVERSES FRON SAN JACINTO (SAMPLE PG-101) 3 TRAVERSES

Sample name Analysis pt Remark	27	28	29	30	2/3 15 um int	3	4	5	6	7
SiO2	58.32	60.23	59.42	59.33	59.20	60.30	60.71	59.99	59.89	59.35
Al2O3	25.92	25.41	25.41	26.30	26.02	25.02	25.27	25.45	25.73	26.29
FeO	0.12	0.10	0.06	0.11	0.11	0.09	0.11	0.05	0.02	0.05
CaO	8.00	7.02	7.12	7.76	7.73	6.37	6.82	6.81	7.22	8.04
BaO	0.04	0.04	0.05	0.04	0.00	0.06	0.06	0.01	0.03	0.03
Na2O	7.04	7.74	7.46	6.98	7.15	7.90	7.68	7.62	7.58	7.00
K2O	0.15	0.18	0.19	0.15	0.11	0.21	0.25	0.22	0.22	0.15
Total	99.59	100.72	99.71	100.67	100.32	99.95	100.90	100.15	100.69	100.91
--Atomic proportions on the basis of 8 oxygens--										
Si	2.620	2.668	2.658	2.630	2.634	2.687	2.682	2.669	2.654	2.627
Al	1.372	1.326	1.340	1.374	1.365	1.314	1.315	1.334	1.344	1.372
Tet cations	3.993	3.994	3.998	4.005	3.999	4.001	3.997	4.003	3.998	3.999
Fe2+	0.005	0.004	0.002	0.004	0.004	0.003	0.004	0.002	0.001	0.002
Ca	0.385	0.333	0.341	0.369	0.369	0.304	0.323	0.325	0.343	0.381
Ba	0.001	0.001	0.001	0.001	0.000	0.001	0.001	0.000	0.001	0.001
Na	0.613	0.665	0.647	0.600	0.617	0.682	0.658	0.657	0.651	0.601
K	0.009	0.010	0.011	0.008	0.006	0.012	0.014	0.012	0.012	0.008
A-site total	1.012	1.012	1.002	0.982	0.996	1.003	1.000	0.996	1.008	0.993
Anorthite	38.22	33.03	34.13	37.70	37.16	30.42	32.42	32.64	34.04	38.47
Albite	60.86	65.90	64.70	61.36	62.21	68.28	66.06	66.09	64.67	60.62
Orthoclase	0.85	1.01	1.08	0.87	0.63	1.19	1.41	1.26	1.24	0.85
Celsian	0.07	0.07	0.09	0.07	0.00	0.10	0.10	0.02	0.05	0.05

PLAGIOCLASE TRAVERSES FRON SAN JACINTO (SAMPLE PG-101) 3 TRAVERSES

Sample name Analysis pt Remark	8	9	10	11	12	13	14	15	16	17
SiO2	59.69	59.47	59.44	60.40	61.04	60.89	61.02	60.73	61.15	60.68
Al2O3	26.14	26.19	26.10	25.43	24.72	24.67	24.81	24.71	25.30	24.86
FeO	0.10	0.02	0.01	0.04	0.00	0.03	0.02	0.02	0.04	0.10
CaO	7.73	7.52	7.43	7.01	6.03	6.39	6.23	6.34	6.31	6.39
BaO	0.06	0.03	0.01	0.00	0.01	0.00	0.01	0.03	0.01	0.00
Na2O	7.18	7.27	7.20	7.55	8.13	7.89	8.11	7.94	8.03	8.18
K2O	0.07	0.08	0.13	0.14	0.10	0.11	0.10	0.11	0.12	0.21
Total	100.97	100.58	100.32	100.57	100.03	99.98	100.30	99.88	100.96	100.42
--Atomic proportions on the basis of 8 oxygens--										
Si	2.638	2.637	2.641	2.674	2.710	2.706	2.704	2.703	2.693	2.692
Al	1.362	1.369	1.367	1.327	1.293	1.292	1.296	1.296	1.313	1.300
Tet cations	4.000	4.006	4.008	4.001	4.003	3.999	4.000	3.999	4.006	3.992
Fe2+	0.004	0.001	0.000	0.001	0.000	0.001	0.001	0.001	0.001	0.004
Ca	0.366	0.357	0.354	0.332	0.287	0.304	0.296	0.302	0.298	0.304
Ba	0.001	0.001	0.000	0.000	0.000	0.000	0.000	0.001	0.000	0.000
Na	0.615	0.625	0.620	0.648	0.700	0.680	0.697	0.685	0.686	0.704
K	0.004	0.005	0.007	0.008	0.006	0.006	0.006	0.006	0.007	0.012
A-site total	0.990	0.988	0.982	0.990	0.993	0.992	0.999	0.995	0.992	1.023
Anorthite	37.11	36.18	36.04	33.64	28.90	30.72	29.63	30.41	30.07	29.80
Albite	62.38	63.30	63.19	65.56	70.51	68.65	69.79	68.91	69.24	69.03
Orthoclase	0.40	0.46	0.75	0.80	0.57	0.63	0.57	0.63	0.68	1.17
Celsian	0.11	0.05	0.02	0.00	0.02	0.00	0.02	0.05	0.02	0.00

PLAGIOCLASE TRAVERSES FRON SAN JACINTO (SAMPLE PG-101) 3 TRAVERSES

Sample name Analysis pt Remark	19	20	21	22	23	24	25	26	27	28
SiO2	60.70	59.18	60.20	59.90	59.26	58.51	59.45	59.18	59.90	60.38
Al2O3	24.78	25.33	25.58	25.38	26.08	26.25	26.12	25.57	25.33	25.08
FeO	0.16	0.10	0.09	0.09	0.08	0.11	0.12	0.04	0.09	0.15
CaO	6.38	7.03	7.16	6.90	7.72	8.02	7.65	7.35	6.74	6.69
BaO	0.00	0.00	0.00	0.00	0.00	0.02	0.00	0.03	0.02	0.00
Na2O	7.92	7.32	7.29	7.60	7.05	7.10	7.21	7.46	7.68	7.64
K2O	0.24	0.18	0.21	0.27	0.24	0.19	0.14	0.13	0.16	0.21
Total	100.18	99.14	100.53	100.14	100.43	100.20	100.69	99.76	99.92	100.15
--Atomic proportions on the basis of 8 oxygens--										
Si	2.698	2.660	2.667	2.667	2.634	2.613	2.636	2.648	2.671	2.685
Al	1.298	1.342	1.336	1.332	1.366	1.382	1.365	1.348	1.331	1.314
Tet cations	3.996	4.002	4.003	3.999	4.001	3.995	4.000	3.996	4.002	3.999
Fe2+	0.006	0.004	0.003	0.003	0.003	0.004	0.004	0.001	0.003	0.006
Ca	0.304	0.339	0.340	0.329	0.368	0.384	0.363	0.352	0.322	0.319
Ba	0.000	0.000	0.000	0.000	0.000	0.000	0.000	0.001	0.000	0.000
Na	0.682	0.638	0.626	0.656	0.608	0.615	0.620	0.647	0.664	0.659
K	0.014	0.010	0.012	0.015	0.014	0.011	0.008	0.007	0.009	0.012
A-site total	1.006	0.991	0.981	1.004	0.992	1.014	0.995	1.009	0.999	0.995
Anorthite	30.38	34.31	34.75	32.90	37.18	38.01	36.67	34.97	32.35	32.22
Albite	68.26	64.65	64.03	65.57	61.44	60.89	62.54	64.24	66.70	66.58
Orthoclase	1.36	1.05	1.21	1.53	1.38	1.07	0.80	0.74	0.91	1.20
Celsian	0.00	0.00	0.00	0.00	0.00	0.03	0.00	0.05	0.04	0.00

PLAGIOCLASE TRAVERSES FRON SAN JACINTO (SAMPLE PG-101) 3 TRAVERSES

Sample name		
Analysis pt	29	30
Remark		
SiO2	61.34	60.99
Al2O3	24.97	25.42
FeO	0.06	0.12
CaO	6.37	6.34
BaO	0.03	0.02
Na2O	7.95	8.00
K2O	0.16	0.19
Total	100.88	101.08
--Atomic proportions on the basis of 8 oxygens--		
Si	2.703	2.685
Al	1.297	1.319
Tet cations	4.000	4.004
Fe2+	0.002	0.004
Ca	0.301	0.299
Ba	0.001	0.000
Na	0.679	0.683
K	0.009	0.011
A-site total	0.992	0.997
Anorthite	30.39	30.12
Albite	68.64	68.77
Orthoclase	0.91	1.07
Celsian	0.05	0.03

PLAGIOCLASE TRAVERSE IN PHENOCRYST NEXT TO K-SPAR - PG-102

Sample name	PG-102									
Analysis pt	1	2	3	4	5	6	7	8	9	10
Remark		15 UM INT								
SiO2	63.62	61.43	61.04	61.83	61.02	60.60	59.26	60.45	60.58	60.56
Al2O3	22.72	24.02	24.27	24.27	24.03	24.39	26.82	24.68	24.50	24.41
FeO	0.01	0.03	0.05	0.04	0.08	0.00	0.04	0.04	0.09	0.07
CaO	3.65	5.63	5.73	5.87	6.04	6.15	6.17	6.27	6.31	6.23
BaO	0.00	0.00	0.00	0.00	0.01	0.01	0.00	0.00	0.00	0.00
Na2O	9.34	8.29	8.11	8.26	8.03	7.88	7.59	7.72	8.08	7.76
K2O	0.15	0.16	0.09	0.09	0.13	0.12	0.13	0.18	0.21	0.17
Total	99.49	99.56	99.29	100.36	99.34	99.15	100.01	99.34	99.77	99.20
--Atomic proportions on the basis of 8 oxygens--										
Si	2.820	2.738	2.727	2.734	2.728	2.714	2.634	2.703	2.703	2.712
Al	1.187	1.262	1.278	1.265	1.266	1.287	1.405	1.301	1.289	1.288
Tet cations	4.007	3.999	4.004	3.998	3.994	4.001	4.038	4.004	3.992	4.000
Fe2+	0.000	0.001	0.002	0.001	0.003	0.000	0.001	0.001	0.003	0.003
Ca	0.173	0.269	0.274	0.278	0.289	0.295	0.294	0.300	0.302	0.299
Ba	0.000	0.000	0.000	0.000	0.000	0.000	0.000	0.000	0.000	0.000
Na	0.803	0.716	0.702	0.708	0.696	0.684	0.654	0.669	0.699	0.674
K	0.008	0.009	0.005	0.005	0.007	0.007	0.007	0.010	0.012	0.010
A-site total	0.985	0.995	0.984	0.993	0.996	0.986	0.957	0.982	1.016	0.985
Anorthite	17.61	27.04	27.93	28.05	29.14	29.92	30.76	30.65	29.79	30.43
Albite	81.53	72.05	71.54	71.43	70.10	69.37	68.47	68.30	69.03	68.58
Orthoclase	0.86	0.91	0.52	0.51	0.75	0.70	0.77	1.05	1.18	0.99
Celsian	0.00	0.00	0.00	0.00	0.02	0.02	0.00	0.00	0.00	0.00

PLAGIOCLASE TRAVERSE IN PHENOCRYST NEXT TO K-SPAR - PG-102

Sample name Analysis pt Remark	11	12	13	14	15	16	17	18	23	24
SiO2	60.50	60.36	60.35	59.93	59.70	59.75	59.58	59.18	58.95	59.64
Al2O3	24.49	24.76	24.89	25.15	25.08	25.27	25.19	25.36	24.74	24.99
FeO	0.04	0.00	0.08	0.11	0.21	0.07	0.00	0.00	0.02	0.02
CaO	6.34	6.34	6.58	6.70	6.81	6.88	7.09	7.45	7.06	6.76
BaO	0.00	0.00	0.00	0.00	0.00	0.00	0.02	0.00	0.00	0.00
Na2O	7.84	7.83	7.68	7.59	7.67	7.65	7.38	7.16	7.26	7.65
K2O	0.25	0.24	0.27	0.24	0.19	0.20	0.23	0.22	0.22	0.24
Total	99.46	99.53	99.85	99.72	99.66	99.82	99.49	99.37	98.25	99.30
--Atomic proportions on the basis of 8 oxygens--										
Si	2.706	2.697	2.691	2.677	2.672	2.668	2.669	2.656	2.674	2.676
Al	1.291	1.304	1.308	1.324	1.323	1.330	1.330	1.341	1.322	1.322
Tet cations	3.997	4.001	3.999	4.001	3.994	3.998	3.999	3.997	3.996	3.998
Fe2+	0.001	0.000	0.003	0.004	0.008	0.003	0.000	0.000	0.001	0.001
Ca	0.304	0.304	0.314	0.321	0.327	0.329	0.340	0.358	0.343	0.325
Ba	0.000	0.000	0.000	0.000	0.000	0.000	0.000	0.000	0.000	0.000
Na	0.680	0.678	0.664	0.657	0.665	0.662	0.641	0.623	0.638	0.666
K	0.014	0.014	0.015	0.014	0.011	0.011	0.013	0.013	0.013	0.014
A-site total	0.999	0.996	0.997	0.996	1.011	1.006	0.995	0.994	0.995	1.005
Anorthite	30.44	30.49	31.64	32.33	32.56	32.82	34.21	36.04	34.51	32.36
Albite	68.13	68.14	66.82	66.29	66.36	66.04	64.44	62.69	64.21	66.27
Orthoclase	1.43	1.37	1.55	1.38	1.08	1.14	1.32	1.27	1.28	1.37
Celsian	0.00	0.00	0.00	0.00	0.00	0.00	0.04	0.00	0.00	0.00

PLAGIOCLASE TRAVERSE IN PHENOCRYST NEXT TO K-SPAR - PG-102

Sample name Analysis pt Remark	25	26	27	28	29	30	31
SiO2	60.08	60.23	60.01	60.73	59.66	59.72	59.36
Al2O3	25.13	25.20	25.07	25.30	24.79	24.78	25.13
FeO	0.00	0.05	0.11	0.07	0.02	0.08	0.09
CaO	6.74	6.70	6.87	6.89	6.69	6.72	6.73
BaO	0.00	0.00	0.04	0.02	0.05	0.00	0.00
Na2O	7.44	7.40	7.40	7.74	7.71	7.55	7.52
K2O	0.27	0.26	0.24	0.25	0.25	0.24	0.23
Total	99.66	99.84	99.74	101.00	99.17	99.09	99.06
--Atomic proportions on the basis of 8 oxygens--							
Si	2.682	2.683	2.680	2.680	2.682	2.684	2.670
Al	1.322	1.323	1.320	1.316	1.313	1.313	1.332
Tet cations	4.005	4.006	4.000	3.996	3.995	3.997	4.002
Fe2+	0.000	0.002	0.004	0.003	0.001	0.003	0.003
Ca	0.322	0.320	0.329	0.326	0.322	0.324	0.324
Ba	0.000	0.000	0.001	0.000	0.001	0.000	0.000
Na	0.644	0.639	0.641	0.662	0.672	0.658	0.656
K	0.015	0.015	0.014	0.014	0.014	0.014	0.013
A-site total	0.982	0.976	0.988	1.005	1.010	0.998	0.997
Anorthite	32.84	32.84	33.41	32.50	31.92	32.51	32.65
Albite	65.60	65.64	65.13	66.06	66.57	66.10	66.02
Orthoclase	1.57	1.52	1.39	1.40	1.42	1.38	1.33
Celsian	0.00	0.00	0.07	0.03	0.09	0.00	0.00

TWO TRAVERSES ACROSS PLAGIOCLASE NEAR AMPHIBOLE PG-110

Sample name	PG101									
Analysis pt	1/1	2	3	4	5	6	7	8	11	12
Remark	12.7 UM INT									
SiO2	59.88	59.77	60.31	60.00	59.96	59.71	59.32	59.41	58.20	58.95
Al2O3	25.86	25.21	25.01	25.02	25.27	25.93	25.55	25.93	25.64	26.43
FeO	0.09	0.08	0.06	0.01	0.03	0.04	0.01	0.00	0.12	0.07
CaO	6.99	6.89	6.73	6.60	7.04	7.28	7.40	7.44	7.81	7.90
BaO	0.04	0.02	0.05	0.02	0.01	0.03	0.03	0.04	0.00	0.01
Na2O	7.50	7.32	7.53	7.37	7.39	7.34	7.14	7.05	7.03	6.89
K2O	0.26	0.19	0.21	0.78	0.21	0.21	0.21	0.20	0.23	0.23
Total	100.62	99.48	99.90	99.80	99.91	100.54	99.66	100.07	99.03	100.48
--Atomic proportions on the basis of 8 oxygens--										
Si	2.654	2.675	2.687	2.682	2.673	2.649	2.654	2.646	2.628	2.620
Al	1.351	1.330	1.313	1.318	1.328	1.356	1.347	1.361	1.365	1.385
Tet cations	4.005	4.004	4.001	4.000	4.000	4.004	4.001	4.007	3.993	4.005
Fe2+	0.003	0.003	0.002	0.000	0.001	0.001	0.000	0.000	0.005	0.003
Ca	0.332	0.330	0.321	0.316	0.336	0.346	0.355	0.355	0.378	0.376
Ba	0.001	0.000	0.001	0.000	0.000	0.001	0.001	0.001	0.000	0.000
Na	0.645	0.635	0.651	0.639	0.639	0.631	0.619	0.609	0.616	0.594
K	0.015	0.011	0.012	0.044	0.012	0.012	0.012	0.011	0.013	0.013
A-site total	0.995	0.980	0.987	1.000	0.988	0.991	0.987	0.976	1.011	0.986
Anorthite	33.47	33.82	32.63	31.62	34.06	34.96	35.95	36.38	37.54	38.26
Albite	64.98	65.03	66.07	63.90	64.71	63.79	62.78	62.38	61.15	60.39
Orthoclase	1.48	1.11	1.21	4.45	1.21	1.20	1.21	1.16	1.32	1.33
Celsian	0.07	0.04	0.09	0.04	0.02	0.05	0.05	0.07	0.00	0.02

TWO TRAVERSES ACROSS PLAGIOCLASE NEAR AMPHIBOLE PG-110

Sample name										
Analysis pt	13	14	15	16	17	18	19	20	21	22
Remark										
SiO2	58.64	58.62	57.97	57.34	57.00	57.01	56.65	57.18	57.50	57.84
Al2O3	26.37	26.78	26.26	26.95	27.15	27.34	26.88	27.03	26.79	26.52
FeO	0.14	0.19	0.14	0.07	0.06	0.11	0.21	0.07	0.13	0.04
CaO	7.88	7.90	8.16	8.67	9.00	9.05	8.94	8.93	8.80	8.60
BaO	0.00	0.00	0.00	0.00	0.08	0.03	0.03	0.05	0.02	0.04
Na2O	6.84	6.81	6.68	6.38	6.40	6.29	6.19	6.39	6.48	6.63
K2O	0.27	0.25	0.31	0.24	0.23	0.25	0.30	0.25	0.26	0.25
Total	100.14	100.55	99.52	99.65	99.92	100.08	99.20	99.90	99.98	99.92
--Atomic proportions on the basis of 8 oxygens--										
Si	2.617	2.606	2.607	2.577	2.561	2.556	2.564	2.568	2.579	2.594
Al	1.387	1.403	1.392	1.427	1.438	1.445	1.434	1.431	1.416	1.401
Tet cations	4.004	4.009	3.999	4.004	3.998	4.001	3.997	3.998	3.995	3.995
Fe2+	0.005	0.007	0.005	0.003	0.002	0.004	0.008	0.003	0.005	0.001
Ca	0.377	0.376	0.393	0.417	0.433	0.435	0.433	0.430	0.423	0.413
Ba	0.000	0.000	0.000	0.000	0.001	0.001	0.001	0.001	0.000	0.001
Na	0.592	0.587	0.582	0.556	0.557	0.547	0.543	0.556	0.564	0.576
K	0.015	0.014	0.018	0.014	0.013	0.014	0.017	0.014	0.015	0.014
A-site total	0.989	0.984	0.999	0.990	1.008	1.001	1.002	1.004	1.007	1.006
Anorthite	38.29	38.50	39.58	42.29	43.09	43.63	43.59	42.91	42.22	41.13
Albite	60.15	60.05	58.63	56.32	55.45	54.88	54.62	55.57	56.26	57.38
Orthoclase	1.56	1.45	1.79	1.39	1.31	1.44	1.74	1.43	1.49	1.42
Celsian	0.00	0.00	0.00	0.00	0.14	0.05	0.05	0.09	0.04	0.07

TWO TRAVERSES ACROSS PLAGIOCLASE NEAR AMPHIBOLE PG-110

Sample name										PG110
Analysis pt	23	24	25	26	27	29	30	31	32	1/2
Remark										40 UM INT
SiO2	58.47	58.46	56.58	57.77	58.36	58.18	58.44	58.33	58.58	59.61
Al2O3	26.43	26.58	27.95	26.36	26.24	26.46	26.27	26.16	26.32	25.67
FeO	0.19	0.07	0.00	0.07	0.00	0.00	0.00	0.05	0.02	0.20
CaO	8.25	8.23	7.82	8.19	7.98	8.02	8.06	7.99	7.99	7.03
BaO	0.05	0.06	0.11	0.03	0.04	0.03	0.04	0.04	0.11	0.02
Na2O	6.84	6.72	6.73	6.48	6.93	6.78	6.81	6.85	6.89	7.61
K2O	0.29	0.29	0.22	0.32	0.35	0.30	0.28	0.30	0.32	0.23
Total	100.52	100.41	99.41	99.22	99.90	99.77	99.90	99.72	100.23	100.37
	--Atomic proportions on the basis of 8 oxygens--									
Si	2.606	2.605	2.548	2.604	2.614	2.607	2.615	2.616	2.615	2.652
Al	1.388	1.396	1.483	1.400	1.385	1.398	1.386	1.383	1.385	1.346
Tet cations	3.994	4.001	4.031	4.005	3.999	4.005	4.001	3.999	4.000	3.998
Fe2+	0.007	0.003	0.000	0.003	0.000	0.000	0.000	0.002	0.001	0.007
Ca	0.394	0.393	0.377	0.396	0.383	0.385	0.386	0.384	0.382	0.335
Ba	0.001	0.001	0.002	0.001	0.001	0.001	0.001	0.001	0.002	0.000
Na	0.591	0.581	0.588	0.566	0.602	0.589	0.591	0.596	0.596	0.656
K	0.016	0.016	0.013	0.018	0.020	0.017	0.016	0.017	0.018	0.013
A-site total	1.009	0.994	0.979	0.983	1.005	0.992	0.994	0.999	0.999	1.012
Anorthite	39.30	39.65	38.52	40.33	38.09	38.82	38.88	38.49	38.27	33.35
Albite	58.97	58.58	59.99	57.74	59.85	59.39	59.44	59.72	59.72	65.32
Orthoclase	1.64	1.66	1.29	1.88	1.99	1.73	1.61	1.72	1.82	1.30
Celsian	0.09	0.11	0.20	0.05	0.07	0.05	0.07	0.07	0.19	0.03

TWO TRAVERSES ACROSS PLAGIOCLASE NEAR AMPHIBOLE PG-110

Sample name										
Analysis pt	2	3	4	5	6	7	8	9	10	11
Remark										
SiO2	59.30	58.99	58.60	58.80	58.87	58.53	58.88	58.35	58.71	57.48
Al2O3	25.46	25.67	25.96	25.54	25.96	25.82	25.73	25.72	25.95	26.91
FeO	0.10	0.12	0.09	0.09	0.09	0.05	0.07	0.12	0.20	0.08
CaO	7.41	7.28	7.57	7.72	7.56	7.52	7.59	7.78	7.66	8.71
BaO	0.05	0.04	0.04	0.00	0.04	0.07	0.08	0.01	0.00	0.00
Na2O	7.19	7.17	7.11	6.91	7.11	7.16	7.04	7.01	7.11	6.31
K2O	0.31	0.30	0.30	0.31	0.34	0.34	0.34	0.36	0.33	0.28
Total	99.82	99.57	99.67	99.37	99.97	99.49	99.73	99.35	99.96	99.77
	--Atomic proportions on the basis of 8 oxygens--									
Si	2.653	2.645	2.628	2.643	2.632	2.631	2.639	2.628	2.627	2.580
Al	1.342	1.357	1.372	1.353	1.368	1.368	1.359	1.365	1.369	1.424
Tet cations	3.995	4.002	4.000	3.996	4.000	3.998	3.998	3.993	3.996	4.004
Fe2+	0.004	0.004	0.003	0.003	0.003	0.002	0.003	0.005	0.007	0.003
Ca	0.355	0.350	0.364	0.372	0.362	0.362	0.364	0.375	0.367	0.419
Ba	0.001	0.001	0.001	0.000	0.001	0.001	0.001	0.000	0.000	0.000
Na	0.624	0.623	0.618	0.602	0.616	0.624	0.612	0.612	0.617	0.549
K	0.018	0.017	0.017	0.018	0.019	0.019	0.019	0.021	0.019	0.016
A-site total	1.001	0.995	1.003	0.995	1.002	1.009	1.000	1.013	1.010	0.987
Anorthite	35.61	35.29	36.38	37.49	36.27	35.97	36.55	37.23	36.62	42.57
Albite	62.53	62.90	61.83	60.72	61.72	61.97	61.36	60.70	61.50	55.80
Orthoclase	1.77	1.73	1.72	1.79	1.94	1.94	1.95	2.05	1.88	1.63
Celsian	0.09	0.07	0.07	0.00	0.07	0.12	0.14	0.02	0.00	0.00

TWO TRAVERSES ACROSS PLAGIOCLASE NEAR AMPHIBOLE PG-110

Sample name Analysis pt Remark	12	13	14	15	16	17	18	21	22	24
SiO2	56.85	57.38	56.99	57.15	56.68	57.61	57.49	57.65	57.74	58.01
Al2O3	26.77	27.35	26.83	26.68	27.27	26.73	26.23	26.24	26.49	26.49
FeO	0.13	0.09	0.12	0.07	0.13	0.11	0.05	0.05	0.07	0.02
CaO	8.73	9.42	8.72	8.78	9.39	8.89	8.45	8.55	8.24	8.15
BaO	0.00	0.00	0.00	0.00	0.00	0.00	0.01	0.00	0.00	0.00
Na2O	6.55	6.08	6.28	6.40	6.18	6.35	6.52	6.40	6.80	6.66
K2O	0.29	0.27	0.32	0.30	0.26	0.27	0.29	0.28	0.21	0.26
Total	99.32	100.59	99.26	99.38	99.91	99.96	99.04	99.17	99.55	99.59
	--Atomic proportions on the basis of 8 oxygens--									
Si	2.569	2.560	2.574	2.578	2.549	2.583	2.599	2.602	2.596	2.604
Al	1.426	1.438	1.428	1.419	1.445	1.413	1.398	1.396	1.404	1.401
Tet cations	3.995	3.997	4.002	3.997	3.994	3.996	3.997	3.997	4.000	4.005
Fe2+	0.005	0.003	0.005	0.003	0.005	0.004	0.002	0.002	0.003	0.001
Ca	0.423	0.450	0.422	0.424	0.452	0.427	0.409	0.413	0.397	0.392
Ba	0.000	0.000	0.000	0.000	0.000	0.000	0.000	0.000	0.000	0.000
Na	0.574	0.526	0.550	0.560	0.539	0.552	0.572	0.560	0.593	0.580
K	0.017	0.015	0.018	0.017	0.015	0.015	0.017	0.016	0.012	0.015
A-site total	1.018	0.995	0.995	1.004	1.011	0.999	1.000	0.991	1.004	0.987
Anorthite	41.71	45.41	42.61	42.38	44.96	42.94	41.02	41.78	39.62	39.73
Albite	56.64	53.04	55.53	55.90	53.55	55.51	57.28	56.59	59.17	58.76
Orthoclase	1.65	1.55	1.86	1.72	1.48	1.55	1.68	1.63	1.20	1.51
Celsian	0.00	0.00	0.00	0.00	0.00	0.00	0.02	0.00	0.00	0.00

TWO TRAVERSES ACROSS PLAGIOCLASE NEAR AMPHIBOLE PG-110

Sample name Analysis pt Remark	25	26	27	28	29	31	32	33	34	35
SiO2	57.97	58.30	58.50	57.02	56.69	56.78	57.18	57.61	57.90	57.86
Al2O3	26.04	25.94	25.99	26.35	26.58	27.01	26.44	25.64	25.67	25.60
FeO	0.10	0.13	0.16	0.07	0.08	0.06	0.08	0.08	0.05	0.03
CaO	7.79	7.82	7.94	8.55	8.62	9.10	8.47	7.69	7.56	7.59
BaO	0.00	0.00	0.00	0.00	0.00	0.00	0.01	0.06	0.04	0.05
Na2O	6.87	6.98	6.76	6.56	6.60	6.33	6.55	7.10	6.86	6.80
K2O	0.32	0.32	0.31	0.31	0.29	0.29	0.29	0.32	0.32	0.30
Total	99.09	99.49	99.66	98.86	98.86	99.57	99.02	98.50	98.40	98.23
	--Atomic proportions on the basis of 8 oxygens--									
Si	2.616	2.621	2.624	2.586	2.573	2.560	2.588	2.619	2.629	2.631
Al	1.385	1.375	1.374	1.408	1.422	1.435	1.410	1.374	1.374	1.372
Tet cations	4.001	3.996	3.998	3.994	3.995	3.995	3.998	3.993	4.003	4.003
Fe2+	0.004	0.005	0.006	0.003	0.003	0.002	0.003	0.003	0.002	0.001
Ca	0.377	0.377	0.382	0.415	0.419	0.440	0.411	0.375	0.368	0.370
Ba	0.000	0.000	0.000	0.000	0.000	0.000	0.000	0.001	0.001	0.001
Na	0.601	0.609	0.588	0.577	0.581	0.553	0.575	0.626	0.604	0.599
K	0.018	0.018	0.018	0.018	0.017	0.017	0.017	0.019	0.019	0.017
A-site total	1.000	1.009	0.993	1.013	1.020	1.012	1.005	1.023	0.993	0.989
Anorthite	37.81	37.54	38.65	41.13	41.23	43.54	40.97	36.72	37.11	37.44
Albite	60.34	60.63	59.55	57.10	57.12	54.81	57.34	61.35	60.94	60.70
Orthoclase	1.85	1.83	1.80	1.78	1.65	1.65	1.67	1.82	1.87	1.76
Celsian	0.00	0.00	0.00	0.00	0.00	0.00	0.02	0.10	0.07	0.09

TRAVERSE ACROSS A PLAGIOCLASE NEAR AMPHIBOLE - PG-118

Sample name	PG-118									
Analysis pt	1	2	3	4	5	6	7	8	9	10
Remark	15.8 UM INT									
SiO2	63.25	64.63	63.44	63.65	63.37	63.62	63.20	63.11	63.25	63.24
Al2O3	23.51	22.22	23.11	23.47	23.06	23.06	22.95	22.89	22.91	22.80
FeO	0.13	0.16	0.17	0.11	0.11	0.07	0.12	0.05	0.08	0.09
CaO	4.69	2.60	4.38	4.38	4.42	4.37	4.29	4.27	4.26	4.24
BaO	0.00	0.06	0.00	0.02	0.02	0.01	0.04	0.04	0.00	0.03
Na2O	9.08	9.73	8.98	9.10	9.16	8.88	8.90	8.73	9.03	8.90
K2O	0.21	0.50	0.24	0.26	0.31	0.36	0.31	0.34	0.35	0.35
Total	100.87	99.90	100.32	100.99	100.45	100.37	99.81	99.43	99.88	99.65
--Atomic proportions on the basis of 8 oxygens--										
Si	2.778	2.853	2.797	2.789	2.794	2.803	2.801	2.805	2.802	2.806
Al	1.217	1.156	1.201	1.212	1.198	1.197	1.199	1.199	1.196	1.193
Tet cations	3.995	4.009	3.998	4.001	3.993	4.000	4.000	4.004	3.998	3.999
Fe2+	0.005	0.006	0.006	0.004	0.004	0.003	0.004	0.002	0.003	0.003
Ca	0.221	0.123	0.207	0.206	0.209	0.206	0.204	0.203	0.202	0.202
Ba	0.000	0.001	0.000	0.000	0.000	0.000	0.001	0.001	0.000	0.001
Na	0.773	0.833	0.768	0.773	0.783	0.759	0.765	0.752	0.776	0.766
K	0.012	0.028	0.014	0.015	0.017	0.020	0.018	0.019	0.020	0.020
A-site total	1.011	0.991	0.994	0.998	1.014	0.988	0.991	0.977	1.000	0.991
Anorthite	21.95	12.49	20.94	20.70	20.68	20.94	20.65	20.84	20.27	20.41
Albite	76.88	84.55	77.69	77.81	77.56	76.99	77.51	77.11	77.75	77.53
Orthoclase	1.17	2.86	1.37	1.46	1.73	2.05	1.78	1.98	1.98	2.01
Celsian	0.00	0.11	0.00	0.03	0.03	0.02	0.07	0.07	0.00	0.05

TRAVERSE ACROSS A PLAGIOCLASE NEAR AMPHIBOLE - PG-118

Sample name										
Analysis pt	11	12	14	17	18	19	20	21	22	23
Remark										
SiO2	63.51	63.84	62.70	63.53	63.38	64.63	65.83	63.36	63.27	63.15
Al2O3	22.64	22.80	23.81	23.28	23.04	22.10	21.82	23.45	23.30	23.47
FeO	0.04	0.03	0.02	0.04	0.00	0.00	0.00	0.12	0.00	0.01
CaO	4.30	4.28	4.99	4.36	4.41	3.22	2.63	4.52	4.42	4.51
BaO	0.00	0.01	0.00	0.02	0.00	0.00	0.00	0.02	0.02	0.00
Na2O	8.91	9.06	8.65	9.13	8.93	9.84	10.36	8.98	8.81	8.88
K2O	0.34	0.27	0.22	0.22	0.22	0.12	0.15	0.31	0.33	0.36
Total	99.74	100.29	100.39	100.58	99.98	99.91	100.79	100.76	100.15	100.38
--Atomic proportions on the basis of 8 oxygens--										
Si	2.814	2.813	2.765	2.794	2.801	2.850	2.875	2.785	2.793	2.784
Al	1.182	1.184	1.238	1.207	1.200	1.149	1.123	1.215	1.212	1.219
Tet cations	3.997	3.997	4.003	4.000	4.001	3.999	3.998	3.999	4.005	4.003
Fe2+	0.001	0.001	0.001	0.001	0.000	0.000	0.000	0.004	0.000	0.000
Ca	0.204	0.202	0.236	0.205	0.209	0.152	0.123	0.213	0.209	0.213
Ba	0.000	0.000	0.000	0.000	0.000	0.000	0.000	0.000	0.000	0.000
Na	0.765	0.774	0.740	0.778	0.765	0.841	0.877	0.765	0.754	0.759
K	0.019	0.015	0.012	0.012	0.012	0.007	0.008	0.017	0.019	0.020
A-site total	0.990	0.993	0.989	0.998	0.986	1.000	1.009	1.000	0.982	0.993
Anorthite	20.64	20.38	23.87	20.61	21.17	15.21	12.20	21.37	21.29	21.47
Albite	77.41	78.07	74.88	78.11	77.57	84.11	86.97	76.85	76.78	76.49
Orthoclase	1.94	1.53	1.25	1.24	1.26	0.67	0.83	1.75	1.89	2.04
Celsian	0.00	0.02	0.00	0.03	0.00	0.00	0.00	0.03	0.04	0.00

TRAVERSE ACROSS A PLAGIOCLASE NEAR AMPHIBOLE - PG-118

Sample name Analysis pt Remark	24	25	26	27	28	29	30
SiO2	62.98	63.62	62.82	62.91	62.67	62.94	62.74
Al2O3	23.61	23.62	23.32	23.62	23.27	23.69	23.41
FeO	0.03	0.09	0.05	0.04	0.08	0.13	0.09
CaO	4.41	4.69	4.75	4.66	4.78	4.80	4.91
BaO	0.04	0.04	0.00	0.01	0.01	0.01	0.04
Na2O	8.86	8.94	8.61	8.69	8.64	8.53	8.66
K2O	0.37	0.38	0.37	0.37	0.39	0.36	0.40
Total	100.30	101.38	99.92	100.30	99.84	100.46	100.25
--Atomic proportions on the basis of 8 oxygens--							
Si	2.779	2.781	2.783	2.776	2.781	2.774	2.775
Al	1.228	1.217	1.218	1.229	1.217	1.231	1.220
Tet cations	4.007	3.998	4.001	4.005	3.998	4.005	3.995
Fe2+	0.001	0.003	0.002	0.001	0.003	0.005	0.003
Ca	0.209	0.220	0.225	0.220	0.227	0.227	0.233
Ba	0.001	0.001	0.000	0.000	0.000	0.000	0.001
Na	0.758	0.758	0.740	0.744	0.743	0.729	0.743
K	0.021	0.021	0.021	0.021	0.022	0.020	0.023
A-site total	0.989	1.002	0.988	0.986	0.996	0.981	1.002
Anorthite	21.10	21.98	22.87	22.37	22.89	23.22	23.30
Albite	76.72	75.83	75.01	75.50	74.87	74.68	74.37
Orthoclase	2.11	2.12	2.12	2.12	2.22	2.07	2.26
Celsian	0.07	0.07	0.00	0.02	0.02	0.02	0.07

VITA

Peter Gillham George was born April 28, 1958 in Pittsburgh, Pennsylvania. He lived in Sewickley, Pennsylvania until attending Duke University in Durham, North Carolina between 1976 and 1980. He graduated in 1980 with a B.S. in geology and a minor in economics. In 1981 he worked as a field geologist for the mineral exploration firm of E. K. Lehman and Associates, located in Minneapolis, Minnesota. From 1982 to 1985 he completed a master's degree program at Texas A&M University. The title of his thesis was "A paleoenvironmental study of the lower Mississippian Caballero Formation and Andrecito member of the Lake Valley Formation in the south-central Sacramento Mountains, Otero County, New Mexico." In 1987 he began a doctoral program at Louisiana State University. While at LSU his major area of interest was in structural geology, geochronology, and tectonics, with a minor in stratigraphy and sedimentation.

DOCTORAL EXAMINATION AND DISSERTATION REPORT

Candidate: Peter Gillham George

Major Field: Geology

Title of Dissertation: TECTONIC IMPLICATIONS OF FISSION-TRACK THERMOCHRONOLOGY AND AMPHIBOLE THERMOBAROMETRY STUDIES OF THE NORTHERN PENINSULAR RANGES BATHOLITH, SOUTHERN CALIFORNIA

Approved:

Major Professor and Chairman

Dean of the Graduate School

EXAMINING COMMITTEE:

Date of Examination:

April 2, 1993